Development and characterization of novel reversibly switchable red fluorescent proteins with opposing switching modes

Dissertation
for the award of the degree
“Doctor rerum naturalium”
of the Georg-August-Universität Göttingen

within the doctoral program
Biomolecules: Structure - Function - Dynamics
of the Georg-August University School of Science (GAUSS)

submitted by

Isabelle Jansen
from Geilenkirchen

Göttingen, 2019

Thesis Committee:

Prof. Dr. Stefan Jakobs (Referee)
Mitochondrial Structure and Dynamics Group
Department of NanoBiophotonics
Max Planck Institute for Biophysical Chemistry, Göttingen
Clinic of Neurology, University Medical Center Göttingen

Prof. Dr. Helmut Grubmüller (2nd Referee)
Department of Theoretical and Computational Biophysics
Max Planck Institute for Biophysical Chemistry, Göttingen

Prof. Dr. Dr. h.c. mult. Stefan W. Hell
Department of NanoBiophotonics
Max Planck Institute for Biophysical Chemistry, Göttingen

Further members of the Examination Board:

Prof. Dr. Silvio O. Rizzoli
Institute of Neuro- and Sensory Physiology
University Medical Center Göttingen

Prof. Dr. Michael Müller
Institute of Neuro- and Sensory Physiology
University Medical Center Göttingen

Dr. Dieter Klopfenstein
Department of Biophysics
Third Institute of Physics
Georg-August University Göttingen

Date of oral examination:

27th November 2019

Abstract

Since the discovery of the green fluorescent protein (GFP) from the jellyfish *Aequorea victoria,* a multitude of fluorescent proteins have been derived from the original GFP and its homologs by protein engineering. Their characteristics were especially adapted to the requirements of different types of live-cell fluorescence microscopy. This includes super-resolution microscopy techniques, which overcome the diffraction barrier by distinguishing fluorophores based on different molecular states. Fluorescent proteins in the subclass of reversibly switchable fluorescent proteins (RSFPs) can be switched from a fluorescent to a non-fluorescent state and *vice versa* by light of certain wavelengths. These RSFPs can be utilized as fusion tags in reversible saturable optical fluorescence transition (RESOLFT) microscopy to achieve diffraction-unlimited resolution. Compared to the green-emitting RSFPs, the application of red-emitting RSFPs benefits from the longer excitation and switching wavelengths utilized and the associated less phototoxicity. However, the number of red RSFPs applicable for live-cell RESOLFT microscopy is limited until now and the available red RSFPs exhibit undesirable characteristics like dimerization tendency.

This work presents the development of novel red RSFPs for RESOLFT microscopy. In order to identify superior red RSFPs, a microscopic screening of mutant libraries expressed in *E. coli* colonies was employed. To additionally facilitate the screening for improved fluorescent proteins in a mammalian expression system, a monoclonal Bxb1 landing pad cell line was generated using CRISPR/Cas9 genome engineering. Since the application of these Bxb1 landing pad cells enables the expression of only a single mutant from a transfected library in each cell, this strategy was suitable to screen for red RSFPs with higher brightness and offers a large potential to establish further screening approaches.

By semi-rational design and screening, novel red RSFPs with opposing switching modes were generated from bright conventional red fluorescent proteins. Three positive-switching RSFPs were developed on the basis of mRuby2 and two negative-switching RSFPs were derived from mScarlet. All of these five RSFPs are monomeric, feature low residual fluorescence in the off-state (below 5 %), and are among the red RSFPs with the highest molecular brightness known today. The characterization of their performance as fusion tag in transient and stable expressions suggest that the novel red RSFPs are suitable for live-cell microscopy. The quantum yields of the switchable mScarlet variants are the highest determined for red RSFPs to date and the switching kinetics of the new negative-switching RSFPs exceeded those of the recently published rsFusionRed2 and rsFusionRed3. In addition, the generated RSFPs based on mRuby2 outperformed rsCherry in all analyzed

switching characteristics and represent the only red fluorescent and positive-switching candidates for live-cell RESOLFT microscopy. A resolution beyond the diffraction limit was demonstrated utilizing one of the switchable mRuby2 variants in a proof of concept experiment.

Table of contents

1 Introduction

1.1 Light microscopy

The invention and development of light microscopy paved the way to non-invasive investigations of structures and components in living organisms which are not visible to the naked eye. In the 17th century, a light microscope allowed Robert Hook to discover and identify cells [1], the basic elements of living organisms. Since these findings, light microscopes were further improved and soon became an elementary tool in life sciences. In the first types of light microscopes, the visualization of objects was limited to the intrinsic contrast of the examined structures. The development of fluorescence microscopy in combination with labeling with fluorophores enabled the targeted investigation of sub-cellular compartments and processes. Further labeling strategies including genetically encodable fluorescent proteins pushed the examination of biological processes even further [2].

However, already in 1873, Ernst Abbe described that the obtainable resolution in conventional light microscopes is restricted by the diffraction of light, meaning that objects within this diffraction limit cannot be discerned [3]. The full width half maximum (FWHM) of the lateral resolution in the focal plane is given by

$$\Delta r \approx \frac{\lambda}{2n \sin \alpha}$$

and the resolution along the axial axis by

$$\Delta z \approx \frac{2\lambda}{n \sin^2 \alpha}$$

with λ describing the wavelength of the focused light, n the refractive index of the media and α the half aperture angle of the objective lens. Hence, the resolution is dependent on the employed wavelength and on the numerical aperture ($n \sin \alpha$) of the objective lens. Using light of the visible spectrum and objectives with common numerical apertures, the lateral resolution is restricted to about 200 nm and the axial resolution to about 450 nm [4]. Several strategies can improve the contrast and the resolution, like confocal laser scanning microscopy [5] and structured illumination microscopy (SIM) [6]. However, these microscopy techniques are still diffraction-limited and do not allow imaging at the nanoscale. In the 1990s, the first concepts for diffraction-unlimited fluorescence

microscopy emerged and several approaches which overcome the diffraction barrier were reported by now (chapter 1.1.1).

1.1.1 Diffraction-unlimited microscopy techniques

The light microscopy strategies which break the diffraction limit, often referred to as super-resolution microscopy or nanoscopy, utilize at least two different molecular states of the markers applied, typically a fluorescent and a non-fluorescent state. Due to the different states, fluorophores within the diffraction-limited distance become distinguishable. These concepts allow only a small ensemble or even a single molecule to be detectable during the fluorescence readout [4] and can be divided into three groups, the coordinate-stochastic nanoscopy, the coordinate-targeted nanoscopy and nanoscopy with minimal photon fluxes (MINFLUX) [7, 8].

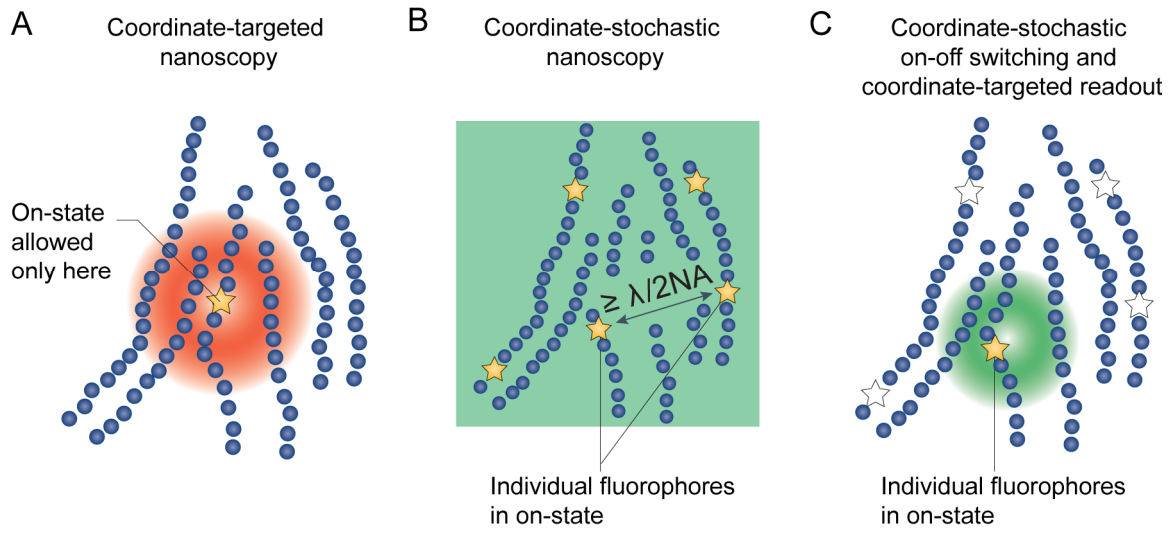

Figure 1.1-1: Diffraction-unlimited microscopy methods.
Different concepts of super-resolution fluorescence imaging techniques. A: Coordinate-targeted nanoscopy methods use a light pattern in combination with light-driven transitions to allow only a small fraction of the fluorophores to be in a detectable state. A doughnut-shaped beam (red) is an example for an applied light pattern. B: Coordinate-stochastic nanoscopy methods utilize stochastic transitions of single fluorophores within the diffraction limit. The technique is implemented by a wide-field illumination and a camera-based readout. The localization of the single fluorophores is calculated from the fluorescence intensity spot. C: The combination of stochastic transitions from non-fluorescent to the fluorescent states with the coordinate targeted readout is applied in MINFLUX imaging. A doughnut-shaped excitation beam (green) can be used for the coordinate-targeted readout. Adapted from Sahl et al., 2017 [7], with permission from Springer Nature.

In the coordinate-stochastic methods, the transitions between the different states of the molecules appear in a stochastic manner. Only a single fluorophore is wanted to emit in the diffraction-limited distance within one frame of the camera-based readout by wide-field illumination (Figure 1.1-1 B). The coordinates of the single fluorophores are calculated by

a Gaussian fit of the detected diffraction-limited fluorescence spot. Examples for coordinate-stochastic methods are stochastic optical reconstruction microcopy (STORM) [9], photoactivated localization microcopy (PALM) [10] and ground state depletion followed by individual molecule return (GSDIM) microcopy [11]. These differ in the strategy used to implement stochastic transitions of single molecules to the fluorescent state.

The second category comprises the coordinate-targeted methods. Here, a light pattern is applied to transfer molecules into a different state at defined positions by exploiting light-driven transitions. The light pattern includes local intensity-zeros where the respective transition does not occur (Figure 1.1-1 A). The coordinate-targeted methods can be implemented by a doughnut-shaped beam or an array with local intensity-zeros (parallelization), with the addition of a fluorescence readout. The resolution in these methods can be approximated by

$$\Delta r \approx \frac{\lambda}{2n \sin\alpha \sqrt{1 + I_{max}/I_s}}$$

with I_{max} being the maximal intensity surrounding the zero and I_S being the saturation intensity at which the amounts of molecules in both states are equal [4].

In the coordinate-targeted method stimulated emission depletion (STED) microscopy, the molecules are transferred from the fluorescent (S_1) to the non-fluorescent state (S_0) by the process of stimulated emission [12]. This concept was the first of the coordinate-targeted methods to be implemented [13]. The light intensities applied for STED microscopy are comparatively high and range from several tens to a hundred $MWcm^{-2}$, because the stimulated emission of the excited molecules in the periphery has to precede the de-excitation by fluorescence emission which occurs in a few nanoseconds [14].

Other coordinate-targeted strategies are based on a different reversible transition to separate the molecules. In ground state depletion (GSD) microscopy, the transition into long-lived dark triplet states and the thermal relaxation are exploited [15]. In addition, the light-driven switching of reversibly switchable fluorescent proteins (RSFPs) between a fluorescent and a non-fluorescent state in both directions can be utilized and was first proposed in 2003 [16]. Due to the long-lived fluorescent and non-fluorescent states, less light intensities are needed for the transitions and range in $kWcm^{-2}$ [14]. Furthermore, fluorescent proteins can be genetically encoded. These two aspects render this coordinate-targeted approach especially suitable for super-resolution microscopy of living cells. Initially, the term reversible saturable optically linear fluorescence transitions (RESOLFT)

included all coordinate-targeted strategies [14, 17]. To date, RESOLFT microscopy is mainly associated with the strategy based on RSFPs and photoswitchable dyes.

In the concept of MINFLUX, the stochastic transtitions from a non-fluorescent to a fluorescent state in combination with coordinate-targeted readout is uitlized to determine the fluorophore localization with high precision [7, 18].

The work presented here focusses on the design and characterization of GFP-like RSFPs suitable for RESOLFT microscopy. Therefore, the class of GFP-like fluorescent proteins is introduced first (chapter 1.2) and then the subclass of RSFPs (chapter 1.3) and their application in RESOLFT microscopy (chapter 1.3.5) is described in more detail.

1.2 GFP-like fluorescent proteins

1.2.1 Naturally occurring fluorescent proteins

The green fluorescent protein from the hydrozoan jellyfish *Aequorea victoria* (avGFP) was first described by Osamu Shimomura and coworkers in 1962 [19] and the first analysis of its chromophore was reported in 1979 [20]. However, it was not until 1992 that avGFP was cloned [21] which was followed by the first demonstration of avGFP as a fluorescent tag in living cells in 1994 [22]. The chromophore of avGFP is formed autocatalytically and the formation is only dependent on molecular oxygen and not on any other cofactors or substrates [23, 24]. This qualifies the genetically encodable fluorescent protein for labeling of whole cells and as fluorescent tag for specific labeling of structures or individual proteins within the cell.

Later on, homologs of avGFP were identified in other species including corals [25-28], crustaceans [29, 30] and lancelets [31, 32]. The first naturally occurring fluorescent protein which emits in the red region of the visible spectrum was DsRed from the mushroom anemone *Discosoma sp.* [25]. Further examples for naturally occurring red fluorescent proteins are asFP595 from the sea anemone *Anemonia sulcate* [33] and eqFP611 from the sea anemone *Entacmaea quadricolor* [26]. While avGFP is monomeric at low concentrations [23], almost all GFP-like proteins from the class of Anthozoa are dimeric or tetrameric [26-28, 34]. Although the sequence homology of the GFP-like proteins from different species is rather low, the overall structure shows a high similarity [35] (chapter 1.2.2).

1.2.2 The overall structure and chromophore maturation

The protein structure of avGFP was reported independently by two groups in 1996 (Figure 1.2-1 A+B) [36, 37]. Later, the structures of avGFP homologs were solved as well and revealed a high similarity (DsRed: Figure 1.2-1 D+E) [38-40]. The sequences of the GFP-like fluorescent proteins consist of 220-240 amino acids [2] which corresponds to a molecular weight of 25-30 kDa [35]. The peptide sequence forms 11 β-sheets. These are connected via loops and are arranged in a beta-barrel structure with an α-helix passing through the center. Oligomeric fluorescent proteins were shown to attach via distinct exterior interfaces of the beta-barrel. The chromophores of the fluorescent proteins are autocatalytically formed within the beta-barrel by three amino acids of the α-helix [41].

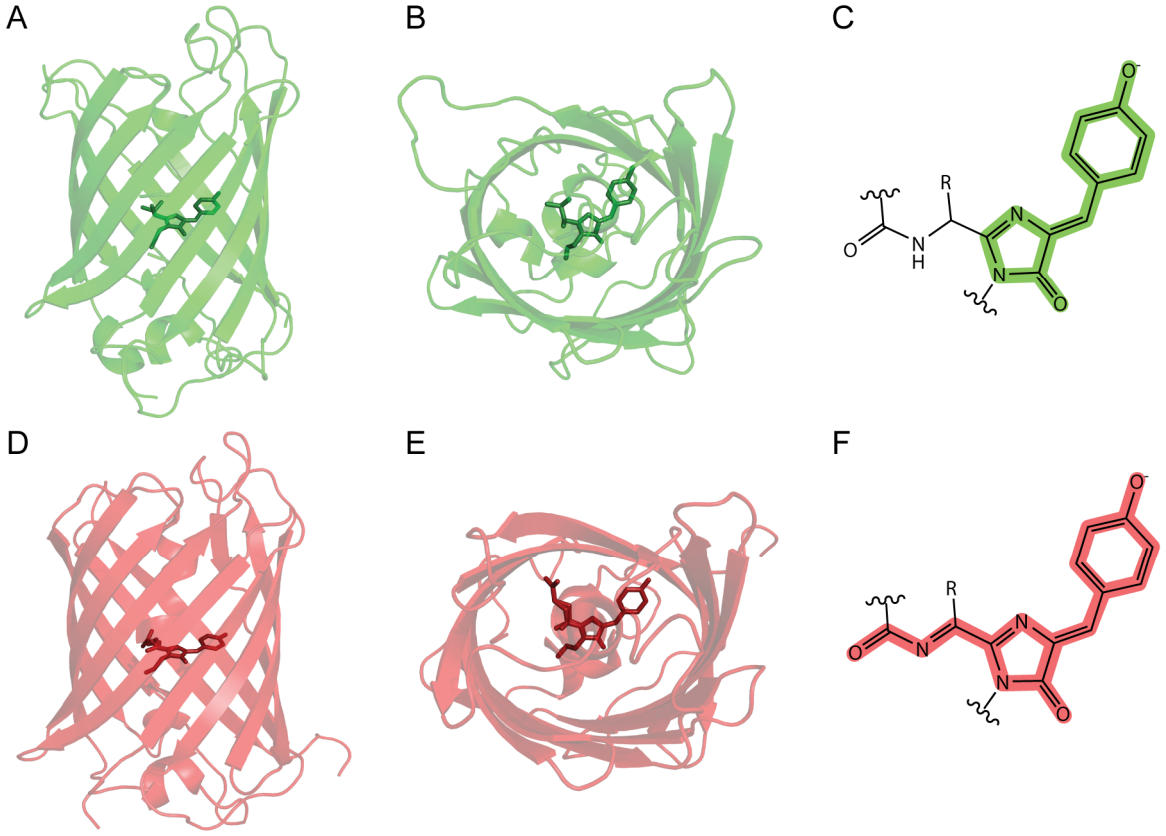

Figure 1.2-1: Beta-barrel structures and chromophores of avGFP and DsRed.
Tertiary structure of avGFP (green) and DsRed (red) from side view (A+D) and top view (B+E). avGFP: PDB 1EMA [36], DsRed: PDB 1ZGO, subunit A [42]. The chromophore inside the beta-barrel is indicated in dark green for avGFP and in dark red for DsRed. The conjugated π-system is marked green or red in the chemical structures of the avGFP (C) or DsRed chromophore (F). Both fluorescent proteins contain a chromophore in the cis-conformation.

In avGFP, the chromophore-forming amino acids are serine, tyrosine and glycine at positions 65-67 [21]. The tyrosine and glycine are highly conserved in naturally occurring fluorescent proteins, whereas the amino acid at the first position in the chromophore differs

among the GFP-like fluorescent proteins. The maturation process of the chromophore can only take place inside the beta-barrel of the folded protein [43]. In avGFP, the maturation is initiated by a nucleophilic attack of the amide nitrogen of amino acid Gly67 on the carbonyl-carbon atom of amino acid Ser65 (Figure 1.2-2 (1)) [44]. The cyclization is most likely followed by an oxidation and a subsequent dehydration (Figure 1.2-2 (2-4)) [45, 46]. The resulting chromophore consists of a hydroxyphenyl ring and an imidazolinone ring connected by a methine bridge (Figure 1.2-1 C). The avGFP chromophore is stabilized in the interior of the beta-barrel by non-covalent interactions and exhibits a conjugated π-system. The excitation of the avGFP chromophore with violet light induces emission of green fluorescence [2, 23].

Compared to the avGFP chromophore, the chromophore of red fluorescent proteins comprises an extended π-system (Figure 1.2-1 F), which explains the higher excitation and emission wavelengths of these proteins [38]. The chromophore of the red fluorescent DsRed is formed by the amino acids glutamine, tyrosine and glycine at the positions 66-68 [47]. The cyclization appears as well by a nucleophilic attack, but the following maturation steps are more complex [46]. The maturation of the DsRed chromophore involves the formation of a blue intermediate (Figure 1.2-2 (5)) containing an acylimine group [48, 49]. The oxidation of this blue intermediate yields the red fluorescent chromophore (Figure 1.2-2 (6)) [48].

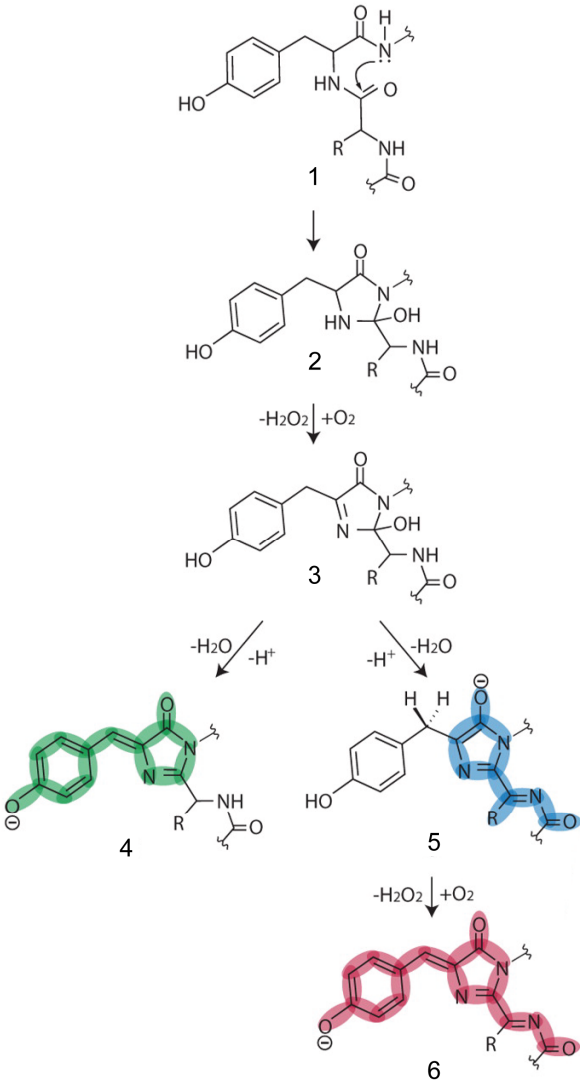

Figure 1.2-2: Maturation of avGFP- and DsRed-like chromophores.
The maturation inside the beta-barrel is initiated by a nucleophilic attack of the nitrogen atom of the third chromophore amino acid on the carbonyl-carbon atom of the first chromophore amino acid (1). By an oxidation of this cyclized product (2), the formation of the imidazolinone ring follows (3). The dehydration yields either the green fluorescent chromophore (4, avGFP) by formation of a methine bridge or a blue fluorescent intermediate (5) by formation of an acylimine group. Proceeding from the blue intermediate, the red fluorescent chromophore (6, DsRed) is formed by an additional oxidation step. Adapted with permission from Dedecker et al., 2013 [35], American Chemical Society.

The maturation process is presumably similar in other red fluorescent proteins including eqFP611 [50], whose chromophore is formed by the amino acids methionine, tyrosine and glycine [26, 39]. In addition, the maturation of some orange or red fluorescent proteins involves further chromophore modification [35]. In asFP595, a protein backbone break appears during the maturation process [51].

The chromophore of the fluorescent proteins can either adopt a *cis*- or a *trans*-conformation at the methine bridge. The crystal structures of a large number of examined GFP-like fluorescent proteins revealed chromophores in the *cis*-conformation (e.g. avGFP [36]). However, fluorescent proteins do exist which exhibit a chromophore in the *trans*-state (e.g. eqFP611 [39]). In addition, the chromophore can be either in an anionic or a neutral form by deprotonation or protonation of the hydroxyphenyl ring. The protonation of this hydroxyl group shifts the absorption band of the chromophore to shorter wavelengths [23]. The conformation and the protonation state of the chromophore are influenced by the chromophore-surrounding amino acids.

1.2.3 Engineering of fluorescent proteins

The initial avGFP and its homologs were modified by protein engineering to adapt their characteristics for different applications [24]. The fluorescent proteins were mutated at specific sites or randomly. Afterwards, the mutants were characterized or the mutant libraries were screened for specific characteristics. One of the first mutants which was generated from avGFP and which is still widely used to date, is the enhanced GFP (EGFP). The F64L and S65T mutations in EGFP are located next to the chromophore and in the chromophore itself and shifted the excitation maximum from 395 nm to 488 nm. The addition of these and further mutations in EGFP improved the molecular brightness (product of quantum yield and extinction coefficient) compared to avGFP [52, 53].

Most of the naturally occurring fluorescent proteins are dimers or tetramers [26-28, 34], which make them unusable in most applications. Hence, the goal was to monomerize the available fluorescent proteins. This was achieved by mutations which disrupt the attachment interfaces on the outside of the beta-barrel. However, the monomerization is commonly accompanied by a strong reduction or even loss of fluorescence [50]. The ability to fluoresce was partly recovered by further mutagenesis and screening. Among others, the monomeric and red fluorescent proteins mRFP1, mRuby and TagRFP were developed from the naturally occurring DsRed, eqFP611 and eqFP578 applying this strategy [27, 54, 55]. Furthermore, for some of the fluorescent proteins, the codon usage was optimized for

expression in the mammalian system [53, 54, 56] and the N- and C-terminus were exchanged by the EGFP termini to improve their performance in fusion constructs [57-59].

1.2.3.1 Tuning the excitation and emission wavelengths

The excitation and emission wavelengths of the naturally occurring fluorescent proteins and their monomeric mutants already covered different parts of the visible spectrum. In addition, protein engineering efforts were capable to produce fluorescent proteins with hypsochromic or bathochromic shifted excitation spectra, emission spectra or both (Figure 1.2-3). This allows multicolor labeling and as a result, imaging of different compartments or proteins in the same cell. Compared to avGFP and EGFP, a bathochromic shift in the excitation and emission spectra was achieved in EYFP by the introduction of the T203Y mutation [36]. The bathochromic shift results from a π-π stacking of the tyrosine at position 203 and the hydroxyphenyl ring of the chromophore [60]. Variants of avGFP with blue-shifted emission spectra were obtained by exchanging the tyrosine located in the chromophore by histidine (blue fluorescent) or tryptophan (cyan fluorescent) and thereby modifying the conjugated π-system [41]. An additional blue fluorescent protein was generated from the red fluorescent protein TagRFP by trapping the blue maturation intermediate [61].

The longer excitation wavelengths needed for orange, red and near-infrared fluorescent proteins in live-cell microscopy have the advantage of reduced autofluorescence, light-scattering and phototoxicity [62]. Furthermore, expanding the color palette in this region of the spectrum provides more options for multicolor imaging. Most red fluorescent proteins were engineered from fluorescent proteins of Anthozoa species [24, 62]. The hypsochromic shift in the spectra of the orange fluorescent protein mOrange [58] compared to its progenitor mRFP1 results from the M65T mutation in the chromophore and cyclization of this residue with the acylimine group [63]. An even further hypsochromic shift was induced in the yellow fluorescent protein mHoneydew by the chromophore mutation Y66W [58].

The shifts to longer wavelengths were attainable by stabilization of the red fluorescent chromophores in the *cis*-form instead of the *trans*-form [64] or introduction of π-π-stacking interactions with amino acids in the chromophore environment [65]. A different strategy involves the stabilization and the extension of the π-system by hydrogen bonds to the phenolat or acylimine group [50, 66]. Thus, the development of red fluorescent proteins with longer excitation and emission wavelengths is highly dependent on interactions of surrounding amino acids with the chromophore. The proteins TagRFP657 (Exc_{max}: 611 nm,

Em_{max}: 657 nm) [67] and TagRFP675 (Exc_{max}: 598 nm, Em_{max}: 675 nm) [68] are examples of available GFP-like fluorescent proteins with long excitation and emission wavelengths. However, the near-infrared fluorescent proteins typically suffer from a low molecular brightness (Figure 1.2-3) [24]. As an alternative, infrared fluorescent proteins on the basis of bacterial phytochromes were introduced, but these are dependent on the binding of the external chromophore biliverdin, which can be disadvantageous in some applications [24].

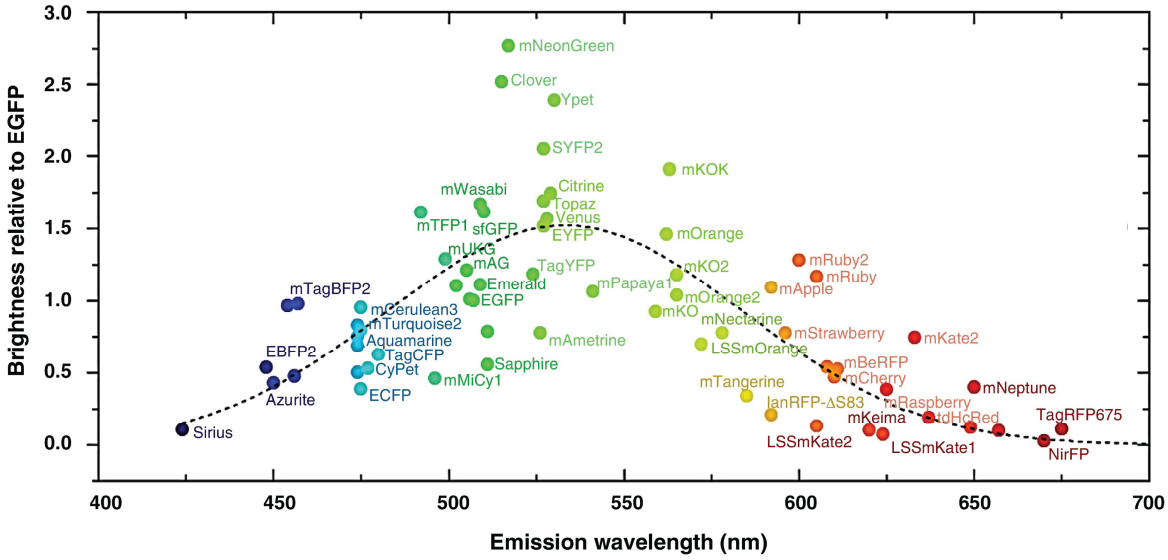

Figure 1.2-3: Brightness and emission wavelengths of GFP-like fluorescent proteins.
Fluorescent proteins emitting in different spectral ranges were developed by protein engineering. The molecular brightness relative to EGFP of the individual proteins is plotted against the respective emission wavelength. The trend of the molecular brightness is indicated by the dashed black line. Adapted from Adam et al., 2014 [69], with permission from Elsevier.

1.2.3.2 Improving further characteristics

In addition to the monomerization and the changes of the spectral properties, the protein engineering was aimed to improve the GFP-like fluorescent proteins regarding other characteristics. A high molecular brightness and a high effective brightness in living cells were targeted, since these are key parameters for most applications [70-72]. Using fluorescent proteins as labels in light microscopy, brighter fluorescent proteins allow to visualize the structure of interest with improved signal-to-noise ratio. Moreover, a lower dose of the excitation light is needed for brighter fluorescent proteins to visualize the respective structure [2]. The effective brightness in living cells is not only affected by the molecular brightness, but also by the expression, folding and maturation rate of the fluorescent proteins [73, 74]. The temperature, the local pH as well as other cellular and environmental factors can additionally have an influence on the effective brightness in cells. However, the comparison of different fluorescent proteins is mainly based on their

molecular brightness [75], since the effective brightness in living cells can vary depending on the applied cell type and experimental setup.

The performance as fusion tag and the cytotoxicity in mammalian cells are further parameters determining the applicability of fluorescent proteins in light microscopy and were as well approached by protein engineering [76]. For applications with long-term illumination like time-lapse imaging, the photostability of the fluorescent proteins is an important factor and was therefore often targeted by mutagenesis and screening [70, 77, 78]. Other characteristics including the fluorescence lifetime, the pH stability [79], the Stokes shift [80, 81] and the performance as fluorescence resonance energy transfer (FRET) acceptor or donor [70, 82] are other parameters which were analyzed in screenings to obtain fluorescent proteins with suitable characteristics for specific applications. For examle, the fluorescent protein mRuby2 is a slightly brighter and more photostable variant of mRuby and was identified by screenings for an improved FRET acceptor [57].

Thus, protein engineering approaches gave rise to a multitude of GFP-like fluorescent proteins with large variations in their characteristics. The structural data of new fluorescent proteins gave insights into the influence of single amino acids and mutations on the characteristics. Since the overall structure and the positions of some highly conserved amino acids show high similarity among all GFP-like fluorescent proteins, this knowledge can guide the choice of mutation sites for other fluorescent proteins [83, 84].

In order to give rise to an additional template for the engineering of red fluorescent proteins, a synthetic gene was generated based on the knowledge about naturally occurring and engineered red fluorescent proteins like mCherry [85]. This synthetic gene template termed mRed7 was applied in mutagenesis and screening rounds which resulted in mScarlet and two further mutants. mScarlet is the monomeric red fluorescent protein with the highest molecular brightness (2.1 fold to EGFP) and the longest fluorescence lifetime to date [85].

The application fields of the GFP-like fluorescent proteins evolved with the occurrence of fluorescent proteins with different characteristics [24]. In addition to the labeling of cells, cellular structures or specific proteins, fluorescent proteins are used in the investigation of protein interactions and movements, in genetically encoded sensors, and in the control of promoter activities [2]. Further application fields emerged with the appearance of phototransformable fluorescent proteins. These can be transformed either irreversibly or reversibly from one state to another by illumination with light [69]. These proteins and in particular the subclass of reversibly switchable fluorescent proteins are described in the next chapter.

1.3 Reversibly switchable fluorescent proteins

In addition to the conventional GFP-like fluorescent proteins, three subclasses of phototransformable fluorescent proteins exist. In the subclass of photoactivatable fluorescent proteins, the proteins can be irreversibly transferred from a non-fluorescent to a fluorescent state, while photoconvertible fluorescent proteins can be irreversibly converted from one emission color to another. The third subclass includes the reversibly switchable fluorescent proteins (RSFPs) [69]. RSFPs can be reversibly switched from a fluorescent on-state to a non-fluorescent off-state and *vice versa* by light of certain wavelengths. Due to their reversible switching, RSFPs are potential probes for super-resolution methods [86], in particular for RESOLFT microscopy (see chapter 1.1.1). This work aimed to develop novel RSFPs, therefore this class is described in detail in the following.

The first GFP-like protein with reversible switching behavior was introduced in 2000 and was named asFP595 [33]. The excitation of this naturally occurring and tetrameric protein with green light yields red fluorescence. Illuminating an ensemble of asFP595 proteins with green light additionally increases the fluorescence emission until all asFP595 proteins are switched to the on-state, whereas the illumination with blue light transfers these proteins to the off-state. The next reported RSFP was the green fluorescent protein Dronpa. This protein is a monomerized mutant of the fluorescent protein 22G, which was derived from a *Pectiniidae* coral [87]. The fluorescence intensity of a Dronpa ensemble decreases when excited with light of 490 nm and the proteins can be switched back to the on-state by illumination with light of 400 nm.

In the following years, the underlying switching mechanisms were investigated (chapter 1.3.4) and key amino acids responsible for the switching were identified. Especially the amino acids in the direct chromophore environment have a direct impact on the switching ability of fluorescent proteins. The mutagenesis of these amino acids changed the switching characteristics of Dronpa [88, 89] and introduced switching to conventional GFP-like proteins including mEGFP or mCherry [90, 91]. Further site-directed mutagenesis in combination with error-prone mutagenesis was able to adjust the characteristics of new RSFPs (see chapter 1.3.3).

1.3.1 Switching modes of RSFPs

The reversible switching between the on- and off-state in RSFPs can be distinguished in three different switching modes: Negative, positive and decoupled switching [88, 92]. In negative-switching RSFPs like Dronpa [87], the light that induces fluorescence emission also switches the proteins off. As a result, the fluorescence intensity decreases until the proteins are entirely switched off (Figure 1.3-1 A). A second wavelength, which is usually 80-130 nm shorter than the off-switching wavelength, can transfer the negative-switching GFP-like proteins back into the on-state [93].

In contrast, in positive-switching RSFPs like asFP595 [33], the excitation wavelength, which induces fluorescence, switches the proteins to the on-state. The on-switching is measurable as an increase of the fluorescence signal (Figure 1.3-1 B). A second shorter wavelength can switch the positive-switching fluorescent proteins into the off-state.

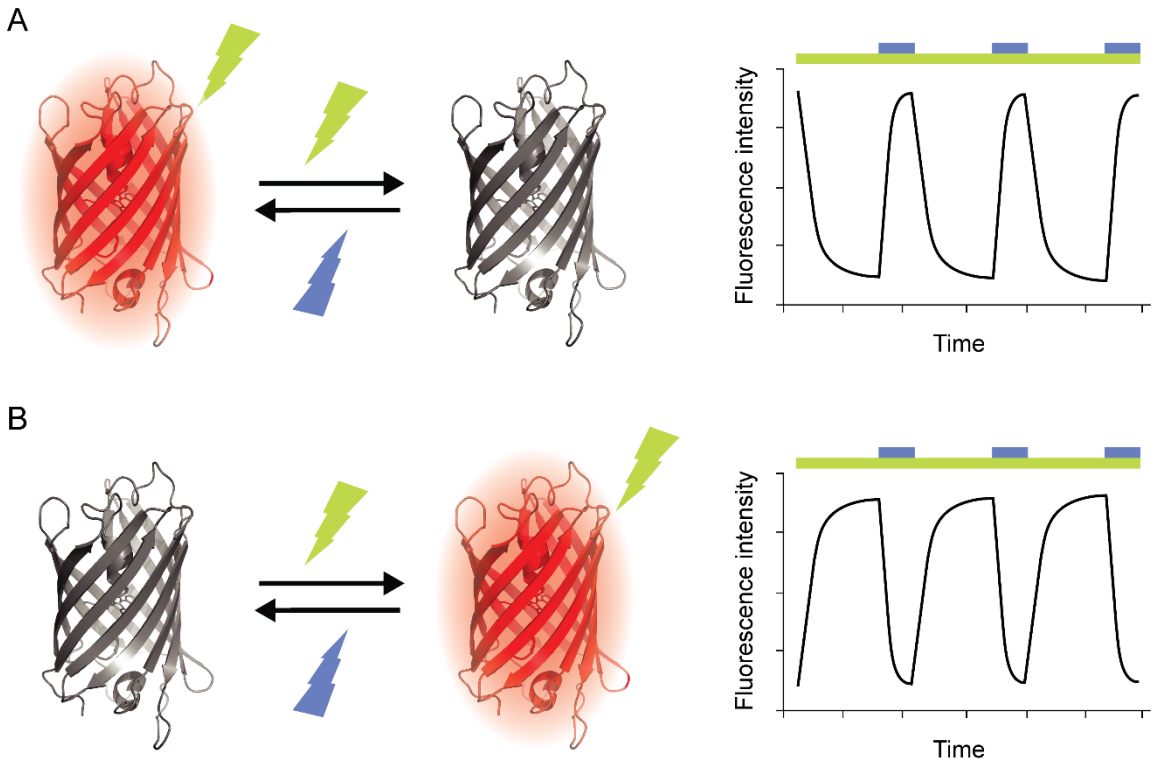

Figure 1.3-1: Negative- and positive-switching mode for red-emitting RSFPs.
Reversible switching illustrated for red fluorescent proteins with negative- or positive-switching mode. The grey fluorescent proteins present the off-state, the red fluorescent proteins present the on-state. A: Negative-switching: The light that is used to induce fluorescence (yellow-green), switches the protein off. A second wavelength switches the protein into the on-state (blue). B: Positive-switching: The light which induces fluorescence switches the protein on (yellow-green). A second wavelengths is used for off-switching (blue). A+B right: Schematic switching curves. The illumination with the light for off-switching yields a reduction in the fluorescence intensity, while the on-switching is visible by an increase in the fluorescence intensity.

In negative- and positive-switching RSFPs, the excitation inducing fluorescence and the switching into one direction are coupled. For RSFPs with decoupled switching mode, an excitation wavelength which induces fluorescence does not provoke switching. Instead, the on- and off-switching are induced by two further wavelengths [92].

1.3.2 Crucial characteristics of RSFPs

Several biological applications of RSFPs have been demonstrated including protein tracking and photochromic FRET, but until now, RSFPs were mostly used in super-resolution microscopy. RSFPs have been applicable in coordinate-stochastic methods [91], protected STED [94], nonlinear SIM [95] and RESOLFT microscopy [90]. Every nanoscopy method relies on specific protein properties, thereby the techniques differ in their requirements [86]. This work focusses on the application of RSFPs in live-cell RESOLFT microscopy, because this method facilitates diffraction-unlimited imaging of living cells with lower light doses than STED microscopy [14].

Since the RSFPs are applied as fusion tags in eukaryotic cells [96, 97], RSFPs with fast maturation, good performance in fusions and low cytotoxicity are desired, preferentially with high molecular and effective cellular brightness (see chapter 1.2.3.2). In contrast to the conventional GFP-like proteins, the RSFPs can adopt two states (on and off) which differ in their molecular brightness [82]. At thermal equilibrium, an ensemble of RSFPs in solution or in living cells can be a mixture of proteins in the on- and in the off-state [88, 91]. This equilibrium state can be calculated by the ratio of the fluorescence signal in the thermal equilibrium to the fluorescence signal in the on-state. To compare the RSFPs regarding their maximal ensemble fluorescence, the examined RSFP ensemble needs to be switched to the on-state before the fluorescence is measured.

Furthermore, the switching characteristics of the RSFPs largely determine their applicability in RESOLFT microscopy. One of these switching parameters is the residual fluorescence signal in the off-state in relation to the fluorescence signal in the on-state [91], which was used in this work to compare RSFPs. Alternatively, the switching contrast can be calculated [82], which is defined as the fluorescence signal in the on-state divided by the fluorescence signal in the off-state. Low residual fluorescence in the off-state or high switching contrast is essential for the application in RESOLFT microscopy [98].

Other important characteristics of RSFPs are their on- and off-switching kinetics [86]. The switching speed is dependent on the applied light intensity and switching wavelengths. For this reason, the absolute switching times can differ using dissimilar methods in different

experimental setups. For a reliable comparison of various RSFPs, the proteins should be expressed in the same type of organism using an equal construct and the switching curves should be acquired with the same microscope using the same light intensities. RSFPs with fast switching kinetics are beneficial for RESOLFT microscopy by reducing the required switching times [96].

The repetitive switching of an RSFP ensemble is accompanied by a reduction in the maximal fluorescence signal due to the destruction of some of the RSFPs in each cycle. This effect is termed switching fatigue. The switching fatigue is related to the process of photobleaching in conventional fluorescent proteins [99], which describes the loss of fluorescence at continuous fluorescence excitation. RSFPs are typically compared by the number of switching cycles until 50 % of the maximal fluorescence signal in the first cycle is reached [96, 100]. Another aspect of switching fatigue can be an increase of the residual fluorescence in the off-state [91] and thereby a reduction of the switching contrast. A low switching fatigue is desirable for RESOLFT microscopy, since the imaging schemes require multiple switching cycles [101].

1.3.3 Engineering of RSFPs

Until now, several RSFPs were developed by introduction of switching to conventional fluorescent proteins or by improving existing RSFPs. Since RSFPs are applied as fusion tags in living cells, the development of new RSFPs was focused on monomeric fluorescent proteins. The generation of new or improved RSFPs usually involves site-directed mutagenesis of the amino acids in the chromophore environment, as these have a major impact on the switching ability of the fluorescent proteins [82, 88, 89, 91, 102]. This approach is often combined with error-prone mutagenesis [82, 88, 91]. The majority of the available RSFPs show a negative-switching mode and more exist which emit in the green part of the spectrum (green RSFPs) than those which emit in the yellow or red part of the spectrum (yellow and red RSFPs) (see chapter 1.3.3.1 and 1.3.3.2).

1.3.3.1 Green and yellow RSFPs

The green RSFPs are commonly switched using the wavelengths 405 nm and 488 nm. The excitation of the green RSFPs at 488 nm induces fluorescence emission. Based on the negative-switching Dronpa [87], further green RSFPs with altered switching characteristics were generated. The site-directed mutagenesis of positions in the direct chromophore environment yielded the faster switching rsFastLime and Dronpa-M159T [89]. Interestingly, the M159Y mutation in Dronpa inverted the switching mode from negative-

to positive-switching. Including this mutation, the positive-switching Padron was evolved from Dronpa using site-directed and error-prone mutagenesis [88]. Padron and its descendant Kohinoor [100] represent the only positive-switching and green fluorescent proteins so far.

A series of green RSFPs with negative-switching mode, namely rsEGFP [90], rsEGFP2 [96], rsGreen1, rsGreenF [103], rsFolder1 and rsFolder2 [104], were developed from mEGFP [105] and superfolder GFP [71], which are both constitutively fluorescent avGFP variants. These RSFPs differ in their expression and maturation efficiencies and show slight differences in their switching characteristics. Especially rsEGFP2 features an extraordinary low switching fatigue and is for this reason most frequently applied in RESOLFT microscopy.

Further green RSFPs were evolved from the photoconvertible fluorescent proteins mEos2 [106] (mGeos-X [107]), mEos3.1 [108] (Skylan-S, Skylan-NS [95, 109]) and mMaple3 [110] (GMars-X [102, 111, 112]) by replacing the histidine in the chromophore and by addition of further mutations. The proteins mIrisFP [113] and NijiFP [114] were as well derived from photoconvertible fluorescent proteins. These two proteins are still photoconvertible (from green to red fluorescent) and additionally negative-switching in both fluorescent forms.

The yellow RSFP Dreiklang [92] and its mutant SPOON [115] are the only RSFPs found with decoupled switching mode. Dreiklang was generated from the avGFP variant Citrine [79] and can be switched to the on-state by light of 365 nm and to the off-state by light of 405 nm [92]. The fluorescence emission of Dreiklang in the on-state can be induced by excitation at 515 nm. Although the decoupled switching mode can be beneficial for RESOLFT microscopy, the two switching wavelengths in the ultraviolet and violet regions of the spectrum and some additional unfavorable switching characteristics (high switching fatigue, slow switching kinetics) limit the use of Dreiklang in live-cell RESOLFT microscopy.

1.3.3.2 Red RSFPs

The available red RSFPs are usually switched with light of 405-510 nm and with light of 540-592 nm with the latter range inducing fluorescence emission. The naturally occurring asFP595 as well as the generated asFP595 mutants are positive-switching and red fluorescent [33, 74, 116]. Although the first proof of concept RESOLFT imaging was performed using purified asFP595, the tetrameric state of asFP595 and its mutants prevent

their application in live-cell RESOLFT microscopy. So far, no monomeric variant of this protein has been reported.

The next introduced red RSFPs were rsCherry and rsCherryRev [91] which were developed from the conventional fluorescent protein mCherry [58]. While rsCherry switches in a positive mode, rsCherryRev is a negative RSFP. The Q163M mutation in the proximity of the chromophore is responsible for the opposing switching mode in rsCherryRev. Further mutagenesis of rsCherryRev in combination with screening yielded the negative-switching rsCherryRev1.4 [98]. This red RSFP showed a dimerization tendency, but was the first red RSFP applicable in live-cell RESOLFT microscopy.

The negative-switching rsTagRFP [117] was generated from the monomeric and red fluorescent protein TagRFP [27]. The absorption spectra of on- and off-switched rsTagRFP proteins feature significant differences, which could not be measured for rsCherryRev. Due to these spectral differences, rsTagRFP was applicable as acceptor in photochromic FRET [117], but no applications in RESOLFT imaging have been shown yet.

The converted red forms of NijiFP [114] and mIrisFP [113] (chapter 1.3.3.1) emit at lower wavelengths (Em_{max}: 569 nm and 578 nm) than the other red RSFPs mentioned above (585-610 nm) [82, 91, 98]. The need for photoconversion with violet light, the dimerization tendency of NijiFP [114] and unfavorable switching characteristics (high switching fatigue, low switching contrast) render both unsuitable for RESOLFT microscopy in the red spectral range.

In the course of this work, the red RSFPs rsFusionRed1, rsFusionRed2 and rsFusionRed3 with negative-switching mode were introduced [118]. These RSFPs were generated based on FusionRed [76], which is a descendant of TagRFP [27]. The variant rsFusionRed1 showed 33.6 % residual fluorescence in the off-state and is thus not suitable for RESOLFT microscopy. The two RSFPs rsFusionRed2 and rsFusionRed3 differ in only one mutation and exhibited a low residual fluorescence in the off-state (8 % and 5 % of the on-state signal). Both showed faster off-switching than other negative-switching red fluorescent proteins (rsCherryRev, rsCherryRev1.4, rsTagRFP). Furthermore, rsFusionRed2 and rsFusionRed3 were successfully applied in parallelized live-cell RESOLFT microscopy [118].

The overall number of available red RSFPs is not only lower, but most green RSFPs also outperform the red RSFPs regarding their molecular brightness and switching characteristics [86]. However, due to the longer switching and excitation wavelengths, red RSFPs with superior switching characteristics would be highly welcome as valuable probes for live-cell RESOLFT microscopy.

1.3.4 Mechanistic aspects of photoswitching

The mechanism of switching in RSFPs was examined by numerous studies utilizing different methods like X-Ray crystallography, NMR spectroscopy, molecular dynamics simulations and ultrafast spectroscopy (e.g. [40, 116, 117, 119-123]). For all examined RSFPs except Dreiklang, *cis-trans* isomerization in the chromophore is involved in switching [124]. Almost all crystal structures of on-switched RSFPs showed a chromophore in the *cis*-conformation, whereas the chromophore in the off-state was found in the *trans*-conformation [99, 124, 125]. The only exception was recently revealed for rsGamillus-S, which exhibited a *trans* chromophore in the on-state and a *cis* chromophore in the off-state [126].

Although the *cis-trans* and *trans-cis* isomerization appears to be a key event in switching, the conformational change alone cannot explain the different fluorescence abilities of the chromophores in the on- and off-states [125]. For most RSFPs, a change in the protonation state induced by the switching process was postulated or confirmed. The chromophore of the negative-switching Dronpa is deprotonated in the on-state and protonated in the off-state [120, 122]. In contrast, the chromophore of its positive-switching variant Padron is deprotonated in the off-state and partially protonated and deprotonated in the on-state [123, 127]. In addition, a higher flexibility of the chromophore in the off-state and the associated non-radiative processes are discussed to contribute to the non-fluorescent state [121]. Another factor could be a change in the planarity of the chromophore [120]. However, the stabilization and distortion of the hydroxyphenyl ring in the on- and off-state vary in the different examined RSFPs [40, 117, 120, 123].

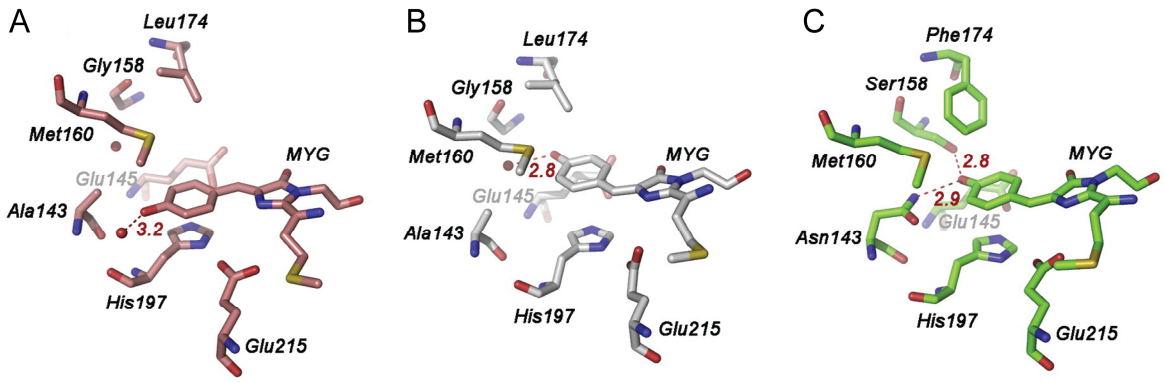

Figure 1.3-2: Chromophore environment of rsTagRFP and TagRFP.
Structures of the direct chromophore environment of rsTagRFP in the on- (A) and off-state (B) in comparison to the chromophore environment of TagRFP (C). In the cis- (A) and trans-conformation (B) of the rsTagRFP chromophore, the hydroxyphenyl ring only adopts hydrogen bonds to internal water molecules (shown in red dashed lines with distances in ångström). The trans chromophore of the non-switching TagRFP is stabilized by hydrogen bonds to Ser158 and Asn143. Adapted from Pletnev et al., 2012 [117], with permission of Elsevier.

In all aspects mentioned, the reversible switching in positive- and negative-switching RSFPs is highly dependent on the chromophore-surrounding amino acids. On the one hand, steric effects might hinder the *cis-trans* isomerization of the chromophore. On the other hand, the amino acids can stabilize one or both conformations by non-covalent bonds and can affect the protonation state. AIready mutational studies of asFP595 revealed the significant impact of the amino acids in the direct chromophore environment, namely A148 and S165, on the switching ability of this protein [116]. The A148S mutation improved the quantum yield and the switching of asFP595. Later, this serine was shown to stabilize the chromophore in the *cis*-form by an additional hydrogen bond to the phenolate group [40].

The introduction of switching to mCherry was achieved by exchanging the isoleucine at position 161 in the close proximity of the chromophore to the smaller and polar amino acid serine. Further mutagenesis of chromophore-surrounding amino acids (among others: S146, Q163) yielded rsCherry and rsCherryRev [91]. In TagRFP, the switching was introduced by the mutations N143A and S158G. The addition of further mutations (among others: F174L) yielded rsTagRFP [117]. In contrast to the former amino acids, the introduced alanine and glycine at positions 143 and 158 are nonpolar. Thus, the hydroxyphenyl ring of the chromophore in rsTagRFP is no more stabilized by hydrogen bonds to the amino acids of the protein scaffold (Figure 1.3-2). In addition, the added mutations enabled the *cis-trans* isomerization [117]. Different to other RSFPs like Dronpa and Padron [120, 121, 123], the crystal structures of rsTagRFP revealed a similar coplanarity in both chromophore conformations [117].

Investigations of the switching in the RSFP Dreiklang with decoupled switching mode revealed a different type of switching mechanism. The off-switching induces a disruption of the π-system by hydration of the imidazolinone ring, while a dehydration during on-switching reverses this effect [92, 128].

1.3.5 Application of RSFPs in RESOLFT microscopy

The first experimental demonstration of RESOLFT microscopy with RSFPs was shown in 2005 using purified asFP595 [17]. In 2011, the first application of RESOLFT microscopy in living cells was demonstrated using the green fluorescent and negative-switching rsEGFP in a point-scanning implementation [90]. In the point-scanning approach, the image is acquired by stepwise scanning and, at each position, a switching pulse scheme is applied (Figure 1.3-3). First, the RSFPs in the focal plane are switched on using a Gaussian beam of the on-switching wavelength. Subsequently, a doughnut-shaped beam with an intensity

zero in the center is applied which switches the RSFPs in the periphery off. Only the RSFPs in the center stay in the on-state. The fluorescence readout is performed by a Gaussian beam for excitation. The pulse scheme is repeated at the next scanning positions and the RESOLFT image is composed of the fluorescence signals at each position.

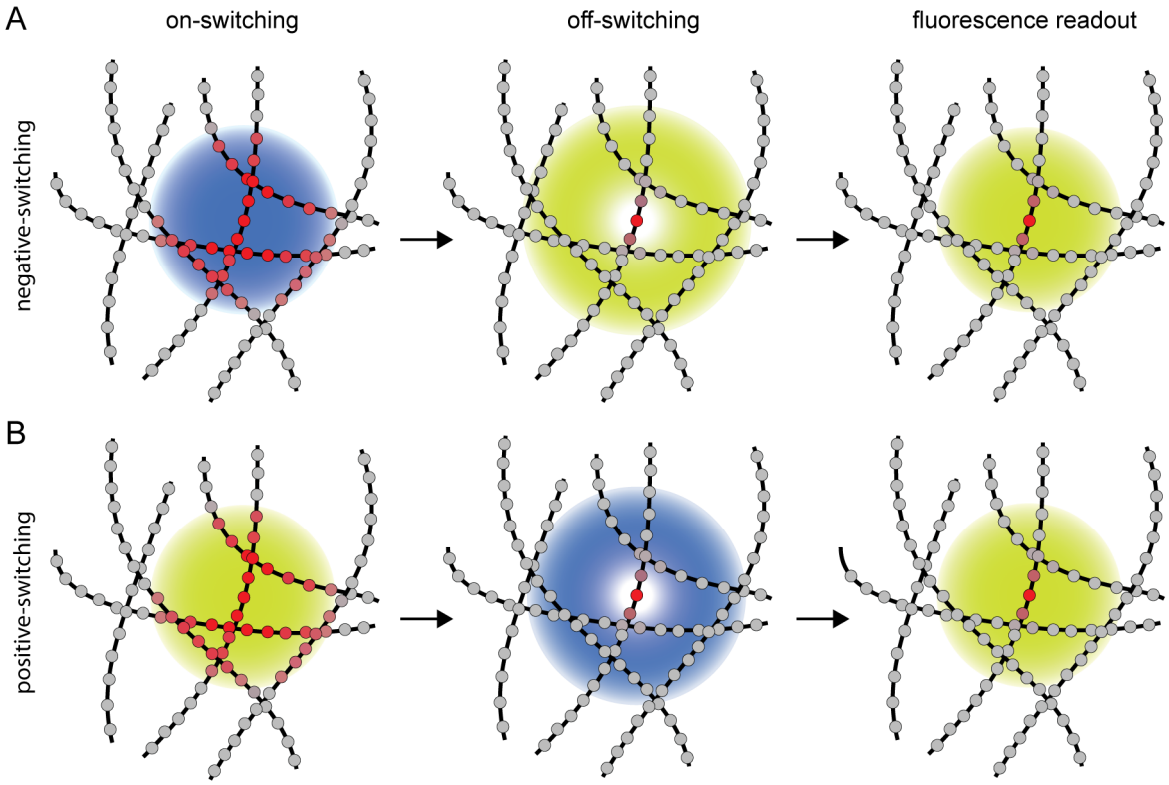

Figure 1.3-3: Point-scanning RESOLFT using negative- or positive-switching RSFPs.
Point-scanning RESOLFT schemes for red RSFPs with negative-switching (A) or positive-switching mode (B) at a single position. First, the RSFPs are switched to the on-state using a Gaussian beam of the on-switching wavelength (left). Next, the RSFPs in the periphery are switched to the off-state using a doughnut-shaped beam of the respective off-switching wavelength (middle). The RSFPs in the center remain in the on-state. Finally, the fluorescence signal of RSFPs in the on-state is readout. The same switching scheme is then applied at the next scanning position. The final RESOLFT image arises from the pixel-by-pixel scanning of the field of interest.

The acquisition times in point-scanning RESOLFT are highly dependent on the switching speed of the RSFPs, since the on- and off-switching are more time-consuming than the fluorescence readout [90, 96, 98]. In order to reduce the imaging times, several parallelized RESOLFT schemes were developed. In these approaches, arrays of intensity zeros are applied to simultaneous facilitate sub-diffraction fluorescence readout at different positions. The on-switching and readout is implemented by wide-field illumination [129, 130] or by individual foci [131]. In the alternative smart-scanning concept, the imaging time and the applied light dose in point-scanning RSOLFT are reduced as a result that the

switching scheme is only applied at those positions with a fluorescence signal higher than a certain threshold [132].

The green RSFP rsEGFP2 is characterized by a low switching fatigue [96] and was applied in multiple RESOLFT implementations. This includes RESOLFT microscopy of endogenous proteins tagged with rsEGFP2 in mammalian cells [97] and rsEGFP2-α-tubulin expressed in tissue and larvae of *Drosophila melanogaster* [133]. These experiments demonstrated the suitability of RESOLFT microscopy, in particular with rsEGFP2, for live-cells and tissue.

The applicability in RESOLFT imaging was as well shown for other green RSFPs with negative-switching mode [102-104, 111, 134] and for the yellow fluorescent protein Dreiklang with decoupled switching [92, 135]. So far, the application of a positive-switching RSFP is restricted to a single demonstration using the green fluorescent Kohinoor [100]. At the beginning of this work, rsCherryRev1.4 was the only red RSFP which was applicable in live-cell RESOLFT microscopy despite its dimerization tendency [98, 130]. In 2018, parallelized live-cell RESOLFT microscopy with the red fluorescent rsFusionRed2 and rsFusionRed3 was reported [118].

Dual channel RESOLFT implementations were based on the different characteristics of specific RSFPs. On the one hand, different switching kinetics and fluorescence lifetimes of two RSFPs were utilized [136]. On the other hand, the different spectral characteristics of the red fluorescent rsCherryRev1.4 and the green fluorescent rsEGFP2 [98] or the yellow fluorescent Dreiklang [130] was exploited. However, dual color RESOLFT microscopy is limited due to the low number of available red RSFPs with suitable characteristics. Thus, the demand for novel red RSFPs with superior switching characteristics is still high.

1.4 Screening of fluorescent proteins and RSFPs

1.4.1 Realized screenings for fluorescent proteins

The large palette of available GFP-like fluorescent proteins including RSFPs were to a large extent generated by protein engineering (see chapter 1.2.3 and 1.3.3). Protein engineering commonly involves the production of mutant libraries, for instance by *in vitro* mutagenesis at selected or random positions. Most mutant libraries were expressed in *Escherichia coli* (*E. coli*) cells, either in liquid cultures or in colonies on agar plates [35, 84]. Subsequently, single mutants were characterized or, in most cases, the mutant libraries were screened. The

chosen screening approach is dependent on the size of the library and the characteristics to be analyzed. The screenings for fluorescent proteins with enhanced brightness, folding or maturation were usually implemented by fluorescence analysis of the transformed *E. coli* cells in flow cytometry or by fluorescence readout of the expressing *E. coli* colonies [32, 54, 58, 76, 85, 137]. Further screening approaches analyzed other characteristics like the fluorescence lifetime, photostability or spectral shifts [35]. The identification of new and improved RSFPs was mostly achieved by on- and off-switching of the proteins expressed in bacterial colonies using a microscope followed by the analysis of the acquired switching data [92, 96, 98, 100, 118]. While the flow cytometry analysis of single cells allows for high throughput, a microscopic screening provides more information and allows the readout of various characteristics at the same time.

The conditions in a cell and the expression differ between mammalian and bacterial cells. Therefore, the effective cellular brightness and other characteristics of fluorescent proteins can also vary in different cell types. Since multiple applications of fluorescent proteins are carried out in eukaryotic cells, the screening of mutant libraries expressed in mammalian cells is preferable [84]. However, the implementation is not practicable by simple transfection of mammalian cells with a mutant library for transient expression. In contrast to the transformation of *E. coli* cells, the transient transfection of mammalian cells yields the uptake and expression of hundreds to thousands of plasmids. For this reason, the transfection of a plasmid library results in the expression of different variants per cell which does not allow to trace changes back to a single mutant.

To date, the realized screenings of fluorescent proteins based on the expression in mammalian cells are limited. For example, the fluorescent proteins mRaspberry and mPlum exhibit bathochromic shifted excitation or emission spectra compared to their template mRFP1.2 and were generated using the B lymphocyte cell line Ramos. The coding sequence of mRFP1.2 was stably introduced to these cells by retroviral infection and the fluorescent protein was mutated *in vivo* utilizing the cell type specific somatic hypermutation [138]. Thus, this approach is restricted to random-mutagenesis. However, the option for rational choice of mutation sites and site-directed mutagenesis is desirable, since this strategy can drastically reduce the size of the library to be screened.

In another approach, mutagenic libraries were generated *in vitro* and were then stably integrated into the genome of mammalian cells using retroviruses. This strategy was applied in the development of the fluorescent protein Kriek which is characterized by a higher photostability compared to its progenitor mCherry [139]. Even if the multiplicity of

infection is kept low, the application of viruses bear the risk of multiple transgene integrations per cell [84]. In addition, the transgene is randomly integrated into the genome in this approach, but the expression of all variants from the same genomic context would be beneficial for the comparison [140]. Due to these disadvantages of the viral approaches, conceivable options for the screenings of mutant libraries exploiting the eukaryotic expression machinery are discussed in the following.

1.4.2 Options for expression of a single fluorescent protein per cell

A perquisite for the screening of fluorescent proteins in mammalian cells is the expression of a single variant from a mutant library per cell. Since this is not feasible by simple transfection of a mutant library, a suitable approach might be the stable integration of a single mutant into the genome of each mammalian cell. Preferably, all variants are expressed from the same genomic locus to avoid effects of the integration sites on the expression [140].

Genome editing using zink finger nucleases [141], transcription activator-like effector nucleases [142] or clustered regularly interspaced short palindromic repeat (CRISPR)/Cas9 [143, 144] allow the knock-in of transgenes to a targeted genomic site. Nevertheless, more than one integration per cell is possible in these methods depending on the copy number of the locus in the genome. Furthermore, the shown off-target effects render these methods inappropriate for screening approaches [145, 146].

The site-specific recombinase techniques are an alternative concept for stable integration of single transgenes into the same genomic context of different cells [147, 148]. In one of these strategies, a single recombinase attachment site is placed in the mammalian host genome using a genome engineering method. A plasmid containing the complementary attachment site can be integrated into the placed attachment site by recombination. The recombination is catalyzed efficiently and precise by a site-specific recombinase [149, 150].

The phage Bxb1 recombinase is such a site-specific recombinase. It is part of the serine recombinase family and mediates the unidirectional recombination of the specific attachment sites Bxb1 attB (38 bp) and Bxb1 attP (52 bp) [147]. It was shown to be the most efficient and accurate out of 15 recombinases in mammalian cells [151]. The application of the Bxb1 recombinase and attachment sites for the stable integration of a transgene into the genome of mammalian cells was successfully demonstrated [152].

Previously, Duportet *et al*. generated Bxb1 landing pad cell lines which contained a single landing pad composed of an upstream CAG promotor and a Bxb1 attP attachment site [140]. These Bxb1 landing pad cells were applied for the stable integration and expression

of multi-gene vectors. A monoclonal Bxb1 landing pad cell line with a single landing pad has the advantage that only a single plasmid can be integrated in the respective cell. At the beginning of this work, a Bxb1 landing pad cell line had not been exploited for the screening of fluorescent proteins.

1.5 Aim of the study

RESOLFT microscopy with RSFPs enables diffraction-unlimited imaging with live-cell compatible light doses. While multiple green RSFPs with suitable characteristics for RESOLFT microscopy exist, the number of red RSFPs is still limited. The molecular brightness of the available red RSFPs is low and most of them exhibit undesirable characteristics (chapter 1.3.3.2). However, RESOLFT microscopy with red RSFPs benefits from the longer switching and fluorescence excitations wavelengths. In addition, red RSFPs can be combined with green RSFPs for dual color imaging. Thus, this work aimed to develop new red RSFPs with superior switching characteristics and higher molecular and cellular brightness than the available red RSFPs.

To facilitate the development of novel red RSFPs with optimized characteristics, screening systems had to be adapted and new screening approaches needed to be developed. This includes the generation of a mammalian Bxb1 landing pad cell line to enable the expression of a single variant from a mutant library per cell. The second part of this work covers the development of novel red RSFPs with positive- and negative-switching mode utilizing site-directed and random mutagenesis in combination with the established screening strategies. Moreover, a detailed characterization of the generated red RSFPs could examine their potential for live-cell RESOLFT microscopy.

2 Materials and methods

All chemical components and reagents used in this work were obtained from Sigma-Aldrich (St. Louis, MO, USA), Merck (Darmstadt, Germany), PanReac Applichem (Darmstadt, Germany), SERVA (Heidelberg, Germany) and VWR (Radnor, PA, USA) unless otherwise indicated.

2.1 Molecular biology methods

2.1.1 Isolation of plasmid DNA from bacterial cultures

Plasmid DNA was isolated from 5 ml or 50 ml *E. coli* cultures using the QIAprep Spin Miniprep Kit or QIAGEN Plasmid Plus Midi Kit (QIAGEN, Hilden, Germany). DNA isolation was performed according to the manufacturer's protocol. DNA concentrations were determined using the NanoDrop1000 Spectrophotometer (Thermo Fisher Scientific, Waltham, MA, USA).

2.1.2 Polymerase chain reaction for cloning and genotyping

Polymerase chain reaction (PCR) [153] was applied to amplify DNA fragments. For cloning of DNA constructs, DNA fragments were either amplified using the *Pfu* or Q5 DNA Polymerase. For genotyping of monoclonal cell lines, PCR reactions were performed on genomic DNA using the Q5 DNA Polymerase protocol. In addition, PCR reactions were conducted for the purpose of mutagenesis as described in chapter 2.1.10.

2.1.2.1 DNA amplification using *Pfu* DNA polymerase

In PCR reactions with the *Pfu* DNA polymerase (2.5 U/µl; biotechrabbit, Hennigsdorf, Germany), the used 10x PCR buffer contained 100 mM Tris-HCl (pH 8.3), 500 mM KCl and 25 mM $MgCl_2$. The deoxyribonucleotide triphosphate (dNTP) stock solution was composed of 10 mM of each dNTP (dATP, dGTP, dCTP, dTTP; Thermo Fisher Scientific, Waltham, MA, USA). The PCR reactions were prepared as described in the following:

50-100 ng template DNA
1 µl sense primer (10 µM)
1 µl antisense primer (10 µM)
5 µl 10x PCR buffer
2 µl dNTP stock solution (10 mM each)
1 µl *Pfu* DNA polymerase
filled up to 50 µl with H_2O

The PCR was carried out with a T-Personal Thermal Cycler (Biometra, Göttingen, Germany) using the following protocol:

Temperature	Time	
94 °C	5 min	
94 °C	1 min	30x
55 °C	1 min	
72 °C	2 min/1 kb	
72 °C	10 min	

2.1.2.2 DNA amplification using Q5 DNA polymerase

For amplification of DNA fragments with the Q5 High-Fidelity DNA Polymerase (2 U/µl; NEB, Ipswich, MA, USA), 5x Q5 Reaction Buffer (NEB, Ipswich, MA, USA) and dNTP stock solution with 10 mM of each dNTP (dATP, dGTP, dCTP, dTTP) were used. The PCR reactions with Q5 DNA Polymerase were prepared according to the following protocol:

50-100 ng plasmid DNA or 150 ng genomic DNA (template)
2.5 µl sense primer (10 µM)
2.5 µl antisense primer (10 µM)
10 µl 5x Q5 Reaction Buffer
1 µl dNTP stock solution (10 mM each)
0.5 µl Q5 DNA Polymerase
filled up to 50 µl with H_2O

The PCR was conducted using the following protocol:

Temperature	Time	
98 °C	2-5 min	
98 °C	20 s	30 x
60-70 °C	20 s	
72 °C	30 s/1 kb	
72 °C	5 min	

2.1.3 Agarose gel electrophoresis

Agarose gels for analysis or purification of DNA fragments were prepared by boiling 1.2 % (w/v) agarose in 1x TAE buffer (40 mM Tris, 20 mM sodium acetate, 1 mM EDTA, set to pH 7.2). The dissolved agarose solution was poured into gel chambers for analytical or preparative gels. The PCR reactions were mixed in the ratio 5:1 with 6x DNA loading buffer (6x TAE buffer, 30 % (v/v) glycerol, 0.15 % (w/v) bromophenol blue, 0.15 % xylene cyanol FF) and were loaded to the gels together with 5 µl GeneRuler 1 kb Ladder (Thermo Fisher Scientific, Waltham, MA, USA). Electrophoresis was carried out in 1x TAE buffer at 70-80 V for 45-50 min. The gel was stained in ethidium bromide solution for 10 min (analytical gels) or 30 min (preparative gels). DNA bands were visualized and documented with the gel documentation system Gel Jet Imager (INTAS Science Imaging Instruments, Göttingen, Germany).

2.1.4 Purification of DNA fragments

PCR products and digested DNA fragments were either purified using the QIAquick PCR Purification Kit (QIAGEN, Hilden, Germany) or with a preparative gel electrophoresis followed by gel extraction using the NucleoSpin Gel and PCR Clean-up Kit (MACHEREY-NAGEL, Düren, Germany). Both kits were applied according to the respective kit instructions.

2.1.5 Restriction

DNA plasmids and purified PCR products were digested with respective enzymes for cloning. 2-3 µg plasmid DNA or the whole purified PCR reaction were mixed with 1 µl of each restriction enzyme (10 U/µl; Thermo Fisher Scientific, Waltham, MA, USA), 4 µl of a suitable restriction buffer (NEBuffer 2, NEB, Ipswich, MA, USA; Buffer O, Thermo Fisher Scientific, Waltham, MA, USA) and, if not contained in the restriction buffer, 4 µl bovine serum albumin (BSA).The mixture was filled up to 40 µl with H_2O and incubated at 37 °C for 2 h. In case of the plasmid backbone DNA, 1 µl FastAP Thermosensitive Alkaline Phosphatase (1 U/µl; Thermo Fisher Scientific, Waltham, MA, USA) was subsequently added to the restriction reactions for dephosphorylation. These mixtures were incubated at 37 °C for further 30 min. All reactions were inactivated at 65 °C for 5-10 min. While linearized plasmids were purified by gel extraction, digested PCR products were purified with the QIAquick PCR purification kit.

2.1.6 Assembly of DNA fragments

2.1.6.1 Ligation of DNA fragments using T4 DNA ligase

For ligation, the restricted and dephosphorylated plasmid backbone and the digested insert DNA fragment were mixed in a 1:3 ratio (20-30 fmol backbone, 60-90 fmol insert). 2 µl T4 DNA ligase buffer (10x) and 1 µl T4 DNA ligase (5 U/µl; Thermo Fisher Scientific, Waltham, MA, USA) were added and the mixture was filled up to 20 µl with H_2O. The ligation mixture was incubated at room temperature for 1 h and subsequently inactivated at 65 °C for 10 min.

2.1.6.2 Gibson Assembly of DNA fragments

For Gibson Assembly [154] of DNA fragments, 1 µl *Dpn*I was added to the PCR reactions prior to the purification in order to digest the methylated template DNA (incubation: at 37 °C for 1 h). The linearized and purified plasmid backbone was mixed with the purified DNA insert in the ratio 1:2 (20-30 fmol backbone, 40-60 fmol insert). 10 µl Gibson Assembly Master Mix (2x; NEB, Ipswich, MA, USA) was added and the reactions were filled up to 20 µl with H_2O. Samples were incubated in a thermal cycler at 50 °C for 40 min.

2.1.7 Dialysis of DNA

The mutagenesis, ligation and Gibson Assembly reactions were dialyzed prior to the transformation of *E. coli*. Therefore, samples were dialyzed on 0.025 µm membrane filters (MF Millipore; Merck Millipore, Darmstadt, Germany) floating on H_2O for 30-40 min.

2.1.8 Sequencing

Plasmid DNA and PCR fragments were sequenced by the company Microsynth Seqlab (Balgach, Switzerland) in Göttingen. For sequencing of plasmid DNA, 0.7 to 1.2 µg DNA were provided in 12 µl H_2O. 3 µl of a suitable primer (10 µM) were added. For sequencing of PCR fragments, the PCR products were purified using the QIAGEN PCR Purification kit and 18 ng DNA per 100 bp were provided in 12 µl H_2O with the addition of 3 µl primer.

2.1.9 Cloning

All clonings conducted in this work were controlled by sequencing. DNA maps in the appendix were created using SnapGene (GSL Biotech LLC, Chicago, IL, USA).

2.1.9.1 Cloning of pBad plasmids for cytosolic expression in *E. coli*

The pBad/His B plasmid was chosen as the expression vector for the cytosolic expression of fluorescent proteins with an N-terminal poly-histidine tag in bacteria. The plasmid pBad-mKalama1 [155] was provided by Robert Campbell (Addgene plasmid #14892; Addgene, MA, USA) and served as backbone by replacing the mKalama1 gene with the coding sequence of the red fluorescent proteins. The pBad plasmid was linearized using *Xho*I and *Eco*RI. The *Pfu* DNA polymerase was used for amplification of the fluorescent protein genes with addition of *Xho*I and *Eco*RI restriction sites (all primers for pBad cloning: see Appendix Table 8). The coding sequence of the fluorescent protein mScarlet was amplified from the plasmid pmScarlet_Giantin_C1 [85] (gift from Dorus Gadella; Addgene plasmid #85048), the mRuby2 gene [57] was amplified from the plasmid pcDNA3.1-Clover-mRuby2 (gift from Kurt Beam, Addgene plasmid #49089) and the FusionRed gene was amplified from the plasmid FusionRed-pBAD [76] (this plasmid differs from the pBad-plasmid used in this work; gift from Michael Davidson, Addgene plasmid #54677). The coding sequences of the RSFPs rsFusionRed2 and rsFusionRed3 were amplified from the plasmids rsFusionRed2-pBAD and rsFusionRed2-pBAD, which were generated by introduction of the published mutations [118] into the plasmid FusionRed-pBAD using site-directed mutagenesis (carried out by Nickels Jensen). The coding sequence of rsCherry [91] was amplified from the plasmid pQE31-rsCherry (laboratory of Prof. Stefan Jakobs, lab ID: P559), the coding sequence of mCherry [58] from plasmid pRSET B-mCherry (gift of Prof. Roger Y. Tsien), the coding sequence of dTomato [58] from plasmid pRSETB-dTomato (gift of Prof. Roger Y. Tsien) and the coding sequence of DsRed [25] from plasmid DsRed1-N1-pRSETA [156]. The PCR products were cloned into the pBad/His B backbone using *Xho*I and *Eco*RI restriction sites and ligation.

2.1.9.2 Cloning of Bxb1 landing pad donor plasmid

A monoclonal Bxb1 landing pad cell line for screening and characterization of fluorescent proteins in mammalian cells was established in this work. The design of the landing pad of Duportet *et al*. [140] was taken as template to some extent to design a Bxb1 attP landing pad suitable for screening. Two Bxb1 landing pad donor plasmids were cloned for CRISPR/Cas9 genome editing of mammalian cells [144, 157]. In addition to the landing pad, the first donor plasmid contains a *cytomegalovirus (*CMV) promotor and a Bxb1 recombinase gene for stable expression of the recombinase. The CRISPR/Cas9 approach using this donor plasmid did not yield positive monoclonal clones, with the result that this experiment is not part of this work. However, this donor plasmid was used for cloning of the second landing

pad donor plasmid. Thus, the cloning of the first donor plasmid is also explained in the following.

The two Bxb1 landing pad donor plasmids were cloned in several consecutive steps. All PCR reactions were performed with the Q5 DNA polymerase. All primers used are listed in Appendix Table 9. A scaffold for the designed landing pad was obtained by gene synthesis (sequence: Appendix I; Genscript, Piscataway, NJ, USA). The plasmid pTRE-TIGHT-EGPF [158] (provided by Rudolf Jaenisch, Addgene plasmid #22074), which contains the homology arms for the adeno-associated virus integration site 1 (AAVS1), served as the vector backbone (from the right homology arm to the bGH PolyA signal). In order to clone the landing pad scaffold into the donor plasmid backbone, primers were designed using the NEBuilder Assembly Tool v2.2 (NEB, Ipswich, MA, USA). The two DNA fragments amplified with these primers were assembled by Gibson Assembly.

Next, the CMV promotor for the expression of the Bxb1 recombinase was cloned into the generated plasmid. For this purpose, the CMV promotor was amplified from the plasmid pmKate21-vimentin (Evrogen #FP318; Evrogen, Moscow, Russia) and cloned into the donor plasmid backbone using *Afl*II and *Pac*I restriction and subsequent ligation. The plasmid thus obtained was used as backbone for the next cloning step. The CAG promotor for the landing pad was amplified from the plasmid pCAGEN [159] (gift from Connie Cepko; Addgene plasmid #11160). The plasmid pCAGEN was restricted with *EcoR*I and *Sal*I prior to the PCR reaction for higher product yields of this GC-rich promoter. In addition, 0.8 M Betaine (5 M stock solution, Sigma-Adrich, St. Louis, MO, USA) and 5 % DMSO were added to this PCR reaction. The PCR product was cloned into the *Mlu*I and *Sal*I sites of the donor plasmid using restriction and ligation (plasmid map: see Appendix Figure 6.1-1). To obtain the final Bxb1 landing pad donor plasmid used in this work, the CMV-Bxb1 recombinase-SV40 polyA element was removed by restriction with *Age*I and subsequent religation with the T4 DNA ligase (plasmid map: see Appendix Figure 6.1-2).

2.1.9.3 Cloning of integration plasmids for the Bxb1 landing pad cell line

To enable stable expression of transgenes in the generated Bxb1 landing pad cells, a basic integration plasmid was designed and cloned which contains the Bxb1 attB site and a small multiple cloning site (MCS). The MCS was intended for the incorporation of fluorescent protein genes or fusion constructs. In addition, a C-terminal element composed of a *porcine teschovirus*-1 2A self-cleaving peptide sequence (P2A) and a Hygromycin resistance gene was included in the basic integration plasmid, which facilitates the selection of genomic modified cells after successful integration by the Bxb1 recombinase. This basic integration

plasmid pInt-MCS-P2A-HygroR was assembled by two DNA fragments. The first DNA fragment was received by gene synthesis (sequence: Appendix II; Genscript, Piscataway NJ, USA). For the second fragment, the backbone of the plasmid pmKate2-vimentin (Evrogen #FP318) without CMV promotor was amplified by PCR using the Q5 Polymerase protocol (all primers: see Appendix Table 10). The two DNA fragments were assembled using *Nhe*I and *Xho*I restriction and subsequent ligation (plasmid map: see Appendix Figure 6.1-3).

The generated plasmid pInt-MCS-P2A-HygroR was then used to generate a series of integration plasmids for stable expression of different transgenes and fusion constructs. The Hygromycin resistance gene was replaced by either the coding sequence of mEGFP or the coding sequence of mCherry using *Sac*I and *Xma*I restriction. For this purpose, the coding sequence of mEGFP [105] was amplified from the plasmid pQE31-mEGFP [160] (provided by Tim Grotjohann; lab ID: P640) and the coding sequence of mCherry was amplified from the plasmid pBad-mCherry (see chapter 2.1.9.1). Restriction and ligation into the linearized vector resulted in the plasmids pInt-MCS-P2A-mEGFP and pInt-MCS-P2A-mCherry. In addition, the coding sequence of mEGFP with altered codon usage at the N- and C-terminal ends (codEGFP) was cloned alike into the integration plasmid using a different primer combination (see Appendix Table 10). The resulting plasmid pInt-MCS-P2A-codEGFP simplifies the screening procedure, as some fluorescent proteins have the same N- and C-terminal ends as mEGFP. An integration plasmid without any C-terminal tag was cloned by amplifying the entire basic integration plasmid except for the P2A-HygroR element with the addition of *Bam*HI restriction sites to both DNA ends. The *Bam*HI restriction of the PCR product and religation yielded the plasmid pInt-MCS.

For the stable expression of cytoskeletal fusion constructs in the Bxb1 landing pad cell line, the vimentin and keratin coding sequences were cloned into different integration plasmids. The vimentin gene was amplified from pmKate2-vimentin (Evrogen #FP318) and the keratin gene from pTagRFP-keratin (Evrogen #FP369). The coding sequences of the two cytoskeleton proteins were cloned into the integrations plasmids by *Kpn*I and *Xba*I restriction sites and ligation. An overview of the integration plasmids together with the lab IDs is given in Appendix Table 11.

For the characterization of the Bxb1 landing pad cell line, the coding sequences of mEGFP and mRuby2 were cloned into the MCS site of various integrations plasmids according to Table 1 (primer sequences are listed in Appendix Table 12). To screen for improved Ru63 variants in the Bxb1 landing pad cell line, the error-prone protocol described in

chapter 2.1.10.3 was applied. The error-prone Ru63 variants were then cloned into the plasmid pInt-MCS-P2A-mEGFP.

Table 1: Cloning of specific integration plasmids.
Primer sequences are listed in Appendix Table 12.

Construct	Amplicon	Primer (lab ID)		Restriction sites used
		forward	reverse	
pInt-mEGFP-P2A-HygroR	mEGFP	7596	7597	*Xba*I, *Bam*HI
pInt-mRuby2-P2A-HygroR	mRuby2	7598	7599	*Xba*I, *Bam*HI
pInt-mRuby2-P2A-mEGFP	mRuby2	7598	7599	*Xba*I, *Bam*HI
pInt-Keratin-mEGFP-P2A-HygroR	mEGFP	7761	8185	*HindIII EcoRI*
pInt-Vimentin-mEGFP-P2A-HygroR	mEGFP	7761	7597	*Hind*III, *Bam*HI
pInt-Keratin-mRuby2-P2A-mEGFP	mRuby2	7602	8186	*Hind*III, *Eco*RI
pInt-Keratin-Ru63-P2A-mEGFP	Ru63	7602	8186	*Hind*III, *Eco*RI

2.1.9.4 Cloning of fusion constructs for expression in mammalian cells

Various plasmids were cloned to control the correct expression and localization of RSFP fusion constructs in mammalian cells. Table 2 lists the generated expression plasmids along with the respective cloning details. The primer sequences of the corresponding primer numbers are listed in Appendix Table 13. All plasmids were cloned by exchanging the fluorescent protein genes in the available expression plasmids with the coding sequence of the intended red RSFP (FP in Table 2). In order to do this, the coding sequences of the RSFPs were amplified using the *Pfu* DNA polymerase PCR protocol. The PCR products were then cloned into the vector backbones using the stated restriction enzymes and DNA assembly method. As Sc10 and Sc21 contain an internal *Not*I restriction site, the Gibson Assembly method was applied for some of these constructs.

The plasmids pEGFP-Hist1H2BN (Homo sapiens histone 1, H2BN; lab ID: P766) and pmEGFP-PTS (peroxisomal targeting signal; lab ID: P1272) (both published in Kamper *et al*., 2018 [161]) were used as backbones for cloning of Histone1 and PTS fusion constructs. The plasmid Caveolin1-mEGFP-N (plasmid map: see Appendix Figure 6.1-4; lab ID: P1219) was cloned earlier in the research group of Prof. Stefan Jakobs and was available for cloning of Caveolin1 fusion constructs. The plasmid pcDNA3.1_Lifeact-EGFP was a gift of Carola Gregor (plasmid map: see Appendix Figure 6.1-5). In addition, the plasmids pTagRFP-keratin (Evrogen #FP369), pDsRed1-Mito (mitochondrial targeting sequence; #6928-1, Clontech, CA, USA, provided by Peter Lipp, UKS Homburg), pmKate2-vimentin (Evrogen #FP318) and pEF/myc/ER (endoplasmic reticulum signal; Invitrogen, Thermo Fisher Scientific, Waltham, MA, USA) were used as backbones for cloning.

For the comparison of the expression and maturation in mammalian cells, constructs of red RSFPs with a C-terminal P2A-mEGFP sequence were produced. The P2A-mEGFP served

as an internal expression reference. The plasmid mEGFP-N (lab ID: P1184) was cloned earlier in the research group of Prof. Stefan Jakobs (PCR on the mEGFP gene with primers TCCACCGGTCGCCACCATGGTGAGCAAGGGCGAGGAGCTGTTC, GTCGCGGCC-GCTACTTGTACAGCTCGTCCATGCCGAGAG, cloned into the backbone of TagRFP-N (Evrogen #FP142) using *Age*I, *Not*I restriction sites) and was chosen as vector backbone. The coding sequences of the red RSFPs were amplified with addition of the C-terminal P2A sequence. The PCR products were cloned into the mEGFP-N plasmid at the 5' end of the mEGFP gene (see Table 2).

Table 2: Cloning of mammalian expression vectors.
Primers, restrictions and DNA assembly methods for the respective fusion constructs are listed. FP: fluorescent protein. Primer sequences are listed in Appendix Table 13.

Fusion construct	Amplicon/FP	Primer (lab ID)		Restriction		DNA assembly method
		forward	reverse	PCR product	vector	
Caveolin1-FP	Sc21	4605	4604	/	*Age*I, *Not*I	Gibson Assembly
	Ru87	5532	4604	*Age*I, *Not*I	*Age*I, *Not*I	ligation
Keratin-FP	Sc21	7674	4604	/	*Kpn*I, *Not*I	Gibson Assembly
	Ru87	5532	4604	*Kpn*I, *Not*I	*Kpn*I, *Not*I	ligation
Lifeact-FP	Sc21	8723	8724	/	*Bam*HI, *Not*I	Gibson Assembly
	Ru87	8719	8720	*Bam*HI, *Not*I	*Bam*HI, *Not*I	ligation
Mito-FP	Sc21	4605	4604	/	*Age*I, *Not*I	Gibson Assembly
	Ru87	5532	4604	*Age*I, *Not*I	*Age*I, *Not*I	ligation
Vimentin-FP	Sc10; Sc21	7674	4604	*Bam*HI	*Bam*HI	Gibson Assembly
	Ru63; Ru85; Ru87	5532	4604	*Age*I, *Not*I	*Age*I, *Not*I	ligation
FP-ER	Sc10; Sc21	9244	9246	/	*Sal*I, *Not*I	Gibson Assembly
	Ru63; Ru85; Ru87	9245	9247	*Sal*I, *Not*I	*Sal*I, *Not*I	ligation
FP-Histone1	Sc10; Sc21	9243	9241	*Nhe*I, *Bgl*II	*Nhe*I, *Bgl*II	ligation
	Ru63; Ru85; Ru87	8640	9242	*Nhe*I, *Bgl*II	*Nhe*I, *Bgl*II	ligation
FP-PTS	Sc10; Sc21	9240	9241	*Nhe*I, *Bgl*II	*Nhe*I, *Bgl*II	ligation
	Ru63; Ru85; Ru87	8639	9242	*Nhe*I, *Bgl*II	*Nhe*I, *Bgl*II	ligation
FP-P2A-mEGFP	Sc10, Sc21	9411	9412	*Age*I, *EcoR*I	*Age*I, *EcoR*I	ligation
	rsFusionRed2; rsFusionRed3	9415	9416	*Age*I, *EcoR*I	*Age*I, *EcoR*I	ligation
pInt-Keratin-FP	Sc10; Sc21	8854	8855	*Hind*III, *Eco*RI	*Hind*III, *Eco*RI	ligation
	Ru63; Ru85; Ru87	7602	8439	*Hind*III, *Eco*RI	*Hind*III, *Eco*RI	ligation
Vimentin-FP-Donor	Sc10	9249	9250	/	*Not*I, *Nco*I	Gibson Assembly
	Ru87	8359	8360	*Not*I, *Nco*I	*Not*I, *Nco*I	ligation

The stable expression of cytoskeleton proteins tagged with the novel RSFPs was investigated in monoclonal cell lines. Hence, pInt-Keratin-FP constructs were generated (vector backbone: see chapter 2.1.9.3). In addition, donor plasmids were prepared for Sc10 and

Ru87 in order to tag the endogenous vimentin gene using CRISPR/Cas9 genome editing. For this, the plasmid pUC57-VIM-Dreiklang-Donor [162] (provided by Michael Ratz) was used as vector backbone as it contains the homology arms for integration of the fluorescent proteins at the 3' end of the endogenous vimentin gene.

2.1.10 Mutagenesis

For the development of novel red RSFPs, three different PCR-based mutagenesis strategies were applied to add specific or random mutations into the fluorescent protein template in the pBad vector. After each mutagenesis protocol, the plasmids containing the mutated fluorescent proteins were dialyzed and used for transformation of *E. coli* cells (see chapter 2.2.2). After one to two days of growth and expression at 37 °C, the agar plates were used for screening (see chapter 2.4.1). For the analysis of the amino acids and the mutation sites in the beta-barrel structures, available crystal structures of mRuby and mScarlet (PDB files 3U0N and 5LK4) were visualized in PyMOL Molecular Graphic System (version 1.8; Schrödinger, New York, NY, USA).

2.1.10.1 Site-directed mutagenesis

The site-directed mutagenesis based on the QuickChange™ protocol (Stratagene, La Jolla, CA USA) was applied to mutate one specific amino acid. The chosen amino acid was exchanged to a predetermined or to a random amino acid. Therefore, primers were designed, which were complementary to the template sequence except for the base triplet of the mutation site (primers: see Appendix Table 14). In addition to the introduction of a mutation, the conducted PCR reaction was used to amplify the entire plasmid. The 10x PCR buffer and dNTP stock solution mentioned in the PCR protocol for the *Pfu* DNA Polymerase (see chapter 2.1.2.1) were also used in this protocol:

200 ng template DNA
1 µl sense mutation primer (10 µM)
1 µl antisense mutation primer (10 µM)
5 µl 10x PCR buffer
1 µl dNTP stock solution (10 mM each)
1 µl *Pfu* DNA polymerase
filled up to 50 µl with H_2O

The following PCR protocol was applied:

Temperature	Time	
95 °C	30 s	
95 °C	1 min	16 x
55 °C	1 min	
68 °C	10 min	
68 °C	10 min	

Following the PCR reaction, the template DNA was removed by digestion with 1 µl *Dpn*I at 37 °C overnight.

2.1.10.2 Multiple-site mutagenesis

For mutagenesis of several specific amino acids in one PCR reaction, the protocol of the multiple-site mutagenesis of Sawano and Miyawaki [163] was chosen. This mutagenesis strategy is divided into two PCR reactions. In the first PCR, the mutated sense strand of the entire plasmid is synthesized by applying several 5' phosphorylated sense primer, which are complementary to the template except for the base triplet to be mutated (primers: see Appendix Table 14). The 10x *Taq* DNA ligase buffer and the *Taq* DNA ligase (40 U/µl; NEB, Ipswich, MA, USA) were added to ligate the synthesized DNA strands. The PCR reactions were prepared as described in the following:

200-400 ng template DNA
1.4 µl of each 5' phosphorylated sense mutation primer (10 µM)
2.5 µl 10x PCR buffer
2.5 µl 10x *Taq* DNA ligase buffer
1 µl dNTP stock solution (10 mM each)
1 µl *Pfu* DNA polymerase
0.5 µl *Taq* DNA ligase
filled up to 50 µl with H_2O

The first PCR was conducted using the following protocol:

Temperature	Time	
65 °C	5 min	
95 °C	2 min	
95 °C	30 s	18x
55 °C	30 s	
65 °C	10 min	
75 °C	7 min	

After this PCR reaction, 1 µl *Dpn*I and 1.5 µl of an antisense primer, binding the pBad-vector backbone, were added. The *Dpn*I digestion of the template DNA and the second PCR for the amplification of the antisense DNA strand were performed using the following protocol:

Temperature	Time	
37 °C	60 min	
95 °C	30 s	
95 °C	30 s	2x
55 °C	1 min	
70 °C	10 min	

2.1.10.3 Error-prone mutagenesis

Error-prone (ep) mutagenesis was used to insert a few random mutations into a fluorescent protein template. The PCR protocol of Leung *et al*. [164] served as basis for the applied protocol. In the ep PCR reaction, *Taq* DNA polymerase (GoTaq G2 DNA Polymerase, 40 U/µl; Promega, Madison, WI, USA) was used to amplify the fluorescent protein from the respective pBad plasmid. To obtain the desired mutation rate, $MnCl_2$ (10 mM stock solution) and an ep dNTP stock solution with unequal ratios of the dNTPs (2mM dATP, 2 mM dGTP, 10 mM dCTP, 10 mM dTTP; Thermo Fisher Scientific, Waltham, MA, USA) were added to the PCR reactions. The 10x ep PCR buffer contained 100 mM Tris-HCl (pH 8.3), 500 mM KCl, 70 mM $MgCl_2$ and 0.1 % (w/v) gelatin (from bovine skin, type B; Sigma-Adrich, St. Louis, MO, USA). Primers used for cloning of mRuby2 and mScarlet into the pBad vector (see Appendix Table 8) were also used in the ep PCR reactions:

1 µg template DNA
10 µl sense primer (10 µM)
10 µl antisense primer (10 µM)
10 µl 10x ep PCR buffer
10 µl 10x ep dNTP stock solution
1.5-2.5 µl $MnCl_2$ (10 mM)
2 µl *Taq* DNA polymerase
filled up to 100 µl with H_2O

Each 100 µl PCR reaction was divided into four PCR reaction tubes, which were incubated using the following PCR program:

Temperature	Time	
95 °C	1 min	
95 °C	30 s	30x
55 °C	45 s	
72 °C	1 min 30 s	
72 °C	2 min	

After the ep PCR reaction, the divided reactions were pooled again. The PCR fragments were purified using gel extraction and cloned into the pBad-backbone using the *Eco*RI and *Xho*I restrictions sites and ligation.

2.1.11 Genotyping of monoclonal cell lines

The genomic DNA from monoclonal cell line cultures was isolated using the GenElute Mammalian Genomic DNA Miniprep Kit (Sigma-Adrich, St. Louis, MO, USA) according to the manufacturer's protocol. Genomic DNA concentrations were determined with the NanoDrop1000 Spectrophotometer (Thermo Fisher Scientific, Waltham, MA, USA). To verify the appropriate genetic modification of the generated cell lines, the genomic DNA sequences to be examined were amplified in PCR reactions using the Q5 DNA polymerase (primers: see Appendix Table 15). The presence and size of the PCR products were controlled in analytical agarose gels. Additionally, PCR products were purified with the QIAquick PCR Purification Kit and sequenced using the primers of the PCR reaction.

2.2 Cell biological methods

2.2.1 *Escherichia coli* culture

The *E. coli* strain DH5α (MAX Efficiency DH5αF'IQ Competent Cells; Life Technologies, CA, USA) was used for cloning purposes and plasmid amplification, while the *E. coli* strain TOP10 (TOP10 Electrocomp Kits; Invitrogen, Waltham, MA, USA) was used for protein expression. *E. coli* cells were cultivated at 37 °C either in liquid lysogeny broth (LB) medium [165] composed of 0.5 % (w/v) yeast extract (PanReac Applichem, Darmstadt, Germany), 1 % (w/v) peptone (from Casein (pancreatic digest); PanReac Applichem, Darmstadt, Germany), 0.5 % (w/v) NaCl and 0.5 % 1N NaOH, or on agar plates (1.4 % (w/v) agar in LB medium). Agar plates were prepared in 9.2 cm round dishes or 12 x 12 cm square dishes. The growth medium was supplemented either with 50 µg/µl ampicillin or 50 µg/µl

kanamycin (both PanReac AppliChem, Darmstadt, Germany) for selection and with 0.02 % arabinose (Sigma-Adrich, St. Louis, MO, USA) for induction of protein expression.

2.2.2 Transformation of *E. coli*

E. coli cells were transformed using electroporation. Electro-competent *E. coli* strains were prepared by a modified protocol initially described by Dower *et al.* [166]. An overnight culture of the respective *E. coli* strain (DH5α, TOP10) was used to inoculate LB medium with a volume ratio of 1:100. The *E. coli* cells were cultured in LB medium at 37 °C to an optical density of 0.6-1 at the wavelength of 600 nm. Cells were then incubated on ice for 30 min and afterwards centrifuged at 4 °C and 4811x g for 15 min. The supernatant was discarded, the bacterial pellets were resuspended in 1:1 volume of chilled H_2O compared to the initial culture volume and again pelleted by centrifugation. The next washing step was performed with 1:2 volume of chilled H_2O. After another centrifugation step, the cells were washed in 1:50 volume of 10% (v/v) glycerol. The cells were pelleted by centrifugation and the supernatant was discarded. The cells were resuspended in 1:500 volume of 10 % (v/v) glycerol, aliquoted in 50 µl portions to 1.5 ml tubes, flash frozen in liquid nitrogen and stored at -80 °C.

For the transformation, electroporation cuvettes (2 mm gap size; cell projects, Harrietsham, United Kingdom) were chilled on ice. 50-150 µl ice-cold water were added to one tube of electro-competent *E. coli* cells. Cells were thawed on ice and carefully resuspended. 1 µl isolated plasmid DNA or 5 µl of the dialyzed reaction were pipetted into the cooled cuvette. 50 µl of the electro-competent bacteria solution were added and gently mixed. The *E. coli* cells were electroporated in the Bio-Rad Gene Pulser (Bio-Rad, Hercules, CA, USA) at 2.5 kV, 200 Ω and 25 µF. Immediately after electroporation, 1 ml LB medium was added to the cells. After resuspension, the cells were transferred to a 1.5 ml tube and incubated at 37 °C for 1 h while shaking.

For screening (chapter 2.4.1), cloning (chapter 2.1.9) and protein purification (chapter 2.3.1), the transformation reactions were plated on agar plates with a suitable antibiotic for selection and with 0.02 % arabinose in case of TOP10 cells. The plates were incubated for one to two days at 37 °C. For screening of RSFPs using the Bxb1 landing pad cell line, 700 µl of the transformation reaction were used for inoculation of 50 ml LB medium.

2.2.3 Mammalian cell culture

U2OS and HeLa cell lines as well as all generated monoclonal cell lines were cultivated in Dulbecco's Modified Eagle's Medium (DMEM) (with 4.5 g/L D-glucose, GlutaMAX, phenol red; Thermo Fisher Scientific, Waltham, MA, USA) supplemented with 10 % fetal bovine serum (FBS) (FBS Superior; Biochrom, Berlin, Germany), 1 mM sodium pyruvate (100 mM stock solution; Sigma-Aldrich, St. Louis, MO, USA), 100 U/ml penicillin and 100 µg/ml streptomycin (10,000 unit/ml, 10,000 µg/ml stock solution; Biochrom, Berlin, Germany). Cells were grown at 37 °C and 5 % CO_2 in well plates or T25 flasks (TC, Standard; Sarstedt, Nürnbrecht, Germany). For passaging of cells, the culture medium was removed and the cells were washed twice with warm phosphate buffered saline (PBS; 137 mM NaCl, 2.7 mM KCl, 10 mM Na_2HPO_4, 1.76 mM KH_2PO_4, set to pH 7.4). After removal of the PBS, the cells were covered with 0.05 % trypsin/0.02 % EDTA solution (10x stock solution; Biochrom, Berlin, Germany) and incubated at 37 °C until the cells were released from the well or flask bottom. The trypsin reaction was stopped by adding three- to four-fold volume of medium. Cells were seeded to a new flask or well.

For transfections and for imaging purposes, mammalian cells were seeded into 6-well plates either with circular cover glasses (diameter of 18 mm, No 1.5H; Marienfeld Superior, Lauda-Königshofen, Germany) for microscopy or without. Cells were transfected the next day (see chapter 2.2.4). Cover glasses with transfected cells or with cells of the generated monoclonal cell lines were mounted to microscope slides with cavities filled with 25 mM HEPES buffered DMEM without phenol red (Thermo Fisher Scientific, Waltham, MA, US).

2.2.4 Transfection of mammalian cells

For transfection of mammalian cells, 2-4 µg plasmid DNA were diluted in 400 µl serum- and antibiotic-free DMEM medium. 6 µl of the TurboFect Transfection Reagent (Thermo Fisher Scientific, Waltham, MA, USA) were added and reactions were vortexed for 15 s. After a short centrifugation, the transfection reactions were incubated at room temperature for 15 min and then added dropwise to the respective well. The cells were further incubated at 37 °C and 5 % CO_2. If cells were cultivated longer than one day after transfection, the medium was substituted the next day.

In order to stably integrate an integration plasmid into the Bxb1 attP site, cells of the Bxb1 landing pad cell line were cotransfected with 1 µg of the respective integration plasmid and 1 µg of the plasmid pCAG-NLS-HA-Bxb1 [167] (gift from Pawel Pelczar; Addgene plasmid

#51271). The plasmid pCAG-NLS-HA-Bxb1 enables transient expression of the Bxb1 recombinase with a nuclear localization signal.

For the tagging of an endogenous vimentin gene using CRISPR/Cas9 genome editing, U2OS cells were cotransfected with 2 µg of the respective vimentin-FP-donor plasmid (chapter 2.1.9.4) and 2 µg of the plasmid px330-VIM-gRNA1 [97, 162] (provided by Michael Ratz; lab ID: P2463) encoding the Cas9 protein and the gRNA GCGCAAGATAGATTTGGAAT. The transfection protocol for the generation of the Bxb1 landing pad cell line differed from this protocol (see chapter 2.2.4.1).

2.2.4.1 Transfection for the generation of Bxb1 landing pad cell lines

For the generation of the Bxb1 landing pad cell line using CRISPR/Cas9 genome engineering, HeLa cells were cotransfected with the Bxb1 landing pad donor plasmid (chapter 2.1.9.2) and the plasmid px458-AAVS1 gRNA2 (gift of Till Stephan; lab ID: P2120; backbone: pSpCas9(BB)-2A-GFP [143]), which encodes the Cas9 protein and the gRNA sequence TGTCCCTAGTGGCCCCACTG. 100 µl serum- and antibiotic-free DMEM medium were mixed with 1.2 µg of the px458-AAVS1 gRNA2 plasmid, 1.8 µg of the Bxb1 landing pad donor plasmid and 10.5 µl of the FuGENE HD Transfection Reagent (Promega, Madison, WI, USA). The mixture was vortexed for 1 min and incubated at room temperature for 20 min. After the incubation time, the complete transfection reaction was added dropwise to the respective well. Cells were further cultivated at 37 °C and 5 % CO_2. These transfected cells were selected using the antibiotic Puromycin (see chapter 2.2.5) prior to the single-cell sorting into 96 well plates (see chapter 2.2.6).

2.2.5 Antibiotic selection of cells

Antibiotic selection of genomic edited cells was realized by incubation in culture medium supplemented with 1.25 µg/ml Puromycin (10 mg/ml stock solution; Invivogen, San Diego, CA, USA) or 400 µg/ml Hygromycin B (50 mg/ml stock solution; Calbiochem, Darmstadt, Germany). After three to four days, the antibiotic medium was replaced by the standard cultivation medium. The Hygromycin B selection of K21 cells with positive integration was controlled in the Cytation 3 Cell Imaging Multi-Mode Reader (BioTek, Winooski, VT, USA) using the 465 nm LED.

2.2.6 Flow cytometry of mammalian cells

Flow cytometry was used for sorting of single mammalian cells into 96-well plates in order to generate monoclonal cell lines. Moreover, flow cytometry was applied for analysis of the expression and maturation of RSFPs in HeLa cells. For these experiments, a group-modified BD Influx cell sorter (BD Biosciences, Franklin Lakes, NJ, USA) was used. The mammalian cells were released from the flask or well bottoms with trypsin as described above (chapter 2.2.3). The released cells were centrifuged at 100x g. Afterwards, the cell pellets were resuspended in PBS. The PBS washing step was performed twice and subsequently cells were again resuspended in PBS. The cells were sorted and analyzed by using lasers at 488 nm (Genesis CX488; Coherent, Santa Clara, CA, USA) and 561 nm (Jive 75; Cobalt, Solna, Sweden) for excitation. The green fluorescence was detected in the range of 495-525 nm, while the two detection windows of 570-640 nm and above 645 nm (645 LP filter) were analyzed for red fluorescence.

2.2.7 Generation of monoclonal cell lines

After single-cell sorting into 96-well plates using the flow cytometer, cells were cultivated for 2-3 weeks. Cell colonies were then released from the 96-well plate bottom by removing the culture medium and adding 100 µl Accutase Cell Detachment Solution (Capricorn Scientific, Ebsdorfergrund, Germany). After 15 min of incubation at room temperature, cells were resuspended and transferred to a 24-well plate containing 1 ml culture medium per well. The monoclonal cell line cultures were further cultivated, characterized and positive clones were frozen for long-time storage (see chapter 2.2.8).

To screen for positive Bxb1 landing pad cell lines, a part of the cell clones were seeded in additional 24-well plates and cotransfected with pCAG-NLS-HA-Bxb1 and pInt-mEGFP-P2A-HygroR (chapter 2.2.4). Transfected cell clones were controlled for green fluorescence in the Cytation 3 Cell Imaging Multi-Mode Reader (BioTek, Winooski, VT, USA) using the 465 nm LED. For all other generated monoclonal cell lines, the stable transgene expression was directly controlled in confocal microscopy (see chapter 2.4.2). In addition, genotyping using PCR reactions (see chapter 2.1.11) was performed to control for the accurate genomic modification.

2.2.8 Freezing of mammalian cell lines

For long-time storage of the generated monoclonal cell lines, cells were released from the well or flask bottom using trypsin (chapter 2.2.3). After addition of cell culture medium, the

entire cell suspension of a 24-well or 1/3 cell suspension of a T25 flask were centrifuged at 100x g for 5 min. The cell pellets were resuspended in 1 ml freezing medium (DMEM supplemented with 20 % FBS, 10 % dimethyl sulfoxide (Hybri-Max; Sigma-Aldrich, St. Louis, MO, USA)) and transferred into a 1.8 ml cryo tube. The tube was immediately placed in a -80 °C freezer inside a freezing container. After at least 24 h, the cryo tube was transferred into a nitrogen tank for long-time storage.

2.3 Characterization of purified fluorescent proteins

2.3.1 Isolation of histidine-tagged fluorescent proteins

Solutions of purified fluorescent proteins were used to analyze the spectral characteristics, the pH stability and the oligomerization state of the RSFPs of interest (see chapters below). For protein purifications, the fluorescent proteins were expressed with an N-terminal poly-histidine tag from the respective pBad plasmid in TOP10 colonies grown on 12 x 12 cm square agar plates at 37 °C for two days (induction of the protein expression by arabinose). Two agar plates were used per fluorescent protein and per purification.

2.3.1.1 Isolation of switchable mScarlet variants and proteins for comparison

For the isolation of the switchable mScarlet variants and the fluorescent proteins for comparison, 2-3 ml binding buffer (20 mM sodium phosphate, 0.5 M NaCl, 20 mM imidazole, pH 7.4, prepared using the His Buffer Kit; GE Healthcare, Chicago, IL, USA) were added to each agar plate and the bacterial colonies were scraped up using cell scrapers (Blade 25; Sarstedt, Nürnbrecht, Germany). The bacteria were resuspended and 1.8-2 ml of the suspension were transferred to a 2 ml tube on ice. Lysozyme (SERVA, Heidelberg, Germany) (stock solution: 50 mg/ml) was added to a final concentration of 1 mg/ml for the lysis of the bacterial cells. After 3-4 h of incubation, 80 µl protease inhibitor were added (1 tablet solved in 2 ml H_2O, cOmplete, EDTA-free Protease Inhibitor Cocktail; Roche Diagnostics, Rotkreuz, Switzerland). The samples were frozen in liquid nitrogen and subsequently thawed in warm water. After five freeze-thaw cycles, 0.5 µl Benzonase nuclease (250 U/µl; Sigma-Aldrich, St. Louis, MO, USA) was added to each sample and incubated for 15 min. The samples were centrifuged at 16,200x g and 4 °C for 1.5-3 h to separate the protein solution from the cell fragments. The supernatant was transferred to a new 2 ml tube and stored at 4 °C. On the next day, the proteins were again centrifuged at 16,200x g and 4 °C for 0.5-2 h.

The histidine-tagged fluorescent proteins were isolated from other proteins by Ni-NTA affinity chromatography using the spin columns His SpinTrap (GE Healthcare, Chicago, IL, USA). Three spin columns were used per fluorescent protein. All centrifugation steps were carried out at 100x g for 1 min. The spin columns were washed with 600 µl binding buffer and the flow through was discarded. Up to 600 µl of the supernatant containing the fluorescent proteins were added to the spin columns and the columns were incubated on a rotator for 30 min. After the next centrifugation step, the remaining protein samples were added to the spin columns, again incubated on the rotator for 30 min and centrifuged. Subsequently, the spin columns were washed twice with 600 µl binding buffer and twice with 200 µl washing buffer (20 mM sodium phosphate, 0.5 M NaCl, 50 mM imidazole pH 7.4). For elution of the fluorescent proteins, 200 µl elution buffer (20 mM sodium phosphate, 0.5 M NaCl, 500 mM imidazole pH 7.4) were added to the columns and incubated for 5 min. After centrifugation, the elution step was repeated once or twice. Eluted samples of equal fluorescent proteins were united.

The purified protein samples were concentrated at 2700x g to a final volume of 150-400 µl using the Vivaspin Turbo 4 Ultrafiltration Units (10,000 MWCO; Sartorius, Göttingen, Germany). The buffer of the concentrated protein samples was exchanged using illustra NAP5 columns (Sephadex G-25; GE Healthcare, Chicago, IL, USA), which were equilibrated with protein buffer (100 mM Tris, 150 mM NaCl, set to pH 7.5). The protein samples were added to the NAP5 columns and when the samples had sunk, protein buffer was added again. Once the proteins eluted (visible by the color of the proteins), the protein solutions were collected.

2.3.1.2 Purification of switchable mRuby2 variants and reference proteins

Since the final switchable mRuby2 variants precipitated during the protein isolation protocol described in chapter 2.3.1.1, the protocol was adjusted for the isolation of these RSFPs and for the fluorescent proteins for comparison. The changes include the addition of 1 mM EDTA to the binding buffer. The *E. coli* colonies on the agar plates were scraped off as described in chapter 2.3.1.1 and incubated with 1 mg/ml lysozyme on ice for 2 h. After the addition of the protease inhibitor, cells were lysed by sonication (duty cycle 40, output control 4, 4x 15 s, 3 mm tip, Sonifier 450; Branson Ultrasonics, Danbury, CT, USA). The incubation with Benzonase at room temperature was followed by addition of DTT (1 M stock solution) to a final concentration of 1 mM. Cell fragments were separated by centrifugation at 16,200x g and 20 °C. The supernatants were stored covered at room temperature overnight.

For protein isolation and buffer exchange, 1 mM EDTA and 1 mM DTT were added to the binding, washing, elution and protein buffer. Apart from that, the proteins in the supernatant were isolated with His SpinTraps columns as described in chapter 2.3.1.1. The elution step was only performed twice. The eluted proteins were not concentrated, but immediately transferred into the protein buffer using the NAP5 columns as described above. Purified proteins were stored covered at room temperature and characterized within the next three days.

2.3.2 Determination of protein concentration

The protein concentration of isolated fluorescent protein samples was determined using the Bio-Rad Protein Assay (Bio-Rad, Hercules, CA, USA), which is based on the method of Bradford [168]. 1-3 µl protein sample were diluted in 800 µl H_2O and 200 µl Protein Assay Dye Reagent Concentrate (Bio-Rad, Hercules, CA, USA) was added. After 5 min of incubation, the absorbance at 600 nm was measured. The protein concentration was calculated using a BSA standard curve.

2.3.3 Sodium dodecyl sulfate polyacrylamide gel electrophoresis

The isolation of the fluorescent proteins was controlled by sodium dodecyl sulfate polyacrylamide gel electrophoresis (SDS-PAGE). The SDS gels were composed of a 5 % stacking gel and a 15 % separation gel. For two separation gels, the following components were mixed and poured into Mini-PROTEAN Tetra spacer plates (Bio-Rad, Hercules, CA, USA):

3.45 ml H_2O
3.75 ml separation gel buffer (1.5 mM Tris-HCl, pH 8.8)
7.5 ml 30 % (w/v) acrylamide / 0.8 % (w/v) biscarcylamide (Rotiphorese Gel 30; Carl Roth, Karlsruhe, Germany)
150 µl 10 % (w/v) SDS
150 µl 10 % (w/v) ammonium persulfate (APS)
15 µl tetramethylethylenediamine (TEMED)

The gel solutions were covered with water-saturated isopropanol. When the gels were completely polymerized, the isopropanol was discarded. The stacking gels were prepared as described in the following and poured onto the separation gel:

5.6 ml H_2O
2.5 ml stacking gel buffer (0.5 mM Tris-HCl pH 6.8)
1.7 ml 30 % (w/v) acrylamide / 0.8 % (w/v) biscarcylamide
100 µl 10 % (w/v) SDS
100 µl 10 % (w/v) APS
10 µl TEMED

A comb for 10 wells was inserted to prepare sample slots. 10 µl of the protein samples (0.2 µg/µl) were mixed with 2 µl of a 6x SDS loading buffer (0.35 M Tris-HCl pH 6.8, 10.28 % (w/v) SDS, 36 % (v/v) glycerol, 0.6 M DTT, 0.012 % (w/v) bromophenol blue) and boiled at 95 °C for 5 min. The protein samples and 5 µl of the size standards PageRuler Prestained Protein Ladder (Thermo Fisher Scientific, Waltham, MA, USA) were loaded to the 15 % SDS gels placed in the Mini-PROTEAN Tetra Cell system (Bio-Rad, Hercules, CA, USA). The proteins were separated in SDS running buffer (25 mM Tris-HCl pH 6.8, 192 mM glycerol, 0.1 % (w/v) SDS) at 20-40 mA.

The proteins in the SDS gels were stained in protein staining solution (0.05 % (w/v) Coomassie Brilliant Blue R-250, 25 % (v/v) isopropanol, 10 % (v/v) acetic acid) for 30 min. The stained gels were destained in 10 % (v/v) acetic acid and afterwards recorded in the Amersham Imager 600 (GE Healthcare, Chicago, IL, USA) in colorimetric epi-illumination mode.

2.3.4 Analytical size-exclusion chromatography

The oligomeric state of the fluorescent proteins was controlled by analytical size-exclusion chromatography in a Superdex 200 Increase 10/300 L column (GE Healthcare, Chicago, IL, USA) using the chromatography system ÄKTA pure (GE Healthcare, Chicago, IL, USA). The size-exclusion chromatography was conducted at 6 °C and at a constant flow rate of 0.75 ml/min (protein buffer, see chapter 2.3.1.1). 250 µl of the purified protein solutions diluted to 10 µM were applied to the column. The elution of proteins was detected by absorption measurements at 280 nm.

2.3.5 Measurement of absorption spectra

The absorption spectra of isolated protein samples were measured in a quartz cuvette with an optical path length of 1.5 mm (105-252-QS; Hellma, Müllheim, Germany) using the Cary 4000 UV VIS spectrophotometer (Varian, Palo Alto, CA, USA). The protein samples were diluted in protein buffer to an absorption of about 0.1 at 280 nm. For data analysis, baselines

were subtracted from the spectra. The corrected spectra were normalized to 280 nm peak absorbance and the spectra of replicates were averaged.

For the absorption spectra of on- and off-states, Sc10 and Sc21 were switched in a quartz cuvette with an optical path length of 1 mm (QS; Hellma, Müllheim, Germany) and subsequently spectra were recorded. The switching was performed by illumination of the protein samples with a fiber coupled mercury vapour lamp (Leica Microsystems, Wetzlar, Germany) for 1 min. For off-switching, a 550/40 nm band pass filter was used, while a 450/40 nm band pass filter was used for on-switching. The relaxation from the off-state to the equilibrium state was observed for Sc10 and Sc21 by repeated measurements without further illumination. The peak absorption of the deprotonated red chromophore at 570 nm was plotted against the time to determine the thermal relaxation kinetics and fitted by a monoexponential function using the iteration algorithm Levenberg Marquardt in OriginPro 2016 (OriginLab, Northampton, MA, USA).

2.3.6 Measurement of excitation and emission spectra

The excitation and emission spectra were recorded for the same protein samples used in the measurements of absorption spectra. Measurements were performed in the quartz cuvette with an optical path length of 1.5 mm (105-252-QS; Hellma, Müllheim, Germany) using the Cary Eclipse fluorescence spectrophotometer (Varian, Palo Alto, CA, USA). The slit size was set to 5 nm. For the spectra of mScarlet and the switchable mScarlet variants, the PMT voltage was set to 560-570 V, and for the spectra of mRuby2 and the switchable mRuby2 variants to 600 V. The excitation and emission spectra of replicates were averaged and normalized to the fluorescence maximum, respectively.

2.3.7 Determination of quantum yields and extinction coefficients

The quantum yield (QY) and the extinction coefficient (ε) were determined for the switchable mRuby2, mScarlet and FusionRed proteins. For this purpose, the absorption and emission spectra of the RSFP and of the respective reference protein were measured consecutively in the same cuvette, as described in chapter 2.3.5 and 2.3.6. The protein mRuby2 served as reference for Ru63, Ru85 and Ru87, mScarlet for Sc10 and Sc21 and FusionRed for rsFusionRed2 and rsFusionRed3. For Sc10 and Sc21, the QY and ε of the on-state (on-switching with band pass 450/40 nm: see chapter 2.3.5) was determined additionally to the QY and ε of the equilibrium state.

For the determination of ε, the absorption spectra were corrected and normalized to the absorption at 280 nm as described in chapter 2.3.5. As the extinction coefficient at 280 nm did not differ for the RSFPs and their respective reference protein, no further corrections were necessary. To calculate the ε, the ratio of the peak absorbance (deprotonated chromophore) of the RSFP to the peak absorbance of the reference protein was multiplied with the published ε of the reference protein.

For the relative determination of the QY, the integral of the emission spectrum was divided by the absorbance at the chosen excitation wavelength. The ratio of this value for the RSFP to the value for the respective reference protein was multiplied with the published QY of the reference protein to determine the QY of the RSFP (relative method). In addition, the absolute QY for Sc10 and Sc21 was measured using the quantum yield spectrometer Quantarus-QY Absolute PL (Hamamatsu Photonics, Hamamatsu, Japan). The protein concentrations were adopted to a maximal absorption of 0.1 at 540 nm by dilution with protein buffer. For Ru63, Ru85 and Ru87, the absolute QY was measured by Alexey I. Chizhik (Third Institute of Physics, Georg August University, Göttingen) using nanocavity-based fluorescence quantum yield measurements described in Chizhik *et al*., 2013 [169].

2.3.8 Measurement of the pH stability and pH-dependent absorption spectra

To investigate the influence of the pH on the absorption and fluorescence of the generated RSFPs, the purified fluorescent protein samples were diluted in buffers of different pH to an end concentration of 5 µM (dilution: 1:20 for Ru63, Ru85, Ru87; 1:40 for Sc10, Sc21). Each buffer contained 150 mM NaCl. Additionally, the buffers of pH 3 to 5.5 were composed of 100 mM citric acid, and the buffers of pH 6 to 7 of 100 mM KH_2PO_4. The buffers of pH 7.5 to 8.5 consisted of 100 mM Tris, and the buffers of pH 9 to 10 of 100 mM Glycin. The pH values were adjusted with 1 N NaOH or 1N HCl.

The absorption spectra and the fluorescence of the different pH samples (3 replicates each) were measured with respective blanks in 96-well plates (UV Star Microplate; Greiner Bio-One, Kremsmünster, Österreich) using the Cytation 3 Cell Imaging Multi-Mode Reader (BioTek, Winooski, VT, USA). For data anaylsis, the spectra of the respective blanks were subtracted first, then the baselines. The corrected absorption spectra of the replicates were averaged and normalized to the absorption at 280 nm. For the determination of the pK_a values, the fluorescence of the replicates were averaged, normalized to pH 9.5 and plotted against the pH values of the buffers. The curves were fitted to the function

$y = maxvalue/(1+(pH/pK_a)^{slope})$ [170] using the iteration algorithm Levenberg Marquardt in OriginPro 2016 (OriginLab, Northampton, MA, USA).

2.3.9 Determination of the fluorescence lifetimes

The fluorescence lifetimes of Sc10 and Sc21 was determined using the fluorescence lifetime spectrometer Quantaurus-Tau (Hamamatsu Photonics, Hamamatsu, Japan). 10,000 counts were acquired to obtain fluorescence decay curves of the purified Sc10 and Sc21 samples excited with the LED at 590 nm. The instrument response function was measured using 0.1 µm microspheres (Polybead Amino Microspheres 0.10µm; Polysciences, Warrington, PA, USA). The fluorescence decay curves were fitted with a 2nd order exponential fit to read out the average fluorescence lifetimes $<\tau>$. The fluorescence lifetimes of Ru63, Ru85 and Ru87 were measured and provided by Alexey I. Chizhik (see chapter 2.3.7).

2.4 Microscopy

2.4.1 Automated microscopy for screening and switching characterization

The screening for improved switchable fluorescent proteins and the switching characterization of RSFPs were performed with an automated microscope, which was constructed earlier within the research group. The automated microscope is based on a Leica DM5500 B upright microscope (Leica Microsystems, Wetzlar, Germany) equipped with a 20x/0.4 NA objective (N Plan; Leica Microsystems, Wetzlar, Germany). Four lasers with the wavelengths of 405 nm (MLD, 100 mW), 445 nm (MLD, 50 mW), 488 nm (MLD, 50 mW) and 561 nm (Jive, 50 mW) (all: Cobolt, Solna, Sweden) were used in this work. The beam splitter HC BS R561 and the bandpass filter 605/70 ET (AHF analysentechnik, Tübingen, Germany) were used to separate the excitation and emission light. The fluorescence signal was detected by a photomultiplier tube (Hamamatsu Photonics, Hamamatsu, Japan). The microscope was controlled by a custom-made software programmed within the group using the LabVIEW platform (National Instruments, Austin, TX, USA). The sample rate was set to 10-200 µs depending on the switching times. An autofocus using the 561 nm laser with an intensity of 1.9 kWcm^{-2} was applied before each measurement. All measurements were conducted at room temperature. The implementation of the screening and the characterization of RSFPs as well as the investigated switching parameters are described in the following.

2.4.1.1 Screening for new and improved red RSFPs

The mutant fluorescent protein libraries (see chapter 2.1.10) were expressed cytosolic in bacterial colonies on agar plates grown at 37 °C for two days. The screening for new and improved RSFPs was realized by direct movement to positions of selected colonies or by stepwise automated scanning for colonies. In the second approach, a short 561 nm laser pulse was applied at each position. Only if the fluorescence read-out was higher than a defined threshold, the switching scheme was applied. For switching, light of 561 nm (9.2-14.5 $kWcm^{-2}$) and 445 nm (2.5-14.9 $kWcm^{-2}$) was used alternating. The chosen switching scheme was adjusted to the switching characteristics of the template protein. The alternating irradiation at 445 nm (14.9 $kWcm^{-2}$) for 10 ms and at 561 nm (14.5 $kWcm^{-2}$) for 22 ms represents an exemplary switching scheme, which was applied for the screening of positive-switching RSFPs. The negative-switching RSFPs were switched for instance by alternating irradiation at 445 nm (2.5 $kWcm^{-2}$) for 20 ms and at 561 nm (14.5 $kWcm^{-2}$) for 170 ms.

The acquired switching data was analyzed in respect to the fluorescence signal in the on-state, the residual fluorescence in the off-state, the switching fatigue and the switching speed (see chapters 2.4.1.3-2.4.1.5). If switching curves with improved characteristics were obtained, the respective colony was picked and used for inoculation of an overnight culture (5 ml). Thereupon, the pBad plasmid with the RSFP variant was isolated (chapter 2.1.1) and the added mutations were analyzed by sequencing (chapter 2.1.8). New RSFP variants were characterized using the automated microscope and if appropriate, applied as templates for the next mutagenesis and screening round.

2.4.1.2 Switching characterization of new red RSFPs

The red RSFPs to be analyzed were as well expressed cytosolic from pBad plasmids in bacterial colonies on agar plates. For the detailed characterization of switching, the automated microscope was directed to selected bacterial colonies, where a suitable switching scheme was applied for the respective analysis. To compensate for variations caused by expression differences and technical fluctuations, the switching scheme was applied to 5 or 10 colonies at two or three different days each. An overview of the switching schemes and analysis are given in the following. The applied light intensities and switching times are given in the results part.

2.4.1.3 Effective cellular brightness in *E. coli* and off-state fluorescence

Both, novel RSFPs and mutant RSFP libraries were analyzed regarding their fluorescence signal in the on-state and the residual fluorescence in the off-state. To analyze these two

parameters, the positive-switching RSFPs were switched into the off-state at 445 nm and subsequently switched completely on at 561 nm. The effective ensemble brightness was read out by the fluorescence signal in the on-state. The residual fluorescence in the off-state was obtained by dividing the first measurement point of the on-switching curve by the averaged last 10 points. The negative-switching red RSFPs were first switched to the on-state at 445 nm and subsequently switched completely off at 561 nm. The first point of the off-switching curve was used to determine the effective ensemble brightness in the on-state. The averaged last 10 points of the off-switching curve was divided by the first point to obtain the residual fluorescence in the off-sate.

2.4.1.4 Switching kinetics

During screening for faster switching red RSFPs, the halftime of the 561 nm induced switching curves was roughly estimated using the custom-made screening software. For the final RSFP variants, the switching halftimes of the on- and off-switching were analyzed in more detail. To do this, the RSFPs were switched off (positive-switching) or on (negative-switching) with light of 445 nm and subsequently switching curves were acquired by irradiation with varying 561 nm laser intensities. These switching curves were fitted by a biexponential function (ExpDec2 or ExpGro2) using the iteration algorithm Levenberg Marquardt in OriginPro 2016 (OriginLab, Northampton, MA, USA). The switching halftimes for each 561 nm laser intensity was determined.

The switching of red RSFPs with light of 445 nm cannot be tracked due to insufficient fluorescence emission induced by this wavelength. However, to obtain switching curves of the 445 nm switching, the proteins were first completely switched on (positive-switching) or off (negative-switching) with light of 561 nm and then irradiated at 445 nm with varying switching times (0-500 ms). This was followed by a fluorescence readout using light of 561 nm. The ratio of the first readout signal to the fluorescence signal in the on-state was plotted against the 445 nm switching times. The resulting switching curves were then fitted and analyzed as described above. In addition, switching curves were acquired by simultaneous irradiation at 405 nm, 445 nm or 488 nm and at 561 nm. These curves were analyzed as well.

2.4.1.5 Switching fatigue

Another parameter analyzed in the screening and characterization is the switching fatigue of the RSFPs occurring through the destruction of the fluorescent proteins during repetitive switching. In the screening for improved RSFPs, all RSFP variants on the same agar plate

were repetitively switched with the same switching scheme. In the evaluation, the ratio of the on-state fluorescence signals in the first and in the last switching cycle was compared for all variants. The residual fluorescence in the off-state of the last switching cycle was additionally analyzed.

To compare the switching fatigue of the new developed RSFPs with the switching fatigue of published RSFPs, the fluorescent proteins were switched on and off for 250-500 switching cycles. The illumination duration were chosen on the basis that the RSFPs were switched on to 90 % (negative-switching) or 95 % (positive-switching) of the maximal fluorescence signal. The off-switching times were selected that each protein was switched off by 95 % of its potential off-switching range (1-0.95*(1–relative fluorescence in the off-state)).

To compare the switching fatigue for different switching wavelengths, a fixed switching scheme was applied for 100-250 switching cycles. All switching fatigue curves were normalized to the second switching cycle to exclude incomplete switching and altered bleaching behavior often found in the first switching cycle.

2.4.1.6 Equilibrium state and relaxation kinetics

The equilibrium state of the red RSFPs was determined by dividing the first fluorescence signal without previous irradiation except for the autofocus by the fluorescence signal in the on-state using the same 561 nm laser intensity. A break of 15 s was applied between the autofocus and the measurements.

For the final switchable mRuby2 variants, the thermal relaxation from the on- and off-state to the thermal equilibrium was investigated using the automated microscope. This was realized by switching the proteins completely on (30 ms 561 nm, 14.5 $kWcm^{-2}$) or off (12 ms 445 nm, 14.9 $kWcm^{-2}$) followed by a break with varying length. Next, the switchable mRuby2 variants were irradiated with light at 561 nm (14.5 $kWcm^{-2}$) for 30 ms. The ratio of the first fluorescent signal after the break to the on-state signal was plotted against the duration of the break.

2.4.2 Confocal microscopy of fusion constructs

The confocal imaging of RSFP fusion constructs expressed in mammalian cells was performed at the confocal laser scanning microscope Leica TCS SP8 (Leica Microsystems, Wetzlar, Germany) using a 63x/1.4 NA oil objective (HC PL APO CS2; Leica Microsystems, Wetzlar, Germany). The fluorescent proteins were excited at 561 nm. Sc10 and Sc21 were

simultaneously irradiated at 458 nm for on-switching of the proteins. The pinhole was set to 1 Airy unit and the fluorescence emission was detected from 570 nm to 630 nm.

2.4.3 Characterization of the new RSFPs for RESOLFT microscopy

The red RSFPs developed in this work were analyzed for their applicability in live-cell RESOLFT nanoscopy. Two different RESOLFT microscopes were used for these experiments depending on the switching mode of the respective RSFP (see below).

2.4.3.1 Characterization of switchable mRuby2 variants for RESOLFT microscopy

For the switching of Ru63, Ru85 and Ru87 fused to vimentin and for the establishment of RESOLFT imaging, an RESOLFT quad scanning microscope (Abberior Instruments, Göttingen, Germany) was adapted to the needs of the red positive-switching RSFPs by Sebastian Schnorrenberg. The RESOLFT microscope, which is based on an Olympus IX83 inverted microscope stand, was extended by a 561 nm laser (Jive 500 mW; Cobalt, Solna, Sweden) for on-switching and readout with a Gaussian profile. Furthermore, a laser diode at 445 nm (MLD 80 mW, fiber pigtailed; Cobalt, Solna, Sweden) was added to the microscope. The Easy3D Upgrade (spatial light modulator for 400-700 nm; Abberior Instruments, Göttingen, Germany) enabled a doughnut-like shape for the 445 nm beam in the focal plane, which was used for off-switching.

A 100x/1.4 NA oil objective (UPLSAPO; Olympus, Tokyo, Japan) was used for imaging and the pinhole was set to 1 Airy unit for all measurements. The fluorescence signal was detected above 568 nm using an avalanche photodiode (APD). The RESOLFT microscope was controlled by the software Imspector (Imspector0.12.10680M; Abberior Instruments, Göttingen, Germany). The alignment of the laser beams was controlled by the beam reflection at 80 nm gold beads and its detection with a photomultiplier tube (Figure 2.4-1). The point spread functions were additionally controlled using TetraSpeck Microspheres (0.1 µm; Thermo Fisher Scientific, Waltham, MA, USA) and fluorescence detection by the APD.

A pulse generator (9520 Series; Quantum Composers, Bozeman, MT, USA) was utilized for the pixel-wise acquisition of switching curves. The vimentin fusion constructs were irradiated with the 445 nm doughnut-shaped beam (0.48 $kWcm^{-2}$) for 8 ms to switch the RSFPs off. After a break of 2 ms, the positive-switching proteins were switched on with the 561 nm Gaussian-shaped beam (0.43 $kWcm^{-2}$) for 20-25 ms. The switching curves of all pixels of the chosen section were added up.

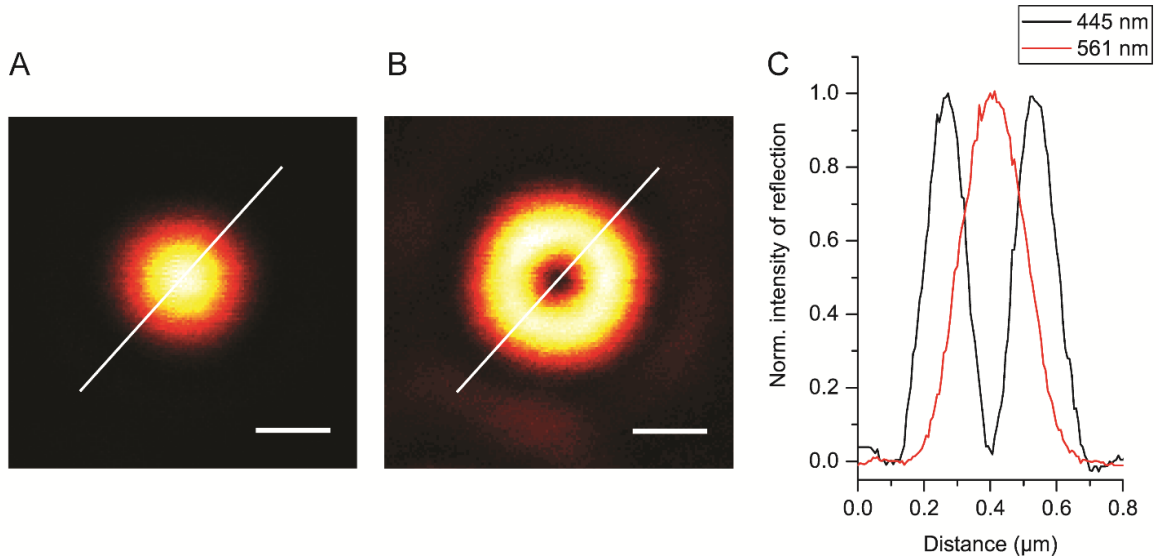

Figure 2.4-1: Examples for beam reflections at gold beads.
Example for the alignment of the RESOLFT microscope used for the positive-switching mRuby2 variants. A: Reflection of the 561 Gaussian-shaped beam B: Reflection of the 445 nm doughnut-shaped beam. Scale bars: 0.2 µm. C: Overlay of the line profiles of the cross sections shown in A and B. The fluorescence was normalized to the maximal signal. Black: 445 nm doughnut-shaped beam; red: 561 nm Gaussian-shaped beam.

The RESOLFT imaging of the keratin18-Ru63 filaments was conducted pixel-by-pixel with a dwell-time of 4.95 ms. The applied pulse scheme was 2 ms on-switching with the 561 nm Gaussian-shaped beam (0.64 $kWcm^{-2}$), followed by 2 ms off-switching with the 445 nm doughnut-shaped beam (0.48 kW/cm^{-2}) and subsequent readout for 944 µs by excitation at 561 nm (0.64 $kWcm^{-2}$). The confocal image of the same image section was acquired by 2 ms on-switching with the Gaussian 561 nm beam and subsequent readout for 944 µs by excitation at 561 nm (0.43 $kWcm^{-2}$). The images of the first 200 µs readout time was used for comparison of the confocal and the RESOLFT image.

2.4.3.2 Characterization of switchable mScarlet variants for RESOLFT microscopy

A RESOLFT microscope built by Abberior Instruments (Göttingen, Germany) was used for the switching of Sc10, Sc21, rsFusionRed2 and rsFusionRed3 fused to vimentin. The microscope is equipped with a 405 nm and a 561 nm laser. The 561 nm beam is divided into two beam paths. One of them can be modulated by a spatial light modulator to either a Gaussian or a doughnut-shaped beam. The pinhole was set to 1 Airy unit and a 100x/1.4 NA oil objective (UPLSAPO; Olympus, Tokyo, Japan) was used for all measurements. The microscope was controlled by the software Imspector (Imspector16.1.7707; Aberrior Instruments, Göttingen, Germany). The fluorescence emission was detected in the range of 580 to 630 nm. The alignment of the three beams was done as described in chapter 2.4.3.1.

The switching curves of the vimentin fusion constructs were acquired pixel-by-pixel using a pulse generator (9400 Series; Quantum Composers, Bozeman, MT, USA). The red negative-switching RSFPs were switched on for 12 ms by irradiation with the Gaussian-shaped 405 nm beam (0.35 or 1.65 $kWcm^{-2}$). Subsequently, the proteins were switched off using the modulatable 561 nm beam with a Gaussian profile (1.44 $kWcm^{-2}$). The switching curves of all pixels were added up.

2.4.4 Image analysis

The recorded confocal and RESOLFT images were imported in the image processing package FIJI [171, 172] and the lookup tables “Red Hot” or “Green” were applied. For the confocal images of the fusion constructs (chapter 3.2.4 and 3.3.5), the background was subtracted (max. 2 counts) and the color table was adjusted to the maximal signal. All images were exported as TIFF files. In the RESOLFT image, the line profiles (three pixel width) were extracted and fitted using a Lorentz-fit in OriginPro 2016 (OriginLab, Northampton, MA, USA).

3 Results

This work aimed to develop novel reversibly switchable fluorescent proteins (RSFPs) emitting in the red region of the visible spectrum. For this purpose, screening approaches were established and tailored to the development of red-emitting RSFPs (chapter 3.1). By applying these screening systems, novel positive-switching RSFPs were generated from the template protein mRuby2 (chapter 3.2) and negative-switching RSFPs were developed from the fluorescent protein mScarlet (chapter 3.3). The new RSFPs were characterized in detail regarding their switching and spectral properties, their applicability as fusion tag and their use in RESOLFT microscopy.

3.1 Development of screening assays to identify and characterize new RSFPs

To date, the search for fluorescent proteins and RSFPs with improved properties has been implemented mostly by the expression of mutant libraries in *E. coli* followed by the screening of these libraries (chapter 1.4.1). Likewise, the development of novel RSFPs in this work was mainly based on the microscopic screening of bacterial colonies expressing fluorescent protein mutants (chapter 3.1.1). To complement this well-established and beneficial screening approach, an alternative concept was established based on the screening of mammalian cells expressing single fluorescent protein variants (chapter 3.1.2).

3.1.1 Microscopic screening of red RSFPs expressed in *E. coli* colonies

A custom built microscope (chapter 2.4.1) facilitates the comparison of fluorescent protein variants expressed in bacterial colonies regarding their fluorescence and switching characteristics. An automated microscope and the workflow of screening were well-established in the research group and in the past, this screening technique was already applied for the generation of other RSFPs like rsEGFP2 [96].

The workflow was adjusted to provide a suitable approach for the development of red RSFPs (Figure 3.1-1). In each screening round, the mutagenesis strategy was chosen first. The analysis of the structure and the sequence comparison to published fluorescent proteins and RSFPs guided the selection of mutation sites for the (multiple) site-directed mutagenesis. Alternatively, error-prone mutagenesis was applied. Consequently, a library of pBad

plasmids containing mutated versions of the respective red fluorescent protein was generated by one of the described protocols (chapter 2.1.10) and was used for the transformation of *E. coli* cells (chapter 2.2.2). On the resulting agar plates, each colony expressed only a single fluorescent protein variant.

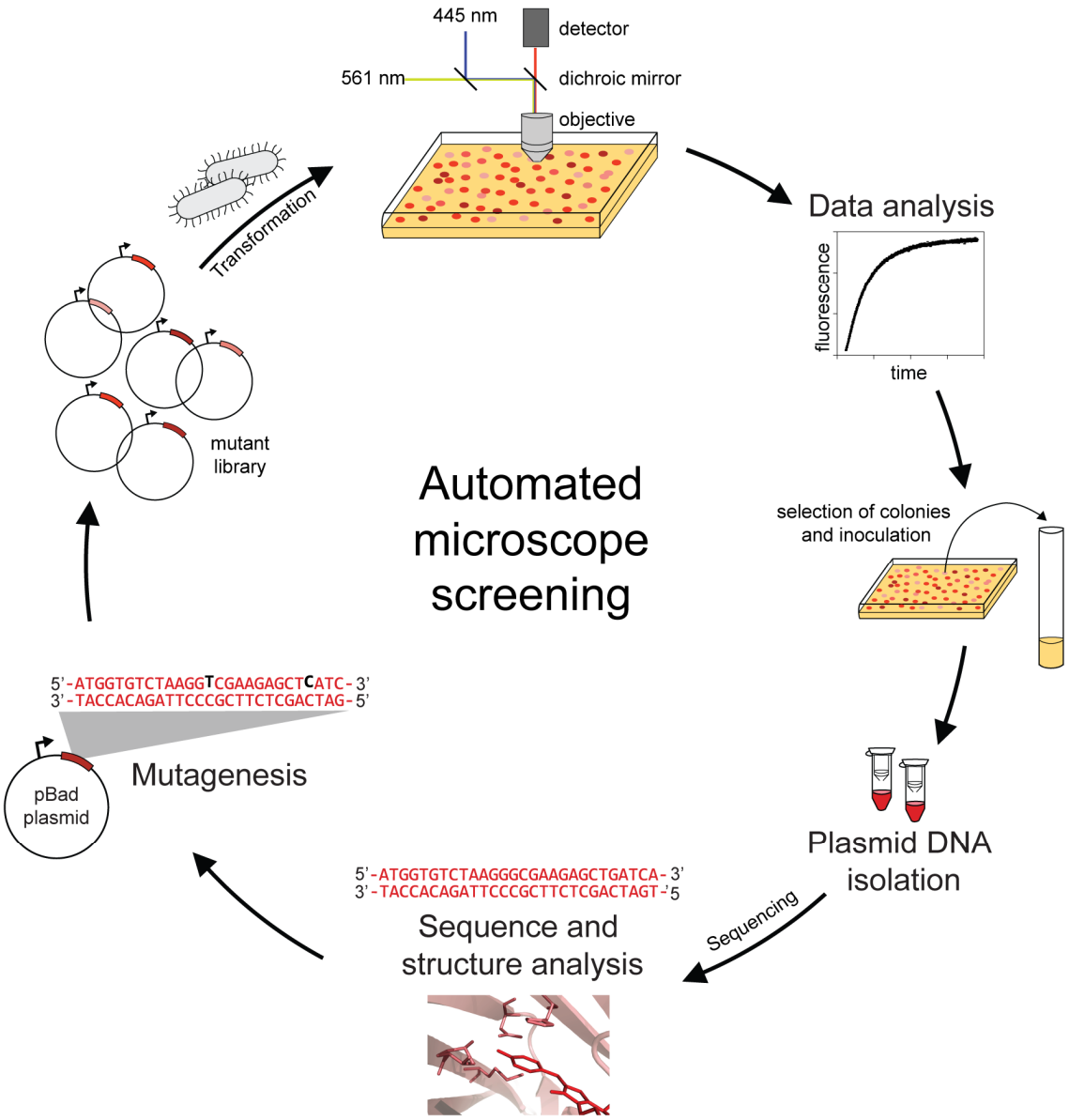

Figure 3.1-1: Screening for improved RSFPs using the automated microscope.
An overview of the mutagenesis and screening workflow using the automated microscope is shown (starting at the bottom). The chosen mutagenesis strategy is derived from the analysis of the coding sequence and the structure of the template protein. Consequently, a library of mutated template genes is generated and used for the transformation of E. coli. Each colony growing on the resulting agar plates expresses one variant. The automated microscope identifies the expressing clones and illuminates the fluorescent proteins by alternating irradiation with light of 445 nm and 561 nm. The resulting fluorescence is detected and the data is analyzed. Colonies expressing an RSFP with improved characteristics are picked to inoculate an overnight culture, respectively. The plasmid DNA is isolated and the obtained mutations are examined by sequencing. The analysis of the mutation sites can guide the next mutagenesis strategy.

The automated microscope was used to determine the switching characteristics of the red-emitting mutants expressed in the bacterial colonies. The wavelengths 445 nm and 561 nm were chosen as switching wavelengths due to the switching characteristics of other red RSFPs like rsCherry and rsCherryRev [91]. In all screenings, a switching scheme of alternating illumination at 445 nm and 561 nm was applied and the resulting fluorescence was detected. If the template protein was switchable, the illumination times were adjusted to switch the template protein completely on and off (chapter 2.4.1.1).

In the following data analysis step, the characteristics of the fluorescence development in the different switching cycles was quantified. It was screened for RSFPs with a high fluorescence in the on-state, a low residual fluorescence in the off-state, a high switching speed and a low switching fatigue (chapters 2.4.1.3-2.4.1.5), since these characteristics determine the applicability of RSFPs in RESOLFT microscopy (chapter 1.3.2). The colonies expressing RSFP variants with at least one improved switching characteristic compared to the template protein were selected if all other characteristics were not drastically impaired. However, the introduction of switching to a fluorescent protein as well as the improvement of the switching contrast or switching speed in a RSFP is commonly accompanied by a reduction in the ensemble brightness, which was tolerated to some extent.

The chosen colonies were used to inoculate overnight cultures (chapter 2.2.1) and the plasmid DNA was isolated (chapter 2.1.1). The mutations were analyzed by sequencing (chapter 2.1.8) and as appropriate, the new fluorescent protein variants were used as templates in the next mutagenesis and screening round.

The microscopic screening of RSFPs expressed in *E. coli* colonies comprises various advantages like the detailed switching characterization for each variant and the rapid process of this approach. Thus, this type of screening was mainly applied in this work for the development of the new red RSFPs (chapter 3.2.1 and 3.3.1). However, the main application field of RSFPs has been and will be the expression of fusion constructs in mammalian cells. Hence, an additional screening system based on the expression in mammalian cells was established (chapter 3.1.2).

3.1.2 Establishment of a mammalian landing pad cell line for screening

This work aimed to establish a new screening system to identify improved fluorescent proteins based on the expression in mammalian cells. For the screening, it is necessary to ensure that only a single fluorescent protein variant of a mutant library is expressed in each mammalian cell. Since this is not feasible by simple transfection, a site-specific recombinase

approach was chosen to achieve this. Similar to the approach of Duportet *et al.* [140] (chapter 1.4.2), a suited Bxb1 landing pad cell line was generated. The concept of the Bxb1 landing pad cell line for screening is described in the following.

3.1.2.1 Conception of a Bxb1 landing pad cell line for screening

A Bxb1 landing pad cell was defined as a suitable option to enable single variant expression in mammalian cells, which is required for the screening of fluorescent proteins. In this approach, a landing pad is placed in the genome of a mammalian cell. The landing pad selected in this work consists of the constitutive CAG promoter and a downstream Bxb1 attP site (see the middle of Figure 3.1-2). The landing pad is placed into the AAVS1 locus (19q13.4 qtr), a well-characterized locus for the knock-in of gene cassettes and known to facilitate long-term expression of transgenes [158, 173]. Important for the concept is, that only a single landing pad is integrated into the genome.

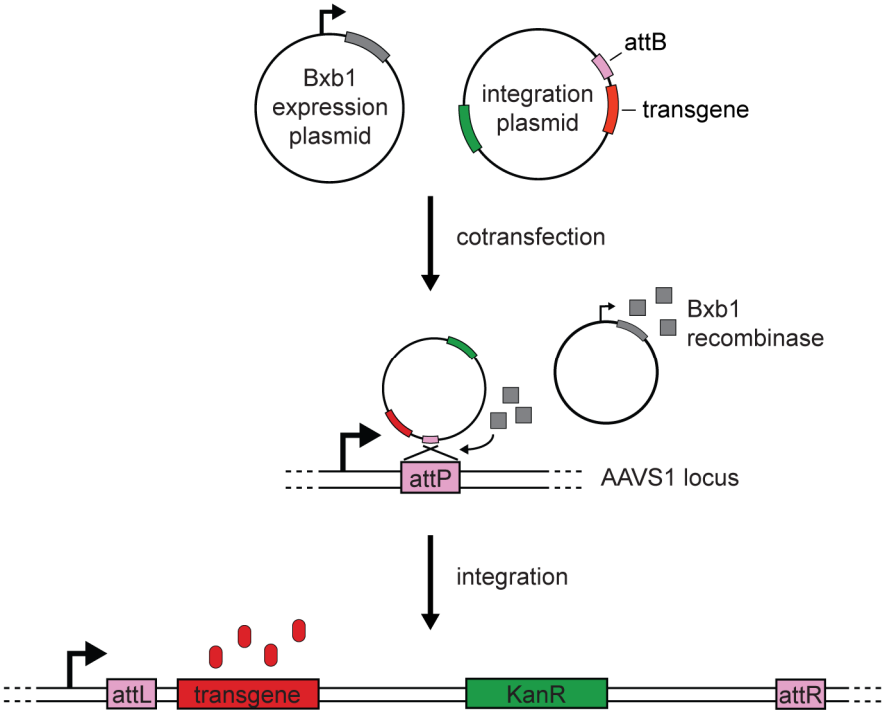

Figure 3.1-2: Integration of an integration plasmid into the Bxb1 landing pad.
A schematic overview of the Bxb1 recombinase-mediated integration event. A Bxb1 expression plasmid and an integration plasmid encoding a transgene next to the Bxb1 attB site, are used for cotransfection of the Bxb1 landing pad cell line. The landing pad is located in the AAVS1 locus and is composed of a CAG promoter and the Bxb1 attP site. The Bxb1 recombinase is transiently expressed from the Bxb1 expression plasmid and catalyzes the integration of the complete integration plasmid into the landing pad by recombination via the attB and attP sites. Accordingly, the transgene is stably expressed by the CAG promoter of the landing pad.

Once a monoclonal cell line with a single landing pad is generated, cells of this Bxb1 landing pad cell line can be used for the stable integration and expression of a single transgene (e.g.

a fluorescent protein mutant) per cell (Figure 3.1-2). This is done by the cotransfection of these cells with a Bxb1 recombinase expression plasmid and a promoter-less integration plasmid containing the Bxb1 attB site and the transgene (downstream the attB site). In successfully transfected cells, the Bxb1 recombinase is transiently expressed, which can then mediate the integration of an integration plasmid into the genome via the attP site in the landing pad and the attB site on the integration plasmid. By this recombination, the complete plasmid is integrated into the genome. Since the recombination catalyzed by the Bxb1 recombinase is unidirectional, only a single plasmid can be integrated per cell. The transgene of the integrated plasmid is then stably expressed under the control of the CAG promoter in the landing pad (shown below in Figure 3.1-2).

This concept is suitable for the screening of fluorescent proteins in mammalian cells. The cells of the Bxb1 landing pad cell line can be cotransfected with the Bxb1 expression plasmid and a mutant library of integration plasmids encoding the fluorescent protein variants. As the integration plasmid does not contain a promoter for transient expression, only the fluorescent protein variant integrated into the landing pad is expressed in the cell. The cells with a positive recombination event can be used for screening and comparison of the fluorescent protein variants (see chapter 3.1.2.5). Thus, various integration plasmids (chapter 3.1.2.2) and a Bxb1 landing pad cell line (chapter 3.1.2.3) were generated in this work.

3.1.2.2 Preparation of basic integration plasmids

Prior to the generation of the monoclonal Bxb1 landing pad cell line, a set of integration plasmids (pInt) was prepared for different applications and flexible use of the cell line (Table 3; cloning: chapter 2.1.9.3). Each integration plasmid contains the Bxb1 attB site for the recombination step and a multiple coning site (MCS) to add the coding sequence of a fluorescent protein (a plasmid map of pInt-MCS-P2A-HygroR is shown in the Appendix Figure 6.1-3).

The generated integration plasmids can be used to compare the expression, maturation and fluorescence characteristics of fluorescent proteins in a Bxb1 landing pad cell line, for instance by flow cytometry. An additional transgene can be stably expressed by using the P2A self-cleaving linker [174] (see Table 3). The P2A sequence is inserted between two transgenes and during translation a cleavage occurs within the P2A linker due to the skip of a peptide bond within the proline-glycine-proline motif.

Table 3: Prepared basic integration plasmids.
MCS: Multiple cloning site, HygroR: Hygromycin resistance gene, codEGFP: coding sequence of mEGFP with altered codon usage at the N- and C-terminus.

Integration plasmids
pInt-MCS-P2A-HygroR
pInt-MCS-P2A-mEGFP
pInt-MCS-P2A-mCherry
pInt-MCS
pInt-Vimentin-MCS-P2A-HygroR
pInt-Vimentin-MCS-P2A-mEGFP
pInt-Vimentin-MCS-P2A-mCherry
pInt-Vimentin-MCS
pInt-Keratin-MCS-P2A-HygroR
pInt-Keratin-MCS-P2A-mEGFP
pInt-Keratin-MCS-P2A-mCherry
pInt-Keratin-MCS
pInt-MCS-P2A-codEGFP

While the integration plasmids containing the P2A-HygroR element allow for selection of cells with positive integration by Hygromycin B treatment, the integration plasmids containing the P2A-mEGFP or P2A-mCherry can be used for normalization to the expression level in each cell, based on the fluorescence signal of mEGFP or mCherry. The integration plasmids with keratin or vimentin fusion constructs can be applied to control the tagging performance of the fluorescent proteins. Additional fusion constructs can be cloned in the future.

3.1.2.3 CRISPR Cas9 knock-in of a Bxb1 landing pad into the AAVS1 locus

The method of CRISPR/Cas9 genome editing [143, 144] was chosen to integrate a Bxb1 landing pad into the AAVS1 locus of HeLa cells. The plasmid pTRE-TIGHT-EGFP [158] served as backbone for the cloning of a suitable donor plasmid (chapter 2.1.9.2). The pTRE-TIGHT-EGPF plasmid already contained homology arms for the knock-in into the PPP1R12C intron 1 (AAVS1 locus). In this plasmid, an element composed of a splicing acceptor site, a *thosea asigna* virus 2A self-cleaving peptide sequence (T2A) and a Puromycin resistance gene is placed downstream of the left homology arm. This element facilitates the expression of the Puromycin resistance gene by the endogenous PPP1R12C promoter, if the knock-in was successful. The landing pad consisting of the CAG promoter and the Bxb1 attP site was assembled into the donor plasmid with addition of a simian virus 40 (SV40) polyA sequence and a cHS4 insultor to shield the landing pad from endogenous genes (plasmid map of the applied donor plasmid: Appendix Figure 6.1-2).

Accordingly, HeLa cells were cotransfected with the Bxb1 landing pad donor plasmid and the plasmid px458-AAVS1 gRNA2 encoding the Cas9 protein and an appropriate gRNA

sequence for the AAVS1 locus (chapter 2.2.4.1). The transfected cells with positive knock-ins were selected by Puromycin treatment (chapter 2.2.5). The remaining cells were used to generate monoclonal cell lines by single-cell sorting and the screening for a functional Bxb1 landing pad cell line was realized by an integration assay. In this assay, cells of each monoclonal cell line were contransfected with the Bxb1 expression plasmid pCAG-NLS-HA-Bxb1 [167] and the integration plasmid pInt-mEGFP-P2A-HygroR (chapter 2.2.7). As a result, the clone K21 was identified as a functional Bxb1 landing pad cell line by the positive expression of mEGFP. In the following, the cell line based on this clone will be called K21.

In Figure 3.1-3 A, the expected genomic situation for a successful knock-in is presented. Three genotyping PCR reactions were performed on the isolated genomic DNA of K21 cells and non-edited HeLa cells (chapter 2.1.11). The first PCR amplifies the DNA strand from the CAG promoter to the right homology arm (expected size: 1081 bp; PCR1 in Figure 3.1-3 A). As expected, the PCR only yielded a PCR product for the K21 cells containing the Bxb1 landing pad (Figure 3.1-3 C). Sequencing of this PCR product confirmed the expected sequences and an intact Bxb1 attP site. In the second genotyping PCR, a landing pad- and a genome-specific primer were applied (PCR2 in Figure 3.1-3 A). Once more, only the PCR with the genomic DNA of K21 cells resulted in a PCR product with the anticipated size (1439 bp; Figure 3.1-3 D). Sequencing of this PCR product verified the knock-in into the AAVS1 locus.

In the third PCR, a PCR product of 441 bp is amplified for the wild-type AAVS1 locus as template (Figure 3.1-3 B). PCR products of this size were received from the genomic DNA of HeLa and K21 cells (Figure 3.1-3 E). Consequently, the K21 cells contain at least one wild-type and one edited AAVS1 locus. For the application of the K21 cells in a screening approach, a single landing pad knock-in is necessary. However, the copy number of the AAVS1 locus in HeLa cells is not entirely clear, since karyograms of HeLa cells showed varying numbers of chromosome 19 from two to three with addition of marker chromosomes [175, 176]. Thus a single or a double knock-in of the landing pad is possible. Furthermore additional off-target knock-ins would be conceivable. Therefore, further characterizations of the generated Bxb1 landing pad cell line K21 are presented in the next chapter.

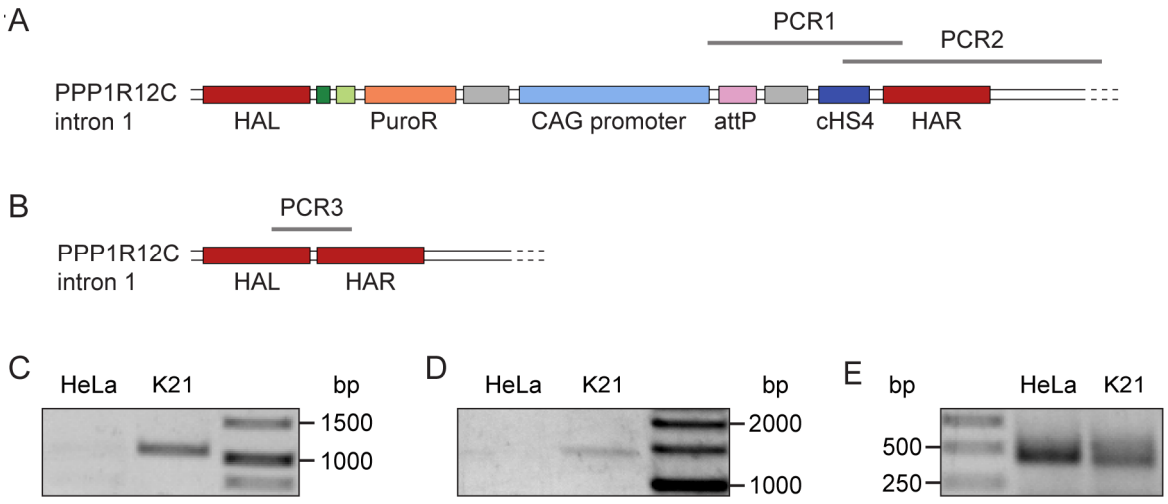

Figure 3.1-3: Verification of the Bxb1 landing pad knock-in for cell line K21.
A: Scheme for the successful knock-in of the Bxb1 landing pad into the PPP1R12C intron 1 (AAVS1 locus) of HeLa cells using CRISPR/Cas9 genome editing. B: Representation of the wild-type locus; sequences of the homology arms are indicated. A+B: Dark red: homology arm left (HAL)/right (HAR), dark green: splicing acceptor site, light green: T2A, orange: Puromycin resistance gene, grey: SV40 polyA, light blue: CAG promoter, pink: Bxb1 attP site, dark blue: cHS4 insulator. Expected DNA fragments of the genotyping PCRs (PCR1-3) are highlighted. C-E: Genotyping PCRs on genomic DNA of HeLa and K21 cells analyzed in analytical gel electrophoresis. C: PCR products of PCR1 in A, expected size: 1081 bp. D: Control of the knock-in localization, PCR2 in A, expected size: 1439 bp. E: The PCR yields a product of 441 bp for wild-type chromosomes (PCR3 in B).

3.1.2.4 Characterization of the generated Bxb1 landing pad cell line K21

Several specific integration plasmids were cloned (chapter 2.1.9.3, Table 1) to characterize the generated Bxb1 landing pad cell line and the stable expression of fusion constructs in these cells. In all experiments, the cells of the K21 cell line were cotransfected with 1 µg of the Bxb1 expression plasmid (pCAG-NLS-HA-Bxb1) and 1 µg of each integration plasmid. To determine the integration efficiency of this approach, the plasmid pInt-mEGFP-P2A-HygroR was used. Five days after transfection, the analysis of 20,000 cells in flow cytometry revealed that 1.15 % of the single cells displayed green fluorescence higher than the autofluorescence of HeLa cells. The expression level varied considerably, as the fluorescence signal ranged from approximately 10 to 2,500 a.u. (Figure 3.1-4 A).

Another batch of K21 cells was cotransfected with pCAG-NLS-HA-Bxb1, pInt-mEGFP-P2A-HygroR and pInt-mRuby2-P2A-HygroR. In the analysis of 20,000 cells in flow cytometry five days after transfection, 0.64 % of the cells exhibited detectable green fluorescence and 0.44 % of the cells exhibited detectable red fluorescence (Figure 3.1-4 B). No cells were detected which displayed both green and red fluorescence, neither in flow cytometry analysis nor in fluorescence microscopy (data not shown). Thus, a double knock-in of the Bxb1 landing pad is determined to be unlikely.

After contransfection of K21 cells with pCAG-NLS-HA-Bxb1 and pInt-mRuby2-P2A-mEGFP, the K21 cells with positive integration showed both, red (mRuby2) and green (mEGFP) fluorescence (Figure 3.1-5 A). The fluorescence signals of mRuby2 and mEGFP were correlated in flow cytometry (Figure 3.1-4 C). Hence, the expression of mEGFP from integrated plasmids with P2A-mEGFP can serve as an internal reference for the expression level in screening approaches.

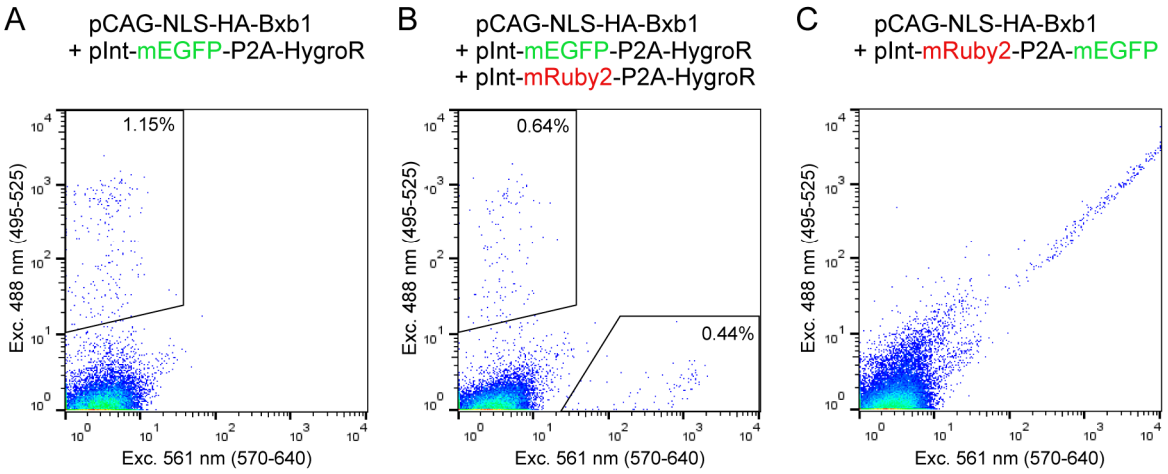

Figure 3.1-4: Expression of fluorescent proteins in K21 cells analyzed in flow cytometry.
Flow cytometry analysis of K21 cells cotransfected with different integration plasmids and the Bxb1 expression plasmid. The green fluorescence (Exc: 488 nm, Em: 495-525 nm) measured for single cells is plotted against the red fluorescence (Exc: 561, Em: 570-640 nm). A: 20,000 cells cotransfected with pCAG-NLS-HA-Bxb1 and pInt-mEGFP-P2A-HygroR were analyzed 5 days after transfection; 1.15 % of the cells were green fluorescent. B: 20,000 cells cotransfected with pCAG-NLS-HA-Bxb1, pInt-mEGFP-P2A-HygroR and pInt-mRuby2-P2A-HygroR were analyzed 5 days after transfection; 0.64 % green and 0.44 % red fluorescent cells. No two-colored cells were detected. C: 50,000 cells cotransfected with pCAG-NLS-HA-Bxb1 and pInt-mRuby2-P2A-mEGFP were analyzed 6 days after transfection. The green fluorescence is correlated to the red fluorescence for cells with positive integration.

In the following, different integration plasmids with fusion constructs and selection markers were analyzed. Therefore, K21 cells were cotransfected with the Bxb1 recombinase expression plasmid and the respective integration plasmid. K21 cells with a successfully integrated pInt-mEGFP-P2A-HygroR plasmid could be enriched by incubation in Hygromycin-containing medium (400 µg/µl). After 4 days of selection, almost all cells showed stable expression of mEGFP (Figure 3.1-5 C). The integration of the plasmids pInt-Keratin-mEGFP-P2A-HygroR (Figure 3.1-5 B), pInt-Vimentin-mEGFP-P2A-HygroR (Figure 3.1-5 D) and pInt-Ker-mRuby2-P2A-mEGFP (Figure 3.1-5 E) into the landing pad of K21 cells resulted in the expression of the cytoskeleton fusion constructs with a characteristic localization pattern. For the integration of pInt-Ker-mRuby2-P2A-mEGFP, the mEGFP signal was detectable in the cytoplasm and in the nucleus (Figure 3.1-5 E right).

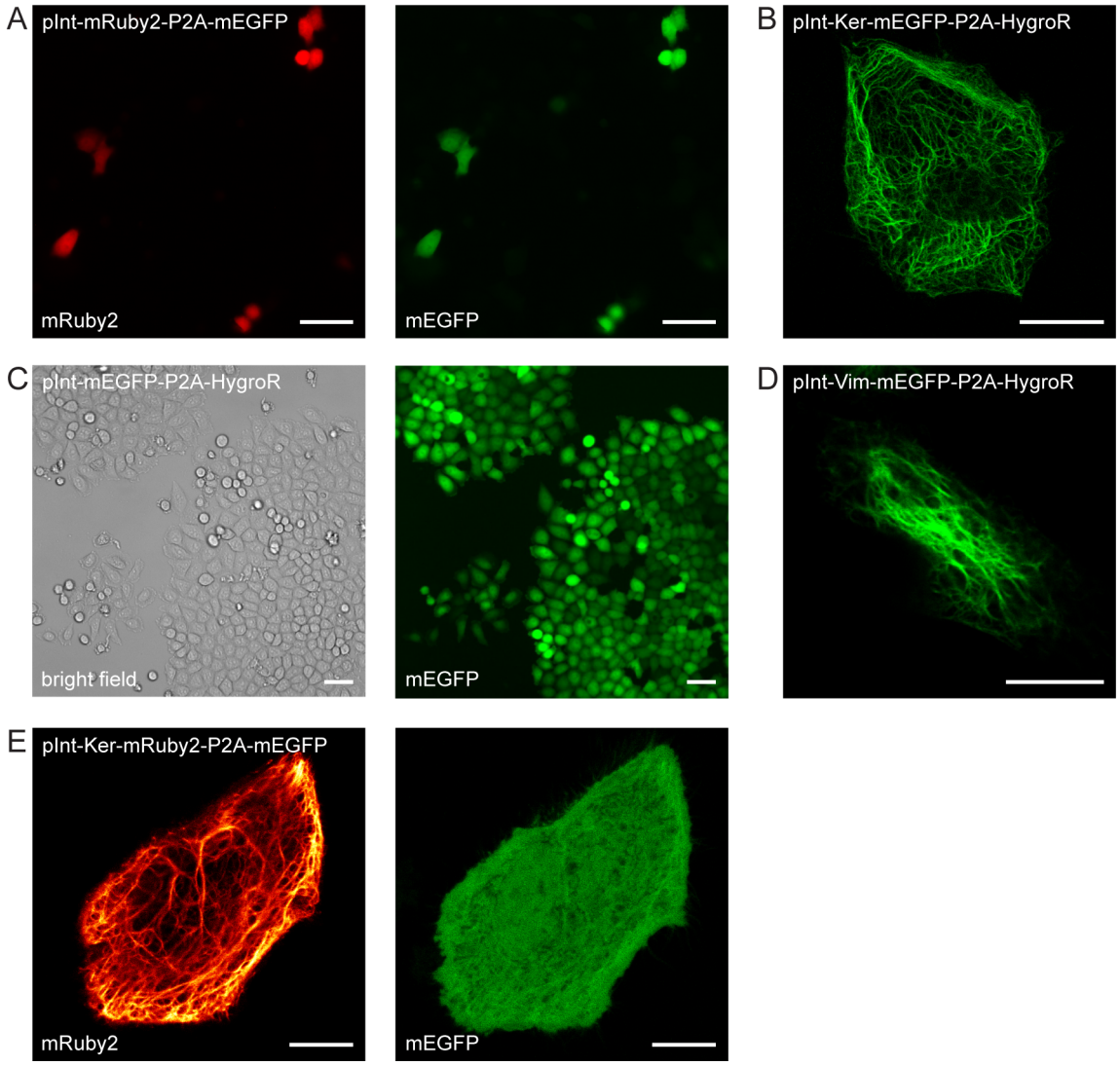

Figure 3.1-5: Stable expression of fusion constructs in K21 cells.
Cells of the Bxb1 landing pad cell line K21 were cotransfected with the respective integration plasmid and the Bxb1 expression plasmid (pCAG-NLS-HA-Bxb1). A: Integration of the plasmid pInt-mRuby2-P2A-mEGFP yields the expression of mRuby2 and mEGFP resulting in both red (left) and green (right) fluorescent cells. B: Expression of keratin18-mEGFP in a K21 cell after integration of the plasmid pInt-Keratin-mEGFP-P2A-HygoR into the landing pad (confocal image). C: K21 cells were transfected with the plasmids pCAG-NLS-HA-Bxb1 and pInt-mEGFP-P2A-HygroR. 5 days after transfection, the cells were selected with Hygromycin B (400 µg/µl) for 4 days (images acquired in the imaging plate reader, see chapter 2.2.5). The Hygromycin selection enriched cells with successful plasmid integration. D: Expression of Vimentin-mEGFP after integration of the plasmid pInt-Vimentin-mEGFP-P2A-HygroR (confocal image). E: Expression of keratin18-mRuby2 (left) and mEGFP (right) after integration of the plasmid pInt-Keratin-mRuby2-P2A-mEGFP (confocal images). Scale bars: A, C: 50 µm; B, D, E: 10 µm.

This indicates that the integration of the plasmids into the Bxb1 landing pad of the K21 cells occur as assumed and presented in chapter 3.1.2.1 (Figure 3.1-2). Additionally, the correct and complete integration of an integration plasmid into the landing pad was verified. In order to do this, a monoclonal cell line was generated by cotransfection of K21 cells with the plasmids pCAG-NLS-HA-Bxb1 and pInt-Keratin-Ru63-P2A-mEGFP (Ru63: developed

RSFP in this work) with following single-cell sorting of fluorescent cells. A monoclonal cell line with an integrated pInt-Keratin-Ru63-P2A-mEGFP plasmid (Figure 3.1-6 A) was identified by the expression of the keratin construct. The genomic DNA was isolated and used for genotyping PCRs. The size of the PCR products was controlled in analytic gel electrophoresis and met the expectations (Figure 3.1-6 B; PCR1: 2214 bp, PCR2: 2310 bp, PCR3: 1374 bp, PCR 4: 1439 bp). The sequencing of the PCR products verified the accurate integration of the plasmid pInt-Keratin-Ru63-P2A-mEGFP into the landing pad of the K21 cells.

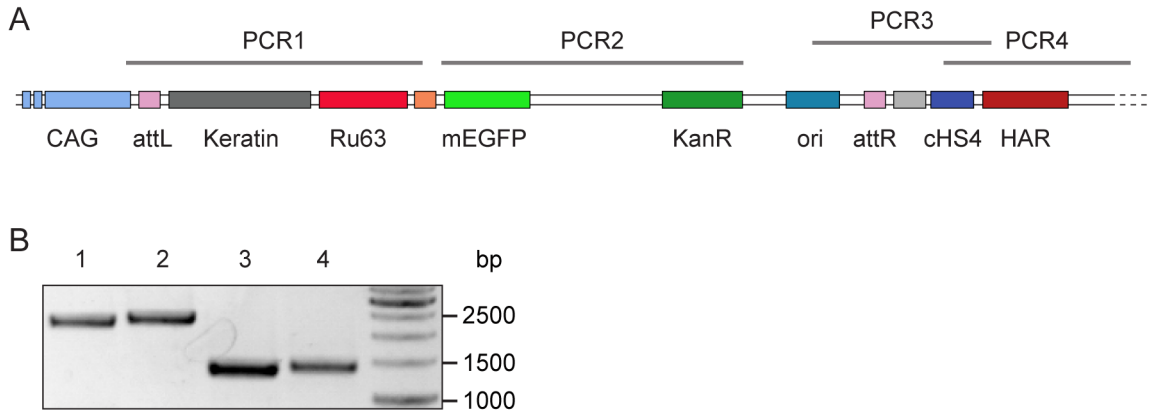

Figure 3.1-6: Control of the integration of an integration plasmid into the landing pad.
A: Expected genomic arrangement after successful integration of the plasmid pInt-Keratin-Ru63-P2A-mEGFP into the Bxb1 landing pad of K21 cells catalyzed by the Bxb1 recombinase. Light blue: CAG promoter, pink: attL and attR resulting from recombination event, dark grey: keratin18, red: Ru63, orange: P2A, light green: mEGFP, dark green: Kanamycin resistance gene (KanR), greenish-blue: ColE1 origin (ori), light grey: SV40 polyA, dark blue: insulator cHS4, dark red: homology arm right (HAR). Expected DNA fragments of the genotyping PCRs are indicated (PCR1-4). B: PCR products of the genotyping PCRs on genomic DNA of the monoclonal K21 cell line with the integrated plasmid pInt-Keratin-Ru63-P2A-mEGFP analyzed in analytical gel electrophoresis. Expected PCR product size: PCR1: 2214 bp, PCR2: 2310 bp, PCR3: 1374 bp, PCR 4: 1439 bp.

3.1.2.5 Screening for improved fluorescent proteins using the K21 cell line

The generated Bxb1 landing pad cell line K21 was used to screen libraries of fluorescent proteins for the effective brightness and expression performance in mammalian cells. At the beginning of the screening workflow (Figure 3.1-7), a library of integration plasmids with mutant fluorescent proteins was prepared using error-prone mutagenesis (chapter 2.1.10). In the applied screenings, the integration plasmid pInt-MCS-P2A-codEGFP served as backbone in order to take the expression level into account. The generated plasmid library was then used for the cotransfection of K21 cells along with the Bxb1 expression plasmid. In the cotransfected cells, only one plasmid can be integrated into the landing pad by the Bxb1 recombinase.

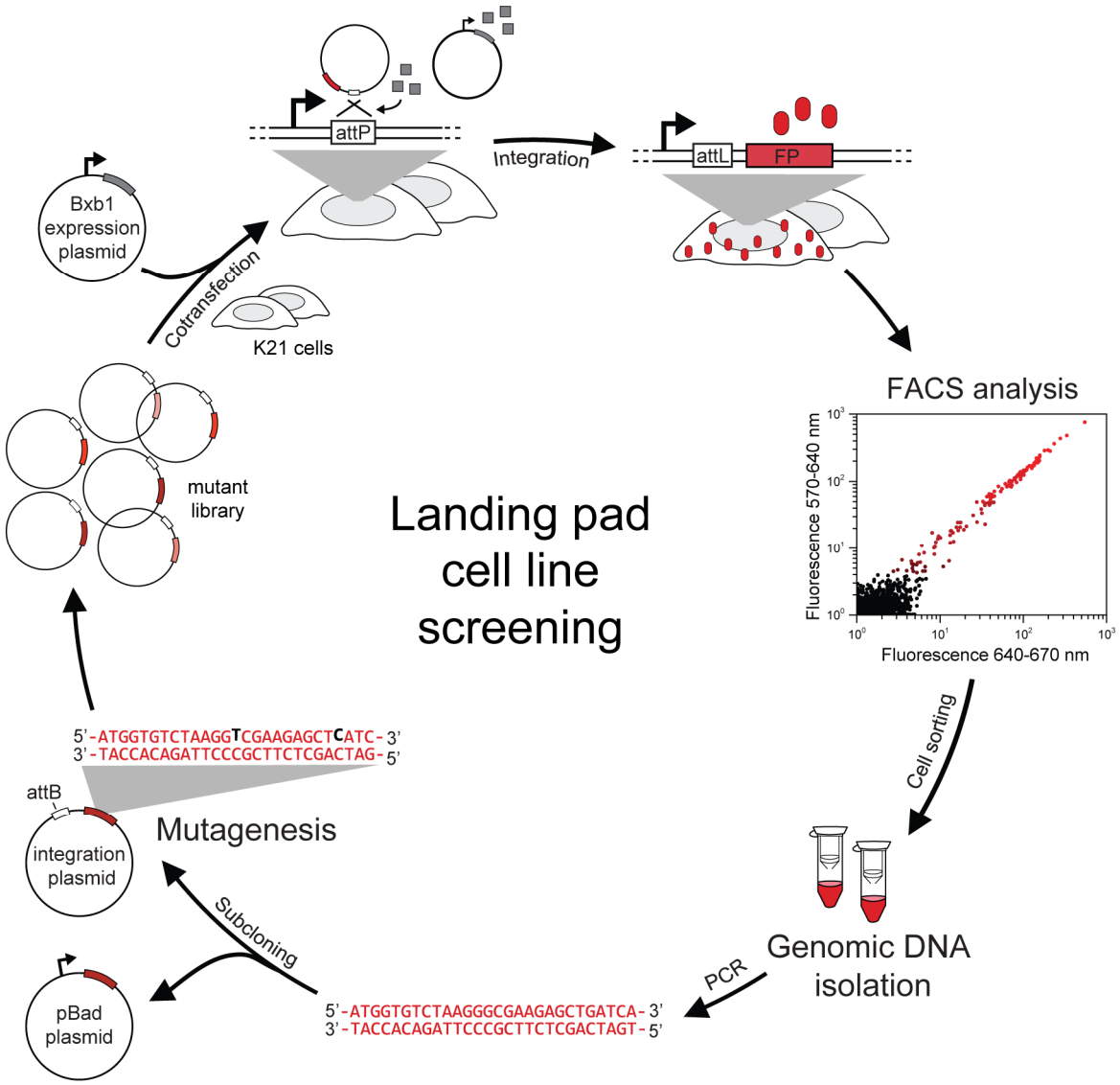

Figure 3.1-7: Screening for fluorescent proteins with improved brightness in K21 cells.
A schematic overview of the screening for fluorescent proteins (FP) or RSFPs with enhanced brightness or improved expression using the landing pad cell line K21 (starting at the bottom). One of the described mutagenesis protocols is applied to generate a library of integration plasmids with mutant fluorescent proteins. The integration plasmid library and the Bxb1 expression plasmid are used for cotransfection of K21 cells. In each cell, only one of the transfected integration plasmids can be integrated into the landing pad by the transiently expressed Bxb1 recombinase. The respective mutant is expressed after the recombination step. Cells expressing different mutants can be compared in the fluorescence activated cell sorting (FACS), and the cells with the highest fluorescence intensity are sorted into a well plate. The genomic DNA of the cells is isolated and the coding sequences of the fluorescent protein variants are amplified by PCR. For the application of directed evolution, further rounds of mutagenesis and screening can be applied. Alternatively, the coding sequences of the mutants can be cloned into pBad plasmids and their characteristics can be analyzed using the automated microscope.

After five to seven days, the fluorescence signals were analyzed by flow cytometry. The cells with the highest fluorescence intensity or the cells with the highest red-to-green fluorescence ratio were sorted for further cultivation. The genomic DNA of these cells was isolated and the coding sequences of the selected protein variants were amplified by PCR.

The PCR products were used for an additional round of mutagenesis and screening or alternatively the coding sequences of the fluorescent protein variants were cloned into the pBad vector for analysis of the mutants in *E. coli*.

In summary, a Bxb1 landing pad cell line was generated, which enables single variant expression per cell. A screening system based on this cell line was established for the development of novel fluorescent proteins. The protocols for the microscopic screening of *E. coli* colonies and the protocols for the screening of K21 cells using flow cytometry were specifically adapted for the development of red RSFPs. The development of novel red RSFPs using these screening systems is described in the following.

3.2 Novel positive-switching red RSFPs based on mRuby2

This work aimed to develop novel red-emitting and reversibly switchable fluorescent proteins with excellent characteristics. The non-switching fluorescent protein mRuby2 [57] was considered to be an appropriate template to design new RSFPs. mRuby2 is a bright fluorescent protein (ε: 113,000 $M^{-1}cm^{-1}$, QY: 0.38) emitting in the red region of the visible spectrum with its maximum at 600 nm. Furthermore, mRuby2 was shown to be applicable in a large number of fusion constructs. The chromophore of its precursor mRuby was found to adopt a *trans*-conformation in crystal form 1 at pH 8.5 and a mixture of *cis*- and *trans*-conformations in the crystal form 2 at pH 8.0 [177]. The development of novel red RSFPs from this template protein is described in the following.

3.2.1 Development of novel RSFPs by screening of mutant mRuby2 libraries

3.2.1.1 An initial variant for the development of positive-switching RSFPs

The amino acids in the chromophore pocket were shown to have a great influence on the switching ability of red fluorescent proteins (chapter 1.3.4). The mutagenesis of these amino acids can introduce switching into non-switching proteins as a result of changing the hydrogen bonding network or providing space for the *cis-trans* isomerization [82, 91]. Hence, the amino acids in the proximity of the chromophore of mRuby2 were mutated using site-directed and multiple-site mutagenesis. The resulting mutant libraries were expressed in bacterial colonies and screened by alternating irradiation with 445 nm and 561 nm using the automated microscope (chapter 2.4.1). A mutant with the mutation M164T was found to be switchable in a positive-switching mode, since the light of 561 nm

switched the protein slightly on, while illumination with light of 445 nm attenuated the fluorescence.

So far, only the tetrameric asFP595 and the monomeric rsCherry were available red fluorescent and positive-switching proteins [33, 91], but both were not applicable in live-cell RESOLFT microscopy. Thus, it was aimed to develop positive-switching RSFPs with improved characteristics derived from the mRuby2-M164T mutant, albeit the brightness of this mutant was reduced compared to the template protein.

3.2.1.2 Switching and screening of positive-switching red RSFPs

The microscopic screening (chapter 2.4.1 and 3.1.1) was applied to identify superior red RSFPs derived from the mRuby2-M164T mutant. Figure 3.2-1 shows exemplary switching curves for a positive-switching red RSFP acquired with the automated microscope. Light of 561 nm, which efficiently excites the proteins, was used for on-switching, while light of 445 nm was applied to switch the RSFPs off. Accordingly, the screening was performed by alternating irradiation at 561 and 445 nm (chapter 2.4.1.1).

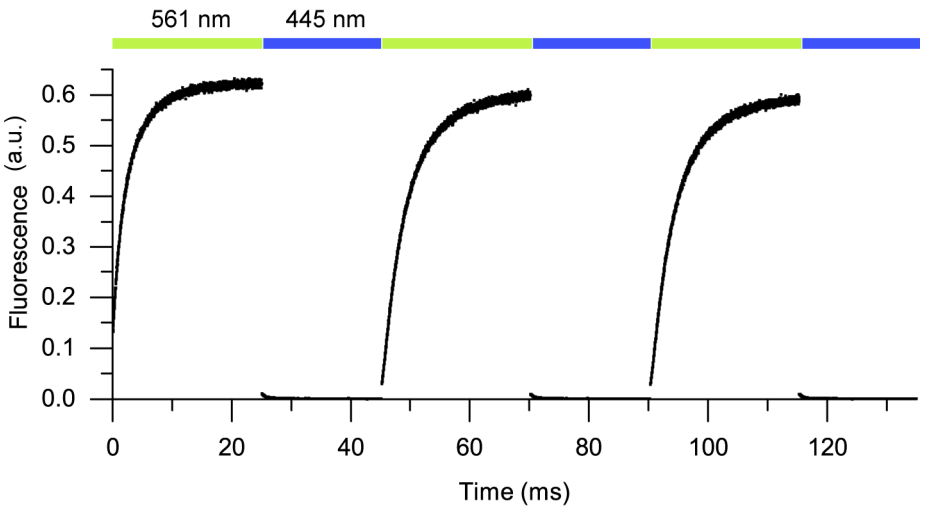

Figure 3.2-1: Switching of a red-emitting and positive-switching fluorescent protein.
The graph shows an example for the switching of a positive-switching red RSFP expressed in E. coli using the automated microscope (in particular: switching curves of Ru87 are shown, see chapter 3.2.1.3). As indicated, the fluorescence signal resulting from the alternating irradiation with light of 561 nm and 445 nm is plotted against the time. The red RSFPs show almost no red fluorescence after irradiation at 445 nm.

The analysis of the switching characteristics was primarily based on the on-switching process. It was screened for positive-switching mRuby2 variants with the highest brightness and contrast between the on and the off-state, meaning the highest maximal fluorescence signal in the on-state and the lowest possible residual fluorescence in the off-state. The residual fluorescence in the off-state was determined by the ratio of the first to the averaged

last points of the on-switching curve. Furthermore, a low halftime for the on-switching process as well as a low switching fatigue were preferred. The switching fatigue was measured by the reduction of the on-state fluorescence signal per switching cycle upon repetitive switching.

3.2.1.3 Evolution of positive-switching red RSFPs from mRuby2-M164T

Several consecutive rounds of mutagenesis and screening were performed for the generation of new improved positive-switching red RSFPs from mRuby2-M164T (Ru27). Both, random and site-directed mutagenesis were applied in this process with the addition of one to three mutations in each round (Figure 3.2-2 A). Only crystal structures of the progenitor mRuby were available (Figure 3.2-2 B). In the screening of randomly mutated libraries, mainly variants with mutations in loops or outside the beta-barrel structure were identified. The amino acids A63, T162 and M164 were mutated specifically due to their close proximity to the chromophore (Figure 3.2-2 close-up). The mutagenesis of C176 was conducted due to the structural based investigations of photobleaching by Duan *et al.* [99]. Ten generated mutants were compared using the same switching protocol in the automated microscope (alternating: 12 ms 445 nm with 6.6 $kWcm^{-2}$ and 24 ms 561 nm with 14.5 $kWcm^{-2}$) (Figure 3.2-3). For each mRuby2 variant, the measurements were performed at ten bacterial colonies grown at 37 °C for two days.

With each screening round, the residual fluorescence in the off-state relative to the fluorescence in the on-state decreased (Figure 3.2-3 B). Using the given switching times and light intensities, the residual fluorescence in the off-state was noticeable higher in the second switching cycle for the variants from Ru27 to Ru63. After the off-switching, the fluorescence of the initial variant Ru27 was reduced to 78 % of the maximal signal in the first switching cycle. The three final variants Ru63, Ru85 and Ru87 showed a residual fluorescence in the off-state of below 5 % in the first cycle and of below 7 % in the second cycle.

The addition of the mutations M67L (Ru34) and T162A (Ru37) strongly reduced the ensemble brightness in bacterial colonies, measured by the maximal fluorescence signal in the on-state (Figure 3.2-3 A). It should be noted that the M67L mutation directly modifies the structure of the chromophore. This reduction of the ensemble brightness could be partly recovered in the last mutagenesis and screening rounds (Ru63, Ru85, Ru87).

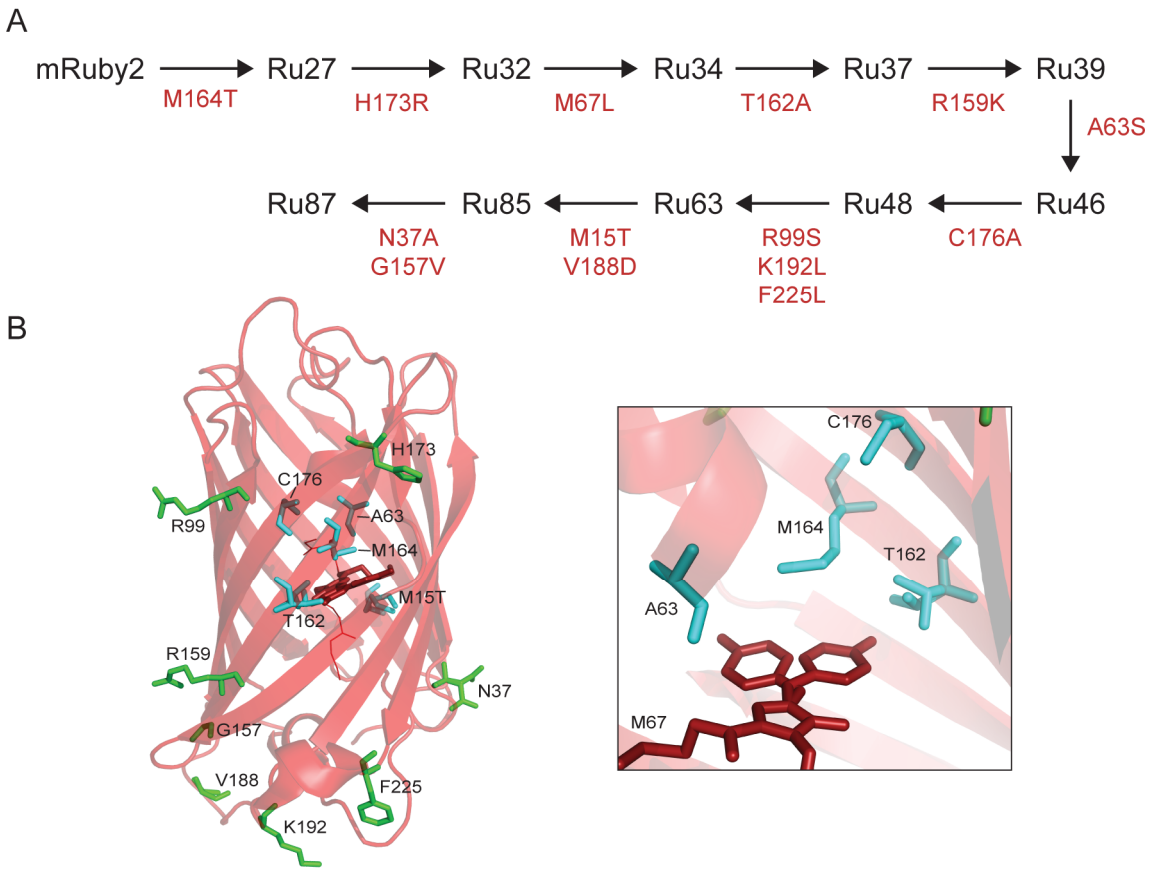

Figure 3.2-2: Development of positive-switching red RSFPs on basis of mRuby2.
A. Evolution of the red-emitting and positive-switching mRuby2 variants. The mutations added at each step are given below the arrows. B: Localization of the mutation sites (original amino acids) mapped in the structure of mRuby [177] (PDB: 3U0N) visualized with PyMOL. The crystal structure of mRuby crystal form 2 at pH 8.0 revealed chromophores in both, the cis and the trans-conformation. Green: amino acids outside the beta-barrel, cyan: amino acids inside the beta-barrel, dark red: chromophore. Left: Overview of the mutations in the overall structure. Right: Close-up of the chromophore and mutation sites in the direct chromophore environment (mutation site M67: part of the chromophore).

Using laser light of 561 nm with an intensity of 14.5 $kWcm^{-2}$, an on-switching halftime of 3 ms was determined for the initial variant Ru27. The addition of the mutations M67L (Ru34) and R159K (Ru39) increased the on-switching halftime by 48 and 34 %, though this was reverted by the mutations T162A (Ru37) and A63S (Ru46) (Figure 3.2-3 C). The switching scheme for the comparison of the variants was not adjusted to the respective switching kinetics, which partially does not allow for the direct comparison of the switching fatigue, since photobleaching of the on-state proteins appears at prolonged illumination. However, the addition of the mutation C176A (Ru48) did not change the on-switching kinetics (Figure 3.2-3 C), but reduced the switching fatigue, as the fluorescence in the on-state of cycle 54 compared to the first cycle was 77 % instead of 60 % (Figure 3.2-3 D).

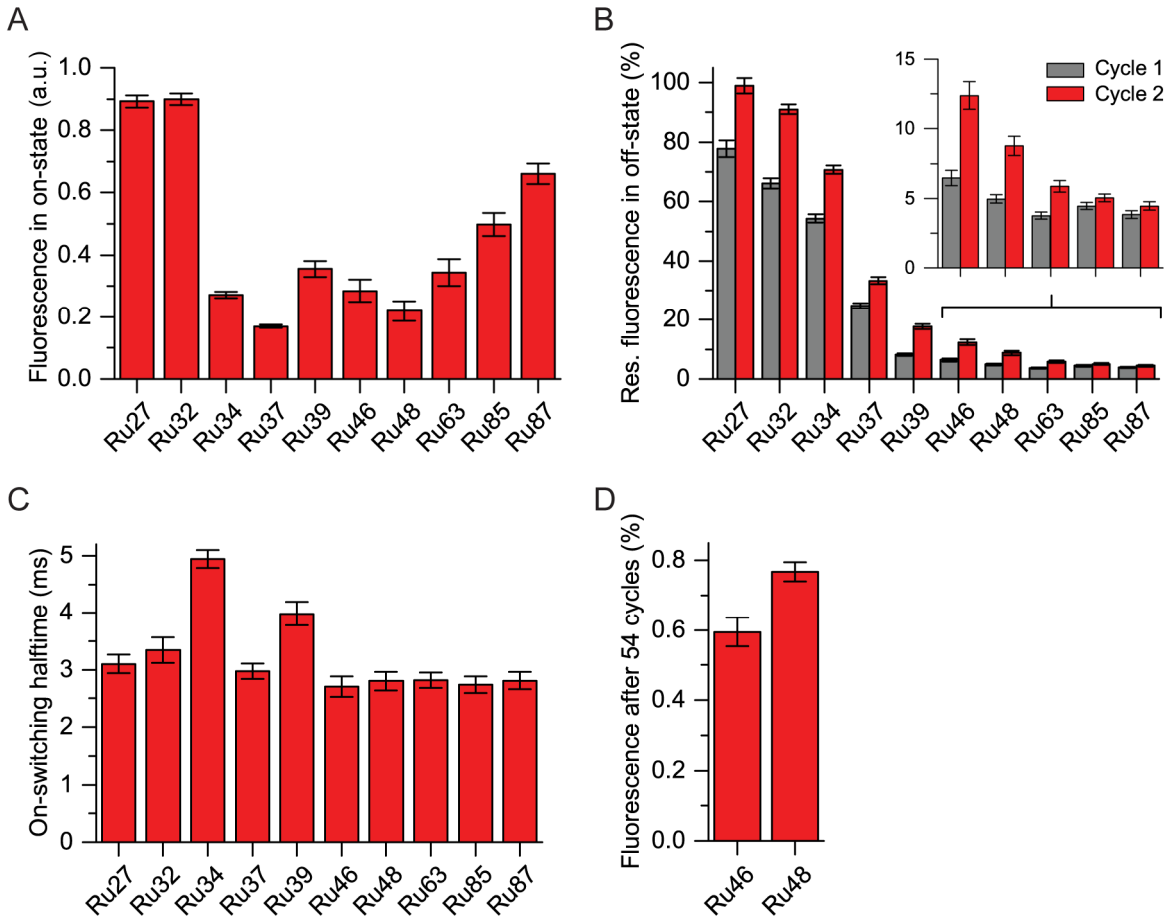

Figure 3.2-3: Characteristics of positive-switching mRuby2 variants found in screenings.
The switching characterization of the positive-switching mRuby2 variants representing the individual rounds of mutagenesis and screening (mutations added in each round: see Figure 3.2-2 A). The switching scheme for all variants: alternating 12 ms 445 nm (6.6 kWcm^{-2}) and 24 ms 561 nm (14.5 kWcm^{-2}) illumination, 54 switching cycles. 10 bacterial colonies grown at 37 °C for 2 days were selected for each measurement. A: Fluorescence signal in the on-state (switching cycle 1). B: Residual fluorescence in the off-state for switching cycle 1 (grey) and 2 (red) normalized to the on-state. Inset: close-up for Ru46-Ru87 with smaller scales for the y-axis. C: On-switching halftimes (switching cycle 1). D: The ratio of the fluorescence signal in the on-state of cycle 54 relative to cycle 1.

The three final variants Ru63, Ru85 and Ru87 were determined to be the most promising new red RSFPs, since they showed the best switching characteristics like the lowest residual fluorescence in the off-state. The switching characteristics did not vary considerably between these variants, only the ensemble brightness measured in the *E. coli* colonies was higher for Ru85 and even higher for Ru87. However, Ru63 contains less mutations, especially outside the beta-barrel, and was therefore further characterized along with Ru85 and Ru87.

The new RSFP Ru63 differs from mRuby2 by ten mutations (A63S, M67L, R99S, R159K, T162A, M164T, H173R, C176A, K192L, F225L). Ru85 was obtained from Ru63 by addition of the two mutations M15T and V188D, while the addition of N37A and G157V to Ru85

revealed Ru87 (sequence alignment with mRuby2: Appendix Figure 6.2-1). In the following, Ru63, Ru85 and Ru87 were characterized in detail regarding their switching properties. In addition, the new RSFPs were compared to the only available monomeric, red fluorescent and positive-switching protein, rsCherry [91].

3.2.2 Switching characterization of Ru63, Ru85 and Ru87 expressed in *E. coli*

The detailed switching characterization of Ru63, Ru85 and Ru87 and the comparison to rsCherry was performed by the expression in *E. coli* colonies and the acquisition of switching curves using the automated microscope at room temperature (chapter 2.4.1.2). The thermal relaxation from the off- and on-state to the equilibrium was investigated in two independent experiments (different transformations) with measurements at four colonies for each data point. All other characterizations were done in three independent experiments with measurements at four to ten colonies for each data point.

3.2.2.1 Ensemble brightness and off-state fluorescence of positive RSFPs

First, the ensemble brightness in *E. coli* colonies was compared for Ru63, Ru85, Ru87 and rsCherry. Therefore, the bacterial colonies were grown at 30 °C or 37 °C for two days (Figure 3.2-4 A). The RSFPs were completely switched on with light of 561 nm (14.5 $kWcm^{-2}$) and the on-state fluorescence signal was measured. For the switchable mRuby2 variants, the fluorescence in the on-state was higher for the colonies grown at 37 °C than for the colonies grown at 30 °C (factor 1.5 to 1.8). The expression at 37 °C yielded a 1.3 times higher fluorescence for Ru85 and a 1.8 times higher fluorescence for Ru87 in comparison to Ru63.

The RSFP rsCherry was barely expressed at 37 °C (reduced by the factor of 0.15 compared to 30 °C) and exhibited a 1.9 to 4.5-fold lower fluorescence in the on-state than Ru63, Ru85 and Ru87 at 30 °C. However, spectral differences between the switchable mRuby2 variants and rsCherry might slightly contribute to a lower fluorescence signal for rsCherry. For further characterizations, rsCherry was expressed at 30 °C and the switchable mRuby2 variants at 37 °C.

The residual fluorescence in the off-state relative to the on-state fluorescence was as well determined for the positive-switching RSFPs. The proteins were switched off with light of 445 nm (14.9 $kWcm^{-2}$) and switched on with light of 561 nm (14.5 $kWcm^{-2}$). Under this condition, the determined residual fluorescence in the off-state ranged from 4.3-5.1 % for the three switchable mRuby2 variants in both, the first and the second switching cycle

(Figure 3.2-4 B). A residual fluorescence in the off-state of 16 % in the first cycle and of 25 % in the second cycle was measured for rsCherry. A lower residual fluorescence in the off-state of 10 % in the first and 16 % in the second switching cycle was measured for rsCherry, when lower light intensities were used (445 nm: 2.5 kWcm^{-2}, 561 nm: 3.2 kWcm^{-2}; data not shown). However, the switching contrast of each switchable mRuby2 variant was still superior.

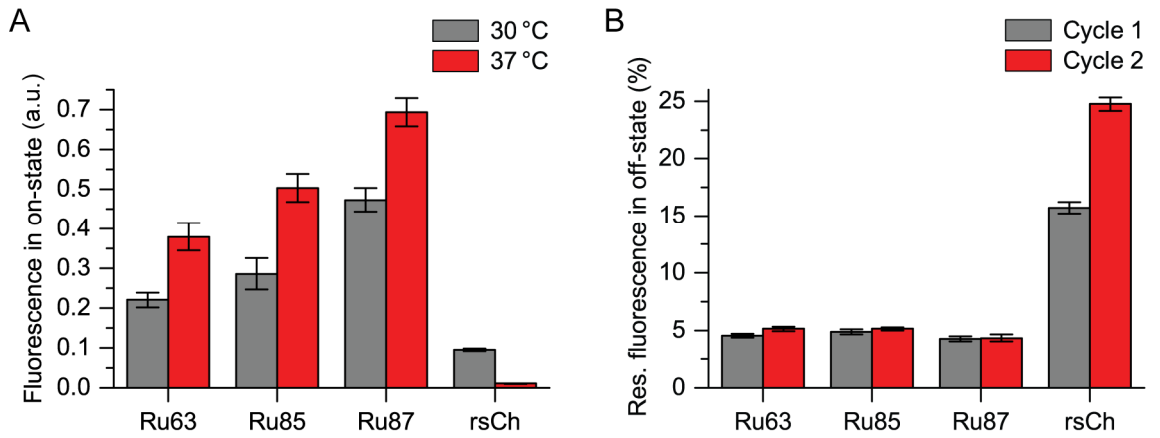

Figure 3.2-4: Ensemble brightness and off-state fluorescence of positive RSFPs.
Comparison of the novel positive-switching proteins Ru63, Ru85 and Ru87 with rsCherry. For all measurements: 445nm: 14.9 kWcm^{-2}, 561 nm: 14.5 kWcm^{-2}. Switching schemes for Ru63, Ru85, Ru87: 12 ms 445 nm, 30 ms 561 nm; for rsCherry: 140 ms 445 nm, 400 ms 561 nm. A: The fluorescence in the on-state of cycle 1 for the different RSFPs expressed at 30 °C (grey) or 37 °C (red) for two days. The mean values and error bars of a single experiment with 10 colonies each are shown. Two repetitions of the experiment yielded comparable ratios. B: The residual fluorescence in the off-state relative to the fluorescence in the on-state in switching cycle 1 (grey) or 2 (red). rsCherry was expressed at 30 °C, Ru63, Ru85 and Ru87 were expressed at 37 °C. The values measured at 10 colonies in each experiment were averaged. The mean values and error bars of three independent experiments are shown.

3.2.2.2 On-switching kinetics of positive-switching proteins

For the measurements of on-switching curves, the positive-switching red RSFPs were switched off by 445 nm laser illumination (14.9 kWcm^{-2}) before the on-switching curves were acquired using light of 561 nm (14.5 kWcm^{-2}). The on-switching curves demonstrated substantial faster on-switching kinetics for the switchable mRuby2 variants than for rsCherry (Figure 3.2-5 A+B). At the applied 561 nm laser intensity, the determined on-switching halftimes of Ru63, Ru85 and Ru87 were 19 times lower than the halftime of rsCherry (Figure 3.2-5 C). In addition, the 561 nm light intensity for on-switching was varied from 3.2 to 63.1 kWcm^{-2} for Ru63, Ru85 and Ru87. These laser intensities yielded on-switching halftimes from 0.3 to 15.7 ms (Figure 3.2-5 D). The on-switching halftimes at each laser intensity was comparable for the three variants. The on-switching halftimes and the laser intensities were not linearly related in the examined intensity range.

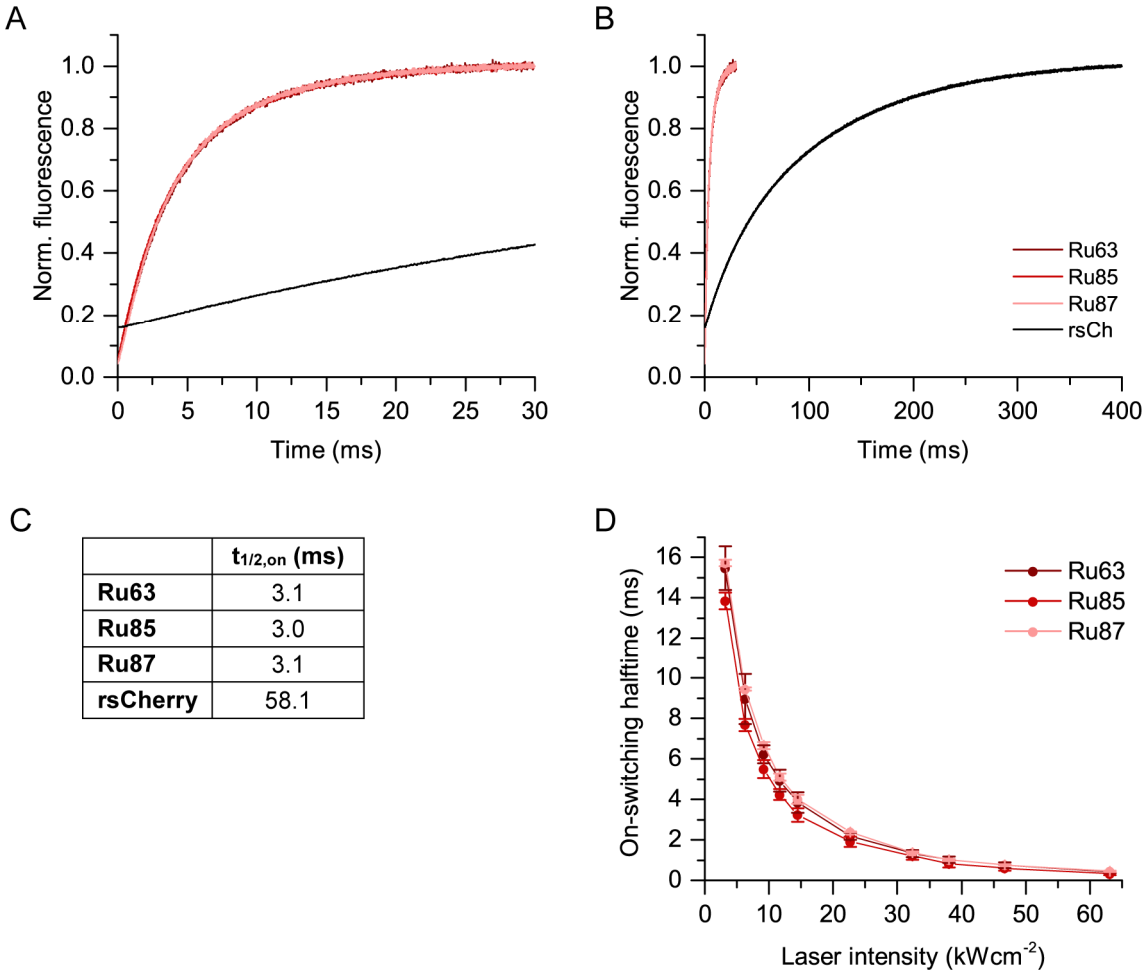

C

	$t_{1/2,on}$ (ms)
Ru63	3.1
Ru85	3.0
Ru87	3.1
rsCherry	58.1

Figure 3.2-5: On-switching kinetics of positive-switching red RSFPs.
A+B: On-switching curves of Ru63 (dark red), Ru85 (medium red), Ru87 (light red) and rsCherry (black) for two different x-axis scales. The curves are normalized to the on-state fluorescence. Switching scheme (445nm: 14.9 kWcm^{-2}; 561 nm: 14.5 kWcm^{-2}) for Ru63, Ru85, Ru87: 12 ms 445 nm, 30 ms 561 nm; for rsCherry: 140 ms 445 nm, 400 ms 561 nm. The averaged curves measured at 10 colonies are shown. Two additional experiments with 10 colonies each showed comparable on-switching kinetics. C: On-switching halftimes determined for the switching curves presented in A+B using a biexponential function. D: The on-switching halftimes in dependency of the 561 nm laser intensity for Ru63, Ru85 and Ru87. The measurements of 4 colonies at each of three experiments were averaged first and the mean values and error bars of the three independent experiments are shown.

3.2.2.3 Off-switching kinetics of positive-switching proteins

Due to the insufficient fluorescence emission induced by the irradiation at 445 nm, the off-switching curves for the positive-switching RSFPs were obtained by modulation of the 445 nm off-switching times (chapter 2.4.1.4). The first fluorescence signal after off-switching received by excitation at 561 nm (14.5 kWcm^{-2}) was normalized to the fluorescence in the on-state and plotted against the off-switching time (Figure 3.2-6). The off-switching times for the chosen 445 nm laser intensity (2.5 kWcm^{-2}) were as well considerably lower for the switchable mRuby2 variants than for rsCherry. The determined

off-switching halftimes were 0.67 ms for Ru63, 0.48 ms for Ru87, 0.51 ms for Ru87 and 48 ms for rsCherry.

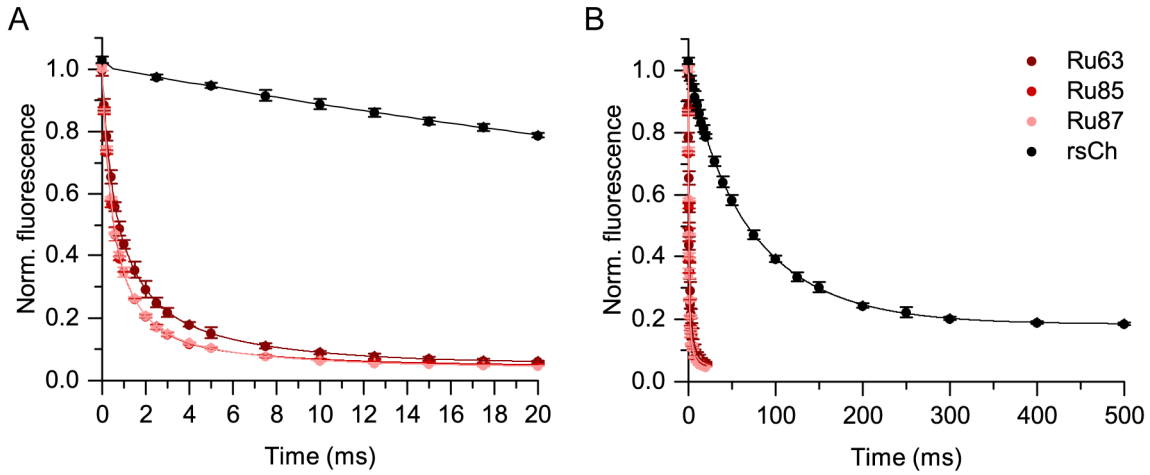

Figure 3.2-6: Off-switching kinetics of positive-switching red RSFPs.
A+B: Off-switching curves of Ru63 (dark red), Ru85 (medium red), Ru87 (light red) and rsCherry (black) for two different x-axis scales. Switching scheme (445nm: 2.5 kWcm^{-2}; 561 nm: 14.5 kWcm^{-2}) for Ru63, Ru85, Ru87: 25 ms 561 nm, 0-20 ms 445 nm, 25 ms 561 nm; for rsCherry: 400 ms 561 nm; 0-500 ms 445 nm; 400 ms 561 nm. The first fluorescence after off-switching divided by the on-state fluorescence signal was plotted against the 445 nm switching time. The curves were fitted by a biexponential function. In a single experiment, each data point was measured at 5 different colonies. The mean values and error bars of the three independent experiments are shown.

3.2.2.4 Switching fatigue of positive-switching proteins

For the comparison of switching fatigue, the positive-switching RSFPs were repetitively switched on and off to 95 % (chapter 2.4.1.5) using light of 561 nm (14.5 kWcm^{-2}) and 445 nm (2.5 kWcm^{-2}). The irradiation times for switching the proteins to 95 % (listed in Figure 3.2-7 B) were determined on the basis of the on- and off-switching curves acquired with the same laser intensities (Figure 3.2-5, Figure 3.2-6). In Figure 3.2-7 the minimal and maximal signal of each on-switching curve was normalized to the maximal signal of the second switching cycle. Using these light intensities, rsCherry showed extremely high switching fatigue, resulting in a loss of switching after 40 cycles. In switching cycle 40, the maximal fluorescence signal was reduced to 58 % for rCherry and only to 85-89 % for the switchable mRuby2 variants (Figure 3.2-7 C). The switching fatigue curves revealed, that Ru63, Ru85 and Ru87 could be switched more than 350 times before the maximal fluorescence decreased to 50 %. The minimal fluorescence signal represents the fluorescence in the off-state, which increased for all three switchable mRuby2 variants during repetitive switching, but strongest for Ru63.

A

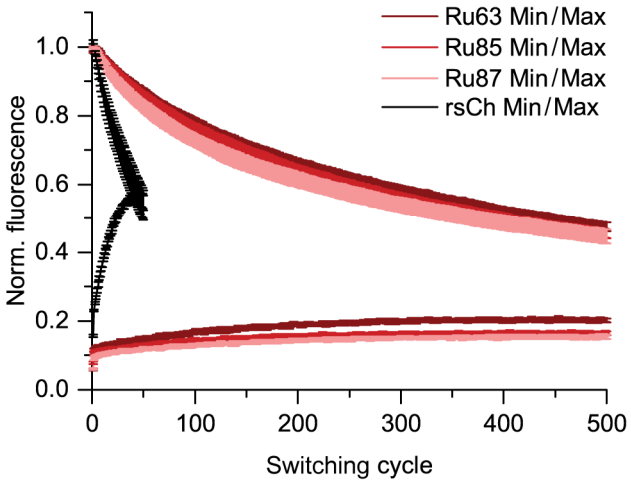

B

	Switching 445 nm (ms)	Switching 561 nm (ms)
Ru63	6.7	15.3
Ru85	4.5	15.3
Ru87	4.9	15.6
rsCh	218.7	259.2

C

	Max. signal cycle 40	Cycles until 50 %
Ru63	89%	431
Ru85	88%	423
Ru87	85%	367
rsCh	58%	/

Figure 3.2-7: Switching fatigue of positive-switching red RSFPs.
A: Repeated switching of Ru63 (dark red), Ru85 (medium red), Ru87 (light red) and rsCherry (black). The proteins were switched off with 445 nm (2.5 kWcm^{-2}) and on with 561 nm (14.5 kWcm^{-2}) to 95 % on the basis of the switching curves measured before (switching times: see B). Ru63, Ru85, Ru87: 500 switching cycles; rsCherry: 40 switching cycles. The switching curves were normalized to the maximal fluorescence in cycle 2. The minimal and maximal fluorescence signal of the on-switching curve are plotted against the switching cycle. The mean values and error bars of one experiment with 10 colonies each are shown. Two repetitions of the experiment yielded comparable results. B: Applied switching times for the switching fatigue measurements C: The table lists the maximal signal in switching cycle 40 relative to cycle 2 and the number of cycles until 50 % of the maximal fluorescence of cycle 2 is reached. These values were determined using averaged curves of three individual experiments.

3.2.2.5 Alternative off-switching wavelengths for Ru63, Ru85 and Ru87

The wavelengths 405 nm and 488 nm are typical switching wavelengths for green RSFPs. In order to examine the potential for simultaneous switching in dual color RESOLFT, these wavelengths were tested as alternative off-switching wavelengths for Ru63, Ru85 and Ru87. The proteins were switched on with light of 561 nm (3.2 kWcm^{-2}) and subsequently switching curves were acquired by simultaneous laser irradiation at 561 nm (2.6 kWcm^{-2}) and 405 nm, 445 nm or 488 nm. Using light of 445 nm with an intensity of 2.5 kWcm^{-2}, the off-switching was dominant. Adjusting the laser intensities to 7.5 kWcm^{-2} for 405 nm and to 10.4 kWcm^{-2} for 488 nm, off-switching curves with comparable switching kinetics were observed (Figure 3.2-8 A, C, E). After 10 ms of simultaneous switching, the fluorescence signal of each variant was decreased to a similar level for the three different wavelengths (Ru63: 17.7-18.7 %, Ru85: 11.7-13.0 %, Ru87: 11.9-12.0 %).

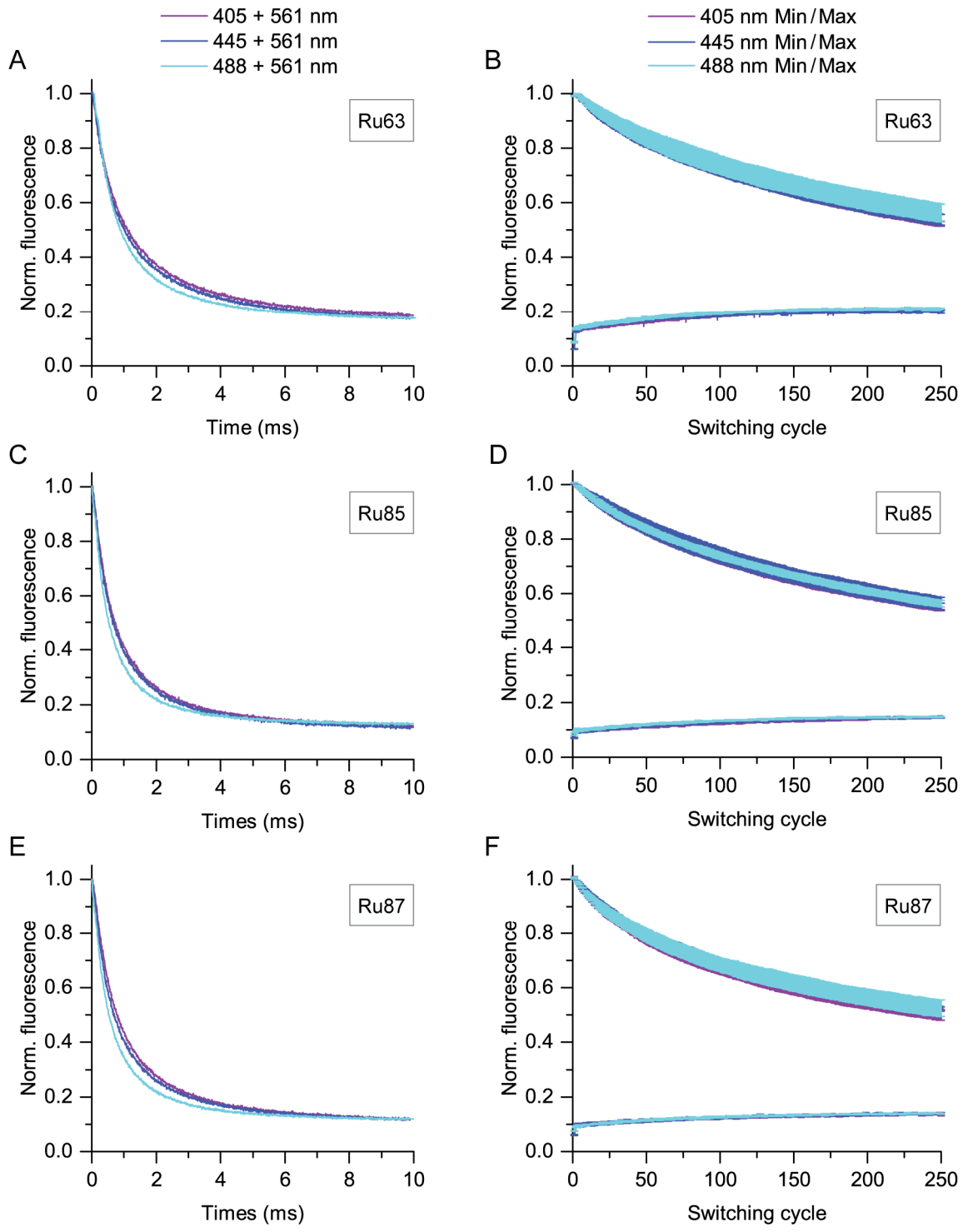

Figure 3.2-8: Alternative off-switching wavelengths for Ru63, Ru85 and Ru87.
405 nm: purple, 7.5 kWcm^{-2}; 445 nm: blue, 2.5 kWcm^{-2}; 488 nm: cyan, 10.4 kWcm^{-2}. Averaged curves of three individual experiments with 5 colonies each. A (Ru63), C (Ru85), E (Ru87): Off-switching curves resulting from simultaneous laser irradiation at 561 nm (2.6 kWcm^{-2}) and at 405, 445 or 488 nm after switching into the on-state (80 ms 561 nm, 3.2 kWcm^{-2}). The fluorescence was normalized to the on-state fluorescence. B (Ru63), D (Ru85), F (Ru87): Switching fatigue curves for the different off-switching wavelengths, 250 switching cycles. Switching scheme: Alternating 7 ms 405 nm, 445 nm or 488 nm and 20 ms 561 nm (14.5 kWcm^{-2}).The minimal and maximal fluorescence signal of the on-switching curves were normalized to the maximal signal in cycle 2 and plotted against the switching cycle.

The laser intensities for 405 nm, 445 nm and 488 nm which were found to induce similar switching kinetics were used for repetitive switching of Ru63, Ru85 and Ru87 (Figure 3.2-8 B, D, F). The same switching scheme was applied for all measurements and 250 switching cycles were acquired. For each switchable mRuby2 variant, the switching fatigue curves for the different off-switching wavelengths were comparable. Thus, 405 nm and 488 nm represent potential alternatives to 445 nm for the off-switching of Ru63, Ru85 and Ru87, however, higher light intensities are necessary to achieve the same effect.

3.2.2.6 Equilibrium state and thermal relaxation from the on- and off-state

Finally, the equilibrium state and the thermal relaxation from the on- and off-state to the thermal equilibrium were investigated utilizing the automated microscope (chapter 2.4.1.6). The measurements revealed 10 % of the on-state fluorescence signal at the equilibrium of Ru63, 32 % at the equilibrium of Ru85 and 20 % at the equilibrium of Ru87 (Figure 3.2-9). Interestingly, the equilibrium state differs for the three variants, although all other characteristics analyzed so far showed a high similarity.

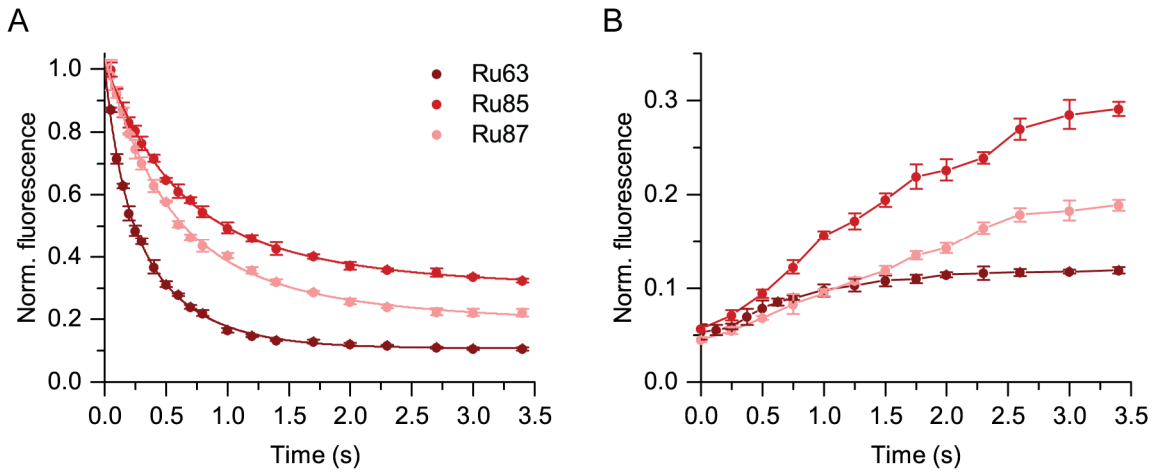

Figure 3.2-9: Thermal relaxation to the equilibrium state for Ru63, Ru85 and Ru87.
A+B: Dark red: Ru63, medium red: Ru85, light red: Ru87. A: The thermal relaxation from the on-state to the equilibrium after 30 ms of on-switching at 561 nm (14.5 kWcm^{-2}). The relaxation curves were fitted using a biexponential function. B: The thermal relaxation from the off-state to the equilibrium state after 12 ms of off-switching at 445 nm (14.9 kWcm^{-2}). A+B: The proteins were switched on (A) or off (B) and the fluorescence after varying breaks was measured by 561 nm excitation (14.5 kWcm^{-2}). The first fluorescence signal after the break was normalized to the on-state signal and plotted against the duration of the break. The mean values and error bars of a single experiment with measurements at 4 colonies for each data point are presented. A repetition of both experiments yielded comparable result.

The thermal relaxation from the on- (Figure 3.2-9 A) and off-state (Figure 3.2-9 B) was tracked for Ru63, Ru85 and Ru87. All three proteins relaxed from the on- and off-state to the equilibrium in less than 4 s. The determined halftimes for the relaxation from the on-

state revealed that Ru63 ($t_{1/2,on\text{-}relax}$ = 216 ms) relaxed 2.1-2.2 times faster than Ru85 ($t_{1/2,on\text{-}relax}$ = 478 ms) and Ru87 ($t_{1/2,on\text{-}relax}$ = 470 ms). No halftimes were determined for the relaxation from the off-state. However, Ru63 relaxed also faster from the off-state than Ru85 and Ru87.

To conclude on the performed switching characterizations, the switchable mRuby2 variants Ru63, Ru85 and Ru87 outperformed the only available monomeric, positive-switching red RSFP rsCherry in all analyzed switching characteristics. Most switching characteristics of the three variants Ru63, Ru85 and Ru87 were comparable. The major differences were found in the equilibrium state of the proteins and in the ensemble brightness measured in *E. coli*. The wavelengths 405 nm and 488 nm represent suitable alternatives for the off-switching. All three variants were analyzed further in the following.

3.2.3 Characterization of isolated Ru63, Ru85 and Ru87 protein samples

For further characterizations, all three mRuby2 variants were expressed in *E. coli* and isolated. The standard protein purification protocol had to be adjusted, because the isolated Ru63, Ru85 and Ru87 proteins tended to precipitate (protocol: chapter 2.3.1.2). The switchable mRuby2 variants could be purified in a sufficient quantity and purity (controlled in SDS-PAGE, see Appendix Figure 6.3-1 A) when 1 mM EDTA and 1 mM DTT were added to the buffers and sonication was used for lysis. The fluorescent proteins mRuby2, mCherry and dTomato were purified using the same protocol for comparison.

3.2.3.1 Spectral characteristics of the switchable mRuby2 variants

The absorption spectra of the purified Ru63, Ru85 and Ru87 samples in comparison to the absorption spectrum of mRuby2 revealed a distinct lower absorption of the deprotonated chromophore in the range of 500 to 600 nm (Figure 3.2-10 A). In this range, the Ru63 absorption spectrum displayed a main and a minor maximum, while Ru85 and Ru87 showed a broad absorption peak in this region (Figure 3.2-10 B). The main maximum is shifted from 560 nm for the template protein mRuby2 to 570 nm for Ru63, 565 nm for Ru85 and 562 nm for Ru87. For the three switchable variants, an absorption maximum in the region of 390 to 400 nm was detected, which might be the absorption of an incomplete matured chromophore (chapter 1.2.2). For Ru85 and Ru87 a smaller maximum at about 450 nm was visible, which might be the absorption band of the protonated chromophore. No changes in the absorption spectra were detectable when the protein solutions of Ru63, Ru85 and Ru87 were illuminated with blue or yellow-green light for switching

(chapter 2.3.5; data not shown). This might be due to the rapid relaxation of these RSFPs from the on- and off-state to the equilibrium (see chapter 3.2.2.6).

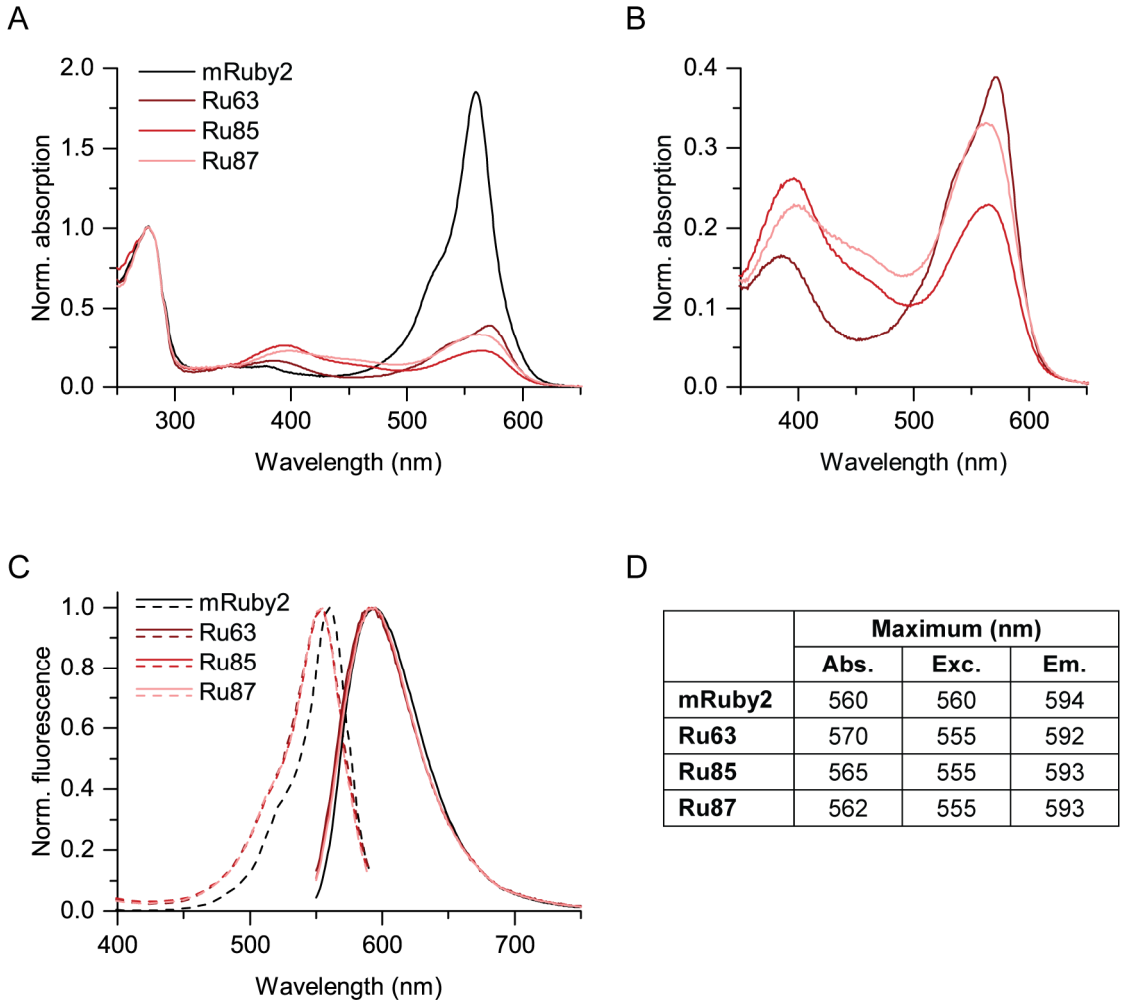

	Maximum (nm)		
	Abs.	**Exc.**	**Em.**
mRuby2	560	560	594
Ru63	570	555	592
Ru85	565	555	593
Ru87	562	555	593

Figure 3.2-10: Spectra of mRuby2 and the generated switchable variants.
A-C: black: mRuby2, dark red: Ru63, medium red: Ru85, light red: Ru87. Averaged spectra of three independent protein samples. A+B: Absorption spectra normalized to the maximum absorbance at 280 nm. B: Detailed section of the absorption spectra from 350-650 nm for Ru63, R85 and Ru87. C: Excitation (dashed lines, Em: 600 nm) and emission spectra (solid lines, Exc: 540 nm) normalized to the maximal fluorescence. D: Wavelengths at maximal absorption or fluorescence.

The shape of the excitation spectrum was similar for mRuby2 and the switchable variants, but the maxima were shifted by 5 nm to the blue region of the spectrum for Ru63, Ru85 and Ru87 (Figure 3.2-10 C). The emission spectra of mRuby2 and the switchable variants were comparable as well, with shifts of 1-2 nm (Figure 3.2-10 D).

3.2.3.2 Fluorescence and extinction characteristics of Ru63, Ru85 and Ru87

The quantum yield (QY) of Ru63, Ru85 and Ru87 was measured by two different methods (chapter 2.3.7). In the first method based on the emission spectra, the quantum yield was

determined relative to the published quantum yield of mRuby2 (QY: 0.38 [57]). As the switchable mRuby2 variants are not stable in the on-state (chapter 3.2.2.6), the quantum yield could only be determined for the RSFPs in the equilibrium state in this method. Applying the relative method, low quantum yields of 3.8-7.7 % were measured (Table 4). In the second method, the quantum yield was determined using the nanocavity-based method [169]. This method is independent from the state of the RSFPs, since the method is based on the measurement of fluorescence lifetimes and detects only fluorescent molecules. The nanocavity-based method yielded substantial higher quantum yields of 18-20 % for the switchable mRuby2 variants (conducted by Alexey I. Chizhik, Third Institute of Physics, Georg August University, Göttingen). Despite the different values determined in the two methods, the highest quantum yield was determined for Ru87 in both methods. The QY published for rsCherry is only about 2 % [178].

Table 4: Fluorescence and extinction characteristics of Ru63, Ru85 and Ru87.
QY (absolute method): Single measurement, fluorescence lifetime: Two independent protein samples (measured by Alexey I. Chizhik). QY (relative method) and extinction coefficient: Three independent protein samples.

FP	QY (%)		ε ($M^{-1}cm^{-1}$)	Lifetime (ns)
	relative method (spectra)	nanocavity-based method		
Ru63	3.8 ± 0.1	18	24,021 ± 3513	1.13
Ru85	7.4 ± 0.3	17	14,098 ± 2280	1.20
Ru87	7.7 ± 0.4	20	20,464 ± 3603	1.25
mRuby2	38*		113,000*	2.5*

** Data taken from [57]*

For Ru63, Ru85 and Ru87, the extinction coefficient (ε) of the deprotonated chromophore was determined in the equilibrium state and relative to the published value of mRuby2 (113,000 $M^{-1}cm^{-1}$). The extinction coefficients of Ru63, Ru85 and Ru87 were distinctly lower than the extinction coefficient of mRuby2 (Table 4) and also lower than the one of rsCherry (80,000 $M^{-1}cm^{-1}$ [178]). The fluorescence lifetimes decreased by the factor of 2.0-2.2 for all three variants in comparison to their template protein mRuby2.

3.2.3.3 The pH stability of Ru63, Ru85 and Ru87

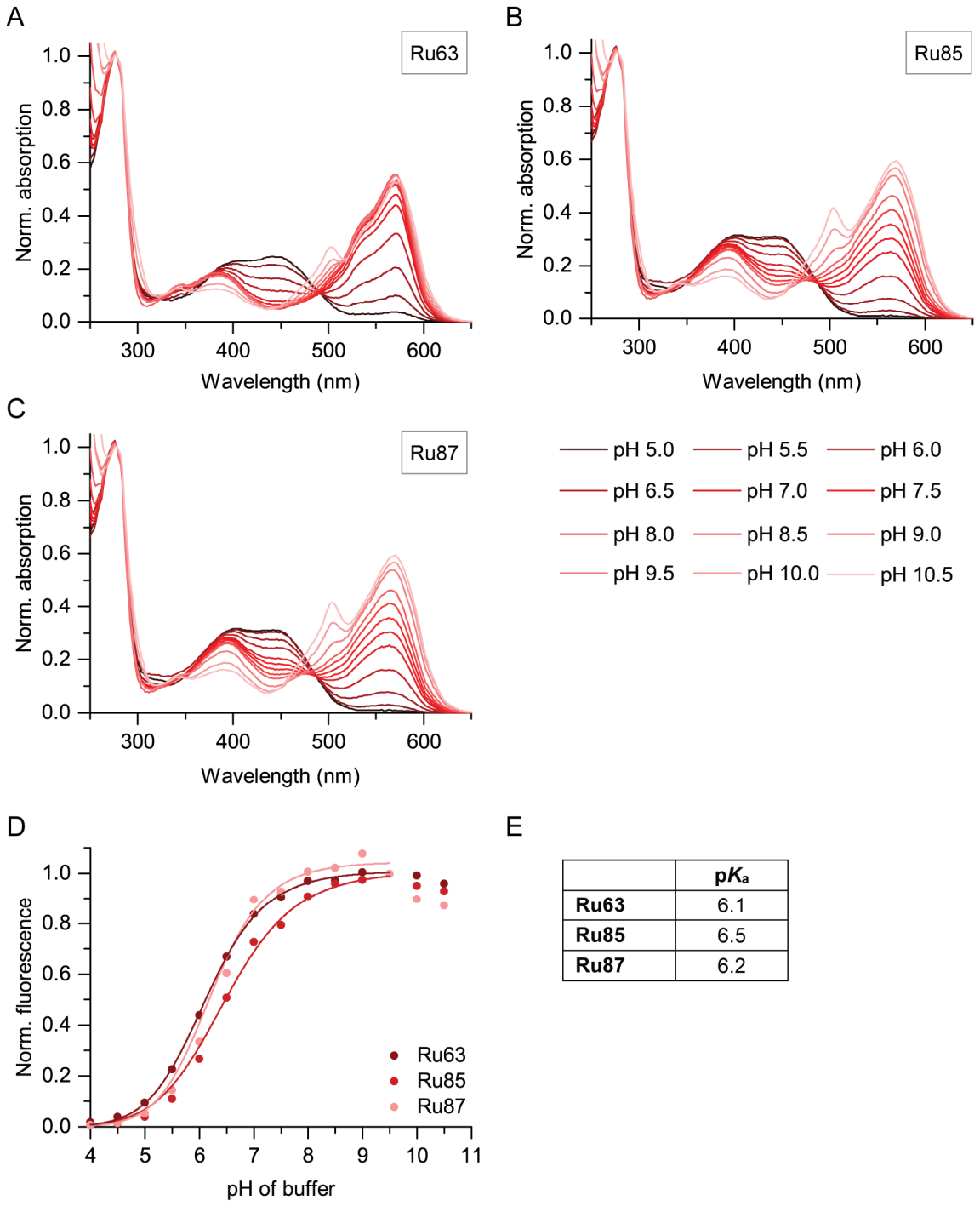

	pK_a
Ru63	6.1
Ru85	6.5
Ru87	6.2

Figure 3.2-11: Effect of the pH on absorption and fluorescence of Ru63, Ru85 and Ru87.
A-C: Absorption spectra of the novel positive-switching RSFPs at different pH values (pH 5.0 to 10.5 in red shades from dark to light) normalized to the absorption at 280 nm. A: Ru63, B: Ru85, C: Ru87. Averaged spectra of three replicates are plotted. An independent repetition yielded comparable results. D: Fluorescence signals (Exc: 560 nm, Em: 595 nm) of protein samples diluted in different pH buffers normalized to the fluorescence at pH 9.5. Dark red: Ru63, medium red: Ru85, light red: Ru87. Averaged values of two independent experiments with three replicates each and fit functions of the data (see chapter 2.3.8) from pH 4 to 9.5 are shown. E: pK_a values determined from data in D.

The influence of the pH on the absorption spectra and on the fluorescence was examined by dilution of the purified Ru63, Ru85 and Ru87 samples in buffers with different pH values (chapter 2.3.8). For all of the three proteins, the absorption between 520 and 600 nm increased with rising pH values, which was assigned to be the absorption of the deprotonated chromophore (Figure 3.2-11 A-C). In this range, the absorption of Ru63 reached its maximum at pH 8.0, while the absorption of Ru85 and Ru87 increased until the highest tested pH value of 10.5. The absorption band between 430 and 470 nm emerged with decreasing pH values and was assigned to be the absorption of the chromophore with a protonated hydroxyphenyl ring. At particularly high pH values (9-10.5) an additional sharp absorption maximum at about 500 nm became apparent.

For the analysis of the pH stability, the fluorescence of the isolated proteins samples in the different pH buffers were measured by exciting the proteins at 560 nm and detecting the emission at 595 nm (Figure 3.2-11 D). The fluorescence of Ru63, Ru85 and Ru87 increased with higher pH values due to the deprotonation of the chromophores. However, the fluorescence slightly decreases above pH 9-9.5 and this is especially visible for Ru87. This effect might occur by unfolding of the proteins at high pH values. Fitting of the data from pH 4 to 9.5 (function: see chapter 2.3.8) determined the pK_a values of the switchable mRuby2 variants to 6.1-6.5 (Figure 3.2-11 E).

3.2.3.4 The oligomeric state of the switchable mRuby2 variants

The oligomeric state of the novel red RSFPs was determined by analytical size-exclusion chromatography (chapter 2.3.4). The purified protein samples of dTomato, mCherry, mRuby2 and the switchable mRuby2 variants were diluted to 10 µM and were applied independently to the size-exclusion column at 6 °C. The elution of the proteins was detected by absorption measurements at 280 nm (Figure 3.2-12). The dimeric protein dTomato [58] eluted with a retention volume of 14.75 ml. The proteins mCherry and mRuby2 are both monomers [57, 58], however, the retention volumes of these two proteins were slightly different with 16.04 ml for mCherry and 16.55 ml for mRuby2. Ru63 eluted at 16.24 ml, Ru85 at 16.28 ml and Ru87 at 16.30 ml, which is in the range of the monomeric proteins mCherry and mRuby2.

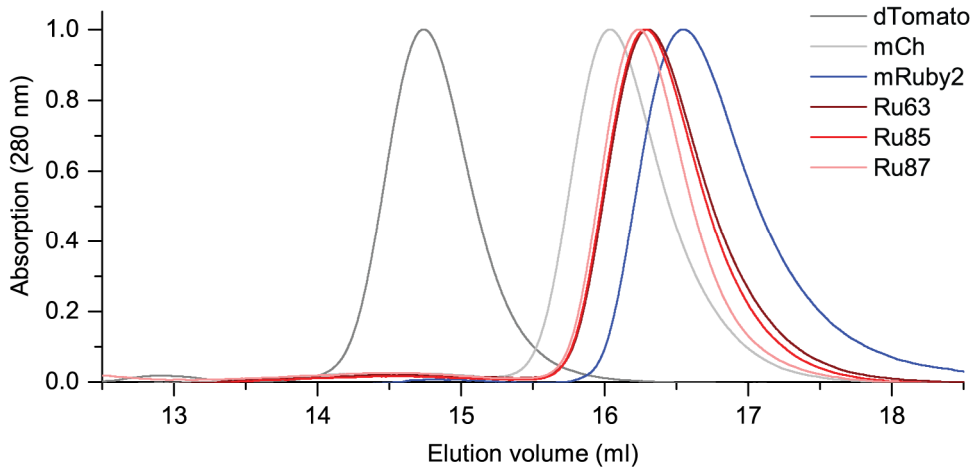

Figure 3.2-12 Size-exclusion chromatography of Ru63, Ru85 and Ru87.
Analytical size-exclusion chromatography of mRuby2, mCherry, dTomato and the generated mRuby2 variants. All proteins were isolated from bacteria with the same purification protocol (see chapter 2.3.1.2). 10 µM protein samples were applied to a Superdex 200 Increase 10/300 L column with a flow rate of 0.75 ml/min at 6 °C. The chromatography profiles at 280 nm are shown. Dark grey: dTomato (dimer); light grey: mCherry (monomer); blue: mRuby2 (monomer); dark red: Ru63; medium red: Ru85; light red: Ru87.

In summary, the characterization of the isolated protein samples revealed some differences for Ru63, Ru85 and Ru87. For instance, the absorption spectra differed for the three variants (Figure 3.2-10). The determined pK_a value for Ru85 (6.5) was slightly higher compared to the pK_a values of Ru63 (6.1) and Ru87 (6.2). All three variants were determined to be monomeric. The variant Ru87 was characterized by the highest quantum yield. In total, Ru87 showed small advantages in some characteristics (e.g. ensemble brightness in *E. coli*, quantum yield). Hence, the investigation of the performance as fusion tags was partly focused on Ru87, but also the characterization of Ru63 and Ru85 was further pursued.

3.2.4 The positive RSFPs used as fusion tags in fluorescence microscopy

An important application of RSFPs is the use as fusion tags in mammalian cells and the imaging of these fusion constructs using conventional or super-resolution microscopy. Hence, the performance of the switchable mRuby2 variants as fusion tag was controlled with a focus on Ru87. The transient expression in various constructs (chapter 3.2.4.1) as well as the stable expression in keratin and vimentin constructs (chapter 3.2.4.2) were analyzed.

3.2.4.1 Transient expression of Ru63, Ru85 and Ru87 in fusion constructs

To control the performance of Ru87 in fusions, eight different fusion constructs were generated (chapter 2.1.9.4), which target different cellular compartments. The prepared

plasmids were used for the transfection of HeLa cells. The day after transfection, the transiently expressed fusion constructs were imaged using confocal microscopy (chapter 2.4.2). The expected localizations were observed for all eight constructs (Figure 3.2-13).

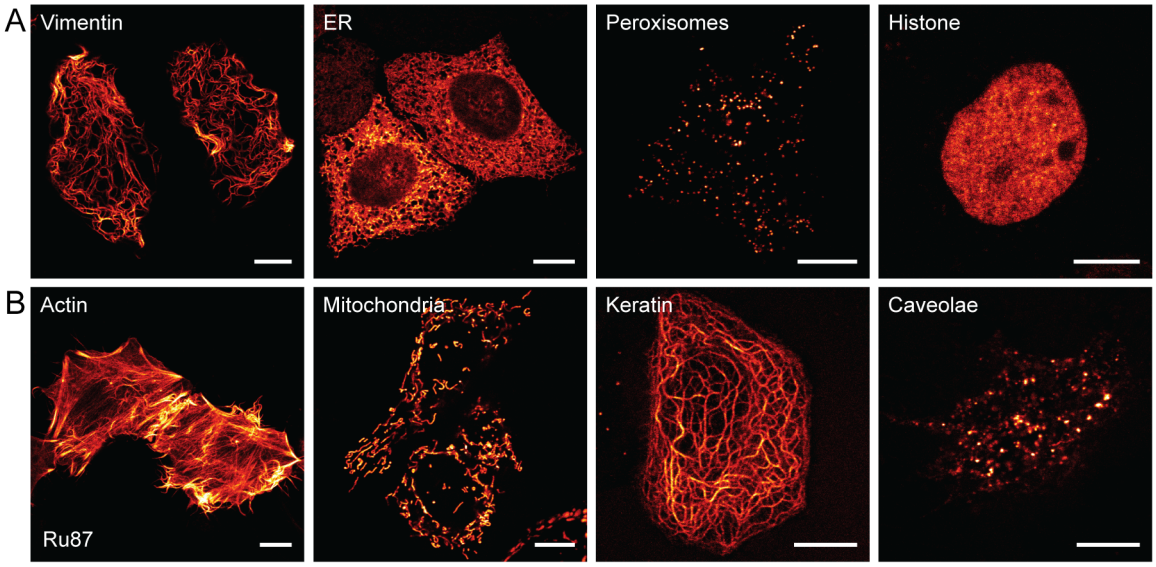

Figure 3.2-13: Fusion constructs of the switchable Ru87 expressed in HeLa cells.
Confocal images of Ru87 fusion constructs transiently expressed in HeLa cells and excited at 561 nm. A (from left to right): Vimentin-Ru87, Ru87-ER (ER signal), Ru87-PTS (peroxisomal targeting signal), Ru87-Histone1 (H2BN). B (from left to right): Lifeact-Ru87, Mito-Ru87 (mito targeting signal), Keratin-Ru87 (keratin18), Caveolin1-Ru87. Scale bars: 10 µm.

Cytoskeleton components were visualized by the expression of Lifeact, vimentin and keratin constructs. In addition, Ru87 was targeted to the cell organelles mitochondria, endoplasmic reticulum (ER) and peroxisomes by fusion to the respective targeting signal peptides. The localization to the nucleus and caveolae were achieved by Histone1 H2BN and Caveolin1 fusions. While Ru87 was applied as an N-terminal tag for the ER signal, the peroxisomal targeting signal and for Histone1, it served as a C-terminal tag in all other fusions. Consequently, Ru87 was applicable for targeting different cell compartments as N- or C-terminal tag in HeLa cells and will be probably suitable as a tag in other applications as well.

Since Ru87 performed well in the tested fusion constructs and contained all mutations of Ru63 and Ru85, the two variants Ru63 and Ru85 were assumed to be applicable in the same fusion constructs. Nevertheless, the fusion constructs of vimentin, the ER signal, the peroxisomal targeting signal and Histone1 were also generated and tested for these two RSFPs. Confocal imaging of HeLa cells transfected with the Ru63 and Ru85 constructs revealed the same expected localizations (Figure 3.2-14).

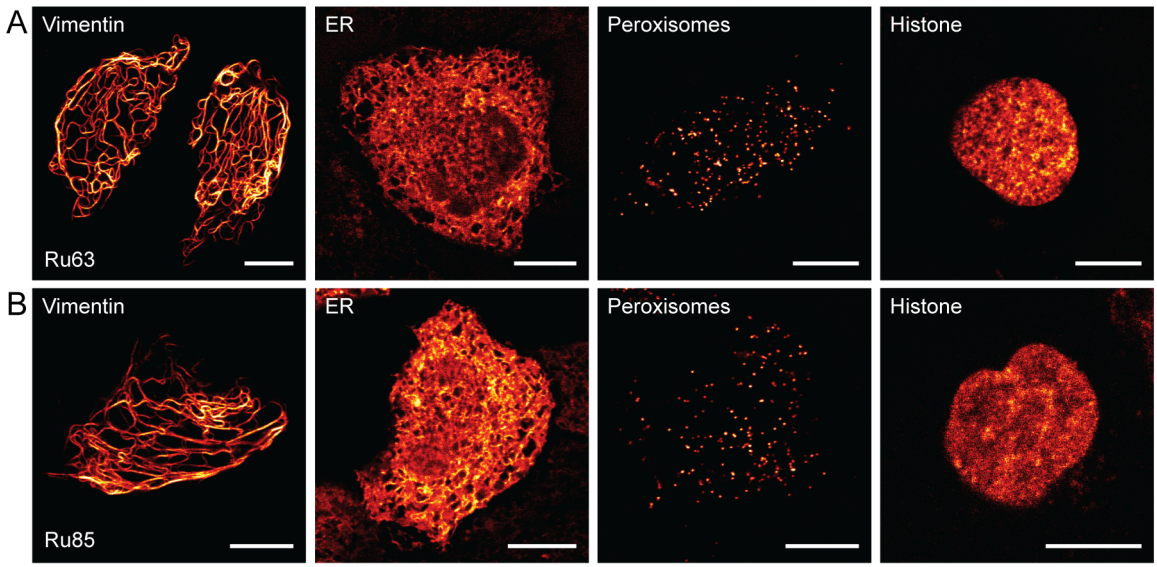

Figure 3.2-14: Fusion constructs of Ru63 and Ru85 expressed in HeLa cells.
Confocal images of Ru63 (A) and Ru85 (B) fusion constructs transiently expressed in HeLa cells and excited at 561 nm. A (from left to right): Vimentin-Ru63, Ru63-ER (ER signal), Ru63-PTS (peroxisomal targeting signal), Ru63-Histone1. B (from left to right): Vimentin-Ru85, Ru85-ER (ER signal), Ru85-PTS (peroxisomal targeting signal), Ru85-Histone1. Scale bars: 10 µm.

3.2.4.2 Stable expression of Ru63, Ru85 and Ru87 constructs

The stable expression of fusion constructs gains more and more importance in cell biology. To test the applicability of Ru63, Ru85 and Ru87 in long-term expressions, monoclonal cell lines stably expressing keratin fusions were generated using the K21 cell line developed in this work (chapter 3.1.2). For this, K21 cells were cotransfected with the plasmids pCAG-NLS-HA-Bxb1 and pInt-Keratin-Ru63, pInt-Keratin-Ru85 or pInt-Keratin-Ru87. Single fluorescent cells were sorted into 96 well plates. For each approach, a stably expressing monoclonal cell line was selected and imaged in confocal microscopy (Figure 3.2-15 A-C). The expression of the keratin fusion constructs was detected in all three cell lines with normal morphology of the cells. A genotyping PCR was conducted on the isolated genomic DNA of these cell lines using a landing pad specific (binding at the end of the CAG promoter) and an mRuby2 specific primer (expected size: 2144 bp). The PCR products were analyzed in gel electrophoresis (Figure 3.2-15 D) and by sequencing. The integration of the plasmids into the Bxb1 landing pad of the K21 cells was thereby verified.

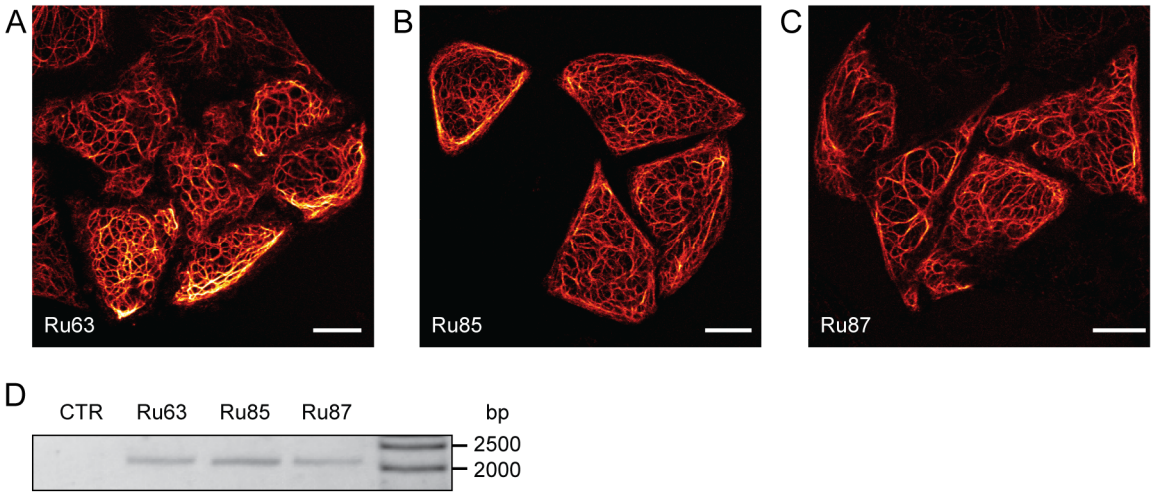

Figure 3.2-15: Stable expression of keratin tagged with Ru63, Ru85 or Ru87.
Monoclonal cell lines were generated by cotransfection of K21 cells with pCAG-NLS-HA-Bxb1 and pInt-Keratin-Ru63/Ru85/Ru87 and single-cell sorting using flow cytometry. A-C: Confocal images of the monoclonal cell lines stably expressing the keratin fusion constructs (Exc: 561 nm). Scale bars: 10 µm. A: Keratin18-Ru63, B: Keratin18-Ru85, C: Keratin18-Ru87. D: PCR products of the genotyping PCRs on genomic DNA of K21 cells (CTR) and of the monoclonal cell lines in A-C analyzed in gel electrophoresis. Expected PCR product size: 2144 bp.

Furthermore, endogenous tagging of the vimentin gene with the Ru87 coding sequence was tested using a comparable CRISPR/Cas9 approach as described in Ratz *et al*., 2015 [97]. Therefore, U2OS cells were cotransfected with the Vimentin-Ru87 donor plasmid and the plasmid encoding the gRNA and Cas9 (chapter 2.1.9.4, chapter 2.2.4). The knock-in of the Ru87 coding sequence was targeted to the C-terminal end of the endogenous vimentin gene. Monoclonal cell lines were generated as described (chapter 2.2.7) and a cell line with positive knock-in was identified in confocal microscopy (Figure 3.2-16 A).

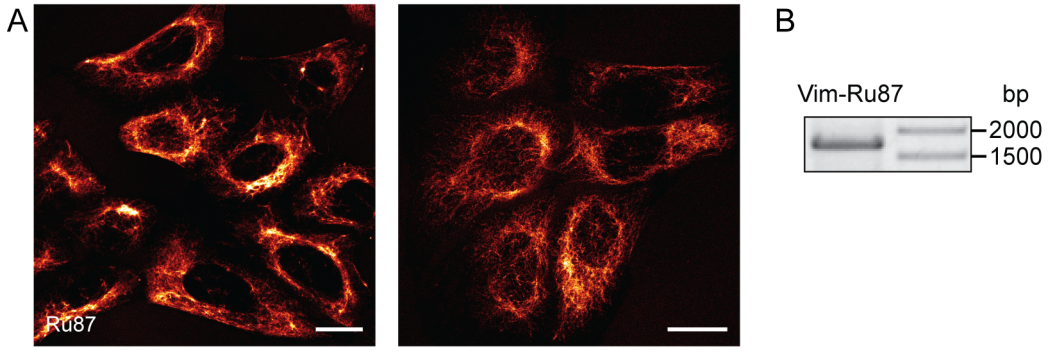

Figure 3.2-16: Tagging of endogenous vimentin with Ru87.
CRISPR/Cas9 genome editing was used to tag endogenous vimentin with Ru87 in U2OS cells. A monoclonal cell lines was generated. A: Confocal images of the monoclonal cell line stably expressing the vimentin-Ru87 fusions (Exc: 561 nm). Scale bars: 20 µm. B: The PCR product of the genotyping PCR on genomic DNA of the monoclonal cell line in A analyzed in analytical gel electrophoresis. Expected PCR product size: 1722 bp.

The knock-in was controlled by a genotyping PCR using a genome-specific and a Ru87 specific primer (expected product: 1722 bp). Analysis of the PCR product by gel electrophoresis (Figure 3.2-16 B) and sequencing verified the knock-in into the vimentin locus. If the cell line is homozygous or heterozygous tagged was not determined.

Cytotoxicity tests were not performed in this work, however, the four generated cell lines were viable, proliferated and stably expressed the fusion constructs for the time of cultivation (weeks to months). The experiments revealed the utility of the switchable mRuby2 variants for the stable expression in mammalian cells. In the next step, the novel positive-switching RSFPs were characterized for their application in live-cell RESOLFT microscopy.

3.2.5 Characterization of Ru63, Ru85 and Ru87 for RESOLFT microscopy

To examine, which of the three novel RSFPs is most suitable for the application in live-cell RESOLFT microscopy, switching curves of Ru63, Ru85 and Ru87 expressed in mammalian cells were acquired. For this purpose, vimentin fusion constructs of the red RSFPs were transiently expressed in HeLa cells. For the switching at each pixel, the pulse generator in the RESOLFT microscope for positive-switching red RSFPs was utilized (chapter 2.4.3.1).

A

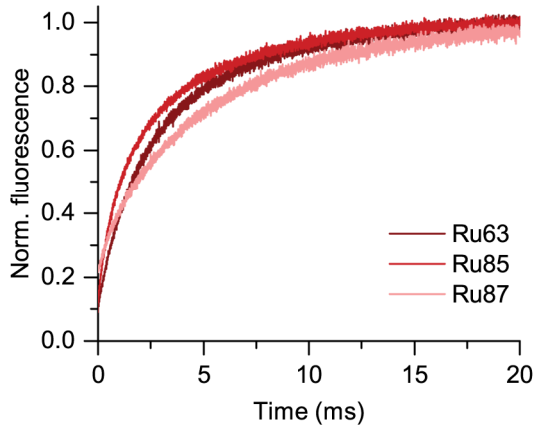

B

	Residual fluo. in off-state	$t_{1/2,on}$ (ms)
Ru63	10.0 ± 0.8 %	2.1 ± 0.2
Ru85	14.0 ± 1.0 %	1.5 ± 0.1
Ru87	22.3 ± 0.8 %	3.1 ± 0.1

Figure 3.2-17: Switching of Ru63, Ru85 and Ru87 in mammalian cells.
A: Vimentin fusion constructs with Ru63 (dark red), Ru85 (medium red) or Ru87 (light red) were transiently expressed in HeLa cells. The proteins were switched off for 8 ms with the doughnut-shaped 445 nm beam (0.48 kWcm^{-2}) and switched on for 20 ms (Ru63, Ru85) or 25 ms (Ru87) at 561 nm (0.43 kWcm^{-2}). The on-switching curves were normalized to the on-state and the averaged curves of one experiment with 5 different cells are shown. B: Residual fluorescence in the off-state relative to the on-state and on-switching halftimes determined for three independent experiments (5 cells each).

In the added switching curves of each pixel, the highest residual fluorescence in the off-state was found for Ru87 (22.3 %), whereas the lowest off-state signal of 10 % was measured for Ru63 (Figure 3.2-17). In contrast to the on-switching kinetics measured in *E. coli* (Figure 3.2-5), the on-switching halftimes for Ru63, Ru85 and Ru87 expressed in the vimentin constructs differed (Figure 3.2-17 B). Although the on-switching halftime of Ru85 was 29 % lower than the on-switching halftime of Ru63, Ru63 was chosen for the establishment of RESOLFT imaging due to the lower residual fluorescence in the off-state (10 % instead of 14 %).

The generated K21 cell line stably expressing keratin-Ru63 (chapter 3.2.4.2) was selected for the first establishment of RESOLFT imaging. For this purpose, the proteins were first switched on with light of 561 nm (2 ms, Gaussian beam, 0.64 kWcm^{-2}), then the Ru63 proteins in the periphery were switched off with the doughnut-shaped 445 nm beam (2 ms, 0.48 kW/cm^{-2}), and finally the fluorescence signal was readout with light of 561 nm (944 µs, Gaussian beam, 0.64 kWcm^{-2}). Afterwards the corresponding confocal image was acquired by on-switching (2 ms) and subsequent readout with light of 561 nm (944 µs, 0.43 kWcm^{-2}). Both, the confocal and RESOLFT images were acquired pixel-by-pixel.

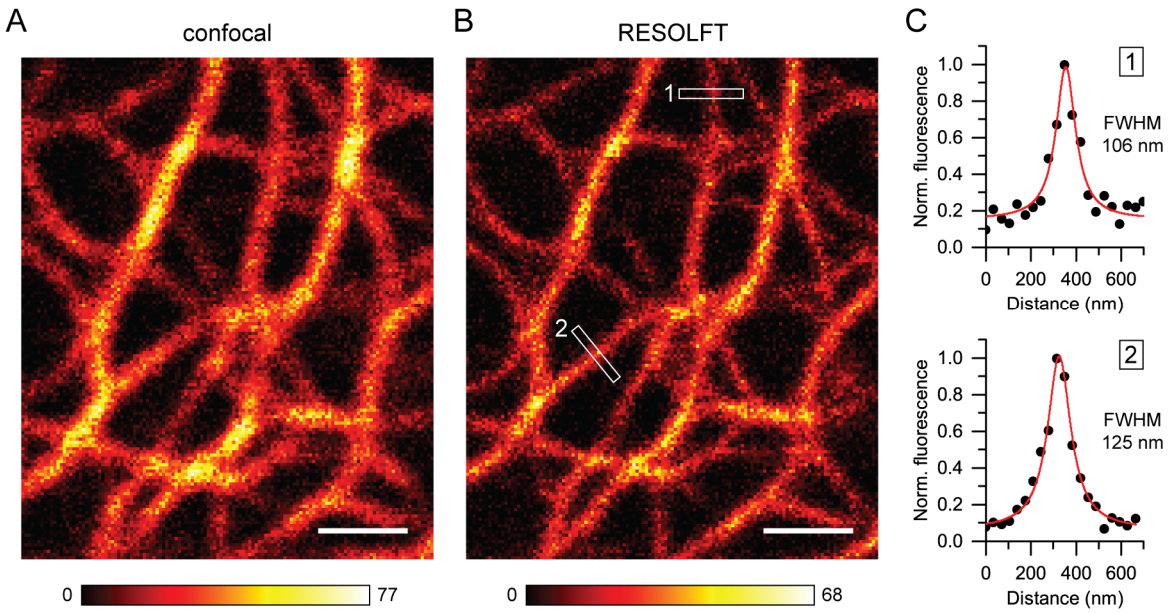

Figure 3.2-18: Point-scanning RESOLFT microscopy using the positive-switching Ru63.
Confocal (A) and RESOLFT (B) microscopy of K21 cells stably expressing keratin-Ru63. Both images display raw data with a pixel size of 35 nm. The color table is given below the respective image. The pinhole was set to 1 Airy unit. Scale bars: 1 µm. Imaging schemes: A: 2 ms on-switching with the Gaussian 561 nm beam, 944 µs readout with the Gaussian 561 nm beam (both 0.43 kWcm^{-2}). B: 2 ms on-switching with the Gaussian 561 nm beam (0.64 kWcm^{-2}), 2 ms off-switching with the doughnut-shaped 445 nm beam (0.48 kW/cm^{-2}), 944 µs readout with the Gaussian 561 nm beam (0.64 kWcm^{-2}). A+B: Only the images of the first 200 µs of the readout are shown. B: The line profiles 1 and 2 were measured at the indicated positions with a three pixels width. C: The lines profiles 1 (above) and 2 (below), as indicated in B, were normalized to the maximal fluorescence and fitted with a Lorentz function (red line). The FWHM was determined using the fit function.

The highest resolution improvement was measured in the RESOLFT image displaying only the fluorescence signals of the first 200 µs of the readout (Figure 3.2-18 A+B). The resolution was analyzed by drawing perpendicular line profiles across the keratin filaments. FWHM of 106 nm and 125 nm were determined (Figure 3.2-18 C), thus a resolution lower than the diffraction-limit was achieved. A slight shift in the field of view was observed from the RESOLFT to the confocal image due to cellular movements or mechanical drift (compare line profiles confocal and RESOLFT image: Appendix Figure 6.3-2). This RESOLFT image represents the first attempts to establish RESOLFT microscopy with the new positive-switchable mRuby2 proteins. To my knowledge, this is the first live-cell RESOLFT image applying a red RSFP with positive-switching mode.

3.3 Novel negative-switching red RSFPs based on mScarlet

In 2017, Bindels *et al.* introduced a new red fluorescent protein named mScarlet [85]. To date, mScarlet is the brightest monomeric fluorescent protein (ε: 100,000 $M^{-1}cm^{-1}$, QY: 0.70) which emits in the red spectral region (maximum: 594 nm). Due to this advantage, mScarlet was selected as template protein for the development of new negative-switching red RSFPs. [85]. The evolution and the characterization of switchable mScarlet proteins is described in this chapter.

3.3.1 Development of novel RSFPs by screening of mutant mScarlet libraries

3.3.1.1 Initial mutagenesis and screening for switchable mScarlet variants

For the development of switchable mScarlet proteins, a mutant mScarlet library was prepared, expressed in bacterial colonies and screened by alternating irradiation at 445 nm and 561 nm using the automated microscope as described before (chapter 3.1.1). Comparable to the development of switchable mRuby2 variants (chapter 3.2.1), the amino acids in the proximity of the chromophore were mutated first in mScarlet. The mutagenesis of the amino acids S147, I162 and M164 yielded various negative-switching variants. All switching variants showed lower cellular brightness than mScarlet. In this initial mutagenesis and screening round, the highest negative-switching capability was measured for the variant mScarlet-I162Q, M164G (Sc1).

At the beginning of this project, the application of red negative-switching RSFPs in live-cell RESOLFT microscopy had only been demonstrated for rsCherryRev1.4, which exhibits

dimerization tendency [98]. Hence, it was aimed to generate monomeric and superior RSFPs with a negative-switching mode from the variant mScarlet-I162Q, M164G. During the process of the development, new negative-switching red RSFPs were introduced by Pennacchietti *et al*. in 2018, which were obtained by mutagenesis of FusionRed. The two RSFPs rsFusionRed2 and rsFusionRed3 were shown to be applicable in live-cell RESOLFT microscopy [118].

3.3.1.2 Switching and screening of negative-switching red RSFPs

The screening for negative-switching mScarlet variants with improved characteristics was performed by alternative on- and off-switching in the automated microscope. Exemplary switching curves for a negative-switching red RSFP are presented in Figure 3.3-1. Laser irradiation at 445 nm was used for on-switching of the RSFPs, while light of 561 nm was used for off-switching.

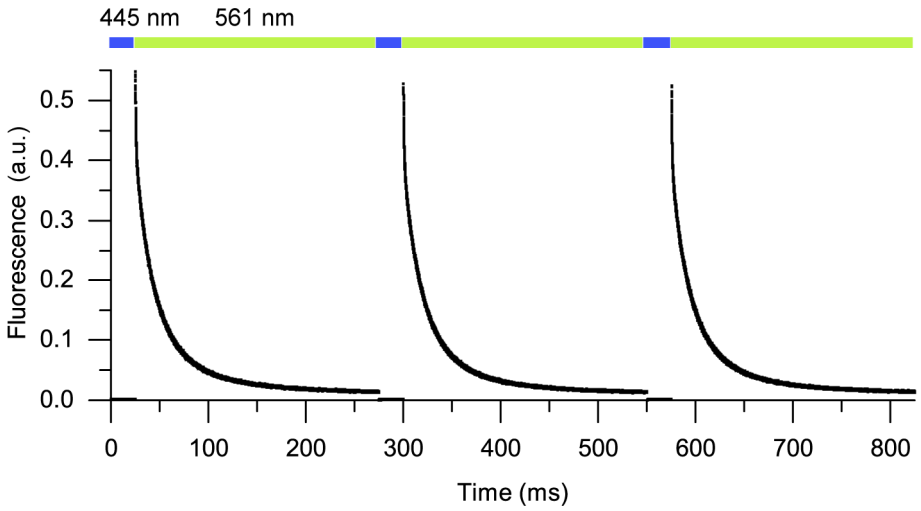

Figure 3.3-1 Switching of a red fluorescent and negative-switching protein.
The graph shows an example for the switching curves of a negative-switching red RSFP expressed in E. coli colonies which were acquired in the automated microscope (in particular: switching curves of Sc21 are shown, see chapter 3.3.1.3). As indicated above the graph, the fluorescence signal resulting from alternating irradiation at 445 nm and 561 nm is plotted against the time. The red RSFPs show no red fluorescence after excitation at 445 nm.

In the screenings, the switching was performed repetitively (chapter 2.4.1.1). The analysis of the switching characteristics was based primarily on the off-switching process. As already described for the screening of mRuby2 variants, switchable mScarlet variants with low residual fluorescence in the off-state, high fluorescence in the on-state, low switching halftimes and low switching fatigue were preferred. The residual fluorescence in the off-state was determined by the ratio of the averaged last points to the first point of the respective off-switching curve.

3.3.1.3 Evolution of negative-switching RSFPs from mScarlet-I162Q, M164G

Mainly site-directed mutagenesis was performed to generate novel negative-switching RSFPs with favorable characteristics in a few mutagenesis and screening rounds. Figure 3.3-2 gives an overview of the mutations added in each round (A) and displays the positions of the mutation sites in the beta-barrel structure of mScarlet (B). To compare the generated variants (Figure 3.3-2 C-F), the same switching scheme was applied for all variants expressed in *E. coli* colonies using the automated microscope (30 ms 445 nm with 2.5 $kWcm^{-2}$, 170 ms 561 nm with 14.5 $kWcm^{-2}$).

Using the given switching scheme and light intensities, the initial variant mScarlet-I162Q, M164T (Sc1) featured an off-switching halftime of 8.9 ms (Figure 3.3-2 F) and 17.2 % residual fluorescence in the off-state (Figure 3.3-2 D). A saturated mutagenesis was performed at position 164 for Sc1 and revealed that an alanine at position 164 (Sc8) reduced the residual fluorescence in the off-state to 13.2 %. However, the addition of this mutation also reduced the fluorescence in the on-state by 25 % (Figure 3.3-2 C).

The site-specific mutation S147G (Sc10) was chosen due to its proximity to the chromophore and strongly reduced the fluorescence in the off-state to 3.2 %. It increased the fluorescence in the on-state by 45 %. In addition, the switching fatigue was strongly reduced, which was observed by a higher on-state fluorescence in cycle 54 relative to cycle 1 (63 % instead of 27 %; Figure 3.3-2 E).

The screening of an error-prone Sc10 library revealed that position R217 can affect the switching characteristics of the switchable mScarlet proteins. The saturated site-directed mutagenesis of this position determined R217Q (Sc19) as most beneficial. In addition, the mutation D161K (Sc21) was introduced based on the findings of Shaner *et al*., who showed that this mutation improved the folding efficiency of mOrange2 (there: E160K) [77]. The D161K mutation improved the ensemble brightness in the on-state, which was reduced by the addition of the mutation R217Q. Both mutation sites were positioned outside the beta-barrel structure (Figure 3.3-2 B close-up). In comparison to Sc10, the addition of R217Q and D161K in Sc21 slightly reduced the residual fluorescence in the off-state (2.2 %) and slightly increased the fluorescence in the on-state. Using the given light intensities, the determined off-switching halftimes differed for the two RSFPs and were 8.9 ms for Sc10 and 5.6 ms for Sc21 (Figure 3.3-2 F).

The negative-switching RSFPs Sc10 and Sc21 were both chosen for further characterizations. Sc10 differs from mScarlet by only three mutations and exhibited already preferable characteristics. Sc21 contains five mutations and was additionally selected due to

the slight improvements in switching (sequence alignment: Appendix Figure 6.2-2). Both variants were characterized in detail regarding their switching characteristics and were compared to the recently published rsFusionRed2 and rsFusionRed3, which were suggested to be the fastest switching red RSFPs so far and to feature a lower residual fluorescence in the off-state than rsCherryRev1.4 [118].

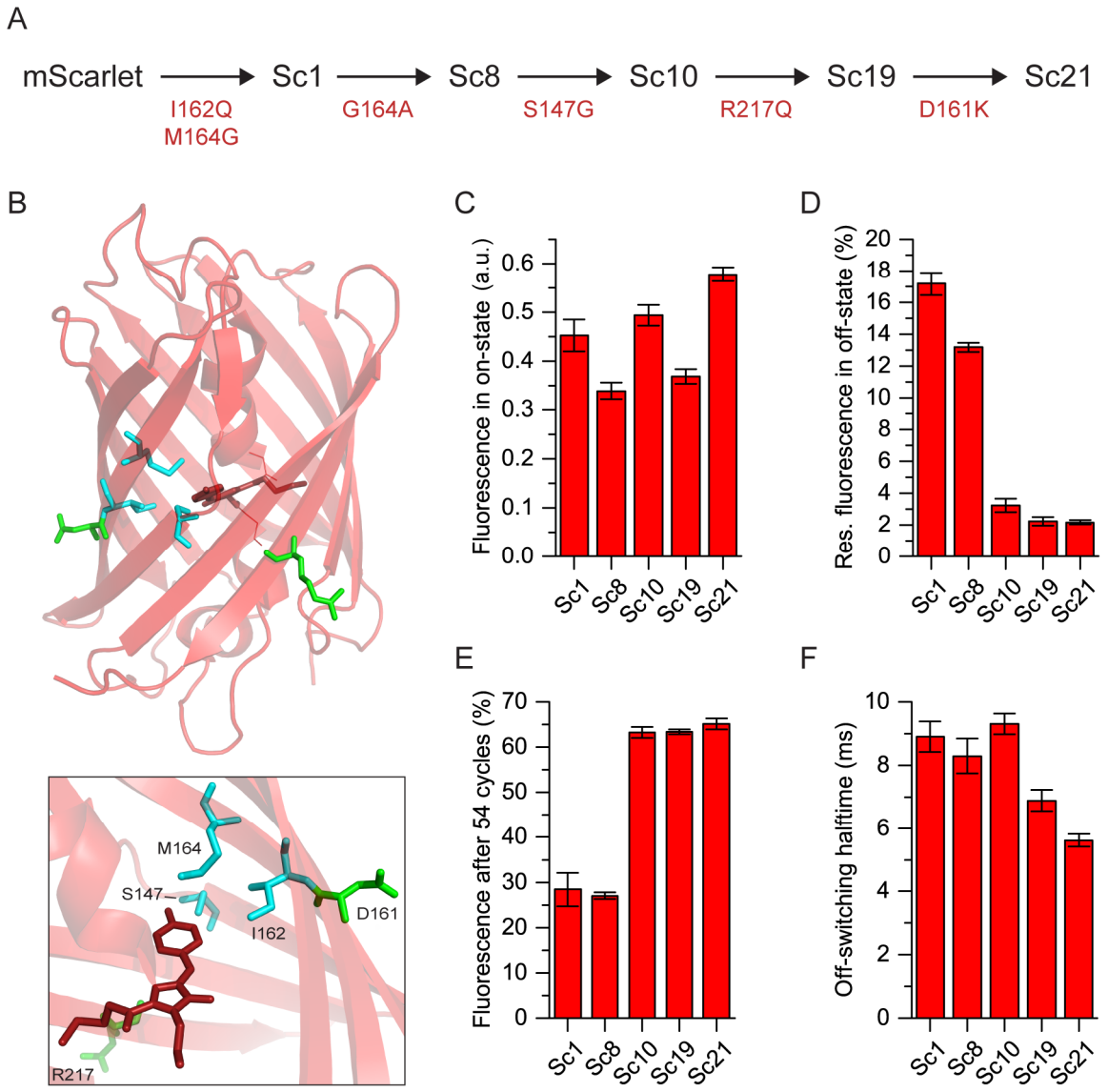

Figure 3.3-2: Development and characterization of negative-switching mScarlet variants.
A. Evolution of the red-emitting and negative-switching mScarlet variants. The mutations added at each step are given below the arrows. B: Localization of the mutation sites (original amino acids) mapped in the structure of mScarlet [85] (PDB: 5LK4) using PyMOL. Green: amino acids outside the beta-barrel, cyan: amino acids inside the beta-barrel, dark red: chromophore. Top: Overview of all mutations in the protein structure of mScarlet. Bottom: Close-up of the chromophore environment. C-F: The switching characterization of the negative-switching mScarlet variants representing the individual rounds of mutagenesis and screening. The switching scheme for all variants: Alternating 30 ms 445 nm (2.5 kWcm^{-2}) and 170 ms 561 nm (14.5 kWcm^{-2}). 5 bacterial colonies grown at 37 °C for 2 days were selected. C, D and F: Values for switching cycle 1. C: Fluorescence signal in the on-state. D: Residual fluorescence in the off-state. E: The ratio of the fluorescence signal in the on-state of cycle 54 relative to cycle 1. F: Off-switching halftimes.

3.3.2 Detailed switching characterization of Sc10 and Sc21

For the detailed switching characterization of Sc10 and Sc21 and the comparison to rsFusionRed2 and rsFusionRed3, the negative-switching red RSFPs were expressed in bacterial colonies (two days at 37 °C) and switched on and off using the automated microscope (chapter 2.4.1.2). All experiments were performed in two to three independent experiments with measurements at five to ten colonies for each data point.

3.3.2.1 Ensemble brightness, off-state fluorescence and equilibrium state of negative RSFPs

The cellular brightness in *E. coli* was measured by the fluorescence signal in the on-state and was compared for the negative-switching RSFPs. Both, Sc10 and Sc21 exhibited 6.8-8.0 times higher fluorescence in the on-state than rsFusionRed2 and rsFusionRed3 (Figure 3.3-3 A). Furthermore, the residual fluorescence in the off-state was determined and no significant increase was observed from the first to the second switching cycle (Figure 3.3-3 B). The determined residual fluorescence in the off-state ranged from 1.8 to 3.4 % for the different RSFPs with the lowest value measured for Sc21 and the highest for rsFusionRed3.

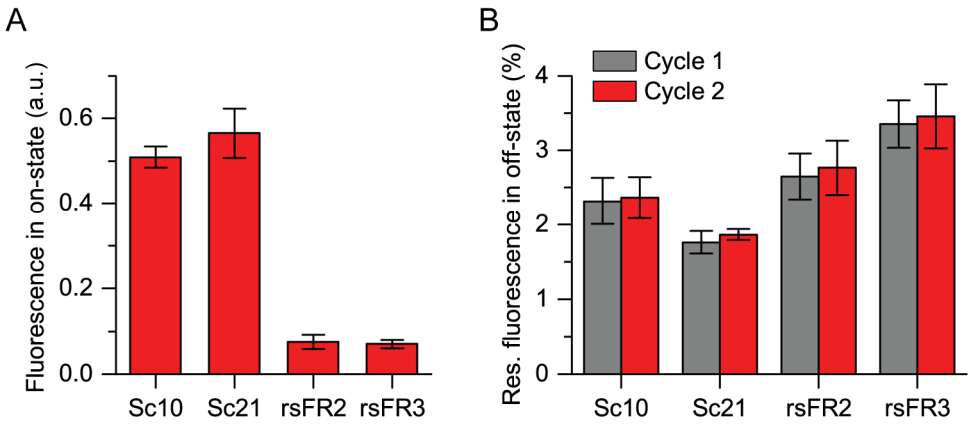

Figure 3.3-3: Ensemble brightness and off-state fluorescence for the negative RSFPs.
Comparison of the novel negative-switching proteins Sc10 and Sc21 with rsFusionRed2 (rsFR2) and rsFusionRed3 (rsFR3) expressed in E. coli. The proteins were switched on with light of 445 nm (1.2 kWcm^{-2}) for 10 ms (Sc10, Sc21) or 100 ms (rsFusionRed2, rsFusionRed3) and subsequently switched off with light of 561 nm (14.5 kWcm^{-2}) for 250 ms (Sc10, Sc21) or 500 ms (rsFusionRed2, rsFusionRed3). In switching cycle 2, the 445 nm switching was extended to 400 ms for rsFusionRed2 and rsFusionRed3 for sufficient on-switching. A: The fluorescence in the on-state in cycle 1. B: Residual fluorescence in the off-state relative to the fluorescence in the on-state in switching cycle 1 (grey) or 2 (red). A+B: The values were measured at 5 colonies each and averaged. The mean values and error bars of three independent experiments are shown.

For Sc10 and Sc21, the equilibrium state was additionally determined (chapter 2.4.1.6). Measurements without previous illumination (except for the autofocus) yielded

92.4 ± 2.9 % fluorescence signal in the equilibrium state relative to the on-state fluorescence for Sc10 and 90.1 ± 1.2 % for Sc21. Hence, the major fraction of the proteins is in the on-state at the thermal equilibrium.

3.3.2.2 Off-switching kinetics of negative-switching RSFPs

To measure the off-switching curves of Sc10, Sc21, rsFusionRed2 and rsFusionRed3, the negative-switching proteins were first switched to the on-state using light of 445 nm (14.9 kWcm^{-2}). Subsequently the off-switching curves were acquired by irradiation at 561 nm (14.5 kWcm^{-2}). The off-switching curves revealed the fastest off-switching kinetic for Sc21 (Figure 3.3-4 A). At the given 561 nm laser intensity, an off-switching halftime of 6.0 ms was determined for Sc21 and an off-switching halftime of 10.5 ms was determined for Sc10. The off-switching halftime of Sc21 was 2.5 and 3.7 times lower than the halftimes of rsFusionRed2 (15.0 ms) and rsFusionRed3 (22.0 ms).

Likewise, the off-switching halftimes for Sc21 at further 561 nm laser intensities (tested range: 6.3 to 63.1 kWcm^{-2}) were lower than those of the other examined negative-switching RSFPs (Figure 3.3-4 B). Sc10 exhibited as well lower switching halftimes than rsFusionRed2 and rsFusionRed3 at all examined laser intensities. For all four proteins, the off-switching halftimes and the laser intensities were not linearly related in the examined intensity range.

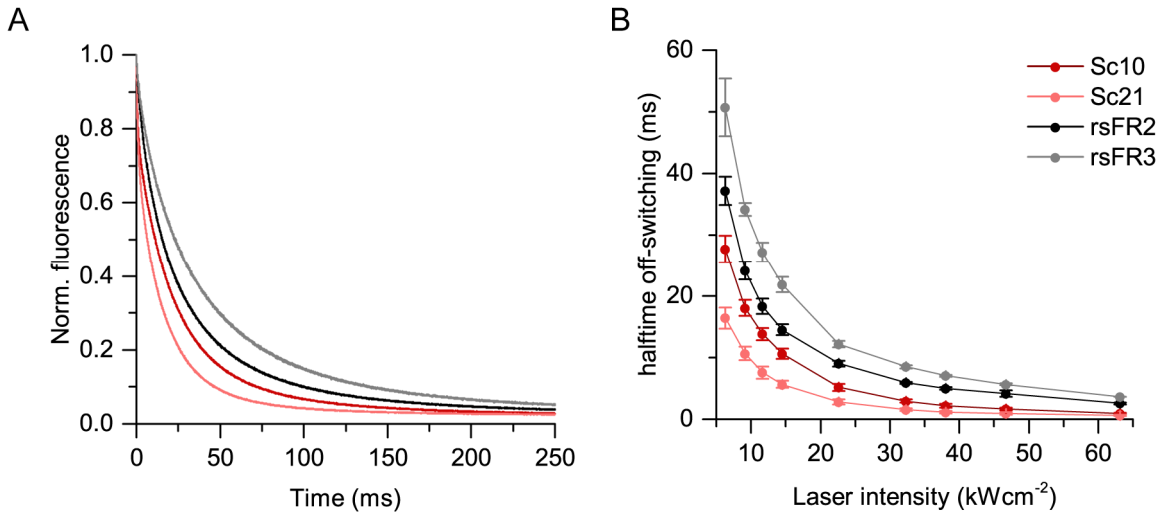

Figure 3.3-4: Off-switching kinetics of negative-switching red RSFPs.
A+B: Dark red: Sc10, light red: Sc21, black: rsFusionRed2, grey: rsFusionRed3. A: Off-switching curves normalized to the on-state. All proteins were first switched on with light of 445 nm (14.9 kWcm^{-2}) for 10 ms. The off-switching curves were then acquired by irradiation at 561 nm (14.5 kWcm^{-2}) for 250 ms (Sc10, Sc21) or 500 ms (rsFusionRed2, rsFusionRed3). The averaged curves measured at 5 colonies are shown. Two additional experiments yielded comparable off-switching kinetics. B: Off-switching halftimes in dependency of the 561 nm laser intensity. The x-axis starts at 5 kWcm^{-2}. The normalized off-switching curves measured at 5 colonies in each experiment were averaged and then the off-switching halftimes were determined. The mean values and error bars of three independent experiments are shown.

3.3.2.3 On-switching kinetics of negative-switching RSFPs

The on-switching of negative-switching red RSFPs cannot be directly detected due to the insufficient fluorescence emission induced by the excitation at 445 nm. Thus, the on-switching curves were obtained by modulation of the 445 nm on-switching times (chapter 2.4.1.4). The fluorescence after on-switching (1.2 $kWcm^{-2}$) was readout using light of 561 nm (14.5 $kWcm^{-2}$). The fluorescence signals were normalized to the fluorescence in the on-state and plotted against the 445 nm switching time (Figure 3.3-5 A+B).

While Sc10 and Sc21 were completely switched on within the irradiation time of 25 ms ($t_{1/2,on}$ = 1.6-1.7 ms), rsFusionRed2 and rsFusionRed3 did not even reach the on-state fluorescence after 400 ms of irradiation. Moreover, the shape of the on-switching curve differed between the switchable FusionRed proteins and the switchable mScarlet proteins.

Due to this discrepancy, the on-switching was additionally investigated by simultaneous irradiation at 561 nm (2.6 $kWcm^{-2}$) and 445 nm (1.2 $kWcm^{-2}$) after full off-switching with light of 561 nm (14.5 $kWcm^{-2}$). For all four negative-switching RSFPs, the on-switching was dominant at the simultaneous irradiation (Figure 3.3-5 C+D). Sc10 and Sc21 were again switched on within 25 ms with slightly reduced on-switching halftimes (Figure 3.3-5 E).

In this approach, the on-switching curves of rsFusionRed2 and rsFusionRed3 reached a plateau within 400 ms of simultaneous irradiation. The on-switching halftimes determined in the simultaneous approach were 19.6 ms for rsFusionRed2 and 20.4 for rsFusionRed3, thus 2.6 and 2.9 times lower compared to the approach with the modulated 445 nm switching times. With both approaches, the on-switching curves demonstrated substantial faster on-switching kinetics for Sc10 and Sc21 than for rsFusionRed2 and rsFusionRed3 at the applied 445 nm light intensities.

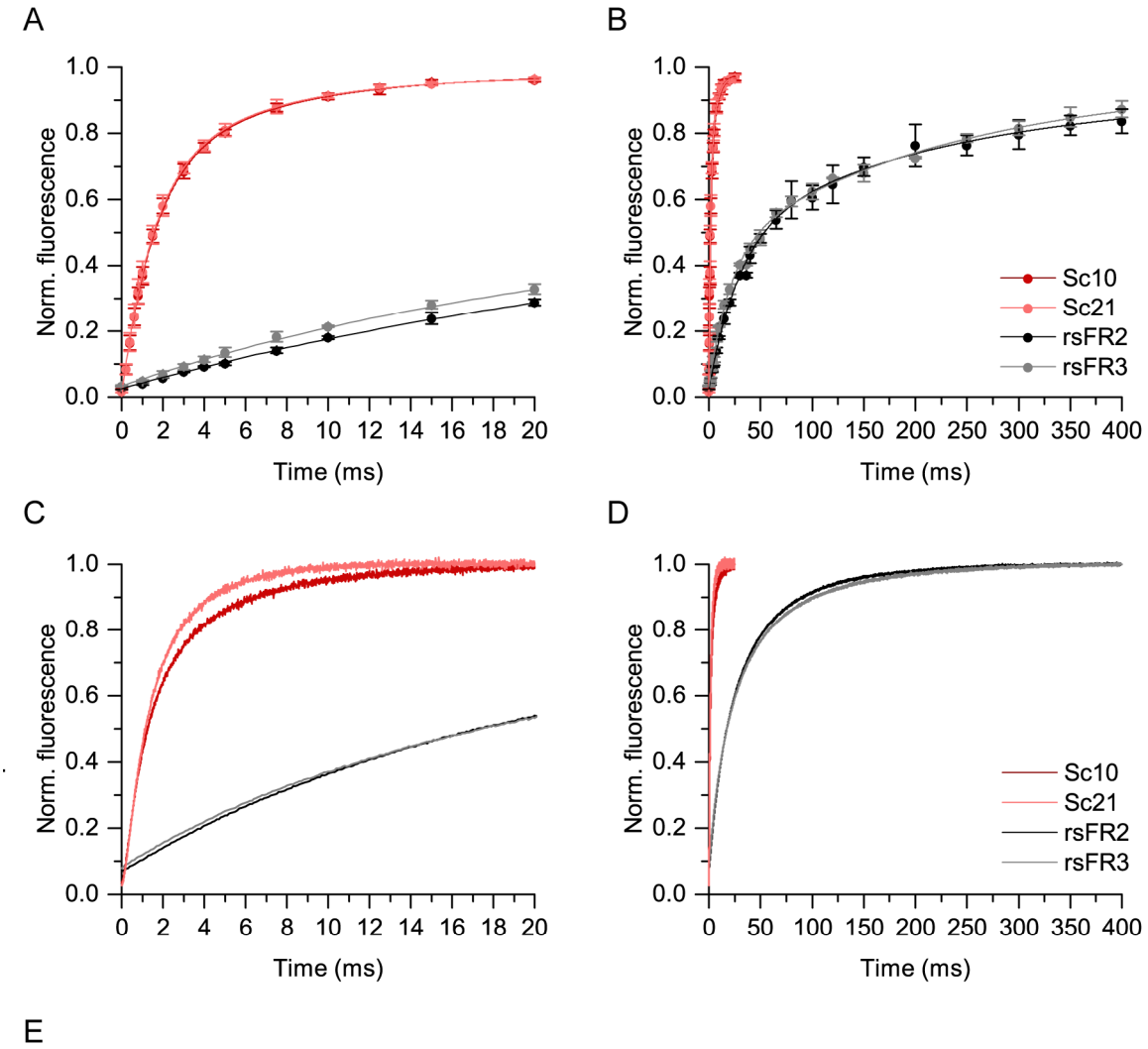

E

	$t_{1/2,on}$ (ms)	
	modulated	simultaneous
Sc10	1.7	1.4
Sc21	1.6	1.2
rsFusionRed2	57.0	19.6
rsFusionRed3	53.5	20.4

Figure 3.3-5: On-switching kinetics of negative-switching red RSFPs.
A-D: Dark red: Sc10, light red: Sc21, black: rsFusionRed2, grey: rsFusionRed3. A+B: On-switching curves after switching into the off-state for two different x-axis scales, measured by the modulation of the 445 nm irradiation times. 445 nm: 1.2 kWcm^{-2}; 561 nm: 14.5 kWcm^{-2}. Switching schemes for Sc10 and Sc21: 250 ms 561 nm, 0-25 ms 445 nm; switching scheme for rsFusionRed2 and rsFusionRed3: 500 ms 561 nm, 0-400 ms 445 nm. The first fluorescence signal after on-switching divided by the on-state fluorescence was plotted against the 445 nm switching time along with the bioexponential fit. In a single experiment, each data point was measured at 5 different colonies. The mean values and error bars of three independent experiments are shown. C+D: On-switching curves acquired by simultaneous irradiation at 445 nm (1.2 kWcm^{-2}) and 561 nm (2.6 kWcm^{-2}) (Sc10, Sc21: 25 ms; rsFusionRed2, rsFusionRed3: 400 ms) after switching into the off-state with 561 nm (14.5 kWcm^{-2}) (Sc10, Sc21: 200 ms; rsFusionRed, rsFusionRed3: 500 ms). Averaged on-switching curves measured at 5 colonies normalized to the on-state. A repetition of the experiment yielded comparable switching curves. E: Determined off-switching halftimes for the switching curves in A-D (left column: A+B; right column: C+D).

3.3.2.4 Switching fatigue of negative-switching RSFPs

Next, the negative-switching RSFPs Sc10, Sc21, rsFusionRed2 and rsFusionRed3 were compared regarding their switching fatigue. Therefore the RSFPs were switched on to 90 % using light of 445 nm (1.2 kWcm^{-2}) and switched off to 95 % using light of 561 nm (14.5 kWcm^{-2}) (chapter 2.4.1.5). The switching times (listed in Figure 3.3-6 B) were chosen on the basis of the measured off-switching curves (Figure 3.3-4 A) and on the basis of the on-switching curves acquired by simultaneous irradiation at 561 and 445 nm (Figure 3.3-5 C+D). 250 switching cycles were acquired.

A

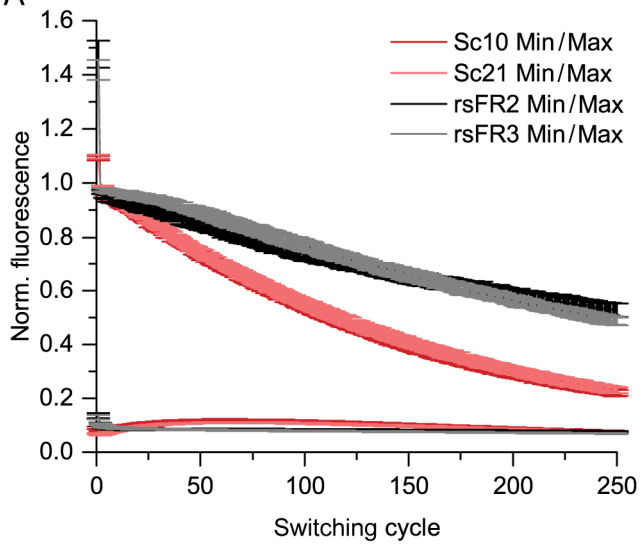

B

	Switching 445 nm (ms)	Switching 561 nm (ms)
Sc10	7.5	75.6
Sc21	7.3	59.4
rsFR2	114.4	110.8
rsFR3	131.8	157.7

C

	Max. signal cycle 100	Cycles until 50 %
Sc10	54 %	111
Sc21	56 %	118
rsFR2	77 %	> 250
rsFR3	75 %	237

Figure 3.3-6: Switching fatigue of negative-switching red RSFPs.
A: 250 switching cycles of Sc10 (dark red), Sc21 (light red), rsFusionRed2 (black) and rsFusionRed3 (grey). The proteins were switched off to 95 % with light of 445 nm (1.2 kWcm^{-2}) and switched on to 90 % with light of 561 nm (14.5 kWcm^{-2}). Switching times: listed in B. The switching curves were normalized to the maximal fluorescence in cycle 2. The minimal and maximal fluorescence signal of the off-switching curves are plotted against the switching cycles. The mean values and error bars of one experiment with measurements at 10 colonies each are shown. Two repetitions of the experiment yielded comparable results. B: Applied switching times for the respective proteins. C: The maximal signal in switching cycle 100 relative to cycle 2, and the number of cycles until 50 % of the maximal fluorescence of cycle 2 is reached. These values were determined using averaged curves of three individual experiments.

The minimal and the maximal signal of the off-switching curves were normalized to the maximal signal in the second switching cycle (Figure 3.3-6 A). Using the stated switching schemes, a smaller fraction of the switchable mScarlet variants (~9 %) and a larger fraction of rsFusionRed2 and rsFusionRed3 (~30 %) could not be switched after the first switching cycle.

The RSFPs Sc10 and Sc21 showed higher switching fatigue than rsFusionRed2 and rsFusionRed3. After 100 switching cycles, the maximal fluorescence signal was reduced to 54-56 % for the switchable mScarlet variants and to 75-77 % for the switchable FusionRed

proteins (Figure 3.3-6 C). While Sc10 and Sc21 could be switched 111 and 118 times before the maximal signal was bleached to 50 %, rsFusionRed3 could be switched 237 times. The maximal signal of rsFusionRed2 was not reduced to 50 % after 250 switching cycles. In the first 70 switching cycles, Sc10 and Sc21 showed a slight increase in the minimal signal, which represents the residual fluorescence in the off-state.

3.3.2.5 Alternative on-switching wavelength for Sc10 and Sc21

The common wavelengths 405 nm and 488 nm were tested as alternatives for the switching of Sc10 and Sc21, like it was already conducted for the positive-switching mRuby2 variants (chapter 3.2.2.5). For this purpose, Sc10 and Sc21 were switched into the off-state with light of 561 nm (3.2 $kWcm^{-2}$) and subsequently on-switching curves were acquired by simultaneous irradiation at 561 nm (2.6 $kWcm^{-2}$) and 405 nm, 445 nm or 488 nm. Applying the light intensities of 4.3 $kWcm^{-2}$ for 405 nm, 1.2 $kWcm^{-2}$ for 445 nm and 5.6 $kWcm^{-2}$ for 488 nm yielded on-switching curves with comparable switching kinetics for both Sc10 ($t_{1/2,on}$=1.1-1.3 ms) and Sc21 ($t_{1/2,on}$=1.0-1.1 ms) (Figure 3.3-7 A+C). In these on-switching curves, a similar fluorescence in the off-state was determined for the different switching wavelengths (Sc10: 4.0-4.2 %, Sc21: 3.1-3.2 %).

The laser intensities for 405 nm, 445 nm and 488 nm which induced similar on-switching kinetics were also applied in switching fatigue experiments (Figure 3.3-7 B+D). The off-switching was performed with light of 561 nm (14.5 $kWcm^{-2}$) and the same switching scheme was applied for all measurements. In the acquired 100 switching cycles, the normalized maximal and minimal signals did not show major differences for the different on-switching wavelengths. Thus, 405 nm and 488 nm represent alternative switching wavelengths, but only if the light intensities are adjusted to higher levels.

To summarize the switching characterization of negative-switching red RSFPs, the advantages of Sc10 and Sc21 over rsFusionRed2 and rsFusionRed3 are the considerable higher ensemble brightness in *E. coli* colonies and the faster on- and off-switching kinetics. The advantage of rsFusionRed2 and rsFusionRed3 is the higher stability in repetitive switching. The determination of the equilibrium state revealed that the major fraction of Sc10 and Sc21 proteins are in the on-state. Furthermore, the wavelengths 405 nm and 488 nm represent suitable alternatives for the on-switching of Sc10 and Sc21. In the following, both switchable mScarlet variants were characterized further.

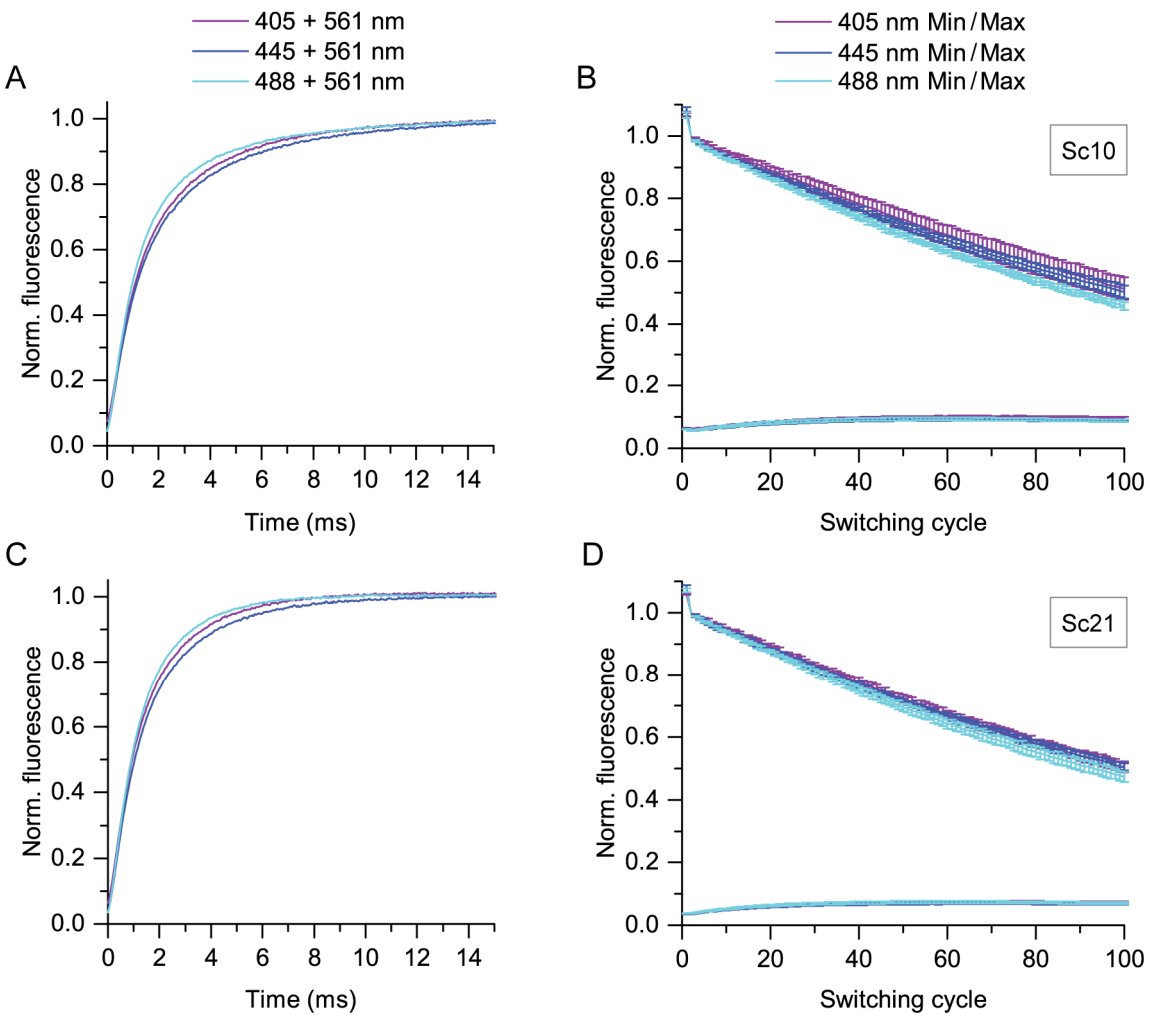

Figure 3.3-7: Switching of Sc10 and Sc21 with alternative on-switching wavelengths.
A-D: 405 nm: purple, 4.3 kWcm^{-2}; 445 nm: blue, 1.2 kWcm^{-2}; 488 nm: cyan, 5.6 kWcm^{-2}. The averaged curves of three individual experiments with measurements at 5 colonies each are plotted. A (Sc10), C (Sc21): On-switching curves resulting from simultaneous irradiation at 561 nm (2.6 kWcm^{-2}) and at 405 nm, 445 nm or 488 nm after switching into the off-state (700 ms 561 nm, 3.2 kWcm^{-2}). The curves were normalized to the on-state fluorescence. B (Sc10), D (Sc21): Switching fatigue curves with different on-switching wavelengths for 100 switching cycles. Switching scheme: alternating 10 ms 405, 445 or 488 nm and 100 ms 561 nm (14.5 kWcm^{-2}). The minimal and maximal fluorescence signals of each off-switching curve were normalized to the maximal signal in cycle 2.

3.3.3 Characterization of isolated Sc10 and Sc21 protein samples

To further characterize the switchable mScarlet variants, Sc10 and Sc21 were expressed in *E. coli* colonies and isolated (protocol: chapter 2.3.1.1). Additionally, mScarlet, mCherry, dTomato, DsRed, FusionRed, rsFusionRed2 and rsFusionRed3 were purified as reference or for comparison using the same protocol. All proteins were isolated in a sufficient quantity and purity, which was controlled by SDS-PAGE (Appendix Figure 6.3-1 B+C).

3.3.3.1 Spectral characteristics of switchable mScarlet variants

The absorption spectra of isolated Sc10, Sc21 and mScarlet samples were recorded and revealed distinct lower absorbance of the deprotonated chromophore at 500 to 600 nm for the switchable variants (Figure 3.3-8 A). The absorption of Sc10 was slightly higher in this range than the absorption of Sc21. All three absorption spectra featured a main absorption maximum at 570 nm and a minor maximum at about 535 nm. The absorption spectra of Sc10 and Sc21 showed an additional absorption band at 400 nm, while the spectrum of mScarlet was characterized by an additional band at 340 nm.

The emission spectra of Sc10 and Sc21 were slightly red-shifted by about 7 nm compared to the emission spectrum of mScarlet (Figure 3.3-8 B). Furthermore, the excitation spectra of mScarlet, Sc10 and Sc21 share a main excitation maximum at 570 nm.

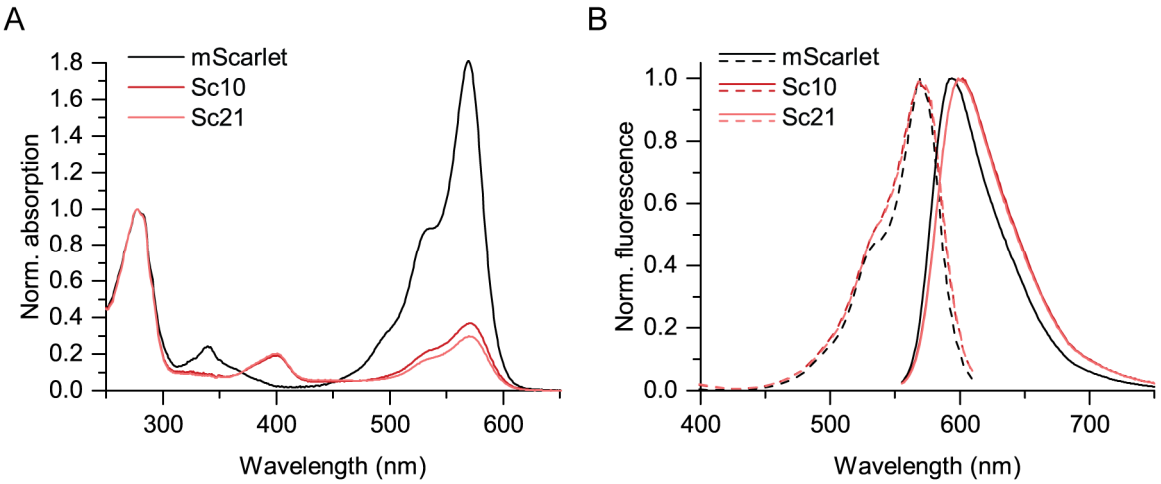

C

	Maximum (nm)		
	Abs.	Exc.	Em.
mScarlet	570	570	594
Sc10	570	570	601
Sc21	570	570	601

Figure 3.3-8: Spectra of mScarlet and generated switchable variants.
A+B: black: mScarlet, dark red: Sc10, light red: Sc21. Averaged spectra of three independent protein samples. A: Absorption spectra normalized to the absorption at 280 nm. B: Excitation (dashed lines, Em: 620 nm) and emission spectra (solid lines, Exc: 545 nm) normalized to the maximal fluorescence. D: Wavelengths of the maximum absorption or fluorescence.

The Sc10 and Sc21 protein solutions were switched in a quartz cuvette (chapter 2.3.5) to measure the absorption spectra of the on- and off-state. Both absorption spectra changed when the protein solutions were illuminated with blue or yellow-green light. The on-switching by illumination with light of 450/40 nm slightly increased the absorption at

570 nm by the factor of 1.1 for Sc10 and of 1.2 for Sc21 (Figure 3.3-9 A+B). Proceeding from the on-switched protein solutions, the illumination with light of 550/40 nm reduced the absorption at 570 nm by the factor of 8.6 for Sc10 and 12.2 for Sc21. In addition, an absorption maximum at 450 nm appeared by the off-switching with light of 550/40 nm. The relaxation from the off-state was monitored by repetitive measurements of the absorption spectra without further illumination. Using the course of the absorption at 570 nm (Figure 3.3-9 C), the determined halftimes for the relaxation from the off-state were 2.0 min for Sc10 and 1.9 min for Sc21.

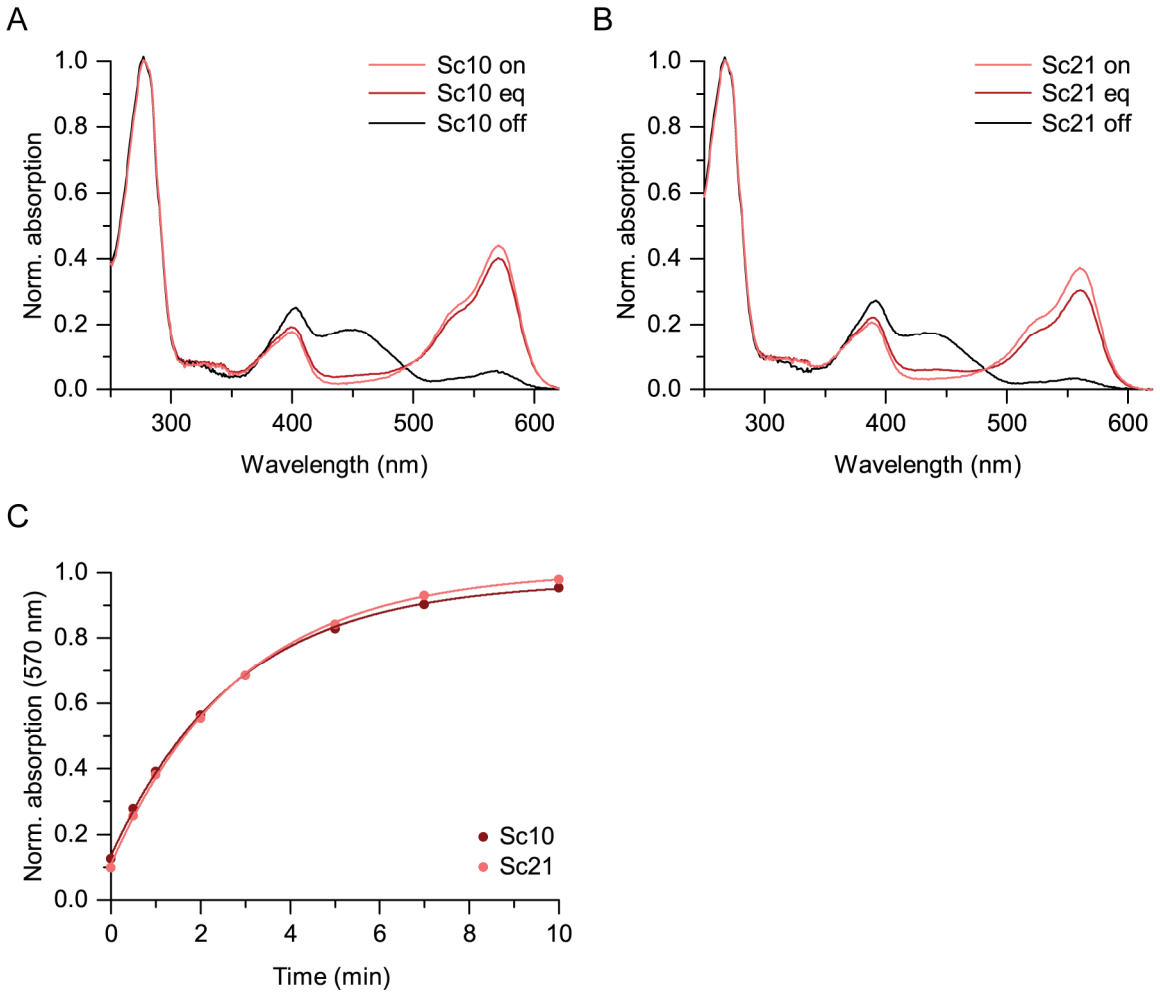

Figure 3.3-9 The absorption changes of switched Sc10 and Sc21 protein solutions.
A+B: Absorption spectra of purified protein samples in the equilibrium state (eq, dark red), after on-switching with light of 450/50 nm for 1 min (on, light red) and after off-switching with light of 550/40 nm for 1 min (off, black). The absorption spectra were normalized to the absorption at 280 nm. A: Sc10, B: Sc21. C: Thermal relaxation from the off-state to the equilibrium state for isolated Sc10 (dark red) or Sc21 (light red) samples after off-switching with yellow-green light for 1 min. The relaxation is visualized by the absorption at 570 nm normalized to the absorption at the equilibrium. The relaxation curves were fitted using a monoexponential function. A-C: A repetition of the experiments yielded comparable results.

3.3.3.2 Fluorescence and extinction characteristics of the negative RSFPs

Two different methods were applied to determine the quantum yields of Sc10 and Sc21 (chapter 2.3.7). In the first method (relative method) based on the emission spectra, the quantum yields of Sc10 and Sc21 was determined relative to the reference mScarlet (QY: 0.70 [85]). The on-switching of the two RSFPs before the measurements did not yield significantly different values and are thus not presented. The quantum yields were additionally determined using the QY spectrometer. Both methods revealed comparable values of 23.6 % and 23.7 % for Sc10 and 24.1 % and 24.7 % for Sc21 (Table 5). These quantum yields of Sc10 and Sc21 exceed all quantum yields which were measured for red-emitting RSFPs so far.

The extinction coefficient ε of the deprotonated chromophore was determined for Sc10 and Sc21 as well relative to the published value of mScarlet (100,000 $M^{-1}cm^{-1}$). Both, the extinction coefficients of the RSFPs in the equilibrium and in the on-state were measured. Slightly higher extinction coefficients were obtained for the on-switched proteins compared to the proteins in the equilibrium (Table 5). The fluorescence lifetimes were reduced from 3.9 ns for mScarlet to 1.8 ns (Sc10) and 1.6 ns (Sc21).

Table 5: Fluorescence and extinction characteristics of switchable mScarlet variants.
QY (relative method) and extinction coefficient: three independent protein samples. QY (QY spectrometer) and fluorescence lifetime: two independent protein samples.

FP	QY (%)		ε ($M^{-1}cm^{-1}$)		Lifetime (ns)
	relative method (spectra)	QY spectrometer	equilibrium	on-state	
Sc10	23.7 ± 0.3	23.6	20,448 ± 923	22,460 ± 302	1.8
Sc21	24.7 ± 1.3	24.1	16,267 ± 788	20,678 ± 699	1.6
mScarlet	70*		100,000*		3.9*

** Data taken from [85]*

The quantum yields and the extinction coefficients were also measured for rsFusionRed2 and rsFusionRed3 using the same protocols. Their template protein FusionRed served as reference protein. Four independent protein samples were isolated for each protein and the determined extinction coefficients varied strongly for the different rsFusionRed2 and rsFusionRed3 samples (Appendix Table 16). In Table 6, only the highest determined extinction coefficient is listed for each protein. Both, the quantum yields and the extinction coefficients determined in this work were lower than the published values (shown in Table 6) [118].

The molecular brightness was calculated by multiplying the quantum yield with the extinction coefficient. For rsFusionRed2 and rsFusionRed3, this calculation resulted in a

2.4-2.5-fold lower molecular brightness determined in this work than in the work of Pennacchietti *et al*. [118]. Consequently, the advantage of the molecular brightness of Sc10 and Sc21 is more apparent when compared to the values measured in this work.

Table 6: Comparison of QY and ε for the negative-switching red RSFPs.
QY: Determined by the relative method (spectra) for three to four independent protein samples.

RSFP	QY (%)		ε ($M^{-1}cm^{-1}$)		Brightness (QY * ε * 10^{-3})	
	this work	published	this work	published	this work	published
Sc10	23.7 ± 0.3	/	22,460 ± 302	/	5.3	/
Sc21	24.7 ± 1.3	/	20,678 ± 699	/	5.1	/
rsFusionRed2	7.2 ± 0.7	12*	25.101**	35500*	1.8	4.3
rsFusionRed3	5.4 ± 0.6	8*	22,678**	38000*	1.2	3.0

** Data taken from [118]*
*** Highest ε determined in four independent measurements, see Appendix Table 16*

3.3.3.3 The pH stability of Sc10 and Sc21

The isolated protein samples of Sc10 and Sc21 were diluted in buffers with different pH values to examine the influence of the pH on the absorption spectra and on the fluorescence (chapter 2.3.8). With increasing pH values, the absorption in the range of 500-600 nm increased, which represents the deprotonated chromophore (Figure 3.3-10 A+B). The reduction of the pH decreased the absorption in this range and at the same time gave rise to an absorptions maximum at about 445 nm, which was assigned to be the absorption of the chromophore with a protonated hydroxyphenyl ring. The pH-dependent changes were comparable for Sc10 and Sc21.

The pH stability of Sc10 and Sc21 was measured by their fluorescence in different pH buffers at 570 nm excitation and 600 nm detection. The fluorescence of Sc10 and Sc21 increased with rising pH values (Figure 3.3-10 C) and revealed high pK_a values of 7.7 for Sc10 and 7.8 for Sc21 (fit fuction: see chapter 2.3.8).

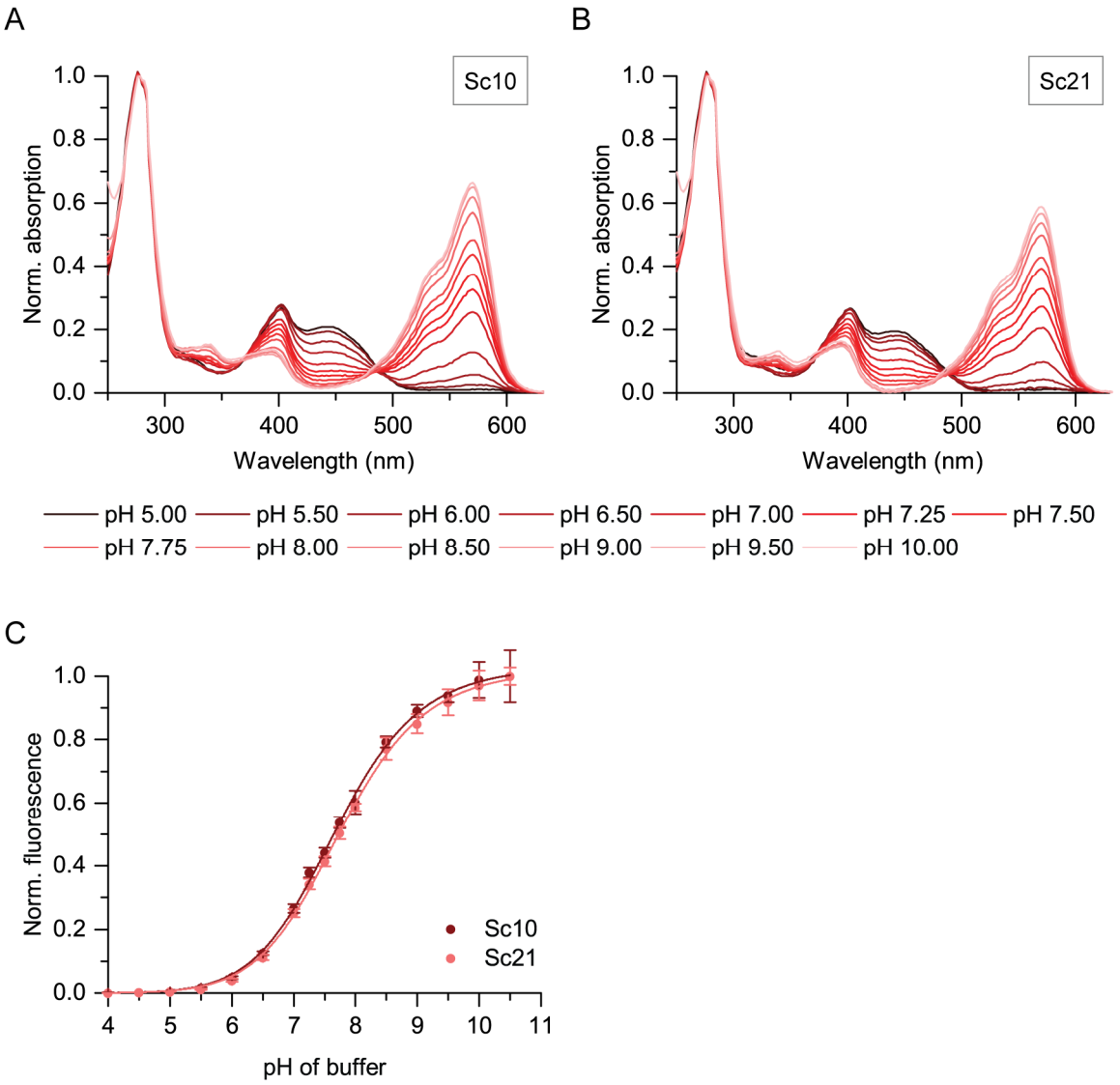

Figure 3.3-10: pH-dependent absorption spectra and pH stability of Sc10 and Sc21.
A+B: Absorption spectra of Sc10 (A) and Sc21 (B) at different pH values: pH 5.0-10.0 in red shades from dark to light red. The spectra are normalized to the absorption at 280 nm. The averaged spectra of three replicates are plotted. Two independent repetitions yielded comparable results. C: Fluorescence (Exc: 570 nm, Em: 600 nm) of protein samples diluted in different pH buffers normalized to the fluorescence at pH 10.5. Dark red: Sc10, light red: Sc21. Averaged values and error bars of three independent experiments with three replicates each. Fits (see chapter 2.3.8) of the data from pH 4.0 to 10.5 are shown.

3.3.3.4 The oligomeric state of the switchable mScarlet variants

Analytical size-exclusion chromatography was applied to determine the oligomeric state of Sc10 and Sc21. The fluorescent proteins DsRed, dTomato, mCherry and mScarlet were additionally analyzed for comparison. All protein samples were diluted to 10 µM and were applied separately to the size-exclusion column. The chromatography profiles which were detected by the absorption at 280 nm are plotted in Figure 3.3-11. The tetrameric DsRed [34] eluted with a retention volume of 13.75 ml, the dimeric dTomato with a

retention volume of 14.71 ml and the monomeric mCherry with a retention volume of 16.01 ml [58]. The monomeric mScarlet eluted with a slightly higher retention volume of 16.16 ml. The RSFPs Sc10 and Sc21 were determined monomeric due to their retention volumes of 16.21 ml and 16.23 ml.

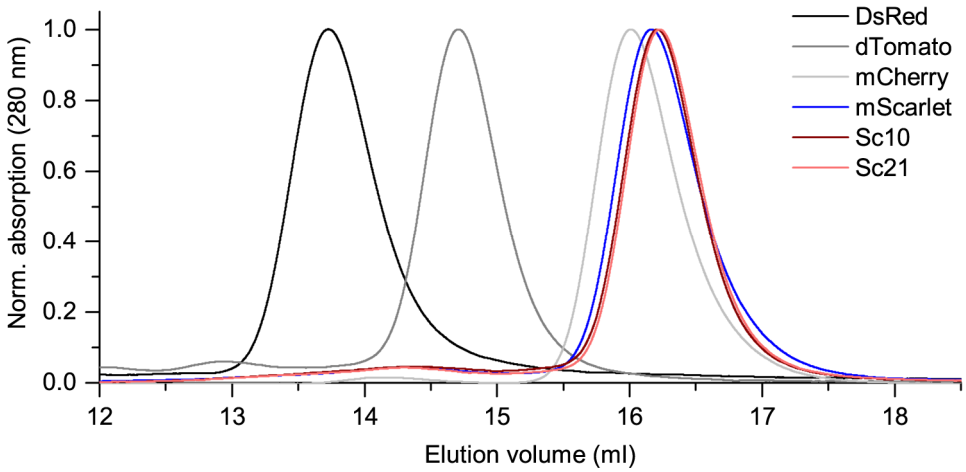

Figure 3.3-11: Size-exclusion chromatography of Sc10 and Sc21.
Analytical size-exclusion chromatography of Sc10, Sc21 and fluorescent proteins for comparison. All proteins were isolated from bacteria with the same purification protocol (see chapter 2.3.1.1). 10 µM protein samples were applied to the Superdex 200 Increase 10/300 L column with a flow rate of 0.75 ml/min at 6 °C. The chromatography profiles at 280 nm are shown. Black: DsRed (tetramer), dark grey: dTomato (dimer), light grey: mCherry (monomer), blue: mScarlet (monomer), medium red: Sc10, light red: Sc21.

To conclude this chapter, the performed characterizations of isolated protein samples showed a high similarity between the two mScarlet variants Sc10 and Sc21. The recorded absorption, excitation and emission spectra of both proteins were comparable. Only the absorption quantity in the range of 500 to 600 nm slightly differed and as a consequence, the determined extinction coefficients were slightly different. Sc10 and Sc21 were both determined monomeric, showed a similar molecular brightness and a comparable response to the change of the surrounding pH. In the following, the expression of the negative-switching RSFPs in mammalian cells was investigated.

3.3.4 Ensemble brightness of the negative-switching RSFPs in HeLa cells

As shown above, the fluorescence in the on-state of Sc10 and Sc21 in *E. coli* colonies was 6.8 to 8.0 times higher than those of rsFusionRed2 and rsFusionRed3 (chapter 3.3.2.1). Since the expression and maturation can differ in bacterial and mammalian cells, the effective cellular brightness in HeLa cells was compared as well. The plasmids Sc10-P2A-mEGFP, Sc21-P2A-mEGFP, rsFusionRed2-P2A-mEGFP and rsFusionRed3-P2A-mEGFP (chapter 2.1.9.4) enable the transient expression of the red RSFPs together with mEGFP in the same

ratio and were used for the transfection of HeLa cells. The day after transfection, the HeLa cells were analyzed in flow cytometry regarding their green and red fluorescence. The ensemble brightness in the equilibrium state was measured, since the RSFPs were not switched on prior to the analysis.

The fluorescence of the individual transfected cells varied considerably (Figure 3.3-12 A). On average, higher red fluorescence signals were measured for the cells expressing Sc10 or Sc21 than for the cells expressing rsFusionRed2 or rsFusionRed3. The red fluorescence signal was normalized to the green fluorescence signal of mEGFP in order to take the introduced plasmid DNA into account. The averaged and normalized red-to-green fluorescence ratio of all fluorescent cells revealed the highest ensemble brightness for Sc10 (set to 1; Figure 3.3-12 B), with a value 1.35-fold higher than for Sc21, 1.66-fold higher than for rsFusioRed2, and 2.60-fold higher than for rsFusionRed3.

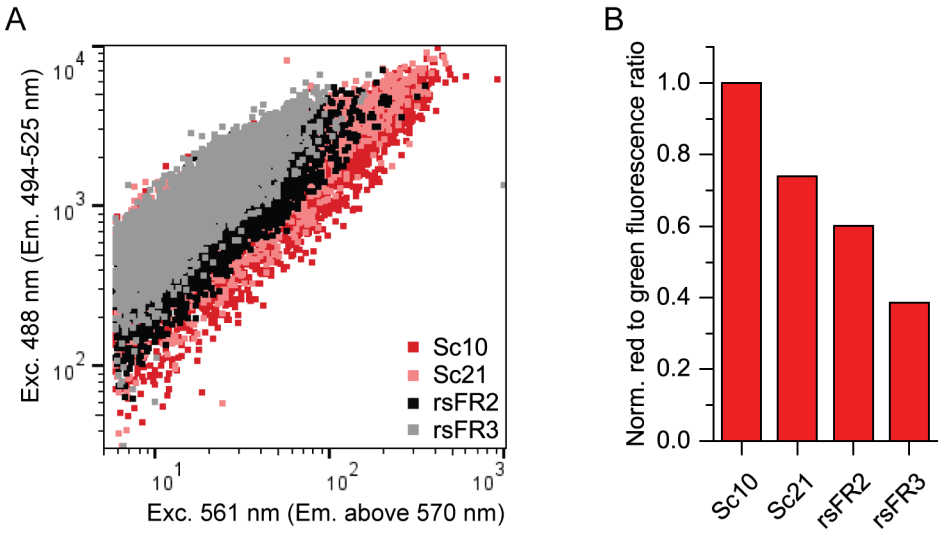

Figure 3.3-12: Expression of the negative-switching red RSFPs in HeLa cells.
A: HeLa cells transfected with Sc10-P2A-mEGFP (medium red), Sc21-P2A-mEGFP (light red), rsFusionRed2-P2A-mEGFP (black) or rsFusionRed3-P2A-mEGFP (grey) were analyzed in flow cytometry the day after transfection. The fluorescence signal occurring from the excitation at 488 nm (detection: 494-525 nm) is plotted against the fluorescence signal resulting from the excitation at 561 nm (detection: sum of fluorescence at 570-640 nm and above 645 nm). 10,000 cells were analyzed, only single cells are displayed. B: The averaged red-to-green ratio of the cells shown in A normalized to the averaged ratio of Sc10-P2A-mEGFP.

3.3.5 The RSFPs Sc10 and Sc21 as fusion tag in fluorescence microscopy

The application of the switchable mScarlet variants as fusion tags was tested by the expression of Sc10 and Sc21 fusion constructs in mammalian cells and their imaging in confocal microscopy (chapter 2.4.2). Since the negative-switching RSFPs are switched off by the excitation light of 561 nm, the imaging of the fusion constructs was performed by

additional and simultaneous irradiation at 458 nm for on-switching. Sc10 and Sc21 were tested in transient expressions (chapter 3.3.5.1) as well as in stable expressions (chapter 3.3.5.2).

3.3.5.1 Transient expression of Sc10 and Sc21 in fusion constructs

The tagging performance of Sc21, the switchable mScarlet variant with most mutations, was controlled in eight different fusion constructs. As already shown for Ru87 (chapter 3.2.4.1), the plasmids encoding the fusion constructs were prepared and used for transfection of HeLa cells. Sc21 was targeted to cytoskeletal structures by fusion to Lifeact, vimentin and keratin, and to different organelles by fusions to the respective targeting signal peptides (ER, mitochondria and peroxisomes). The detection of the Sc21 fluorescence in confocal microscopy revealed the expected localizations (Figure 3.3-13). In addition, the expression of Sc21 fused to Histone1 and Caveolin1 targeted Sc21 to the nucleus and to the caveolae. The successful expression of Sc21 as C- and N-terminal tag and its correct cellular targeting to different cell compartments promotes its applicability in transient expressions.

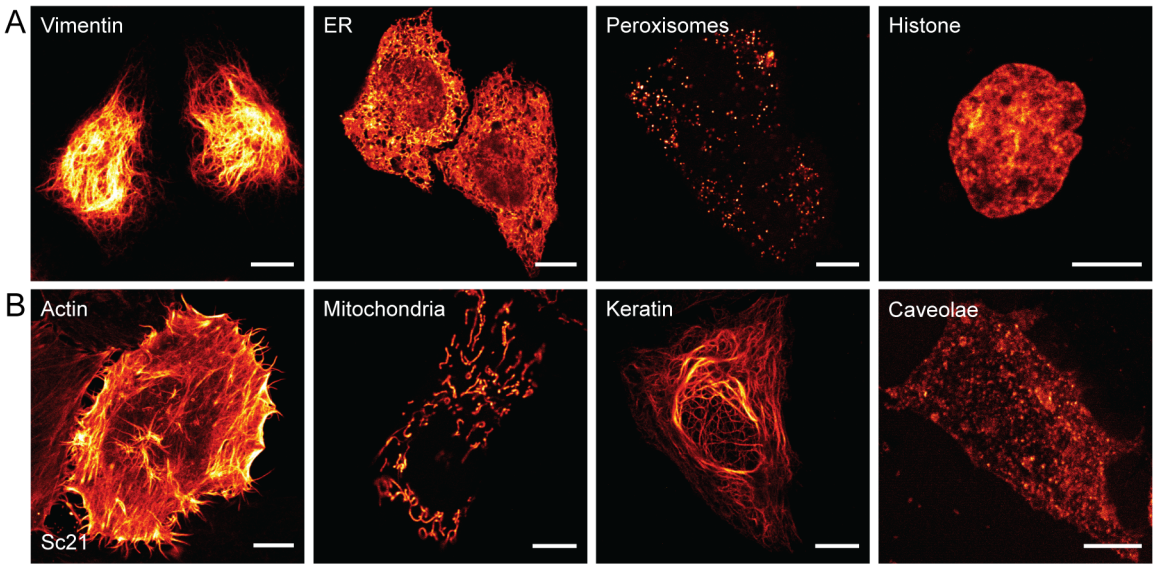

Figure 3.3-13: Fusion constructs of Sc21 expressed in HeLa cells.
Confocal images of Sc21 fusion constructs transiently expressed in HeLa cells. Sc21 was switched on with 458 nm and excited at 561 nm. A (from left to right): Vimentin-Sc21, Sc21-ER (ER signal), Sc21-PTS (peroxisomal targeting signal), Sc21-Histone1 (H2BN). B (from left to right): Lifeact-Sc21, Mito-Sc21 (mito targeting signal), Keratin-Sc21 (keratin18), Caveolin1-Sc21. Scale bars: 10 µm.

The four fusion constructs of vimentin, ER signal, peroxisomal targeting signal and Histone1 were as well generated for Sc10. The transient expression of these constructs in HeLa cells resulted in the expected localizations and revealed their natural occurring pattern (Figure 3.3-14) which suggests also the applicability of Sc10 as fusion tag in microscopy.

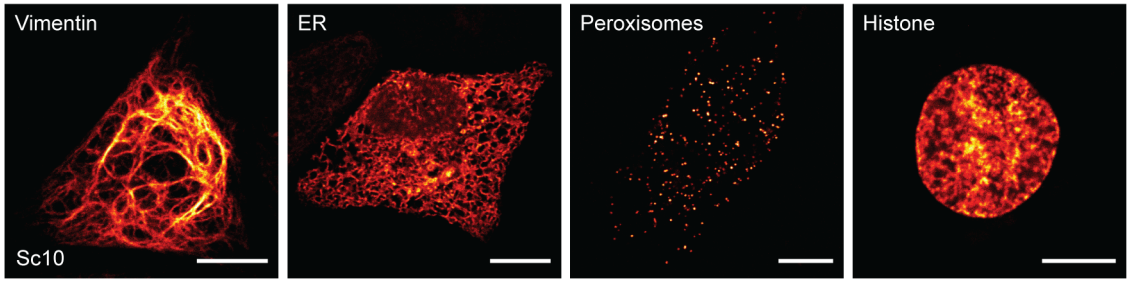

Figure 3.3-14: Fusion constructs of Sc10 expressed in HeLa cells.
Confocal images of Sc10 fusion constructs transiently expressed in HeLa cells, switched on with 458 nm and excited at 561 nm. From left to right: Vimentin-Sc10, Sc10-ER (ER signal), Sc10-PTS (peroxisomal targeting signal), Sc10-Histone1 (H2BN). Scale bars: 10 µm.

3.3.5.2 Stable expression of Sc10 and Sc21 fusion constructs

The application of Sc10 and Sc21 in long-term expression was controlled by the generation of monoclonal cell lines stably expressing keratin fusion constructs. For this purpose, cells of the K21 cell line generated in this work (chapter 3.1.2) were cotransfected with the plasmids pCAG-NLS-HA-Bxb1 and pInt-Keratin-Sc10 or pInt-Keratin-Sc21. Monoclonal cell lines were generated by single-cell sorting of the transfected cells. For both approaches, a monoclonal cell line stably expressing the keratin fusion constructs was identified and imaged in confocal microcopy (Figure 3.3-15 A+B). The expected cytoskeletal structures were observed in the cells.

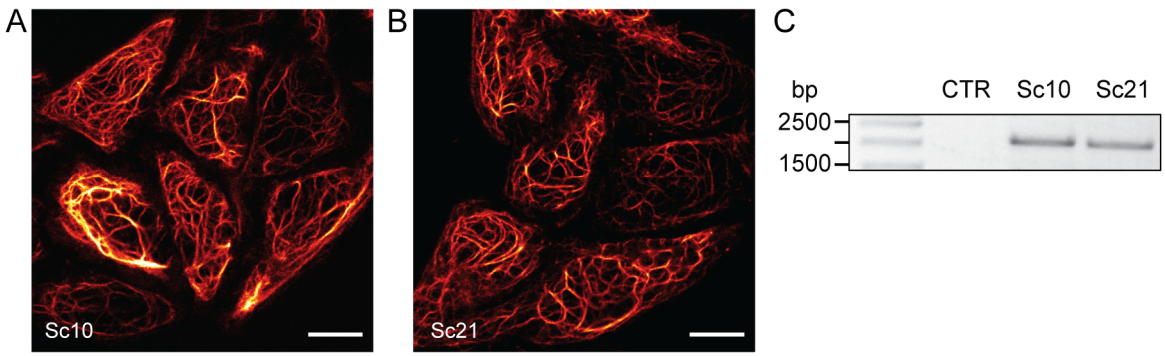

Figure 3.3-15: Stable expression of keratin constructs with Sc10 and Sc21 as fusion tag.
Monoclonal cell lines were generated by cotransfection of K21 cells with pCAG-NLS-HA-Bxb1 and pInt-Ker-Sc10/Sc21 and single-cell sorting in flow cytometry. A+B: Confocal images of the monoclonal cell lines stably expressing the keratin fusion constructs (on-switching: 458 nm, Exc: 561 nm). A: Keratin18-Sc10, B: Keratin18-Sc21. Scale bars: 10 µm. C: PCR products of the genotyping PCRs on genomic DNA of K21 cells (CTR) and of the monoclonal cell lines in A+B analyzed in gel electrophoresis. Expected PCR product size: 2129 bp.

A genotyping PCR was performed on the isolated genomic DNA using a landing pad-specific (binding at the end of the CAG promoter) and a Sc10/Sc21 specific primer

(expected size: 2129 bp). The analysis of the PCR product in gel electrophoresis (Figure 3.3-15 C) and sequencing verified the integration into the Bxb1 landing pad of the K21 cells.

The tagging of the endogenous vimentin gene with the coding sequence of Sc10 was tested using CRISPR/Cas9 genomic editing. For this, U2OS cells were cotransfected with the Vimentin-Sc10 donor plasmid and the plasmid encoding the Cas9 and a suitable gRNA (chapters 2.1.9.4 and 2.2.4). The knock-in of the Sc10 coding sequence was targeted to the C-terminal end of the endogenous vimentin gene. By single-cell sorting of the transfected cells, monoclonal cell lines were generated and a cell line with positive knock-in was identified in confocal microscopy (Figure 3.3-16 A+B). The stable expression of vimentin-Sc10 was detectable in all cells. The genomic DNA of these knock-in cells was isolated and applied in genotyping PCRs with a genome-specific and a Sc10 specific primer. The analysis of the PCR products by gel electrophoresis and sequencing verified the knock-in into the vimentin locus. It was not determined whether the cell line is homozygous or heterozygous tagged.

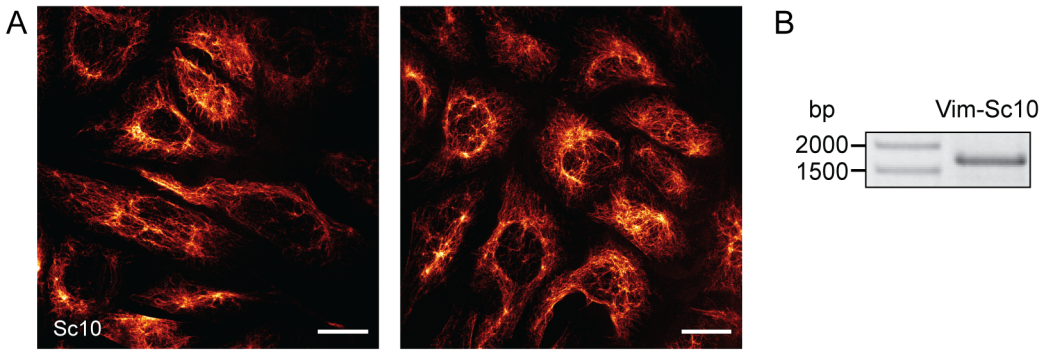

Figure 3.3-16: Tagging of endogenous vimentin with Sc10.
CRISPR/Cas9 genome editing was used to label the endogenous vimentin with Sc10 in U2OS cells. A monoclonal cell line was generated. A: Confocal images of the monoclonal cell line stably expressing the vimentin-Sc10 (on-switching: 458 nm, Exc: 561 nm). Scale bars: 20 µm. B: A genotyping PCR was conducted using the genomic DNA of the monoclonal cell line in A as template. The PCR product was analyzed in gel electrophoresis. Expected PCR product size: 1707 bp.

In all three generated cell lines, the expression of the fusion constructs was stable for the time of cultivation (weeks to months). The cells were viable and proliferated. The examined transient and stable expressions emphasized the applicability of the switchable mScarlet variants as fusion tags in fluorescence microscopy. Finally, Sc10 and Sc21 were characterized for their application in live-cell RESOLFT microscopy.

3.3.6 Characterization of Sc10 and Sc21 for RESOLFT microscopy

To compare the switching of Sc10, Sc21, rsFusionRed2 and rsFusionRed3 under live-cell RESOLFT conditions, the negative-switching RSFPs were transiently expressed in vimentin fusions in HeLa cells. Off-switching curves were acquired utilizing the pulse generator of the RESOLFT microscope for negative-switching red RSFPs (chapter 2.4.3.2). The proteins were switched on for 12 ms with a Gaussian 405 nm beam and the off-switching curves were detected for 80 ms using a Gaussian 561 nm beam (1.44 kWcm^{-2}). To achieve similar values for the residual fluorescence in the off-state, rsFusionRed2 and rsFusionRed3 had to be switched with higher 405 nm laser intensities (1.65 kWcm^{-2}) compared to Sc10 and Sc21 (0.35 kWcm^{-2}). The off-switching curves were acquired in three individual experiments with measurements in five cells per protein.

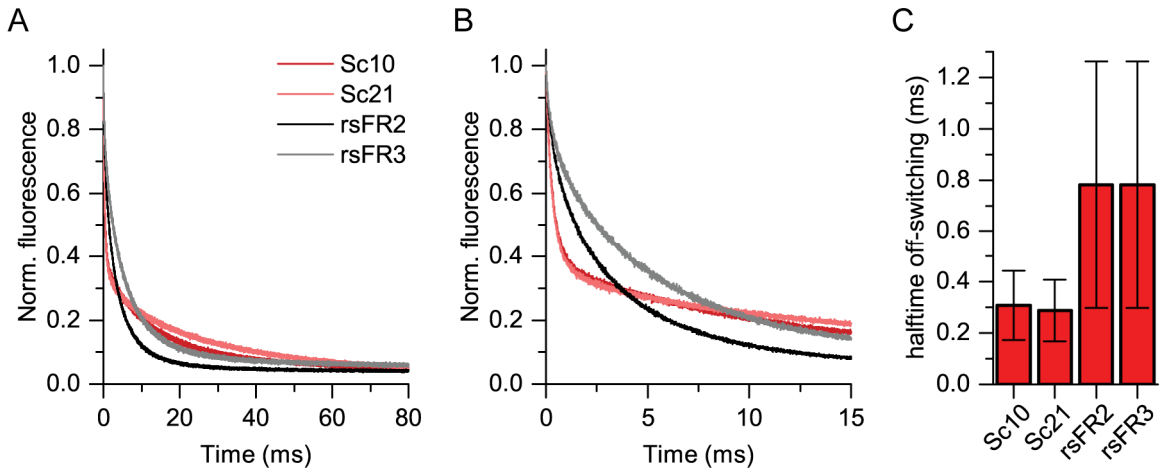

Figure 3.3-17: Switching of negative-switching red RSFPs expressed in HeLa cells.
A+B: Vimentin fusion constructs with Sc10 (dark red), Sc21 (light red), rsFusionRed2 (black) or rsFusionRed3 (grey) were transiently expressed in HeLa cells. The proteins were switched on for 12 ms using light of 445 nm (Sc10, Sc21: 0.35 kWcm^{-2}; rsFusionRed2, rsFusionRed3: 1.65 kWcm^{-2}). The off-switchting curves were acquired by irradiation at 561 nm (1.44 kWcm^{-2}) for 80 ms. The off-switching curves were normalized to the fluorescence in the on-state. Curves of one experiment with 5 different cells were averaged and plotted with different scales in A and B. C: The off-switching halftimes determined in three independent experiments (5 cells each) showing large variations.

The residual fluorescence in the off-state and the off-switching halftimes fluctuated in the different experiments (halftimes: see Figure 3.3-17 C). The off-switching curves of Sc10 and Sc21 showed two distinctly different kinetics (Figure 3.3-17 A+B). In the first 2 ms of the off-switching, the fluorescence was reduced faster for Sc10 and Sc21, while the fluorescence of rsFusionRed2 and rsFusionRed3 was reduced stronger in the following milliseconds. The resulting overall off-switching halftimes were lower for Sc10 and Sc21 than for rsFusionRed2 and rsFusionRed3 (Figure 3.3-17 C). After 80 ms of off-switching, the residual fluorescence relative to the fluorescence in the on-state was comparable for the four

negative-switching RSFPs. Although the measured values fluctuated in the different experiments, the determined residual fluorescence in the off-state were below 8 % in all experiments (4.0-7.7 %).

The switching characteristics in mammalian cells and the performance as fusion tags for transient and stable expression (chapter 3.3.5) indicate that Sc10 and Sc21 might be suitable for live-cell RESOLFT imaging. This needs to be tested in the future. The advantage of rsFusionRed2 and rsFusionRed3 for RESOLFT microscopy might be their lower switching fatigues, which were only analyzed in this work for the RSFPs expressed in *E. coli* (chapter 3.3.2.4). Compared to rsFusionRed2 and rsFusionRed3, the higher molecular and cellular brightness of Sc10 and Sc21 (chapter 3.3.3.2 and 3.3.4), the faster off-switching in the first milliseconds (Figure 3.3-17) and the lower light doses needed for on-switching (chapter 3.3.5) can be advantageous for live-cell RESOLFT microscopy. In comparison to rsCherryRev1.4, Sc10 and Sc21 might be preferential due to their monomeric state (chapter 3.3.3.4) and good performance in fusions (chapter 3.3.5).

4 Discussion

The demand for reversibly switchable red fluorescent proteins with suitable characteristics for the super-resolution method RESOLFT is still high, since the number of available red RSFPs is still low and most red RSFPs have disadvantages. Thus, this work aimed to develop novel red-emitting RSFPs which are applicable in RESOLFT microscopy. To achieve this, a microscopic screening of mutant libraries expressed in *E. coli* colonies was adapted for the development of red RSFPs (chapter 3.1.1). Furthermore, a screening strategy based on the expression in mammalian cells was established (chapter 3.1.2). Based on their high brightness, the two red fluorescent proteins mRuby2 and mScarlet were chosen as templates to develop novel RSFPs (chapter 3.2 and 3.3). Screening of mutant libraries with the established and adapted screening strategies yielded novel positive- and negative-switching red RSFPs with exceptional features.

4.1 Screening for novel RSFPs

4.1.1 The automated microscope for screening and characterization of RSFPs

The search for fluorescent proteins with the ability of being switchable and the search for RSFPs with improved switching characteristics was realized by microscopic screening of *E. coli* colonies each expressing one mutant. Comparable screenings have already been applied for the generation of other RSFPs [92, 96, 98]. In this work, the wavelengths 445 nm and 561 nm were chosen as switching wavelengths (chapter 3.1.1). During the screening, the illumination with those wavelengths was performed alternating and not simultaneously (chapter 3.2.1.2 and 3.3.1.2), since the simultaneous illumination might already cause repetitive switching of single proteins and might not allow for complete on- and off-switching of the protein ensemble.

The microscopic screening enabled a detailed characterization of each expressed variant. The throughput of this screening method is restricted by the number of *E. coli* colonies on the agar plates and by the time needed for the identification of fluorescent colonies, the autofocussing and the illumination protocol. However, the overall process is rapid, since one mutagenesis and screening round, including the isolation of the respective plasmid DNA and sequencing, (Figure 3.1-1) can be accomplished within five days.

The automated microscope was also used for the characterization of the final switchable variants expressed in *E. coli* colonies due to the opportunity to flexibly modulate the switching protocols (chapter 3.2.2 and 3.3.2). The light intensities in this approach exceeded the light intensities which were used in the RESOLFT microscopes for switching of the RSFPs expressed in mammalian cells. Nevertheless, in the case of Ru63, Ru85 and Ru87, the times needed for on-switching were comparable for the switching in *E. coli* colonies with a light intensity of 14.5 $kWcm^{-2}$ (chapter 3.2.2.2) and for the switching in HeLa cells with a light intensity of 0.43 $kWcm^{-2}$ (chapter 3.2.5). An explanation to this intensity discrepancy might be the size of the detection volume due to the non-confocal setup of the automated microscope as well as the scattering and absorption of the light in the first layers of the bacterial colonies. However, the switching data can be used to compare different RSFPs, because this effect is comparable in each colony.

4.1.2 Screening for improved fluorescent proteins in mammalian cells

So far, most approaches of engineering fluorescent proteins were based on the expression of mutants in *E. coli* (e.g.: [54, 58, 85, 118]). The screening of mutant libraries expressed in *E. coli* colonies or in single *E. coli* cells allows for multiparametric analysis and has been capable to produce numerous fluorescent proteins with certain requested properties (chapter 1.2.3). Likewise, the screening of mutant libraries expressed in bacteria yielded new RSFPs in this work (chapter 3.2.1 and 3.3.1). However, the expression in *E. coli* does not present an accurate prediction regarding the characteristics of the fluorescent proteins in mammalian cells. This was also shown in this work, since the ensemble brightness and the switching properties of different RSFP variants differed between the *E. coli* colonies and the HeLa cells (e.g. chapter 3.2.2 and 3.2.5).

The screening of fluorescent proteins in mammalian cells allows for the characterization in a cellular context equal or comparable to the prospective expression host. Furthermore, the screening in mammalian cells will prefer fluorescent proteins with low cytotoxicity. Since the realization of screenings based on the expression in mammalian cells is complicated, only a few applications have been shown [84, 139, 179, 180] (see chapter 1.4.1). However these have certain disadvantages, for instance, the introduction of mutant libraries into mammalian cells using viruses [139] bear the risk of introducing the coding sequences of more than one variant per cell.

In this work, an approach was established which enables single variant expression per mammalian cell, a requirement for the screening of fluorescent proteins. This was achieved

by generating and employing a Bxb1 landing pad cell line (chapter 3.1.2). During the processing of this work, a similar approach was introduced by Matreyek *et al*. [181]. They integrated a landing pad into the AAVS1 locus of HEK cells and used this cell line along with high throughput sequencing to investigate the effect of different N-terminal codons on the expression of EGFP [181].

4.1.2.1 Generation of a Bxb1 landing pad cell line for screening

The Bxb1 landing pad cell line K21 was generated by knock-in of the designed landing pad into the genome of HeLa cells using CRISPR/Cas9 genome engineering (chapter 3.1.2.3). The knock-in of the landing pad was targeted to the AAVS1 locus, and the positive and accurate knock-in was verified by genotyping PCRs and sequencing of the PCR products. A double knock-in of the Bxb1 landing pad is determined to be unlikely (chapter 3.1.2.4), however, it could not be entirely ruled out. As the single knock-in is essential for the specificity of the screening approach, the verification of the single knock-in should be addressed in the future.

The integrated landing pad was composed of a CAG promoter and the Bxb1 attP site. Similar to the approach of Duportet *et al.* [140], a constitutive promoter was selected for the landing pad in this work, whereas Matreyek *et al.* chose a Tet-inducible promoter [181]. A landing pad with an inducible promoter offers the option to not permanently expose the cells to the transgene expression. However, for the screening it is advantageous to have a constitutive promoter, since fluorescent proteins with a low cytotoxicity in permanent expressions will be enriched [84]. In addition, the need for induction prolongs the time between transfection and possible fluorescence analysis. While Matreyek *et al.* controlled the transgene expression 7-11 days after transfection [181], the fluorescence in transfected K21 cells was analyzed 5-6 days after transfection (chapter 3.1.2.4). Moreover, the induction could add a variability to the expression of the fluorescent proteins in each cell.

Different to the generated HeLa K21 cell line in this work, the Bxb1 landing pad cell lines of Duportet *et al.* and Matreyek *et al.* stably express a fluorescent protein (EYFP or mTagBPF2) [140, 181]. After integration of a plasmid into these landing pads, the expression of the respective fluorescent protein is interrupted. Thereby it can be monitored, if an integration event occurred. However, this can be disadvantageous for the screening of fluorescent proteins with emission at similar spectral ranges. Since no fluorescent protein gene is encoded in the landing pad of the K21 cells, the cell line generated in this work can be used for the screening of all types of fluorescent proteins, independent from their spectral characteristics. Furthermore, the monitoring of the integration event is not needed, because

the integration can be detected by the fluorescence of the integrated and expressed fluorescent protein.

4.1.2.2 The efficiency of plasmid integration into the Bxb1 landing pad

To determine the integration efficiency, K21 cells were cotransfected with the Bxb1 expression plasmid and the integration plasmid pInt-mEGFP-P2A-HygroR. 1.15 % of the cells were green fluorescent, but the integration efficiency is presumably higher, since the transfection efficiency was not determined and therefore non-transfected cells could not be excluded. However, this percentage of fluorescent cells was lower than expected from the literature [140, 181]. The highest integration efficiency so far (10 %) was measured for a landing pad cell line generated from HEK cells (non-transfected cells were excluded in the analysis) [140]. The low integration efficiency for the K21 cells increases the amount of cells which have to be analyzed to compare the same quantity of fluorescent protein variants.

Several strategies could improve the integration efficiency. In the applied Bxb1 expression plasmid (pCAG-NLS-HA-Bxb1 [167]), a nuclear localization signal (NLS) was fused to the N-terminus of the Bxb1 recombinase. Since it was shown, that an NLS sequence does not improve the integration efficiency and a fusion to the N-terminus of the Bxb1 recombinase can even reduce the integration efficiency [140], a new expression plasmid for the Bxb1 recombinase without NLS sequence should be generated. Furthermore, it was shown that the transfection of the Bxb1 expression plasmid one day before the transfection of the integration plasmids can improve the integration efficiency [181]. These strategies should be tested to improve the integration efficiency and thereby increase the throughput in the screening of mutant libraries.

4.1.2.3 Screening for brighter fluorescent proteins expressed in K21 cells

Using the generated Bxb1 landing pad cell line K21, a screening for fluorescent proteins with improved brightness was established (chapter 3.1.2.5). This was implemented by *in vitro* mutagenesis, transfection of the mutant library along with the Bxb1 expression plasmid, and fluorescence analysis of the transfected cells in flow cytometry. The variants with the highest red fluorescence signal or the best red-to-green fluorescence ratio were selected by fluorescence-activated cell sorting. The cells were cultivated for a few days to increase the cell number for the subsequent isolation of genomic DNA. The coding sequences of the selected variants were amplified by PCR and cloned into a suitable vector. One mutagenesis and screening round took about three weeks.

In contrast to viral approaches [140], all fluorescent protein variants are expressed from the same genomic locus. For this reason, the fluorescence signals were expected to be more comparable. Surprisingly, the fluorescence signals of the K21 cells with the same integrated plasmid (pInt-mEGFP-P2A-HygroR) varied strongly (Figure 3.1-4 A). This variation might arise from varying expression levels depending on the cell cycle phase or random transcription bursts [182, 183]. Thus, the utilization of the integration plasmids with the element P2A-mCherry or P2A-mEGFP is useful in terms of assigning the quantity of expressed proteins. The correlation of the mRuby2 and mEGFP signals in the K21 cells with integrated pInt-mRuby2-P2A-mEGFP plasmid proved this concept to be suitable (Figure 3.1-4 C).

In the plasmid pInt-MCS-P2A-codEGFP (chapter 3.1.2.2), the codon usage at the N- and C-terminus of the mEGFP gene was modified (codons of the first and last 7-8 amino acids). This plasmid can be used as backbone, if the red template protein applied in the mutagenesis and screening contains EGFP-ends. This minimizes the amount of primers that bind to the mEGFP gene instead of the red fluorescent protein gene when the coding sequences of the selected red variants are extracted from the genomic DNA by PCR.

The screening was applied to identify RSFPs with higher brightness. Mutations which stabilize the chromophore and thereby improve the brightness could at the same time prevent or impair the switching process. For this reason, a higher fluorescence signal of a RSFP mutant measured in flow cytometry can be accompanied by a reduction or loss of switching. Furthermore, the RSFPs were not switched on prior to the flow cytometry analysis, thus a higher detected fluorescence signal might also be a consequence of an altered equilibrium state. Consequently, a combinatory screening was conducted by cloning the coding sequences of the selected mutants into the pBad vector and then controlling the switching abilities of the RSFP variants in the automated microscope. However, it would be preferable to reduce the number of experimental steps by characterizing the switching characteristics of the bright RSFPs directly in the K21 cells (see chapter 4.1.2.4).

The screening for brighter fluorescent proteins based on the K21 cell line might be more suited for non-switching proteins. Related to the development of novel RSFPs, the described protocol could be applied at the beginning to identify brighter template proteins. This is in particular interesting for the development of red RSFPs, because those typically exhibit a low molecular brightness.

4.1.2.4 The potential of the Bxb1 landing pad cell line

Various screening approaches for the evolution of fluorescent proteins are conceivable on the basis of the generated Bxb1 landing pad cell line K21. In this work, the screening of mutant libraries expressed in K21 cells was restricted to the fluorescence analysis in flow cytometry. This type of screening can be used to identify brighter fluorescent protein mutants.

The development of fluorescent proteins with improved tagging performance could be implemented by transfection of the K21 cells with a mutant fusion construct library and an imaging-based screening. The prepared integration plasmids for keratin and vimentin constructs (chapter 3.1.2.2) could be utilized as vector backbone for this. In addition, a screening which identifies RSFPs with improved switching characteristics in mammalian cells is desirable. For this purpose, a suitable setup for repetitive switching and subsequent sorting of single K21 cells is required. A microfluidic cell sorter [139, 184] with several consecutive laser beams for switching and readout could be a solution to this [185].

Moreover, the Bxb1 landing pad cells can be used for the generation of monoclonal cell lines stably expressing a fusion construct. This can be applied to investigate the applicability of new fluorescent proteins in stable expressions (chapter 3.2.4.2 and 3.3.5.2). In addition, it was shown that K21 cells stably expressing keratin fusion constructs can serve as samples for the establishment of RESOLFT imaging due to the higher reproducibility from day to day compared to transient overexpressions (chapter 3.2.5).

To conclude, the advantage of a Bxb1 landing pad cell line for screening is the option for single variant expression per mammalian cell, which is not necessarily given in other approaches like viral transfections. This enables the characterization and comparison of different fluorescent protein variants. In contrast to other published Bxb1 landing pad cell lines, the K21 cell line can be used for screening of all types of fluorescent proteins. In addition, the permanent expression of the single mutant variants should facilitate the selection of fluorescent proteins with low cytotoxicity. In combination with the establishment of further screening techniques, the Bxb1 landing pad cell line K21 offers a great potential for the development of new fluorescent proteins.

4.2 Novel reversibly switchable red fluorescent proteins

The number of applicable red-emitting RSFPs for RESOLFT microscopy is limited, since most of the available red RSFPs exhibit drawbacks like a low switching contrast or a dimerization tendency [91, 98]. Numerous green RSFPs with favorable characteristics exist [93], however using red RSFPs with longer excitation and switching wavelengths leads to reduced phototoxicity, autofluorescence and light-scattering during imaging of living cells [84]. Furthermore, red RSFPs with excellent characteristics can be used along with available green RSFPs in dual color RESOLFT microscopy [98]. In this work, a series of novel RSFPs emitting in the red region of the spectrum were developed. Both, positive- and negative-switching RSFPs with a high switching contrast were generated from non-switching template proteins. The new red RSFPs are potential probes for live-cell RESOLFT microscopy.

4.2.1 Positive-switching RSFPs derived from mRuby2

The red fluorescent protein mRuby2 [57] was chosen as template for the development of novel RSFPs due to its high molecular brightness and its monomeric state. Additionally, no attempts of developing an RSFP on the basis of this protein were reported so far. Mutagenesis of the chromophore-surrounding amino acids followed by screening yielded the slightly switchable Ru27 variant (M164T) (chapter 3.2.1.1). This mutant switched in a positive-switching mode, which was particularly favored, since no positive-switching red RSFPs with characteristics suitable for live-cell RESOLFT microscopy were available.

A high number of mutagenesis and screening rounds were conducted to obtain switchable mRuby2 variants with low residual fluorescence in the off-state (chapter 3.2.1.3). Only the crystal structure of the mRuby2-precursor mRuby was available for the choice and analysis of mutation sites (Figure 3.2-2 B). Among others, the positions T162 and M164 were mutated, which are typical mutation sites for the introduction or improvement of switching as both are located close to the chromophore (chapter 1.3.4). For instance, at least one of these two positions were as well mutated in the development of the red RSFPs rsTagRFP [82], rsCherry and rsCherryRev [91].

The mutation C176A was introduced due to the findings of Duan *et al.* who showed that sulfoxidation of the cysteine at position 171 in IrisFP might be involved in the switching fatigue mechanism of this protein [99]. The addition of the C176A mutation indeed improved the switching fatigue in the switchable mRuby2 variants by about 28 % (Ru48;

chapter 3.2.1.3). Altogether, 10-14 mutations were added in total to generate the final variants Ru63, Ru85 and Ru87, eight of these are located in loops or outside the beta barrel structure.

After the start of this work, the conventional fluorescent protein mRuby3 was reported which is a variant of mRuby2 with 21 mutations. This proteins exhibits a higher molecular brightness and an improved photostability compared to its progenitor [70]. However, one of the key amino acids which improved the characteristics (M164I), is one of the mutation sites in the switchable mRuby2 variants. Furthermore, the addition of the Ru48 mutations to mRuby3 yielded switchable variants, but with worse switching characteristics compared to Ru48 (data not shown, mutations and characteristics of Ru48: see chapter 3.2.1.3). Thus, this template was not further pursued.

4.2.1.1 Comparison of available positive-switching red RSFPs

The switching behavior of Ru63, Ru85 and Ru87 was compared to the only other available monomeric and positive-switching red RSFP, rsCherry [91]. The characterization of these positive-switching RSFPs expressed in *E. coli* colonies revealed that all three switchable mRuby2 variants outperform rsCherry (chapter 3.2.2). Ru63, Ru85 and Ru87 exhibited lower residual fluorescence in the off-state (about 4.5 %) and substantial higher on- and off-switching kinetics. All three could be switched in more than 350 switching cycles until the maximal fluorescence was bleached to 50 %, while rsCherry lost its switching ability within 40 switching cycles. Some negative-switching RSFPs (green and red) were shown to be switchable several hundreds or even thousands times before the on-state signal was reduced to half [96, 98, 118]. However, these results are strongly dependent on the experimental conditions like light intensities, completeness of switching per cycle and the cellular conditions which varied in each measurement.

The only other reported positive-switching red RSFPs are asFP595 and its mutants, which are not applicable in live-cell microscopy due to their obligate tetramerization [33, 74, 116]. By contrast, Ru63, Ru85 and Ru87 were shown to be monomeric in size-exclusion chromatography (chapter 3.2.3.4). Hence, Ru63, Ru85 and Ru87 were identified as the positive-switching RSFPs with the highest potential for the application in live-cell RESOLFT microscopy to date.

4.2.1.2 Further characterization of the RSFPs Ru63, Ru85 and Ru87

A detailed switching characterization and a characterization of the purified protein samples was performed for the final variants Ru63, Ru85 and Ru87 (chapter 3.2.2 and 3.2.3).

Expressed in *E. coli* colonies, the three variants exhibited comparable switching characteristics. However, the determined off-switching halftimes of Ru85 and Ru87 were slightly lower for the applied light intensity (chapter 3.2.2.3) and the residual fluorescence in the off-state increased less in the switching fatigue curves of these two RSFPs (chapter 3.2.2.4). The additional advantage of Ru87 is the highest ensemble brightness measured in *E. coli* (chapter 3.2.2.1). All three switchable mRuby2 variants relaxed from the on- and off-state within 4 s (chapter 3.2.2.6), while most other RSFPs exhibit thermal relaxation times from minutes to hours (e.g. rsTagRFP, Padron, rsEGFP) [82, 88, 90, 118].

A greater difference was found in the equilibrium state (chapter 3.2.2.6) and in the shape of the absorption spectra (chapter 3.2.3.1). The addition of the mutations M15T and V188D increased the equilibrium state from 10 % of the on-state signal (Ru63) to 32 % (Ru85), while further addition of the mutations N37A and G157V, both located in loops, reduced the equilibrium state again to 20 % (Ru87). In the absorption spectra, the change from a main and a minor maximum to a single broad maximum in the range of 500 to 600 nm was introduced by either the M15T or the V188D mutation. The M15T mutation is located inside the barrel and is closer to the chromophore than V188D. However, the explanation for the changes in the spectra and in the equilibrium state remain unclear.

In addition, a small absorption maximum was detected at about 450 nm for Ru85 and Ru87 (Figure 3.2-10 B). As both RSFPs showed a higher fluorescence in the equilibrium state compared to Ru63, this absorption band might represent a fraction of RSFPs in the on-state which can be switched to the off-state by absorption of light at 445 nm. Furthermore, this absorption band might rise from protonated chromophores, since the absorption at this wavelength also increased when the proteins were diluted in buffers with low pH values (Figure 3.2-11). An additional absorption maximum occurred at 500 nm when the Ru63, Ru85 and Ru87 protein samples were diluted in buffers with pH values higher than 9.0. This absorption band cannot be assigned, but due to the high pH values it should arise from the deprotonation of a residue exhibiting a high pK_a value.

No changes in the absorption spectra were measured after illumination of the Ru63, Ru85 and Ru87 protein samples with blue or yellow-green light (chapter 3.2.3.1). However, this might be due to the rapid thermal relaxation and the time needed to start the absorption measurements. Thus, the determination of the quantum yields and extinction coefficients based on the absorption and emission spectra could only be performed for the proteins in the equilibrium state (chapter 3.2.3.2). By contrast, the quantum yield determination based on the nanocavity-based method [169] is independent from the state of the protein. This

might explain the higher quantum yields measured in this method. The quantum yields of Ru63, Ru85 and Ru87 determined in the nanocavity-based method (QYs = 17-20 %) are comparably high for red RSFPs (comparison to other red RSFPs: see chapter 4.2.3). Although it was not measurable, the absorption spectra might change upon switching, like it was shown for Sc10, Sc21 (Figure 3.3-9), rsTagRFP [82] and most green RSFPs [88, 90, 96]. Hence, the extinction coefficients measured for the equilibrium state might not equal the extinction coefficients of the on-state.

All three switchable mRuby2 variants showed high performance as fusion tags in the transient and stable expressions in mammalian cells (chapter 3.2.4). Ru87 was even shown to be applicable in endogenous tagging of vimentin (chapter 3.2.4.2). These experiments in combination with the characterization of the switching in *E. coli* colonies suggest an applicability of all three variants in live-cell RESOLFT microscopy, with Ru87 having small benefits. However, when expressed in vimentin constructs in HeLa cells, the switching curves of Ru63, Ru85 and Ru87 revealed differences to the once measured in *E. coli* concerning the on-switching kinetics and the residual fluorescence in the off-state (Figure 3.2-17). This data suggests the highest applicability of Ru63 for live-cell RESOLFT imaging because it exhibited the lowest fluorescence in the off-state (10 % of the on-state signal). For this reason, Ru63 was chosen for the establishment of live-cell RESOLFT imaging with positive-switching red RSFPs. In the future, the switching characteristics of Ru63, Ru85 and Ru87 should be additionally tested and compared using further fusion construct in order to examine the effect of the localization within the cell and the fusion construct on the switching characteristics. Just recently, it was shown, that the packing can have an influence on the switching mechanism in RSFPs [186] and the binding to another protein can alter switching characteristics [187].

4.2.1.3 Live-cell RESOLFT image utilizing a positive-switching red RSFP

Before the start of this work, live-cell RESOLFT microscopy with red RSFPs had only been implemented with negative-switching proteins [98, 118]. However, only two instead of three laser beams are needed in RESOLFT microscopy with positive-switching RSFPs [100]: A doughnut-shaped beam for off-switching and a Gaussian beam for on-switching and fluorescence readout. The new RSFP Ru63 was selected for the establishment of live-cell RESOLFT imaging with a positive-switching red RSFP. Indeed, a resolution improvement was achieved using a point-scanning approach with a dwell time of about 5 ms per pixel (Figure 3.2-18, protocol: 2.4.3.1). FWHM of 106 and 125 nm were determined in line profiles across the keratin filaments. For comparison, a confocal image was acquired of the

same field of view by 2 ms on-switching and subsequent fluorescence readout. It should be mentioned that this confocal image might exhibit a higher resolution than expected, since the RSFPs, especially the ones in the periphery, might be incompletely switched to the on-state. Thus, the resolution improvement in the RESOLFT image might be less obvious (Appendix Figure 6.3-2). The switching characteristics (chapter 3.2.2 and 3.2.5Figure 3.2-17) and the performance as fusion tag (chapter 3.2.4) suggest that Ru63 is a promising candidate for live-cell RESOLFT microscopy. An adjustment of the RESOLFT imaging scheme could further improve the obtained resolution in the future.

4.2.2 Negative-switching RSFPs derived from mScarlet

Due to its high molecular brightness, the recently introduced and non-switching red fluorescent protein mScarlet [85] was additionally selected as template protein. In contrast to the evolution of Ru63, Ru85 and Ru87, only a few mutagenesis and screening rounds were needed to obtain red RSFPs with low residual fluorescence in the off-state (chapter 3.3.1). In the semi-rational design, mainly saturated site-directed mutagenesis was performed. Similar to the generation of switchable mRuby2 mutants, the mutagenesis of the amino acids at positions 162 and 164 in mScarlet yielded switchable proteins, but this time with a negative-switching mode. In addition, the position S147 was mutated, which was previously shown to be a typical mutation site for the introduction or improvement of switching [82, 91, 118], resulting in the final variant Sc10 (chapter 3.3.1.3). The other final variant Sc21 contains two additional mutations located outside the beta barrel (R217Q, D161K) which mainly improved the off-switching halftime. Also in the development of switchable mRuby2 variants (chapter 3.2.1.3) and other red RSFPs [82, 91, 98], mutation sites in loops or outside the beta-barrel structures were introduced, but these differ for the individual RSFPs. Those mutations might influence the folding of the GFP-like proteins and the exact position of the beta-strands.

4.2.2.1 Comparison of negative-switching RSFPs

During the processing of this work, new negative-switching RSFPs were reported, which were obtained by mutagenesis of FusionRed [118]. Since rsFusionRed2 and rsFusionRed3 were successfully employed in live-cell RESOLFT microscopy and exceeded rsTagRFP and rsCherryRev1.4 concerning off-switching halftimes [118], these two RSFPs were chosen for the comparison to Sc10 and Sc21.

Both, rsFusionRed2 and rsFusionRed3 showed essentially lower ensemble brightness in *E. coli* colonies compared to the negative-switching RSFPs generated in this work (factor of

6.8-8.0; chapter 3.3.2.1). A lower cellular brightness was as well measured in HeLa cells (chapter 3.3.4). However, the determined molecular brightness of Sc10 and Sc21 was only slightly higher than the published values of rsFusionRed2 and rsFusionRed3 (factor 1.2-1.8; chapter 3.3.3.2). Thus, the quantum yield, the extinction coefficient and the resulting molecular brightness were also determined for rsFusionRed2 and rsFusionRed3 using the protocols of this work. As a result, the molecular brightness of rsFusionRed2 and rsFusionRed3 was 2.8 to 4.4-fold lower compared to the values of Sc10 and Sc21. It should be noted, that the maturation varied strongly for rsFusionRed2 and rsFusionRed3 which affected the extinction coefficient determination (Appendix Table 16). However, the published values could not be reached in four experiments and the variation of the measured extinction coefficients indicate problems in the maturation of these proteins.

Expressed in *E. coli* colonies, Sc21 exhibited the lowest fluorescence in the off-state (chapter 3.3.2.1) and the lowest switching halftimes of the four examined negative RSFPs (chapter 3.3.2.2 and 3.3.2.3). In the on-switching using light of 445 nm, the switching speeds of Sc10 and Sc21 clearly exceeded the switching speeds of rsFusionRed2 and rsFusionRed3 (Figure 3.3-5). The high sensitivity of Sc10 and Sc21 to light of 445 nm was also visible in the switching of RSFPs in HeLa cells, since 4.7-fold higher light intensity were applied for the on-switching of rsFusionRed2 and rsFusionRed3 to obtain comparable switching contrasts (chapter 3.3.6). Lower 445 nm light intensities or shorter on-switching times reduce the doses of blue light needed in RESOLFT imaging, thus a lower phototoxicity is expected for the application of Sc10 and Sc21 compared to the application of rsFusionRed2 and rsFuionRed3.

The off-switching curves acquired for Sc10 and Sc21 expressed in HeLa cells revealed substantial higher off-switching kinetics in the first two milliseconds followed by a fluorescence decrease with a slow kinetic (Figure 3.3-17). The impact of this effect on the application of Sc10 and Sc21 in RESOLFT microscopy has to be addressed in the future.

The only advantage of rsFusionRed2 and rsFusionRed3 was found in the switching fatigue experiments (chapter 3.3.2.4). Using the chosen switching scheme, rsFusionRed2 and rsFusionRed3 could be switched 2.0-2.5 times more often until the maximal signal was reduced by half. However, Sc10 and Sc21 were also switched more than 100 times before the signal was reduced to 50 %. In addition, a fluorescence decrease of 30 % was observed from the first to the second switching cycle for rsFusionRed2 and rsFusionRed3 and only by 9 % for Sc10 and Sc21, which was not taken into account for the evaluation of the

switching fatigue. The high loss of the on-state fluorescence is a severe disadvantage for the application of rsFusionRed2 and rsFusionRed3.

4.2.2.2 Further characterization of the RSFPs Sc10 and Sc21

Most examined characteristics of Sc10 and Sc21 were comparable. Both RSFPs are monomeric in size-exclusion chromatography (chapter 3.3.3.4) and both exhibited comparable quantum yields (24-25 %; chapter 3.3.3.2). In difference to the switchable mRuby2 variants, the absorption spectra of the isolated Sc10 and Sc21 protein samples changed upon illumination with blue and yellow-green light (Figure 3.3-9). The off-switching with yellow-green light gave rise to an absorption maximum at about 450 nm, representing the absorption band which can be addressed by blue light for on-switching.

The pK_a value was comparably high for Sc10 and Sc21 (7.7 and 7.8; chapter 3.3.3.3). However, a *cis-trans* or *trans-cis* isomerization at reduced pH values was proven for some proteins like mRuby and Gamillus [126, 177], thus a pH-dependent change of the equilibrium state is conceivable for Sc10 and Sc21. This could be analyzed in the future by examination of the switching ability and the equilibrium state of Sc10 and Sc21 samples diluted in buffers with lower pH values.

The investigation of the absorption change at 570 nm revealed a halftime of about 2 min for the thermal relaxation from the off-state for Sc10 and Sc21 (chapter 3.3.3.1), considerably higher than the relaxation halftimes of Ru63, Ru85 and Ru87 (relaxation halftimes from the on-state: 216-478 ms). Comparable to the switchable mRuby2 variants, the utility of Sc10 and Sc21 as fusion tags in transient and stable expressions in mammalian cells was shown and Sc21 was even applicable in the endogenous tagging of vimentin (chapter 3.3.5). The result of all characterizations is that both, Sc10 and Sc21, are potential candidates for live-cell RESOLFT microscopy, which still needs to be proven in the future. Only the higher switching fatigue shown for Sc10 and Sc21 might limit their use in this method.

4.2.3 Available red-emitting RSFPs

By now, more negative-switching than positive-switching RSFPs are available which emit in the green and red region of the spectrum. In addition, most applications of RESOLFT microscopy utilized negative-switching RSFPs [86]. Also in this work, the generation of positive-switching red RSFPs with favorable characteristics required more effort than the generation of negative-switching red RSFPs (chapter 3.2.1.3 and 3.3.1.3). However, this might also be due to the chosen template proteins.

The novel mRuby2 variants represent the only potential positive-switching and red fluorescent candidates for live-cell RESOLFT microscopy and Ru63 has been shown to be applicable in this super-resolution method (chapter 3.2.5). The poor switching characteristics of rsCherry (chapter 3.2.2) [91] and the tetrameric state of asFP595 [33] restrict their applicability as fusion tags in live-cell RESOLFT microscopy.

In addition to the novel negative-switching mScarlet variants, a few other negative-switching and red-emitting RSFP exist (Table 7). The RSFP rsFusionRed1 was not considered due to its low switching contrast (residual fluorescence in the off-state: 34 %) [118]. From the negative-switching RSFPs, only rsFusionRed2, rsFusionRed3 and rsCherryRev1.4 were applied in live-cell RESOLFT microscopy despite the dimerization tendency of the latter [98, 118]. The switching characteristics of various RSFPs from the literature are difficult to compare because of the different expression and switching conditions applied. However, using the same protocol, Pennacchietti *et al.* presented that rsFusionRed2 and rsFusionRed3 exhibited the fastest off-switching kinetics of the negative-switching RSFPs available at that time [118]. In this work, the off-switching kinetics of the novel RSFPs Sc10 and Sc21 even exceeded the ones of rsFusionRed2 and rsFusionRed3 (chapter 3.3.2.2).

Table 7: Characteristics of available red RSFPs.
Switching mode, absorption, excitation and emission maximum, extinction coefficient, quantum yield, molecular brightness, pK_a and oligomeric state of available red RSFPs.

RSFP	Sw. mode	Abs. max. [nm]	Exc. max. [nm]	Em. max. [nm]	ε [$M^{-1}cm^{-1}$]	QY	Bright-ness (ε * QY)	pK_a	Olig. state	Ref.
Ru63	Pos. sw.	571	555	592	24,000	0.18	4.32	6.1	monomer	this work
Ru85		565	555	593	14,100	0.17	2.40	6.5	monomer	
Ru87		564	555	593	20,500	0.20	4.10	6.2	monomer	
rsCherry		571	n.d.	610	80,000[a]	0.02[a]	1.6	6.0[a]	monomer	[91]
asFP595		572	572	595	n.d.	n.d.	n.d.	n.d.	tetramer	[33]
Sc10	Neg. sw.	570	570	600	22,500	0.24	5.4	7.7	monomer	this work
Sc21		570	570	600	20,500	0.25	5.1	7.7	monomer	
rsFusionRed2		564	580	607	35,500	0.12	4.3	4.7	monomer	[118]
rsFusionRed3		565	580	607	38,000	0.08	3.0	4.7	monomer	[118]
rsCherryRev		572	n.d.	608	84,000[a]	0.005[a]	0.4	5.5[a]	monomer	[91]
rsCherryRev1.4		572	n.d.	609	n.d.	n.d.	n.d.	5.5	dimerization tendency	[98]
rsTagRFP		567	567	585	36,800	0.11	4.0	6.6	monomer	[82]

a: determined in Subach et al., 2009 [178]

All reported red RSFPs suffer from a low molecular brightness (Table 7). The five generated red RSFPs in this work rank among the red RSFPs with the highest molecular brightness. The quantum yield and the molecular brightness determined for Sc10 and Sc21 are the highest values measured for red RSFPs by now. Nevertheless, a strong reduction in the molecular brightness was as well observed for the novel red RSFPs compared to their

template proteins (mRuby2: 43 [57], mScarlet: 70 [85]). Presumably, the introduction of switching allows a higher probability for non-radiative processes [121]. However, it should be noted that the molecular brightness of most available green RSFPs exceed the molecular brightness of the red RSFPs (e.g.: rsEGFP2: 18.3 [96]).

The maturation process of red fluorescent chromophores is more complex than the maturation of green fluorescent chromophores and involves the formation of a blue fluorescent intermediate state, and in some cases even a break in the protein backbone [2, 46, 49, 188]. A fraction of incompletely matured chromophores might be visible in the absorption spectrum of red fluorescent protein samples at lower wavelengths. Interestingly, the absorption spectra of most red RSFPs (Ru63, Ru85, Ru87 (chapter 3.2.3.1), Sc10, Sc21 (chapter 3.3.3.1), rsCherry, rsCherryRev [91], rsCherryRev1.4 [98], rsFusionRed2, rsFusionRed3 [118]) feature a distinct absorption maximum at about 390 to 420 nm and partially a slightly increased absorption in the range of 320-380 nm. While the absorption spectra of their progenitor (mRuby2, mScarlet, mCherry, FusionRed) showed only a (slightly) increased absorption at 320-380 nm, but no distinct absorption maximum at 400 nm (chapter 3.2.3.1, chapter 3.3.3.1, [91] and [76]).

The 400 nm absorption maximum of the red RSFPs fits to the excitation maximum of the blue fluorescent mTagBFP and mCherry-Blue, which was generated from the red fluorescent TagRFP and mCherry by mutagenesis [61]. Among others, the positions 148 and 165 were mutated in these proteins, which are also typical mutations sites to generate RSFPs (positions 143 and 162 in mScarlet and mRuby2). Furthermore, the mutation M65L was introduced to obtain these blue fluorescent variants, which was also added in the switchable mRuby2 variants (here: M67L). It was suggested that the blue fluorescent proteins were obtained by preventing the last maturation steps from the blue intermediate to the red fluorescent proteins [49, 61]. Thus, the distinct absorption maximum might result from a higher fraction of blue fluorescent intermediates. However, this cannot explain the differences between the red RSFPs and their template proteins (not detected for rsTagRFP, rsFusionRed1). Hence, the introduction of switching by mutagenesis of the chromophore-surrounding amino acids might affect the blue intermediate in an additional way.

4.2.4 Switching mechanisms in red RSFPs

Several studies investigated the underlying mechanism of switching in different RSFPs (e.g. [40, 99, 116, 117, 120]). Even today the exact mechanism stays unclear and might differ for the individual RSFPs. In all positive- and negative-switching RSFPs examined by now, *cis*-

trans isomerization is a key event in switching. A change in the planarity and flexibility as well as protonation and deprotonation of the chromophore are discussed to contribute to the different fluorescence abilities of the *cis*- and *trans*-forms [125].

The chromophore of the non-switching mRuby protein adopted a *trans*-conformation in crystal structures at pH 8.5 [177], while the chromophore of mScarlet adopted a *cis*-conformation at pH 7.8 [85]. This raises the question, which conformations the chromophores of the novel RSFPs adopt in the on- and off-states. Structural investigations could reveal insights to this in the future. By now, almost all examined crystal structures of on-switched RSFPs showed a chromophore in the cis-conformation [125]. For instance, the on-state chromophore of rsTagRFP was found in the *cis*-form [117], although its non-switching progenitor TagRFP exhibits a *trans*-chromophore [49]. In contrast, just recently it was shown that the chromophore of the acid-tolerant RSFP rsGamillus-S adopts a *trans*-form in the on-state and a *cis*-form in the off-state [126].

For all switchable mRuby2 and mScarlet proteins, the dilution in buffers with lower pH values gave rise to an absorption maximum at about 450 nm, which was assigned to be the chromophore protonated at the hydroxyphenyl ring (chapter 3.2.3.3 and 3.3.3.3). A comparable absorption maximum was visible in the absorption spectra of the off-switched Sc10 and Sc21 protein solutions (chapter 3.3.3.1). Furthermore, 445 nm represents a wavelength for efficient switching of Ru63, Ru85, Ru87, Sc10 and Sc21 (chapter 3.2.2.5 and 3.3.2.5). Thus, it is reasonable that protonation and deprotonation is involved in the switching mechanism, like it was already shown for other RSFPs [116, 117, 189].

The introduction of switching in mScarlet and mRuby2 was achieved by mutating M164 to smaller amino acids (threonine, glycine, alanine, Figure 3.2-2, Figure 3.3-2). In addition, the amino acid at position 157 was exchanged from a polar to a non-polar amino acid in mScarlet (serine to glycine), while the amino acid at position 162 was mutated from a non-polar to a polar amino acid (isoleucine to glutamine). By contrast, in mRuby2 the amino acid at position 162 was exchanged from a polar to a non-polar amino acid (threonine to alanine). The mentioned mutation sites are located in close proximity to the chromophore. Hence, these mutations might enable switching in the generated RSFPs by offering more space for *cis-trans* isomerization and by changing the hydrogen bonding network, like it was shown for other RSFPs [125]. However, these speculations and the contribution of the other mutations to the switching need to be analyzed in the future, for instance by X-ray crystallography.

4.2.5 Alternative wavelengths for switching

The wavelength of 405 nm, 445 nm and 488 nm were compared for the off-switching of Ru85, Ru85 and Ru87 and for the on-switching of Sc10 and Sc21 (chapter 3.2.2.5 and 3.3.2.5). The adjustment of the light intensities enabled switching with all three wavelengths in a comparable manner. The lowest light intensities were needed for the switching with light of 445 nm and therefore this wavelength is preferred. However, the switching with 405 nm and 488 nm could enable simultaneous on- (Sc10, Sc21) or off-switching (Ru63, Ru85, Ru87) of the red RSFPs along with green RSFPs in dual color RESOLFT microscopy [98]. In addition, a higher switching wavelength is desirable to reduce phototoxicity in living cells while imaging [118], but probably the switching times need to be prolonged or the switching intensities needed to be increased, if light of 488 nm instead of 445 nm is used for switching.

The application of different wavelengths for on-switching was also investigated for rsFusionRed2 and rsFusionRed3 by Pennacchietti *et al.* [118]. There, the switching wavelengths 405 nm, 488 nm and 510 nm were compared. They observed a lower switching fatigue when applying light of 510 nm for on-switching. This is in contrast to the findings of this work, which did not find significant variations for the switching with 405 nm, 445 nm and 488 nm. The differences of both studies might result from the fact, that Pennacchietti *et al.* did not adjust the light intensities to obtain comparable switching kinetics [118] for the different switching wavelengths as it was done in this work.

4.2.6 Future perspective of the novel red RSFPs

Five novel monomeric and red-emitting RSFPs with high switching contrast were developed and characterized in this work. Further mutagenesis and screening could be applied to identify even further improved red RSFPs in the future, for example switchable mScarlet variants with higher photostability. The application of the screening based on the expression in K21 cells might further improve the molecular brightness and the expression in mammalian cells. X-ray crystallography of on- and off-switched crystals [40] or time-resolved serial femtosecond crystallography [190] could give insights into the switching mechanism of the novel RSFPs, which could also guide the rational choice of further mutation sites to improve these proteins.

The characteristics of the RSFPs generated in this work suggest an applicability in live-cell RESOLFT microscopy. However, only for Ru63 a RESOLFT image with a resolution lower than the diffraction limit has already been acquired. In the future, RESOLFT microscopy

with Sc10 and Sc21 might be established and a detailed search for suitable switching schemes could improve the resolution for RESOLFT microscopy utilizing Ru63. Furthermore, different fusion constructs and different switching wavelengths like 405 nm, 488 nm and 590-595 nm could be tested [98, 118]. A parallelized RESOLFT strategy or smart scanning could shorten the imaging times or reduce photobleaching during imaging [118, 129, 130].

This work focused on the application of red RSFPs in RESOLFT microscopy. However, the application in other super-resolution methods like photochromic stochastic optical fluctuation imaging (pcSOFI) [191] or protected STED [94] could be evaluated for the novel red RSFPs in future experiments. In addition, the RSFPs might be tested for optoacoustic imaging [192] and the observed photochromic behavior of Sc10 and Sc21 could allow the application in photochromic FRET (pcFRET) [117].

5 References

1. Hooke, R., *Micrographia, or some physiological descriptions of minute bodies made by magnifying glasses, with observations and inquiries thereupon.* 1665.
2. Chudakov, D.M., Matz, M.V., Lukyanov, S., and Lukyanov, K.A., *Fluorescent proteins and their applications in imaging living cells and tissues.* Physiol Rev, 2010. 90(3): p. 1103-63.
3. Abbe, E., *Beiträge zur Theorie des Mikroskops und der mikroskopischen Wahrnehmung.* Archiv für Mikroskopische Anatomie, 1873. 9(1): p. 413–468.
4. Hell, S.W., *Far-Field Optical Nanoscopy.* Science, 2007. 316(5828): p. 1153-1158.
5. Minsky, M., *Microscopy apparatur. US Patent 3013467 A.* 1961.
6. Gustafsson, M.G., *Surpassing the lateral resolution limit by a factor of two using structured illumination microscopy.* J Microsc., 2000. 198: p. 82-7.
7. Sahl, S.J., Hell, S.W., and Jakobs, S., *Fluorescence nanoscopy in cell biology.* Nat Rev Mol Cell Biol, 2017. 18(11): p. 685-701.
8. Sigal, Y.M., Zhou, R., and Zhuang, X., *Visualizing and discovering cellular structures with super-resolution microscopy.* Science, 2018. 361(6405): p. 880-887.
9. Rust, M.J., Bates, M., and Zhuang, X., *Sub-diffraction-limit imaging by stochastic optical reconstruction microscopy (STORM).* Nat Methods, 2006. 3(10): p. 793-5.
10. Betzig, E., Patterson, G.H., Sougrat, R., Lindwasser, O.W., Olenych, S., Bonifacino, J.S., Davidson, M.W., Lippincott-Schwartz, J., and Hess, H.F., *Imaging intracellular fluorescent proteins at nanometer resolution.* Science, 2006. 313(5793): p. 1642-5.
11. Folling, J., Bossi, M., Bock, H., Medda, R., Wurm, C.A., Hein, B., Jakobs, S., Eggeling, C., and Hell, S.W., *Fluorescence nanoscopy by ground-state depletion and single-molecule return.* Nat Methods, 2008. 5(11): p. 943-5.
12. Hell, S.W. and Wichmann, J., *Breaking the diffraction resolution limit by stimulated emission: stimulated-emission-depletion fluorescence microscopy.* Opt Lett., 1994. 19(11): p. 780-2.
13. Klar, T.A., Jakobs, S., Dyba, M., Egner, A., and Hell, S.W., *Fluorescence microscopy with diffraction resolution barrier broken by stimulated emission.* Proc Natl Acad Sci U S A. , 2000. 97(15): p. 8206-10.
14. Hell, S.W., Dyba, M., and Jakobs, S., *Concepts for nanoscale resolution in fluorescence microscopy.* Curr Opin Neurobiol, 2004. 14(5): p. 599-609.
15. Hell, S.W. and Kroug, M., *Ground-state-depletion fluorscence microscopy: A concept for breaking the diffraction resolution limit.* Applied Physics B, 1995. 60(5): p. 495–497.

16. Hell, S.W., Jakobs, S., and Kastrup, L., *Imaging and writing at the nanoscale with focused visible light through saturable optical transitions.* Applied Physics A: Materials Science & Processing, 2003. 77(7): p. 859-860.

17. Hofmann, M., Eggeling, C., Jakobs, S., and Hell, S.W., *Breaking the diffraction barrier in fluorescence microscopy at low light intensities by using reversibly photoswitchable proteins.* Proc Natl Acad Sci U S A, 2005. 102(49): p. 17565-9.

18. Balzarotti, F., Eilers, Y., Gwosch, K.C., Gynnå, A.H., Westphal, V., Stefani, F.D., Elf, J., and Hell, S.W., *Nanometer resolution imaging and tracking of fluorescent molecules with minimal photon fluxes.* Science, 2017. 355(6325): p. 606-612.

19. Shimomura, O., Johnson, F.H., and Saiga, Y., *Extraction, purification and properties of aequorin, a bioluminescent protein from the luminous hydromedusan, Aequorea.* J Cell Comp Physiol. , 1962. 59: p. 223-39.

20. Shimomura, O., *Structure of the chromophore of Aequorea green fluorescent protein.* FEBS Lett., 1979. 104(2).

21. Prasher, D.C., Eckenrode, V.K., Ward, W.W., Prendergast, F.G., and Cormier, M.J., *Primary structure of the Aequorea victoria green-fluorescent protein.* Gene, 1992. 111(2): p. 229-33.

22. Chalfie, M., Tu, Y., Euskirchen, G., Ward, W.W., and Prasher, D.C., *Green fluorescent protein as a marker for gene expression.* Science, 1994. 263(5148): p. 802-5.

23. Tsien, R.Y., *The green fluorescent protein.* Annu Rev Biochem. , 1998. 67: p. 509-44.

24. Rodriguez, E.A., Campbell, R.E., Lin, J.Y., Lin, M.Z., Miyawaki, A., Palmer, A.E., Shu, X., Zhang, J., and Tsien, R.Y., *The Growing and Glowing Toolbox of Fluorescent and Photoactive Proteins.* Trends Biochem Sci, 2017. 42(2): p. 111-129.

25. Matz, M.V., Fradkov, A.F., Labas, Y.A., Savitsky, A.P., Zaraisky, A.G., Markelov, M.L., and Lukyanov, S.A., *Fluorescent proteins from nonbioluminescent Anthozoa species.* Nat Biotechnol., 1999. 17(10): p. 969-73.

26. Wiedenmann, J., Schenk, A., Röcker, C., Girod, A., Spindler, K.D., and Nienhaus, G.U., *A far-red fluorescent protein with fast maturation and reduced oligomerization tendency from Entacmaea quadricolor (Anthozoa, Actinaria).* Proc Natl Acad Sci U S A, 2002. 99(18): p. 11646-51.

27. Merzlyak, E.M., Goedhart, J., Shcherbo, D., Bulina, M.E., Shcheglov, A.S., Fradkov, A.F., Gaintzeva, A., Lukyanov, K.A., Lukyanov, S., Gadella, T.W., and Chudakov, D.M., *Bright monomeric red fluorescent protein with an extended fluorescence lifetime.* Nat Methods, 2007. 4(7): p. 555-7.

28. Karasawa, S., Araki, T., Nagai, T., Mizuno, H., and Miyawaki, A., *Cyan-emitting and orange-emitting fluorescent proteins as a donor/acceptor pair for fluorescence resonance energy transfer.* Biochem J., 2004. 381: p. 307-12.

29. Shagin, D.A., Barsova, E.V., Yanushevich, Y.G., Fradkov, A.F., Lukyanov, K.A., Labas, Y.A., Semenova, T.N., Ugalde, J.A., Meyers, A., Nunez, J.M., Widder, E.A., Lukyanov,

S.A., and Matz, M.V., *GFP-like proteins as ubiquitous metazoan superfamily: evolution of functional features and structural complexity.* Mol Biol Evol, 2004. 21(5): p. 841-50.

30. Hunt, M.E., Scherrer, M.P., Ferrari, F.D., and Matz, M.V., *Very bright green fluorescent proteins from the Pontellid copepod Pontella mimocerami.* PLoS One, 2010. 5(7): p. e11517.
31. Deheyn, D.D., Kubokawa, K., McCarthy, J.K., Murakami, A., Porrachia, M., Rouse, G.W., and Holland, N.D., *Endogenous green fluorescent protein (GFP) in amphioxus.* Biol Bull. , 2007. 213(2).
32. Shaner, N.C., Lambert, G.G., Chammas, A., Ni, Y., Cranfill, P.J., Baird, M.A., Sell, B.R., Allen, J.R., Day, R.N., Israelsson, M., Davidson, M.W., and Wang, J., *A bright monomeric green fluorescent protein derived from Branchiostoma lanceolatum.* Nat Methods, 2013. 10(5): p. 407-9.
33. Lukyanov, K.A., Fradkov, A.F., Gurskaya, N.G., Matz, M.V., Labas, Y.A., Savitsky, A.P., Markelov, M.L., Zaraisky, A.G., Zhao, X., Fang, Y., Tan, W., and Lukyanov, S.A., *Natural animal coloration can Be determined by a nonfluorescent green fluorescent protein homolog.* J Biol Chem, 2000. 275(34): p. 25879-82.
34. Baird, G.S., Zacharias, D.A., and Tsien, R.Y., *Biochemistry, mutagenesis, and oligomerization of DsRed, a red fluorescent protein from coral.* Proc Natl Acad Sci U S A., 2000. 97(22): p. 11984-9.
35. Dedecker, P., De Schryver, F.C., and Hofkens, J., *Fluorescent proteins: shine on, you crazy diamond.* J Am Chem Soc, 2013. 135(7): p. 2387-402.
36. Ormö, M., Cubitt, A.B., Kallio, K., Gross, L.A., Tsien, R.Y., and Remington, S.J., *Crystal structure of the Aequorea victoria green fluorescent protein.* Science, 1996 273(5280): p. 1392-5.
37. Yang, F., Moss, L.G., and Phillips, G.N.J., *The molecular structure of green fluorescent protein.* Nat Biotechnol., 1996. 14(10): p. 1246-51.
38. Wall, M.A., Socolich, M., and Ranganathan, R., *The structural basis for red fluorescence in the tetrameric GFP homolog DsRed.* Nat Struct Biol., 2000. 7(12): p. 1133-8.
39. Petersen, J., Wilmann, P.G., Beddoe, T., Oakley, A.J., Devenish, R.J., Prescott, M., and Rossjohn, J., *The 2.0-A crystal structure of eqFP611, a far red fluorescent protein from the sea anemone Entacmaea quadricolor.* J Biol Chem, 2003. 278(45): p. 44626-31.
40. Andresen, M., Wahl, M.C., Stiel, A.C., Gräter, F., Schäfer, L.V., Trowitzsch, S., Weber, G., Eggeling, C., Grubmüller, H., Hell, S.W., and Jakobs, S., *Structure and mechanism of the reversible photoswitch of a fluorescent protein.* Proc Natl Acad Sci U S A., 2005. 102(37): p. 13070-4.
41. Heim, R., Prasher, D.C., and Tsien, R.Y., *Wavelength mutations and posttranslational autoxidation of green fluorescent protein.* Proc Natl Acad Sci U S A., 1994. 91(26): p. 12501-4.

42. Tubbs, J.L., Tainer, J.A., and Getzoff, E.D., *Crystallographic structures of Discosoma red fluorescent protein with immature and mature chromophores: linking peptide bond trans-cis isomerization and acylimine formation in chromophore maturation.* Biochemistry, 2005. 44(29): p. 9833-40.

43. Reid, B.G. and Flynn, G.C., *Chromophore formation in green fluorescent protein.* Biochemistry, 1997. 36(22): p. 6786-91.

44. Cubitt, A.B., Heim, R., Adams, S.R., Boyd, A.E., Gross, L.A., and Tsien, R.Y., *Understanding, improving and using green fluorescent proteins.* Trends Biochem Sci. , 1995. 20(11): p. 448-55.

45. Craggs, T.D., *Green fluorescent protein: structure, folding and chromophore maturation.* Chem Soc Rev, 2009. 38(10): p. 2865-75.

46. Wachter, R.M., Watkins, J.L., and Kim, H., *Mechanistic diversity of red fluorescence acquisition by GFP-like proteins.* Biochemistry, 2010. 49(35): p. 7417-27.

47. Gross, L.A., Baird, G.S., Hoffman, R.C., Baldridge, K.K., and Tsien, R.Y., *The structure of the chromophore within DsRed, a red fluorescent protein from coral.* Proc Natl Acad Sci U S A., 2000. 97(22): p. 11990-5.

48. Strack, R.L., Strongin, D.E., Mets, L., Glick, B.S., and Keenan, R.J., *Chromophore formation in DsRed occurs by a branched pathway.* J Am Chem Soc. , 2010. 132(24): p. 8496-505.

49. Subach, O.M., Malashkevich, V.N., Zencheck, W.D., Morozova, K.S., Piatkevich, K.D., Almo, S.C., and Verkhusha, V.V., *Structural characterization of acylimine-containing blue and red chromophores in mTagBFP and TagRFP fluorescent proteins.* Chem Biol, 2010. 17(4): p. 333-41.

50. Hense, A., Nienhaus, K., and Nienhaus, G.U., *Exploring color tuning strategies in red fluorescent proteins.* Photochem Photobiol Sci, 2015. 14(2): p. 200-12.

51. Quillin, M.L., Anstrom, D.M., Shu, X., O'Leary, S., Kallio, K., Chudakov, D.M., and Remington, S.J., *Kindling fluorescent protein from Anemonia sulcata: dark-state structure at 1.38 A resolution.* Biochemistry 2005. 44(15): p. 5774-87.

52. Cormack, B.P., Valdivia, R.H., and Falkow, S., *FACS-optimized mutants of the green fluorescent protein (GFP).* Gene, 1996. 173: p. 33-8.

53. Zhang, G., Gurtu, V., and Kain, S.R., *An enhanced green fluorescent protein allows sensitive detection of gene transfer in mammalian cells.* Biochem Biophys Res Commun., 1996. 227(3): p. 707-11.

54. Kredel, S., Oswald, F., Nienhaus, K., Deuschle, K., Rocker, C., Wolff, M., Heilker, R., Nienhaus, G.U., and Wiedenmann, J., *mRuby, a bright monomeric red fluorescent protein for labeling of subcellular structures.* PLoS One, 2009. 4(2): p. e4391.

55. Campbell, R.E., Tour, O., Palmer, A.E., Steinbach, P.A., Baird, G.S., Zacharias, D.A., and Tsien, R.Y., *A monomeric red fluorescent protein.* Proc Natl Acad Sci U S A., 2002. 99(12): p. 7877-82.

56. Tanida-Miyake, E., Koike, M., Uchiyama, Y., and Tanida, I., *Optimization of mNeonGreen for Homo sapiens increases its fluorescent intensity in mammalian cells.* PLoS One, 2018. 13(1): p. e0191108.

57. Lam, A.J., St-Pierre, F., Gong, Y., Marshall, J.D., Cranfill, P.J., Baird, M.A., McKeown, M.R., Wiedenmann, J., Davidson, M.W., Schnitzer, M.J., Tsien, R.Y., and Lin, M.Z., *Improving FRET dynamic range with bright green and red fluorescent proteins.* Nat Methods, 2012. 9(10): p. 1005-12.

58. Shaner, N.C., Campbell, R.E., Steinbach, P.A., Giepmans, B.N., Palmer, A.E., and Tsien, R.Y., *Improved monomeric red, orange and yellow fluorescent proteins derived from Discosoma sp. red fluorescent protein.* Nat Biotechnol, 2004. 22(12): p. 1567-72.

59. Shinoda, H., Ma, Y., Nakashima, R., Sakurai, K., Matsuda, T., and Nagai, T., *Acid-Tolerant Monomeric GFP from Olindias formosa.* Cell Chem Biol, 2018. 25(3): p. 330-338 e7.

60. Wachter, R.M., Elsliger, M.A., Kallio, K., Hanson, G.T., and Remington, S.J., *Structural basis of spectral shifts in the yellow-emission variants of green fluorescent protein.* Structure, 1998. 6(10): p. 1267-77.

61. Subach, O.M., Gundorov, I.S., Yoshimura, M., Subach, F.V., Zhang, J., Gruenwald, D., Souslova, E.A., Chudakov, D.M., and Verkhusha, V.V., *Conversion of red fluorescent protein into a bright blue probe.* Chem Biol, 2008. 15(10): p. 1116-24.

62. Nienhaus, G.U. and Wiedenmann, J., *Structure, dynamics and optical properties of fluorescent proteins: perspectives for marker development.* Chemphyschem, 2009. 10(9-10): p. 1369-79.

63. Shu, X., Shaner, N.C., Yarbrough, C.A., Tsien, R.Y., and Remington, S.J., *Novel chromophores and buried charges control color in mFruits.* Biochemistry, 2006. 45(32): p. 9639-47.

64. Nienhaus, K., Nar, H., Heilker, R., Wiedenmann, J., and Nienhaus, G.U., *Trans-cis isomerization is responsible for the red-shifted fluorescence in variants of the red fluorescent protein eqFP611.* J Am Chem Soc. , 2008. 130(38): p. 12578-9.

65. Chica, R.A., Moore, M.M., Allen, B.D., and Mayo, S.L., *Generation of longer emission wavelength red fluorescent proteins using computationally designed libraries.* Proc Natl Acad Sci U S A, 2010. 107(47): p. 20257-62.

66. Yoon, E., Konold, P.E., Lee, J., Joo, T., and Jimenez, R., *Far-Red Emission of mPlum Fluorescent Protein Results from Excited-State Interconversion between Chromophore Hydrogen-Bonding States.* J Phys Chem Lett, 2016. 7(12): p. 2170-4.

67. Morozova, K.S., Piatkevich, K.D., Gould, T.J., Zhang, J., Bewersdorf, J., and Verkhusha, V.V., *Far-red fluorescent protein excitable with red lasers for flow cytometry and superresolution STED nanoscopy.* Biophys J, 2010. 99(2): p. L13-5.

68. Piatkevich, K.D., Malashkevich, V.N., Morozova, K.S., Nemkovich, N.A., Almo, S.C., and Verkhusha, V.V., *Extended Stokes shift in fluorescent proteins: chromophore-protein interactions in a near-infrared TagRFP675 variant.* Sci Rep, 2013. 3: p. 1847.

69. Adam, V., Berardozzi, R., Byrdin, M., and Bourgeois, D., *Phototransformable fluorescent proteins: Future challenges.* Curr Opin Chem Biol, 2014. 20: p. 92-102.

70. Bajar, B.T., Wang, E.S., Lam, A.J., Kim, B.B., Jacobs, C.L., Howe, E.S., Davidson, M.W., Lin, M.Z., and Chu, J., *Improving brightness and photostability of green and red fluorescent proteins for live cell imaging and FRET reporting.* Sci Rep, 2016. 6: p. 20889.

71. Pedelacq, J.D., Cabantous, S., Tran, T., Terwilliger, T.C., and Waldo, G.S., *Engineering and characterization of a superfolder green fluorescent protein.* Nat Biotechnol, 2006. 24(1): p. 79-88.

72. Chu, J., Haynes, R.D., Corbel, S.Y., Li, P., Gonzalez-Gonzalez, E., Burg, J.S., Ataie, N.J., Lam, A.J., Cranfill, P.J., Baird, M.A., Davidson, M.W., Ng, H.L., Garcia, K.C., Contag, C.H., Shen, K., Blau, H.M., and Lin, M.Z., *Non-invasive intravital imaging of cellular differentiation with a bright red-excitable fluorescent protein.* Nat Methods, 2014. 11(5): p. 572-8.

73. Heppert, J.K., Dickinson, D.J., Pani, A.M., Higgins, C.D., Steward, A., Ahringer, J., Kuhn, J.R., and Goldstein, B., *Comparative assessment of fluorescent proteins for in vivo imaging in an animal model system.* Mol Biol Cell, 2016. 27(22): p. 3385-3394.

74. Chudakov, D.M., Belousov, V.V., Zaraisky, A.G., Novoselov, V.V., Staroverov, D.B., Zorov, D.B., Lukyanov, S., and Lukyanov, K.A., *Kindling fluorescent proteins for precise in vivo photolabeling.* Nat Biotechnol, 2003. 21(2): p. 191-4.

75. Cranfill, P.J., Sell, B.R., Baird, M.A., Allen, J.R., Lavagnino, Z., de Gruiter, H.M., Kremers, G.J., Davidson, M.W., Ustione, A., and Piston, D.W., *Quantitative assessment of fluorescent proteins.* Nat Methods, 2016. 13(7): p. 557-62.

76. Shemiakina, I.I., Ermakova, G.V., Cranfill, P.J., Baird, M.A., Evans, R.A., Souslova, E.A., Staroverov, D.B., Gorokhovatsky, A.Y., Putintseva, E.V., Gorodnicheva, T.V., Chepurnykh, T.V., Strukova, L., Lukyanov, S., Zaraisky, A.G., Davidson, M.W., Chudakov, D.M., and Shcherbo, D., *A monomeric red fluorescent protein with low cytotoxicity.* Nat Commun, 2012. 3: p. 1204.

77. Shaner, N.C., Lin, M.Z., McKeown, M.R., Steinbach, P.A., Hazelwood, K.L., Davidson, M.W., and Tsien, R.Y., *Improving the photostability of bright monomeric orange and red fluorescent proteins.* Nat Methods, 2008. 5(6): p. 545-51.

78. Davis, L.M., Lubbeck, J.L., Dean, K.M., Palmer, A.E., and Jimenez, R., *Microfluidic cell sorter for use in developing red fluorescent proteins with improved photostability.* Lab Chip, 2013. 13(12): p. 2320-7.

79. Griesbeck, O., Baird, G.S., Campbell, R.E., Zacharias, D.A., and Tsien, R.Y., *Reducing the environmental sensitivity of yellow fluorescent protein. Mechanism and applications.* J Biol Chem, 2001. 276(31): p. 29188-94.

80. Piatkevich, K.D., Hulit, J., Subach, O.M., Wu, B., Abdulla, A., Segall, J.E., and Verkhusha, V.V., *Monomeric red fluorescent proteins with a large Stokes shift.* Proc Natl Acad Sci U S A, 2010. 107(12): p. 5369-74.

81. Shcherbakova, D.M., Hink, M.A., Joosen, L., Gadella, T.W., and Verkhusha, V.V., *An orange fluorescent protein with a large Stokes shift for single-excitation multicolor FCCS and FRET imaging.* J Am Chem Soc, 2012. 134(18): p. 7913-23.

82. Subach, F.V., Zhang, L., Gadella, T.W., Gurskaya, N.G., Lukyanov, K.A., and Verkhusha, V.V., *Red fluorescent protein with reversibly photoswitchable absorbance for photochromic FRET.* Chem Biol, 2010. 17(7): p. 745-55.

83. Kremers, G.J., Gilbert, S.G., Cranfill, P.J., Davidson, M.W., and Piston, D.W., *Fluorescent proteins at a glance.* J Cell Sci, 2011. 124(Pt 2): p. 157-60.

84. Subach, F.V., Piatkevich, K.D., and Verkhusha, V.V., *Directed molecular evolution to design advanced red fluorescent proteins.* Nat Methods, 2011. 8(12): p. 1019-26.

85. Bindels, D.S., Haarbosch, L., van Weeren, L., Postma, M., Wiese, K.E., Mastop, M., Aumonier, S., Gotthard, G., Royant, A., Hink, M.A., and Gadella, T.W., Jr., *mScarlet: a bright monomeric red fluorescent protein for cellular imaging.* Nat Methods, 2017. 14(1): p. 53-56.

86. Shcherbakova, D.M., Sengupta, P., Lippincott-Schwartz, J., and Verkhusha, V.V., *Photocontrollable fluorescent proteins for superresolution imaging.* Annu Rev Biophys, 2014. 43: p. 303-29.

87. Ando, R., Mizuno, H., and Miyawaki, A., *Regulated fast nucleocytoplasmic shuttling observed by reversible protein highlighting.* Science, 2004. 306(5700): p. 1370-3.

88. Andresen, M., Stiel, A.C., Folling, J., Wenzel, D., Schonle, A., Egner, A., Eggeling, C., Hell, S.W., and Jakobs, S., *Photoswitchable fluorescent proteins enable monochromatic multilabel imaging and dual color fluorescence nanoscopy.* Nat Biotechnol, 2008. 26(9): p. 1035-40.

89. Stiel, A.C., Trowitzsch, S., Weber, G., Andresen, M., Eggeling, C., Hell, S.W., Jakobs, S., and Wahl, M.C., *1.8 A bright-state structure of the reversibly switchable fluorescent protein Dronpa guides the generation of fast switching variants.* Biochem J, 2007. 402(1): p. 35-42.

90. Grotjohann, T., Testa, I., Leutenegger, M., Bock, H., Urban, N.T., Lavoie-Cardinal, F., Willig, K.I., Eggeling, C., Jakobs, S., and Hell, S.W., *Diffraction-unlimited all-optical imaging and writing with a photochromic GFP.* Nature, 2011. 478(7368): p. 204-8.

91. Stiel, A.C., Andresen, M., Bock, H., Hilbert, M., Schilde, J., Schonle, A., Eggeling, C., Egner, A., Hell, S.W., and Jakobs, S., *Generation of monomeric reversibly switchable red fluorescent proteins for far-field fluorescence nanoscopy.* Biophys J, 2008. 95(6): p. 2989-97.

92. Brakemann, T., Stiel, A.C., Weber, G., Andresen, M., Testa, I., Grotjohann, T., Leutenegger, M., Plessmann, U., Urlaub, H., Eggeling, C., Wahl, M.C., Hell, S.W., and

Jakobs, S., *A reversibly photoswitchable GFP-like protein with fluorescence excitation decoupled from switching.* Nat Biotechnol, 2011. 29(10): p. 942-7.

93. Zhou, X.X. and Lin, M.Z., *Photoswitchable fluorescent proteins: ten years of colorful chemistry and exciting applications.* Curr Opin Chem Biol, 2013. 17(4): p. 682-90.
94. Danzl, J.G., Sidenstein, S.C., Gregor, C., Urban, N.T., Ilgen, P., Jakobs, S., and Hell, S.W., *Coordinate-targeted fluorescence nanoscopy with multiple off states.* Nature Photonics, 2016. 10(2): p. 122-128.
95. Zhang, X., Zhang, M., Li, D., He, W., Peng, J., Betzig, E., and Xu, P., *Highly photostable, reversibly photoswitchable fluorescent protein with high contrast ratio for live-cell superresolution microscopy.* Proc Natl Acad Sci U S A, 2016. 113(37): p. 10364-9.
96. Grotjohann, T., Testa, I., Reuss, M., Brakemann, T., Eggeling, C., Hell, S.W., and Jakobs, S., *rsEGFP2 enables fast RESOLFT nanoscopy of living cells.* Elife, 2012. 1: p. e00248.
97. Ratz, M., Testa, I., Hell, S.W., and Jakobs, S., *CRISPR/Cas9-mediated endogenous protein tagging for RESOLFT super-resolution microscopy of living human cells.* Sci Rep, 2015. 5: p. 9592.
98. Lavoie-Cardinal, F., Jensen, N.A., Westphal, V., Stiel, A.C., Chmyrov, A., Bierwagen, J., Testa, I., Jakobs, S., and Hell, S.W., *Two-color RESOLFT nanoscopy with green and red fluorescent photochromic proteins.* Chemphyschem, 2014. 15(4): p. 655-63.
99. Duan, C., Adam, V., Byrdin, M., Ridard, J., Kieffer-Jaquinod, S., Morlot, C., Arcizet, D., Demachy, I., and Bourgeois, D., *Structural evidence for a two-regime photobleaching mechanism in a reversibly switchable fluorescent protein.* J Am Chem Soc, 2013. 135(42): p. 15841-50.
100. Tiwari, D.K., Arai, Y., Yamanaka, M., Matsuda, T., Agetsuma, M., Nakano, M., Fujita, K., and Nagai, T., *A fast- and positively photoswitchable fluorescent protein for ultralow-laser-power RESOLFT nanoscopy.* Nat Methods, 2015. 12(6): p. 515-8.
101. Hell, S.W., *Microscopy and its focal switch.* Nat Methods, 2009. 6(1): p. 24-32.
102. Wang, S., Chen, X., Chang, L., Xue, R., Duan, H., and Sun, Y., *GMars-Q Enables Long-Term Live-Cell Parallelized Reversible Saturable Optical Fluorescence Transitions Nanoscopy.* ACS Nano, 2016. 10(10): p. 9136-9144.
103. Duwé, S., De Zitter, E., Gielen, V., Moeyaert, B., Vandenberg, W., Grotjohann, T., Clays, K., Jakobs, S., Van Meervelt, L., and Dedecker, P., *Expression-Enhanced Fluorescent Proteins Based on Enhanced Green Fluorescent Protein for Super-resolution Microscopy.* ACS Nano., 2015. 0(10): p. 9528-41.
104. El Khatib, M., Martins, A., Bourgeois, D., Colletier, J.P., and Adam, V., *Rational design of ultrastable and reversibly photoswitchable fluorescent proteins for super-resolution imaging of the bacterial periplasm.* Sci Rep, 2016. 6: p. 18459.

105. Zacharias, D.A., Violin, J.D., Newton, A.C., and Tsien, R.Y., *Partitioning of lipid-modified monomeric GFPs into membrane microdomains of live cells.* Science, 2002. 296(5569): p. 913-6.

106. McKinney, S.A., Murphy, C.S., Hazelwood, K.L., Davidson, M.W., and Looger, L.L., *A bright and photostable photoconvertible fluorescent protein.* Nat Methods, 2009. 6(2): p. 131-3.

107. Chang, H., Zhang, M., Ji, W., Chen, J., Zhang, Y., Liu, B., Lu, J., Zhang, J., Xu, P., and Xu, T., *A unique series of reversibly switchable fluorescent proteins with beneficial properties for various applications.* Proc Natl Acad Sci U S A, 2012. 109(12): p. 4455-60.

108. Zhang, M., Chang, H., Zhang, Y., Yu, J., Wu, L., Ji, W., Chen, J., Liu, B., Lu, J., Liu, Y., Zhang, J., Xu, P., and Xu, T., *Rational design of true monomeric and bright photoactivatable fluorescent proteins.* Nat Methods, 2012. 9(7): p. 727-9.

109. Zhang, X., Chen, X., Zeng, Z., Zhang, M., Sun, Y., Xi, P., Peng, J., and Xu, P., *Development of a reversibly switchable fluorescent protein for super-resolution optical fluctuation imaging (SOFI).* ACS Nano., 2015. 9(3): p. 2659-67.

110. Wang, S., Moffitt, J.R., Dempsey, G.T., Xie, X.S., and Zhuang, X., *Characterization and development of photoactivatable fluorescent proteins for single-molecule-based superresolution imaging.* Proc Natl Acad Sci U S A, 2014. 111(23): p. 8452-7.

111. Wang, S., Chen, X., Chang, L., Ding, M., Xue, R., Duan, H., and Sun, Y., *GMars-T Enabling Multimodal Subdiffraction Structural and Functional Fluorescence Imaging in Live Cells.* Anal Chem, 2018. 90(11): p. 6626-6634.

112. Wang, S., Shuai, Y., Sun, C., Xue, B., Hou, Y., Su, X., and Sun, Y., *Lighting Up Live Cells with Smart Genetically Encoded Fluorescence Probes from GMars Family.* ACS Sens, 2018. 3(11): p. 2269-2277.

113. Fuchs, J., Bohme, S., Oswald, F., Hedde, P.N., Krause, M., Wiedenmann, J., and Nienhaus, G.U., *A photoactivatable marker protein for pulse-chase imaging with superresolution.* Nat Methods, 2010. 7(8): p. 627-30.

114. Adam, V., Moeyaert, B., David, C.C., Mizuno, H., Lelimousin, M., Dedecker, P., Ando, R., Miyawaki, A., Michiels, J., Engelborghs, Y., and Hofkens, J., *Rational design of photoconvertible and biphotochromic fluorescent proteins for advanced microscopy applications.* Chem Biol, 2011. 18(10): p. 1241-51.

115. Arai, Y., Takauchi, H., Ogami, Y., Fujiwara, S., Nakano, M., Matsuda, T., and Nagai, T., *Spontaneously Blinking Fluorescent Protein for Simple Single Laser Super-Resolution Live Cell Imaging.* ACS Chem Biol, 2018. 13(8): p. 1938-1943.

116. Chudakov, D.M., Feofanov, A.V., Mudrik, N.N., Lukyanov, S., and Lukyanov, K.A., *Chromophore environment provides clue to "kindling fluorescent protein" riddle.* J Biol Chem, 2003. 278(9): p. 7215-9.

117. Pletnev, S., Subach, F.V., Dauter, Z., Wlodawer, A., and Verkhusha, V.V., *A structural basis for reversible photoswitching of absorbance spectra in red fluorescent protein rsTagRFP.* J Mol Biol, 2012. 417(3): p. 144-51.

118. Pennacchietti, F., Serebrovskaya, E.O., Faro, A.R., Shemyakina, II, Bozhanova, N.G., Kotlobay, A.A., Gurskaya, N.G., Boden, A., Dreier, J., Chudakov, D.M., Lukyanov, K.A., Verkhusha, V.V., Mishin, A.S., and Testa, I., *Fast reversibly photoswitching red fluorescent proteins for live-cell RESOLFT nanoscopy.* Nat Methods, 2018. 15(8): p. 601-604.

119. Fron, E., Flors, C., Schweitzer, G., Habuchi, S., Mizuno, H., Ando, R., Schryver, F.C., Miyawaki, A., and Hofkens, J., *Ultrafast excited-state dynamics of the photoswitchable protein Dronpa.* J Am Chem Soc, 2007. 129(16): p. 4870-1.

120. Andresen, M., Stiel, A.C., Trowitzsch, S., Weber, G., Eggeling, C., Wahl, M.C., Hell, S.W., and Jakobs, S., *Structural basis for reversible photoswitching in Dronpa.* Proc Natl Acad Sci USA, 2007. 104(32): p. 13005-9.

121. Mizuno, H., Mal, T.K., Wälchli, M., Kikuchi, A., Fukano, T., Ando, R., Jeyakanthan, J., Taka, J., Shiro, Y., Ikura, M., and Miyawaki, A., *Light-dependent regulation of structural flexibility in a photochromic fluorescent protein.* Proc Natl Acad Sci U S A. , 2008. 105(27): p. 9227-32.

122. Habuchi, S., Ando, R., Dedecker, P., Verheijen, W., Mizuno, H., Miyawaki, A., and Hofkens, J., *Reversible single-molecule photoswitching in the GFP-like fluorescent protein Dronpa.* Proc Natl Acad Sci U S A., 2005. 102(27): p. 9511-6.

123. Brakemann, T., Weber, G., Andresen, M., Groenhof, G., Stiel, A.C., Trowitzsch, S., Eggeling, C., Grubmuller, H., Hell, S.W., Wahl, M.C., and Jakobs, S., *Molecular basis of the light-driven switching of the photochromic fluorescent protein Padron.* J Biol Chem, 2010. 285(19): p. 14603-9.

124. Duan, C., Adam, V., Byrdin, M., and Bourgeois, D., *Structural basis of photoswitching in fluorescent proteins.* Methods Mol Biol, 2014. 1148: p. 177-202.

125. Bourgeois, D. and Adam, V., *Reversible photoswitching in fluorescent proteins: a mechanistic view.* IUBMB Life, 2012. 64(6): p. 482-91.

126. Shinoda, H., Lu, K., Nakashima, R., Wazawa, T., Noguchi, K., Matsuda, T., and Nagai, T., *Acid-Tolerant Reversibly Switchable Green Fluorescent Protein for Super-resolution Imaging under Acidic Conditions.* Cell Chem Biol, 2019.

127. Faro, A.R., Carpentier, P., Jonasson, G., Pompidor, G., Arcizet, D., Demachy, I., and Bourgeois, D., *Low-temperature chromophore isomerization reveals the photoswitching mechanism of the fluorescent protein Padron.* J Am Chem Soc, 2011. 133(41): p. 16362-5.

128. Lacombat, F., Plaza, P., Plamont, M.A., and Espagne, A., *Photoinduced Chromophore Hydration in the Fluorescent Protein Dreiklang Is Triggered by Ultrafast Excited-State*

Proton Transfer Coupled to a Low-Frequency Vibration. J Phys Chem Lett, 2017. 8(7): p. 1489-1495.

129. Chmyrov, A., Keller, J., Grotjohann, T., Ratz, M., d'Este, E., Jakobs, S., Eggeling, C., and Hell, S.W., *Nanoscopy with more than 100,000 'doughnuts'.* Nat Methods, 2013. 10(8): p. 737-40.
130. Chmyrov, A., Leutenegger, M., Grotjohann, T., Schonle, A., Keller-Findeisen, J., Kastrup, L., Jakobs, S., Donnert, G., Sahl, S.J., and Hell, S.W., *Achromatic light patterning and improved image reconstruction for parallelized RESOLFT nanoscopy.* Sci Rep, 2017. 7: p. 44619.
131. Masullo, L.A., Boden, A., Pennacchietti, F., Coceano, G., Ratz, M., and Testa, I., *Enhanced photon collection enables four dimensional fluorescence nanoscopy of living systems.* Nat Commun, 2018. 9(1): p. 3281.
132. Dreier, J., Castello, M., Coceano, G., Caceres, R., Plastino, J., Vicidomini, G., and Testa, I., *Smart scanning for low-illumination and fast RESOLFT nanoscopy in vivo.* Nat Commun, 2019. 10(1): p. 556.
133. Schnorrenberg, S., Grotjohann, T., Vorbruggen, G., Herzig, A., Hell, S.W., and Jakobs, S., *In vivo super-resolution RESOLFT microscopy of Drosophila melanogaster.* Elife, 2016. 5.
134. Testa, I., Urban, N.T., Jakobs, S., Eggeling, C., Willig, K.I., and Hell, S.W., *Nanoscopy of living brain slices with low light levels.* Neuron, 2012. 75(6): p. 992-1000.
135. Jensen, N.A., Danzl, J.G., Willig, K.I., Lavoie-Cardinal, F., Brakemann, T., Hell, S.W., and Jakobs, S., *Coordinate-targeted and coordinate-stochastic super-resolution microscopy with the reversibly switchable fluorescent protein Dreiklang.* Chemphyschem, 2014. 15(4): p. 756-62.
136. Testa, I., D'Este, E., Urban, N.T., Balzarotti, F., and Hell, S.W., *Dual channel RESOLFT nanoscopy by using fluorescent state kinetics.* Nano Lett, 2015. 15(1): p. 103-6.
137. Shcherbo, D., Murphy, C.S., Ermakova, G.V., Solovieva, E.A., Chepurnykh, T.V., Shcheglov, A.S., Verkhusha, V.V., Pletnev, V.Z., Hazelwood, K.L., Roche, P.M., Lukyanov, S., Zaraisky, A.G., Davidson, M.W., and Chudakov, D.M., *Far-red fluorescent tags for protein imaging in living tissues.* Biochem J, 2009. 418(3): p. 567-74.
138. Wang, L., Jackson, W.C., Steinbach, P.A., and R.Y., T., *Evolution of new nonantibody proteins via iterative somatic hypermutation.* Proc Natl Acad Sci U S A, 2004. 101(48): p. 16745-9.
139. Dean, K.M., Lubbeck, J.L., Davis, L.M., Regmi, C.K., Chapagain, P.P., Gerstman, B.S., Jimenez, R., and Palmer, A.E., *Microfluidics-based selection of red-fluorescent proteins with decreased rates of photobleaching.* Integr Biol (Camb), 2015. 7(2): p. 263-73.
140. Duportet, X., Wroblewska, L., Guye, P., Li, Y., Eyquem, J., Rieders, J., Rimchala, T., Batt, G., and Weiss, R., *A platform for rapid prototyping of synthetic gene networks in mammalian cells.* Nucleic Acids Res, 2014. 42(21): p. 13440-51.

141. Moehle, E.A., Rock, J.M., Lee, Y.L., Jouvenot, Y., DeKelver, R.C., Gregory, P.D., Urnov, F.D., and Holmes, M.C., *Targeted gene addition into a specified location in the human genome using designed zinc finger nucleases.* Proc Natl Acad Sci U S A, 2007. 104(9): p. 3055-60.

142. Reyon, D., Tsai, S.Q., Khayter, C., Foden, J.A., Sander, J.D., and Joung, J.K., *FLASH assembly of TALENs for high-throughput genome editing.* Nat Biotechnol, 2012. 30(5): p. 460-5.

143. Ran, F.A., Hsu, P.D., Wright, J., Agarwala, V., Scott, D.A., and Zhang, F., *Genome engineering using the CRISPR-Cas9 system.* Nat Protoc, 2013. 8(11): p. 2281-2308.

144. Mali, P., Yang, L., Esvelt, K.M., Aach, J., Guell, M., DiCarlo, J.E., Norville, J.E., and Church, G.M., *RNA-guided human genome engineering via Cas9.* Science, 2013. 339(6121): p. 823-6.

145. Gaj, T., Gersbach, C.A., and Barbas, C.F., *ZFN, TALEN, and CRISPR/Cas-based methods for genome engineering.* Trends Biotechnol, 2013. 31(7): p. 397-405.

146. Sander, J.D. and Joung, J.K., *CRISPR-Cas systems for editing, regulating and targeting genomes.* Nat Biotechnol, 2014. 32(4): p. 347-55.

147. Brown, W.R., Lee, N.C., Xu, Z., and Smith, M.C., *Serine recombinases as tools for genome engineering.* Methods, 2011. 53(4): p. 372-9.

148. Grindley, N.D., Whiteson, K.L., and Rice, P.A., *Mechanisms of site-specific recombination.* Annu Rev Biochem, 2006. 75: p. 567-605.

149. Mulholland, C.B., Smets, M., Schmidtmann, E., Leidescher, S., Markaki, Y., Hofweber, M., Qin, W., Manzo, M., Kremmer, E., Thanisch, K., Bauer, C., Rombaut, P., Herzog, F., Leonhardt, H., and Bultmann, S., *A modular open platform for systematic functional studies under physiological conditions.* Nucleic Acids Res, 2015. 43(17): p. e112.

150. Zhu, F., Gamboa, M., Farruggio, A.P., Hippenmeyer, S., Tasic, B., Schule, B., Chen-Tsai, Y., and Calos, M.P., *DICE, an efficient system for iterative genomic editing in human pluripotent stem cells.* Nucleic Acids Res, 2014. 42(5): p. e34.

151. Xu, Z., Thomas, L., Davies, B., Chalmers, R., Smith, M., and Brown, W., *Accuracy and efficiency define Bxb1 integrase as the best of fifteen candidate serine recombinases for the integration of DNA into the human genome.* BMC Biotechnol., 2013. 13(87).

152. Russell, J.P., Chang, D.W., Tretiakova, A., and Padidam, M., *Phage Bxb1 integrase mediates highly efficient site-specific recombination in mammalian cells.* Biotechniques, 2006. 40(4): p. 460, 462, 464.

153. Mullis, K., Faloona, F., Scharf, S., Saiki, R., Horn, G., and Erlich, H., *Specific enzymatic amplification of DNA in vitro: the polymerase chain reaction.* Cold Spring Harb Symp Quant Biol., 1986. 51: p. 263-73.

154. Gibson, D.G., Young, L., Chuang, R.Y., Venter, J.C., Hutchison, C.A., and Smith, H.O., *Enzymatic assembly of DNA molecules up to several hundred kilobases.* Nat Methods, 2009. 6(5): p. 343-5.

155. Ai, H.W., Shaner, N.C., Cheng, Z., Tsien, R.Y., and Campbell, R.E., *Exploration of new chromophore structures leads to the identification of improved blue fluorescent proteins.* Biochemistry, 2007. 46(20): p. 904-10.

156. Jakobs, S., Subramaniam, V., Schönle, A., Jovin, T.M., and Hell, S.W., *EGFP and DsRed expressing cultures of Escherichia coli imaged by confocal, two-photon and fluorescence lifetime microscopy.* FEBS Lett., 2000. 479(3): p. 131-5.

157. Cong, L., Ran, F.A., Cox, D., Lin, S., Barretto, R., Habib, N., Hsu, P.D., Wu, X., Jiang, W., Marraffini, L.A., and Zhang, F., *Multiplex genome engineering using CRISPR/Cas systems.* Science, 2013. 339(6121): p. 819-23.

158. Hockemeyer, D., Soldner, F., Beard, C., Gao, Q., Mitalipova, M., DeKelver, R.C., Katibah, G.E., Amora, R., Boydston, E.A., Zeitler, B., Meng, X., Miller, J.C., Zhang, L., Rebar, E.J., Gregory, P.D., Urnov, F.D., and Jaenisch, R., *Efficient targeting of expressed and silent genes in human ESCs and iPSCs using zinc-finger nucleases.* Nat Biotechnol, 2009. 27(9): p. 851-7.

159. Matsuda, T. and Cepko, C.L., *Electroporation and RNA interference in the rodent retina in vivo and in vitro.* Proc Natl Acad Sci USA, 2004. 101(1): p. 16-22.

160. Grotjohann, T., *Generation of Novel Photochromic GFPs: Fluorescent Probes for RESOLFT-type Microscopy at Low Light Intensities, Dissertation*. 2012.

161. Kamper, M., Ta, H., Jensen, N.A., Hell, S.W., and Jakobs, S., *Near-infrared STED nanoscopy with an engineered bacterial phytochrome.* Nat Commun, 2018. 9(1): p. 4762.

162. Ratz, M., *CRISPR-Cas9-mediated protein tagging in human cells for RESOLFT nanoscopy and the analysis of mitochondrial prohibitins, Dissertation*. 2015.

163. Sawano, A. and Miyawaki, A., *Directed evolution of green fluorescent protein by a new versatile PCR strategy for site-directed and semi-random mutagenesis.* Nucleic Acids Res., 2000. 28(16).

164. Leung, D.W., Chen, E., and Goeddel, D.V., *A method for random mutagenesis of a defined DNA segment using a modified polymerase chain reaction.* Technique, 1989. 1: p. 11-15.

165. Bertani, G., *Studies on lysogenesis. I. The mode of phage liberation by lysogenic Escherichia coli.* J Bacteriol. , 1951. 62(3): p. 293-300.

166. Dower, W.J., Miller, J.F., and Ragsdale, C.W., *High efficiency transformation of E. coli by high voltage electroporation.* Nucleic Acids Res., 1988. 16(13): p. 6127-45.

167. Hermann, M., Stillhard, P., Wildner, H., Seruggia, D., Kapp, V., Sanchez-Iranzo, H., Mercader, N., Montoliu, L., Zeilhofer, H.U., and Pelczar, P., *Binary recombinase systems for high-resolution conditional mutagenesis.* Nucleic Acids Res, 2014. 42(6): p. 3894-907.

168. Bradford, M.M., *A rapid and sensitive method for the quantitation of microgram quantities of protein utilizing the principle of protein-dye binding.* Anal Biochem., 1976. 7(72): p. 248-54.

169. Chizhik, A.I., Gregor, I., Ernst, B., and Enderlein, J., *Nanocavity-based determination of absolute values of photoluminescence quantum yields.* Chemphyschem, 2013. 14(3): p. 505-13.

170. Roberts, T.M., Rudolf, F., Meyer, A., Pellaux, R., Whitehead, E., Panke, S., and Held, M., *Identification and Characterisation of a pH-stable GFP.* Sci Rep, 2016. 6: p. 28166.

171. Schindelin, J., Arganda-Carreras, I., Frise, E., Kaynig, V., Longair, M., Pietzsch, T., Preibisch, S., Rueden, C., Saalfeld, S., Schmid, B., Tinevez, J.Y., White, D.J., Hartenstein, V., Eliceiri, K., Tomancak, P., and Cardona, A., *Fiji: an open-source platform for biological-image analysis.* Nat Methods, 2012. 9(7): p. 676-82.

172. Schneider, C.A., Rasband, W.S., and Eliceiri, K.W., *NIH Image to ImageJ: 25 years of image analysis.* Nature Methods, 2012. 9(7): p. 671-675.

173. Smith, J.R., Maguire, S., Davis, L.A., Alexander, M., Yang, F., Chandran, S., ffrench-Constant, C., and Pedersen, R.A., *Robust, persistent transgene expression in human embryonic stem cells is achieved with AAVS1-targeted integration.* Stem Cells, 2008. 26(2): p. 496-504.

174. Kim, J.H., Lee, S.R., Li, L.H., Park, H.J., Park, J.H., Lee, K.Y., Kim, M.K., Shin, B.A., and Choi, S.Y., *High cleavage efficiency of a 2A peptide derived from porcine teschovirus-1 in human cell lines, zebrafish and mice.* PLoS One, 2011. 6(4): p. e18556.

175. Macville, M., Schröck, E., Padilla-Nash, H., Keck, C., Ghadimi, B.M., Zimonjic, D., Popescu, N., and Ried, T., *Comprehensive and definitive molecular cytogenetic characterization of HeLa cells by spectral karyotyping.* Cancer Res. , 1999. 59(1): p. 141-50.

176. Smirnov, E., Kalmárová, M., Koberna, K., Zemanová, Z., Malínský, J., Masata, M., Cvacková, Z., Michalová, K., and Raska, I., *NORs and their transcription competence during the cell cycle.* Folia Biol (Praha), 2006. 52(3): p. 59-70.

177. Akerboom, J., Carreras Calderon, N., Tian, L., Wabnig, S., Prigge, M., Tolo, J., Gordus, A., Orger, M.B., Severi, K.E., Macklin, J.J., Patel, R., Pulver, S.R., Wardill, T.J., Fischer, E., Schuler, C., Chen, T.W., Sarkisyan, K.S., Marvin, J.S., Bargmann, C.I., Kim, D.S., Kugler, S., Lagnado, L., Hegemann, P., Gottschalk, A., Schreiter, E.R., and Looger, L.L., *Genetically encoded calcium indicators for multi-color neural activity imaging and combination with optogenetics.* Front Mol Neurosci, 2013. 6: p. 2.

178. Subach, F.V., Patterson, G.H., Manley, S., Gillette, J.M., Lippincott-Schwartz, J., and Verkhusha, V.V., *Photoactivatable mCherry for high-resolution two-color fluorescence microscopy.* Nat Methods, 2009. 6(2): p. 153-9.

179. Davis, J.N. and van den Pol, A.N., *Viral Mutagenesis as a Means for Generating Novel Proteins.* Journal of Virology, 2009. 84(3): p. 1625-1630.

180. Wang, L. and Tsien, R.Y., *Evolving proteins in mammalian cells using somatic hypermutation.* Nat Protoc, 2006. 1(3): p. 1346-50.

181. Matreyek, K.A., Stephany, J.J., and Fowler, D.M., *A platform for functional assessment of large variant libraries in mammalian cells.* Nucleic Acids Res, 2017. 45(11): p. e102.

182. Raj, A., Peskin, C.S., Tranchina, D., Vargas, D.Y., and Tyagi, S., *Stochastic mRNA synthesis in mammalian cells.* PLoS Biol, 2006. 4(10): p. e309.

183. Volfson, D., Marciniak, J., Blake, W.J., Ostroff, N., Tsimring, L.S., and Hasty, J., *Origins of extrinsic variability in eukaryotic gene expression.* Nature, 2006. 439(7078): p. 861-4.

184. Chen, C.H., Cho, S.H., Tsai, F., Erten, A., and Lo, Y.H., *Microfluidic cell sorter with integrated piezoelectric actuator.* Biomed Microdevices, 2009. 11(6): p. 1223-31.

185. Lychagov, V.V., Shemetov, A.A., Jimenez, R., and Verkhusha, V.V., *Microfluidic System for In-Flow Reversible Photoswitching of Near-Infrared Fluorescent Proteins.* Anal Chem, 2016. 88(23): p. 11821-11829.

186. Chang, J., Romei, M.G., and Boxer, S.G., *Structural Evidence of Photoisomerization Pathways in Fluorescent Proteins.* J Am Chem Soc, 2019.

187. Roebroek, T., Duwe, S., Vandenberg, W., and Dedecker, P., *Reduced Fluorescent Protein Switching Fatigue by Binding-Induced Emissive State Stabilization.* Int J Mol Sci, 2017. 18(9).

188. Miyawaki, A., Shcherbakova, D.M., and Verkhusha, V.V., *Red fluorescent proteins: chromophore formation and cellular applications.* Curr Opin Struct Biol, 2012. 22(5): p. 679-88.

189. Habuchi, S., Dedecker, P., Hotta, J., Flors, C., Ando, R., Mizuno, H., Miyawaki, A., and Hofkens, J., *Photo-induced protonation/deprotonation in the GFP-like fluorescent protein Dronpa: mechanism responsible for the reversible photoswitching.* Photochem Photobiol Sci, 2006. 5(6): p. 567-76.

190. Coquelle, N., Sliwa, M., Woodhouse, J., Schiro, G., Adam, V., Aquila, A., Barends, T.R.M., Boutet, S., Byrdin, M., Carbajo, S., De la Mora, E., Doak, R.B., Feliks, M., Fieschi, F., Foucar, L., Guillon, V., Hilpert, M., Hunter, M.S., Jakobs, S., Koglin, J.E., Kovacsova, G., Lane, T.J., Levy, B., Liang, M., Nass, K., Ridard, J., Robinson, J.S., Roome, C.M., Ruckebusch, C., Seaberg, M., Thepaut, M., Cammarata, M., Demachy, I., Field, M., Shoeman, R.L., Bourgeois, D., Colletier, J.P., Schlichting, I., and Weik, M., *Chromophore twisting in the excited state of a photoswitchable fluorescent protein captured by time-resolved serial femtosecond crystallography.* Nat Chem, 2018. 10(1): p. 31-37.

191. Dedecker, P., Mo, G.C., Dertinger, T., and Zhang, J., *Widely accessible method for superresolution fluorescence imaging of living systems.* Proc Natl Acad Sci U S A, 2012. 109(27): p. 10909-14.

192. Vetschera, P., Mishra, K., Fuenzalida-Werner, J.P., Chmyrov, A., Ntziachristos, V., and Stiel, A.C., *Characterization of Reversibly Switchable Fluorescent Proteins in Optoacoustic Imaging.* Anal Chem, 2018. 90(17): p. 10527-10535.

6 Appendix

6.1 Cloning

Table 8: Primers for cloning of fluorescent protein genes into pBad/His B.

Amplicon	Primer sequence (5' to 3')	Lab ID
mScarlet	AGGGCTCGAGCATGGTGAGCAAGGGCGAGGCA	7577
	CTTCGAATTCTTACTTGTACAGCTCGTCCAT	2944
mRuby2	AGGGCTCGAGCATGGTGTCTAAGGGCGAAGAG	3950
	CAGCCAAGCTTCGAATTCTTA	3744
FusionRed, rsFusionRed2, rsFusionRed3	AGGGCTCGAGCATGGTGTCTAAGGGCGAAGAG	5760
	TTCGAATTCTCATTTACCTCCATCACC	9019
rsCherry, mCherry, dTomato	AGGGCTCGAGCATGGTGAGCAAGGGCGAGGAG	2943
	CTTCGAATTCTTACTTGTACAGCTCGTCCAT	2944
DsRed	AGGGCTCGAGCATGGTGCGCTCCTCCAAGAA	6657
	CTTCGAATTCCTACAGGAACAGGTGGTGGCG	6658

Appendix I: Gene synthesis for Bxb1 landing pad donor plasmid.

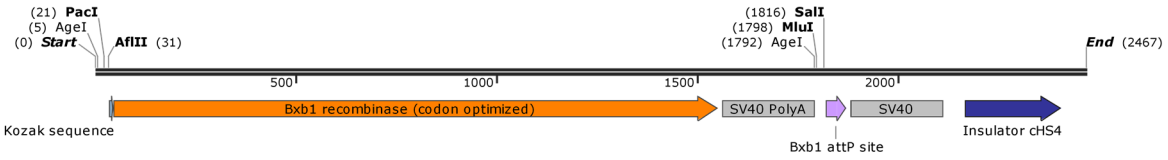

synthesized DNA fragment for Bxb1 landing pad donor plasmid
2467 bp

CATCACCGGTTCGCGATTAATTAAAGCGCTCTTAAGGCCGCCACCATGAGAGCACTGGTGGTCATCCGA
CTGAGTAGGGTCACAGACGCAACAACAAGCCCCGAGAGGCAGCTGGAATCATGTCAGCAGCTGTGCGC
ACAGCGAGGATGGGACGTGGTCGGAGTGGCAGAGGATCTGGACGTGAGCGGCGCTGTCGATCCATTC
GACAGAAAGCGGAGGCCCAACCTGGCAAGGTGGCTGGCTTTCGAGGAACAGCCCTTTGATGTGATCGT
CGCCTACAGAGTGGACAGGCTGACACGCTCTATTCGACATCTGCAGCAGCTGGTGCATTGGGCCGAGG
ACCACAAGAAACTGGTGGTCAGTGCAACTGAAGCCCACTTCGATACCACAACTCCTTTTGCCGCTGTGG
TCATCGCACTGATGGGCACCGTGGCCCAGATGGAGCTGGAAGCTATCAAGGAGCGAAACCGGAGTGG
GAGACTGGTGCCAGACCCCGTCCAGAGAGAGAGGATTCTGGAAGTGTACCACAGGGTGGTCGATAACC
ACGAACCACTGCATCTGGTCGCCCACGACCTGAATAGGCGCGGCGTGCTGAGCCCAAAAGATTATTTTG
CTCAGCTGCAGGGAAGGGAGCCACAGGGACGAGAATGGTCCGCTACCGCCCTGAAGCGGAGCATGAT
CAGTGAGGCTATGCTGGGCTACGCAACTCTGAATGGGAAAACCGTCCGGGACGATGACGGAGCACCAC
TGGTGAGGGCTGAGCCTATTCTGACACGCGAGCAGCTGGAAGCTCTGCGGGCAGAACTGGTGAAAACC
TCCAGAGCCAAACCTGCCGTGAGCACCCCAAGCCTGCTGCTGAGGGTGCTGTTCTGCGCCGTCTGTGG
GGAGCCAGCATACAAGTTTGCCGGCGGGGGAAGAAAACATCCCCGCTATCGATGCCGGTCTATGGGAT
TCCCTAAGCACTGTGGAAACGGCACTGTGGCTATGGCCGAGTGGGACGCCTTTTGTGAGGAACAGGTG
CTGGATCTGCTGGGAGACGCCGAGAGGCTGGAAAAAGTGTGGGTCGCTGGCAGCGACTCCGCTGTGG
AGCTGGCAGAAGTCAATGCCGAGCTGGTGGATCTGACCTCCCTGATCGGATCTCCTGCATATAGGGCA
GGCTCACCACAGCGAGAAGCTCTGGACGCACGAATTGCTGCACTGGCAGCTCGACAGGAGGAACTGGA
GGGGCTGGAAGCACGACCTAGCGGATGGGAGTGGCGAGAAACAGGCCAGCGGTTTGGGGATTGGTGG

AGAGAGCAGGACACAGCAGCCAAGAACACTTGGCTGAGAAGTATGAATGTCAGGCTGACTTTCGATGTG
CGCGGCGGGCTGACCCGAACAATCGATTTTGGCGACCTGCAGGAGTATGAACAGCACCTGAGACTGGG
GAGCGTGGTCGAAAGACTGCACACTGGGATGTCATAGTAACAGCCCATTTCAATATTCGGGCCGGGAAA
TACAGAGGATCACTGCCCCCTTGGGGCTATCTGCCTACCCGGGTGGATGGGGAGTGGCGCGCCACTCT
AGATCATAATCAGCCATACCACATTTGTAGAGGTTTTACTTGCTTTAAAAAACCTCCCACACCTCCCCCTG
AACCTGAAACATAAAATGAATGCAATTGTTGTTGTTAACTTGTTTATTGCAGCTTATAATGGTTACAAATAA
AGCAATAGCATCACAAATTTCACAAATAAAGCATTTTTTTCACTGCATTCTAGTTGTGGTTTGTCCAAACT
CATCAATGTATCTACCGGTACGCGTGTATACTTCGAAGTCGACGTGGTTTGTCTGGTCAACCACCGCGG
TCTCAGTGGTGTACGGTACAAACCCAGCCTCAGCATCCTAGATCATAATCAGCCATACCACATTTGTAGA
GGTTTTACTTGCTTTAAAAAACCTCCCACACCTCCCCCTGAACCTGAAACATAAAATGAATGCAATTGTTG
TTGTTAACTTGTTTATTGCAGCTTATAATGGTTACAAATAAAGCAATAGCATCACAAATTTCACAAATAAAG
CATTTTTTTCACTGCATTCTAGTTGTGGTTTGTCCAAACTCATCAATGTATCTGCCCGGGCCCTCGAGAC
AATTGATTAACATCGATACGTACCGAGTTGGCGCGCCTGGGAGCTCACGGGGACAGCCCCCCCCCAAA
GCCCCCAGGGATGTAATTACGTCCCTCCCCCGCTAGGGGGCAGCAGCGAGCCGCCCGGGGCTCCGCT
CCGGTCCGGCGCTCCCCCCGCATCCCCGAGCCGGCAGCGTGCGGGGACAGCCCGGGCACGGGGAAG
GTGGCACGGGATCGCTTTCCTCTGAACGCTTCTCGCTGCTCTTTGAGCCTGCAGACACCTGGGGGGAT
ACGGGGAAAAAGCTTTAGGCTGAAAGAGAGATTTAGAATGACAGGCGCGCCTGGCTGGCCGGCCAGC

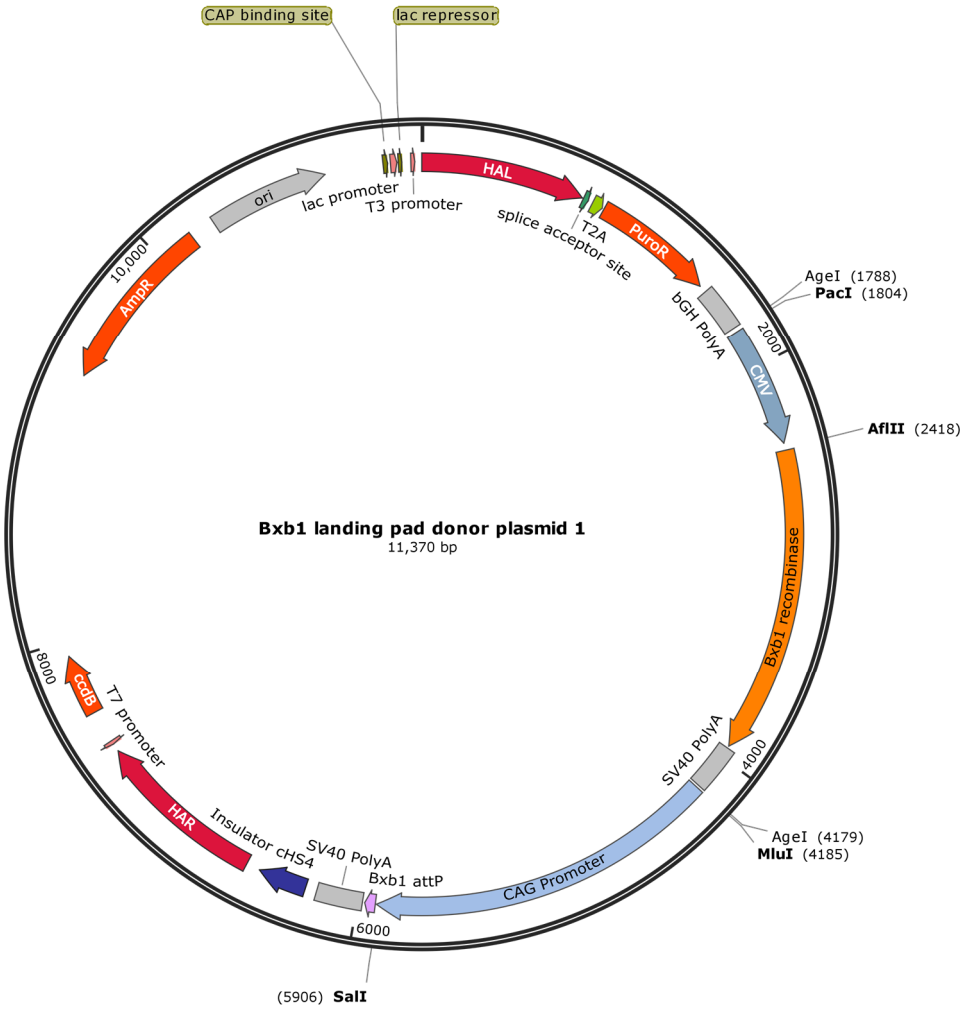

Figure 6.1-1: Bxb1 landing pad donor plasmid with Bxb1 recombinase.
Only the restriction sites used for cloning are shown.

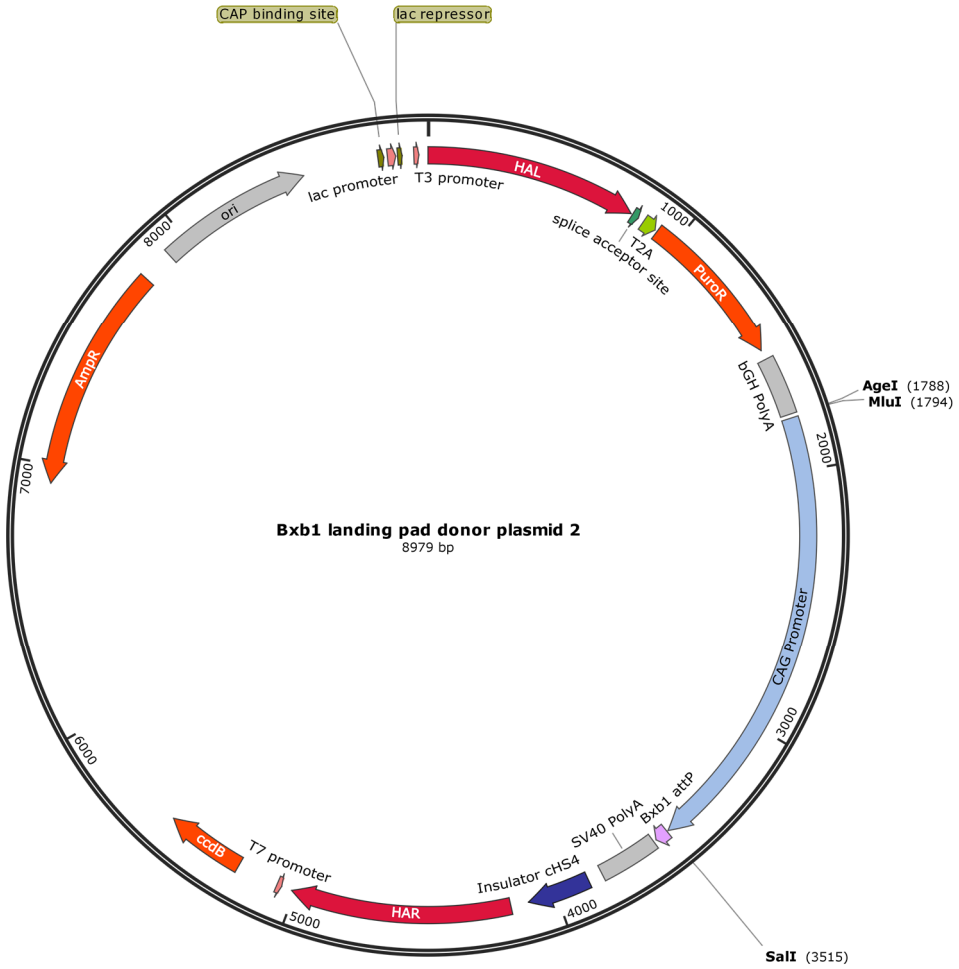

Figure 6.1-2: Bxb1 landing pad donor plasmid 2 used in this work.
Only the restriction sites used for cloning are shown.

Appendix II: Synthesized DNA for preparation of integration plasmids.

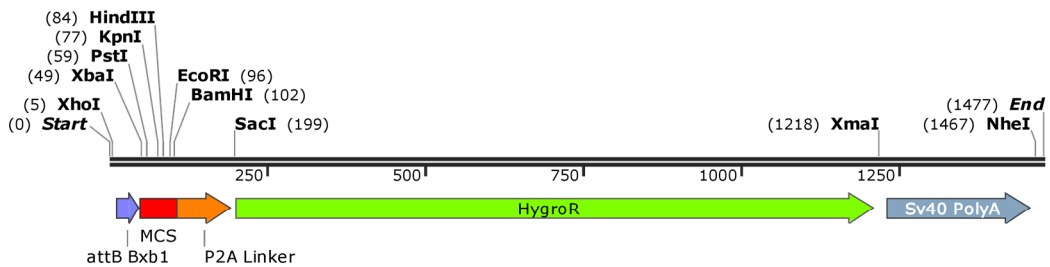

synthesized DNA fragment for integration plasmid
1477 bp

GTGCCTCGAGGGCTTGTCGACGACGGCGGTCTCCGTCGTCAGGATCATTCTAGACTGCAGAACGTTCT
TAAGGGTACCGCTGGAAGCTTCGATCGGAATTCGGATCCGGAAGCGGAGCTACTAACTTCAGCCTGCT
GAAGCAGGCTGGCGACGTGGAGGAGAACCCTGGACCTGCCACCATGAAAAAGCCTGAAGAGCTCCTCA
CCGCGACGTCTGTTGAGAAGTTTCTGATCGAAAAGTTCGACAGCGTCTCCGACCTGATGCAGCTCTCGG
AGGGCGAAGAATCTCGTGCTTTCAGCTTCGATGTAGGAGGGCGTGGATATGTCCTGCGGGTAAATAGCT
GCGCCGATGGTTTCTACAAAGATCGTTATGTTTATCGGCACTTTGCATCGGCCGCGCTCCCGATTCCGG
AAGTGCTTGACATTGGGGAATTTAGCGAGAGCCTGACCTATTGCATCTCCCGCCGTGCACAGGGTGTCA
CGTTGCAAGACCTGCCTGAAACCGAACTGCCCGCTGTTCTGCAACCGGTCGCGGAGGCTATGGATGCG
ATCGCTGCGGCCGATCTTAGCCAGACGAGCGGGTTCGGCCCATTCGGACCGCAAGGAATCGGTCAATA
CACTACATGGCGTGATTTCATATGCGCGATTGCTGATCCCCATGTGTATCACTGGCAAACTGTGATGGA
CGACACCGTCAGTGCGTCCGTCGCGCAGGCTCTCGATGAGCTGATGCTTTGGGCCGAGGACTGCCCC
GAAGTCCGGCACCTCGTGCACGCGGATTTCGGCTCCAACAATGTCCTGACGGACAATGGCCGCATAAC
AGCGGTCATTGACTGGAGCGAGGCGATGTTCGGGGATTCCCAATACGAGGTCGCCAACATCTTCTTCTG
GAGGCCGTGGTTGGCTTGTATGGAGCAGCAGACGCGCTACTTCGAGCGGAGGCATCCGGAGCTTGCA
GGATCGCCGCGGCTCCGGGCGTATATGCTCCGCATTGGTCTTGACCAACTCTATCAGAGCTTGGTTGAC
GGCAATTTCGATGATGCAGCTTGGGCGCAGGGTCGATGCGACGCAATCGTCCGATCCGGAGCCGGGA
CTGTCGGGCGTACACAAATCGCCCGCAGAAGCGCGGCCGTCTGGACCGATGGCTGTGTAGAAGTACTC
GCCGATAGTGGAAACCGACGCCCCAGCACTCGTCCGAGGGCAAAGGAATAGGGCGCCCCCGGGTTAA
TTAACTAGATCATAATCAGCCATACCACATTTGTAGAGGTTTTACTTGCTTTAAAAAACCTCCCACACCTC
CCCCTGAACCTGAAACATAAAATGAATGCAATTGTTGTTGTTAACTTGTTTATTGCAGCTTATAATGGTTA
CAAATAAAGCAATAGCATCACAAATTTCACAAATAAAGCATTTTTTTCACTGCATTCTAGTTGTGGTTTGTC
CAAACTCATCAATGTATCTACGCGTGCTAGCGATCG

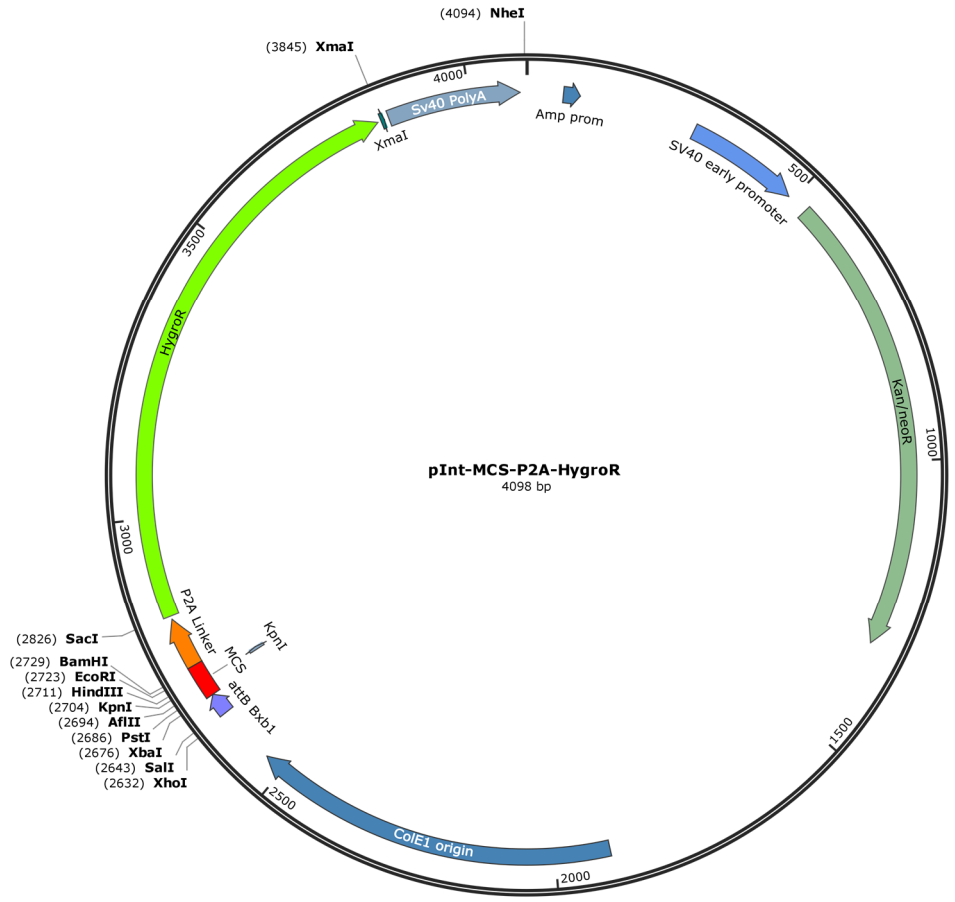

Figure 6.1-3: Basic integration plasmid pInt-MCS-P2A-HygroR.
Only restrictions sites in the MCS and restrictions sites used for cloning are shown.

Table 9: Primers for cloning of the Bxb1 landing pad donor plasmid.

Amplicon	Primer sequence (5' to 3')	Lab ID
landing pad scaffold	CGGTGGGCTCTATGGGTCACCGGTTCGCGATTAATTAAAGCGCT CTTAAGGCCGCC	7561
	CCTGTCCCTAGTAAAGCTGCTGGCCGGCCAGCCAGGCG	7562
donor backbone	AGCTTTACTAGGGACAGGATTG	7563
	GACCCATAGAGCCCACCGCA	7564
CMV promotor	CGATTAATTAATAGTTATTAATAGTAATCAATTACGGGGT	7573
	ACGCTTAAGGTAGCGCTAGCGGATCTGAC	7574
CAG promotor	AGAACGCGTGACATTGATTATTGACTAGTTATTAATAGTAATCAA	7624
	ATAGTCGACTTTGCCAAAATGATGAGACAGCACAATAA	7625

Table 10: Primers for cloning of integration plasmids.

Amplicon	Primer sequence (5' to 3')	Lab ID
integration plasmid backbone	CTTGCTAGCTCAGGTGGCACTTTTCGGGG	7594
	TGACTCGAGATGCATGGCGGTAATACGGTTA	7595
mEGFP, mCherrry	GAAGAGCTCATGGTGAGCAAGGGCGAG	8120
	TAACCCGGGGGCGCCTTACTTGTACAGCTCGTC	8121
codEGFP	GAAGAGCTCGTCTCCAAAGGAGAGGAGCTGTTCACCGGG	8529
	TAACCCGGGGGCGCCTTATTTATAGAGTTCATCCATGCCGAGAG TGATCCC	8531
vimentin	AGCGGTACCGGCTTCAAGGTCATCGTGATGCT	7601
	TCGAAGCTTAGGCATGGTGTCTAAGGGCGAAGA	7602
keratin	CATTCTAGAGCCGCCACCATGAGCTTCACCACTCGCTCC	8183
	AGCGGTACCGGCATGCCTCAGAACTTTGGTGTC	8184

Table 11: Generated integration plasmids with lab ID.
MCS: see Figure 6.1-3.

Integration plasmid	lab ID
pInt-MCS-P2A-HygroR	P2158
pInt-MCS-P2A-mEGFP	P2358
pInt-MCS-P2A-mCherry	P2474
pInt-MCS	P2377
pInt-Vimentin-MCS-P2A-HygroR	P2179
pInt-Vimentin-MCS-P2A-mEGFP	P2374
pInt-Vimentin-MCS-P2A-mCherry	P2489
pInt-Vimentin-MCS	P2398
pInt-Keratin-MCS-P2A-HygroR	P2376
pInt-Keratin-MCS-P2A-mEGFP	P2375
pInt-Keratin-MCS-P2A-mCherry	P2490
pInt-Keratin-MCS	P2399
pInt-MCS-P2A-codEGFP	P2475

Table 12: Primers for cloning of specific integration plasmids.

Amplicon	Primer sequence (5' to 3')	Lab ID
mEGFP, mCherry	CGTTCTAGAGCCGCCACCATGGTGAGCAAGGGCGAGGA	7596
mEGFP, mCherry	GCTGGATCCCTTGTACAGCTCGTCCATGCCG	7597
mRuby2, Ru63	CGTTCTAGAGCCGCCACCATGGTGTCTAAGGGCGAAGAG	7598
mRuby2	GCTGGATCCCTTGTACAGCTCGTCCATCCCA	7599
mRuby2, Ru63	TCGAAGCTTAGGCATGGTGTCTAAGGGCGAAGA	7602
mEGFP	TCGAAGCTTAGGCATGGTGAGCAAGGGCGAGGA	7761
mEGFP	AACGAATTCCTTGTACAGCTCGTCCATGCCG	8185
mRuby2, Ru63	AACGAATTCCTTGTACAGCTCGTCCATCCCA	8186

Table 13: Primers used for cloning of mammalian expression plasmids.

Primer sequence (5' to 3')	lab ID
GTCGCGGCCGCTTACTTGTACAGCTCGTC	4604
TCCACCGGTCGCCACCATGGTGAGCAAGGGCGAG	4605
GACGGTACCGCGGGCCCGGGATCCACCGGTCGCCACCATGGTGTCTAAGGGCGAAGAGCT	5532
TCGAAGCTTAGGCATGGTGTCTAAGGGCGAAGA	7602
GACGGTACCGCGGGCCCGGGATCCACCGGTCGCCACCATGGTGAGCAAGGGCGAGGCAGT	7674
TTAATTCCATGGTTACTTGTACAGCTCGTCCATCCCA	8359
ATATTAGCGGCCGCCGGTAGTGGTTCAGGGATGGTGTCTAAGGGCGAAGAGCTGATC	8360
AACGAATTCTTACTTGTACAGCTCGTCCATCCCA	8439
TCCGCTAGCGCTAATGGTGTCTAAGGGCGAAGA	8639
TCCGCTAGCGCTACCGGTCGCCACCATGGTGTCTAAGGGCGAAGA	8640
AGGGGATCCACCGGTCGCCACCGTGTCTAAGGGCGAAGAGCT	8719
CGAGCGGCCGCTACTTGTACAGCTCGTCCATCC	8720
AGGGGATCCACCGGTCGCCACCGTGAGCAAGGGCGAGGCAGT	8723
CGAGCGGCCGCTACTTGTACAGCTCGTCCATGC	8724
TCGAAGCTTAGGCATGGTGAGCAAGGGCGAGGC	8854
AACGAATTCTTACTTGTACAGCTCGTCCATGCC	8855
GATCCGCTAGCGCTAATGGTGAGCAAGGGCGAGGCA	9240
CACTCGAGATCTGAGTCCGGACTTGTACAGCTCGTCCATGCC	9241
CACTCGAGATCTGAGTCCGGACTTGTACAGCTCGTCCATCCC	9242
TCCGCTAGCGCTACCGGTCGCCACCATGGTGAGCAAGGGCGAGGCA	9243
CTGCAGGTCGACATGGTGAGCAAGGGCGAGGC	9244
CTGCAGGTCGACATGGTGTCTAAGGGCGAAGA	9245
TTCTGCGGCCGCCTTGTACAGCTCGTCCATGC	9246
TTCTGCGGCCGCCTTGTACAGCTCGTCCATCC	9247
CTTGAAGCGGCCGCCGGTAGTGGTTCAGGGATGGTGAGCAAGGGCGAGGCAGTGATC	9249
CAATTTCCATGGTTACTTGTACAGCTCGTCCATGCC	9250
CTTCGAATTCATGGTGAGCAAGGGCGAGGCAGTG	9411
GCGACCGGTTTCATGGTGGCAGGTCCAGGGTTCTCCTCCACGTCGCCAGCCTGCTTCAGCAG GCTGAAGTTAGTAGCTCCGCTTCCCTTGTACAGCTCGTCCATGCCGC	9412
CTTCGAATTCATGGTGAGCGAGCTGATTAAGGAG	9415
GCGACCGGTTTCATGGTGGCAGGTCCAGGGTTCTCCTCCACGTCGCCAGCCTGCTTCAGCAG GCTGAAGTTAGTAGCTCCGCTTCCTTTACCTCCATCACCAGCGCCAC	9416

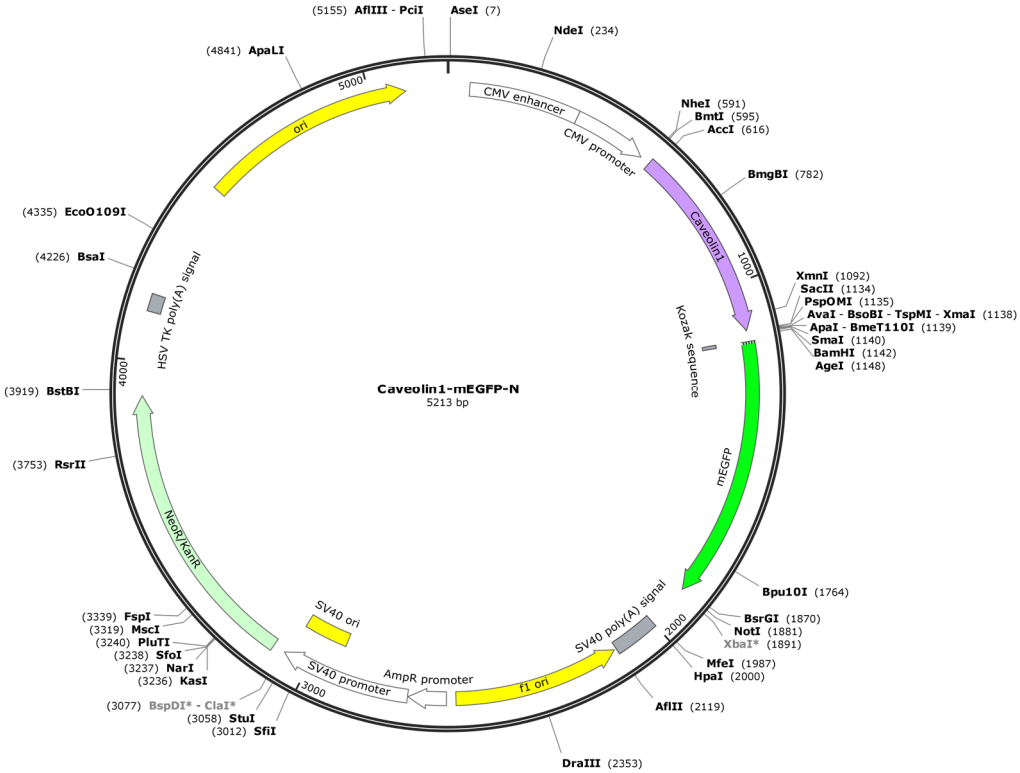

Figure 6.1-4: Plasmid map of Caveolin1-mEGFP-N.
Caveolin1: 597-1130; mEGFP: 1161-1880

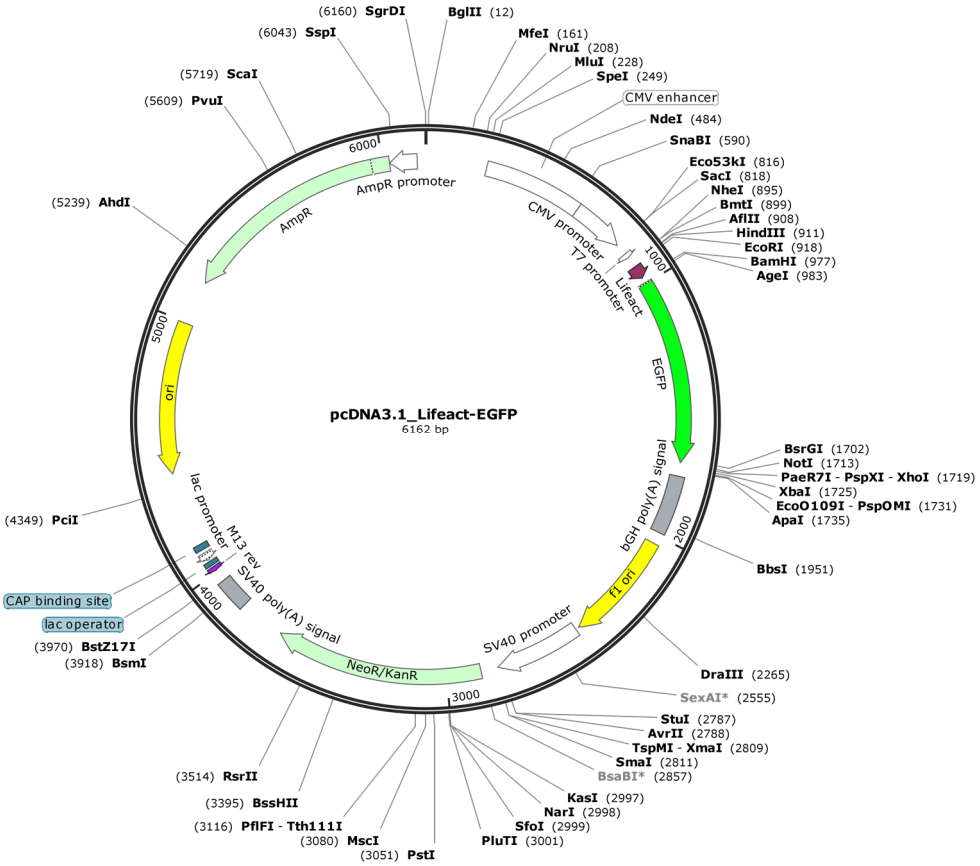

Figure 6.1-5: Plasmid map of pcDNA3.1_Lifeact-EGFP.
Lifeact: 924-974; EGFP: 996-1709.

Table 14: Primers used for mutagenesis of mRuby2 and mScarlet variants.
[Phos] indicates 5' phosphorylation of the respective primer.

Amplicon	Mutagenesis	Obtained mutation	Primer sequence (5' to 3')	Lab ID
mRuby2 variants	Site-directed	T162A	GGTCTGAGGGGATACGCCCATACAGCACTGAAA	6869
		T162A	TTTCAGTGCTGTATGGGCGTATCCCCTCAGACC	6870
		C176A	GGTGGCCGTCTGTCTNNNTCTTTCGTAACAACT	7070
		C176A	AGTTGTTACGAAAGANNNAGACAGACGGCCACC	7071
		N37A	GGTGAAGGAGAAGGCNNNCCGTACATGGGAACT	8479
		N37A	AGTTCCCATGTACGGNNNGCCTTCTCCTTCACC	8480
	Multiple-site	M164T	[Phos]AGGGGATACACTCATNNNGCACTGAAAGTT GAT	6646
		A63S	[Phos]GCCTTTGACATTCTTNNNACGTCGTTCTTGT AT	7012
		F225L	[Phos]CACGCAGTTGCCAAGNNNGCCGGGCTTGG TGGT	7274
		K192L	[Phos]ACCGTCGGGAACATCNNNATGCCCGGTATC CAT	7276
		R99S	[Phos]TGGGAAAGAGTTACGNNNTACGAAGATGGT GGA	7277
		antisense primer	GATTTAATCTGTATCAGG	1640
mScarlet variants	Site-directed	I162Q M164G	GTGCTGAAGGGCGACNNNAAGNNNGCCCTGCGC CTGAAG	8305
		I162Q M164G	CTTCAGGCGCAGGGCNNNCTTNNNGTCGCCCTTC AGCAC	8306
		G164A	AAGGGCGACCAGAAGNNNGCCCTGCGCCTGAAG	8370
		G164A	CTTCAGGCGCAGGGCNNNCTTCTGGTCGCCCTT	8371
		S147G	ATGGGCTGGGAAGCGNNNACCGAGCGGTTGTAC	8307
		S147G	GTACAACCGCTCGGTNNNCGCTTCCCAGCCCAT	8308
		R217Q	GTGGAACAGTACGAANNNTCCGAGGGCCGCCAC	8946
		R217Q	GTGGCGGCCCTCGGANNNTTCGTACTGTTCCAC	8947
		D161K	GGCGTGCTGAAGGGCAAGCAGAAGGCTGCCCTG	9120
		D161K	CAGGGCAGCCTTCTGCTTGCCCTTCAGCACGCC	9121

Table 15: Primers used in genotyping PCRs for generated monoclonal cell lines.

Monoclonal cell line	Amplicon	Primer sequence (5' to 3')	Lab ID
Landing pad cell line K21	wt PCR chromosome 19	CCCCTATGTCCACTTCAGGA	7195
		CAGCTCAGGTTCTGGGAGAG	7196
	CAG to HAR	GCAACGTGCTGGTTATTGTG	5942
		TTCCAAACTGCTTCTCCTCTTGGG	7094
	cHA4 to chromosome 19	GGATCGCTTTCCTCTGAACGCTTC	8052
		GAAGGATGCAGGACGAGAAA	7198
K21 Ker-Ru63-P2A-mEGFP (control of correct integration)	CAG to P2A	GCAACGTGCTGGTTATTGTG	5942
		GTGGCAGGTCCAGGGTTCTCCTC	7779
	mEGFP to KanR	GAAGAGCTCATGGTGAGCAAGGGCGAG	8120
		GGTCAAGCTTTCAGAAGAACTCGTCAAGAAG	5759
	ori to HAR	CTACACCGAACTGAGATACCTACAGCG	7379
		TTCCAAACTGCTTCTCCTCTTGGG	7094
	HAR to chromosome 19	GGATCGCTTTCCTCTGAACGCTTC	8052
		GAAGGATGCAGGACGAGAAA	7198
K21 keratin cell lines	CAG to	GCAACGTGCTGGTTATTGTG	5942
	Ru63/Ru85/Ru87	AACGAATTCTTACTTGTACAGCTCGTCCATCCCA	8439
	Sc10/Sc21	AACGAATTCTTACTTGTACAGCTCGTCCATGCC	8855
U2OS endogenous vimentin-tagged cell lines	vimentin to	CTAATCTGGATTCACTCCCTCTGGTTGATACC	MR847
	Ru87	TTAATTCCATGGTTACTTGTACAGCTCGTCCATCCCA	8359
	Sc10	CAATTTCCATGGTTACTTGTACAGCTCGTCCATGCC	9250

6.2 Sequence alignments of the novel RSFPs with their template proteins

```
          1                              30                              60
mRuby2    MVSKGEELIKENMRMKVVMEGSVNGHQFKCTGEGEGNPYMGTQTMRIKVIEGGPLPFAFD
Ru63      MVSKGEELIKENMRMKVVMEGSVNGHQFKCTGEGEGNPYMGTQTMRIKVIEGGPLPFAFD
Ru85      MVSKGEELIKENMRTKVVMEGSVNGHQFKCTGEGEGNPYMGTQTMRIKVIEGGPLPFAFD
Ru87      MVSKGEELIKENMRTKVVMEGSVNGHQFKCTGEGEGAPYMGTQTMRIKVIEGGPLPFAFD

          61                             90                             120
mRuby2    ILATSFMYGSRTFIKYPKGIPDFFKQSFPEGFTWERVTRYEDGGVVTVMQDTSLEDGCLV
Ru63      ILSTSFLYGSRTFIKYPKGIPDFFKQSFPEGFTWERVTSYEDGGVVTVMQDTSLEDGCLV
Ru85      ILSTSFLYGSRTFIKYPKGIPDFFKQSFPEGFTWERVTSYEDGGVVTVMQDTSLEDGCLV
Ru87      ILSTSFLYGSRTFIKYPKGIPDFFKQSFPEGFTWERVTSYEDGGVVTVMQDTSLEDGCLV

          121                            150                            180
mRuby2    YHVQVRGVNFPSNGPVMQKKTKGWEPNTEMMYPADGGLRGYTHMALKVDGGGHLSCSFVT
Ru63      YHVQVRGVNFPSNGPVMQKKTKGWEPNTEMMYPADGGLKGYAHTALKVDGGGRLSASFVT
Ru85      YHVQVRGVNFPSNGPVMQKKTKGWEPNTEMMYPADGGLKGYAHTALKVDGGGRLSASFVT
Ru87      YHVQVRGVNFPSNGPVMQKKTKGWEPNTEMMYPADGVLKGYAHTALKVDGGGRLSASFVT

          181                            210                        237
mRuby2    TYRSKKTVGNIKMPGIHAVDHRLERLEESDNEMFVVQREHAVAKFAGLGGGMDELYK
Ru63      TYRSKKTVGNILMPGIHAVDHRLERLEESDNEMFVVQREHAVAKLAGLGGGMDELYK
Ru85      TYRSKKTDGNILMPGIHAVDHRLERLEESDNEMFVVQREHAVAKLAGLGGGMDELYK
Ru87      TYRSKKTDGNILMPGIHAVDHRLERLEESDNEMFVVQREHAVAKLAGLGGGMDELYK
```

Figure 6.2-1: Sequence alignment of mRuby2 and final positive-switchable variants.
Amino acid sequences of mRuby2, Ru63, Ru85 and Ru87. Mutations are highlighted in yellow.

```
          1                              30                              60
mScarlet  MVSKGEAVIKEFMRFKVHMEGSMNGHEFEIEGEGEGRPYEGTQTAKLKVTKGGPLPFSWD
Sc10      MVSKGEAVIKEFMRFKVHMEGSMNGHEFEIEGEGEGRPYEGTQTAKLKVTKGGPLPFSWD
Sc21      MVSKGEAVIKEFMRFKVHMEGSMNGHEFEIEGEGEGRPYEGTQTAKLKVTKGGPLPFSWD

          61                             90                             120
mScarlet  ILSPQFMYGSRAFTKHPADIPDYYKQSFPEGFKWERVMNFEDGGAVTVTQDTSLEDGTLI
Sc10      ILSPQFMYGSRAFTKHPADIPDYYKQSFPEGFKWERVMNFEDGGAVTVTQDTSLEDGTLI
Sc21      ILSPQFMYGSRAFTKHPADIPDYYKQSFPEGFKWERVMNFEDGGAVTVTQDTSLEDGTLI

          121                            150                            180
mScarlet  YKVKLRGTNFPPDGPVMQKKTMGWEASTERLYPEDGVLKGDIKMALRLKDGGRYLADFKT
Sc10      YKVKLRGTNFPPDGPVMQKKTMGWEAGTERLYPEDGVLKGDQKAALRLKDGGRYLADFKT
Sc21      YKVKLRGTNFPPDGPVMQKKTMGWEAGTERLYPEDGVLKGKQKAALRLKDGGRYLADFKT

          181                            210                    232
mScarlet  TYKAKKPVQMPGAYNVDRKLDITSHNEDYTVVEQYERSEGRHSTGGMDELYK
Sc10      TYKAKKPVQMPGAYNVDRKLDITSHNEDYTVVEQYERSEGRHSTGGMDELYK
Sc21      TYKAKKPVQMPGAYNVDRKLDITSHNEDYTVVEQYEQSEGRHSTGGMDELYK
```

Figure 6.2-2: Sequence alignment of mScarlet and final negative-switchable variants.
Amino acid sequences of mScarlet, Sc10 and Sc21. Mutations are highlighted in yellow.

6.3 Isolation and characterization of fluorescent proteins

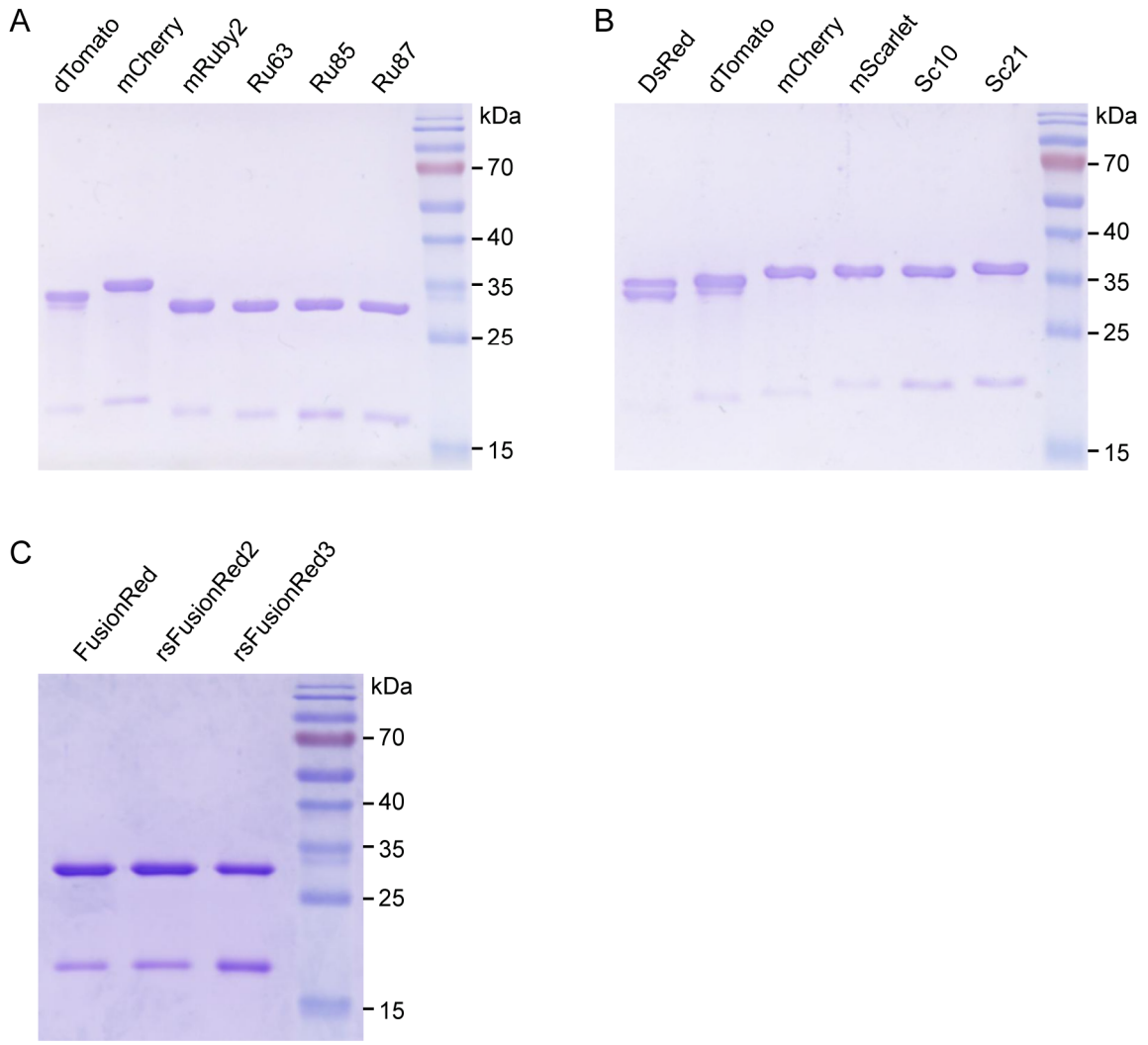

Figure 6.3-1: SDS-PAGE of purified fluorescent protein solutions.
The purity of the isolated fluorescent protein samples was controlled in SDS-PAGE. 2 µg protein was added to each lane. Marker: PageRuler Prestained Ladder. A: Isolated switchable mRuby2 variants and proteins for comparison. B: Isolated switchable mScarlet variants and proteins for comparison. C: Isolated FusionRed, rsFusionRed2 and rsFusionRed3 samples.

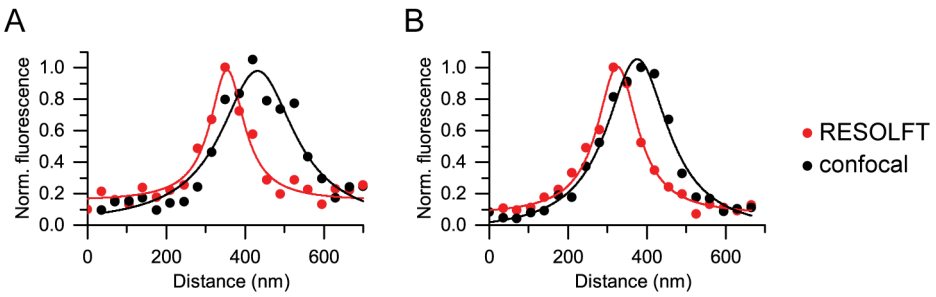

Figure 6.3-2: Comparison of line profiles in the RESOLFT and confocal image using Ru63.
Line profiles at the same positions in the confocal and RESOLFT image of keratin-Ru63 in Figure 3.2-18. The data was fitted using a Lorentz function. Red: RESOLFT, black: confocal image. A: Line profile 1, B: Line profile 2 in Figure 3.2-18. Due to shifts in the field of view, the position of the maximal fluorescence is shifted from the RESOLFT to the confocal image.

Table 16: Determination of ε and QY for rsFusionRed2 and rsFusionRed3.

Protein	Purification	ε [$M^{-1}cm^{-1}$]	QY [%]	Brightness
rsFR2	1	10381	7.7	0.80
	2	7853	7.8	0.61
	3	18413	6.6	1.22
	4	25101	6.6	1.66
	Average	15437	7.2	1.07
	STDEV	7860	0.7	0.46
rsFR3	1	11020	5.8	0.64
	2	9631	5.8	0.56
	3	17660	5.2	0.92
	4	22678	4.6	1.04
	Average	15247	5.4	0.79
	STDEV	6068	0.6	0.23

List of figures

List of tables

Abbreviations

AAVS1	adeno-associated virus integration site 1
Abs	absorption
APS	ammonium persulfate
a.u.	arbitrary unit
bp	base pair
BSA	bovine serum albumin
CMV	*cytomegalovirus*
codEGFP	mEGFP with altered codon usage at the N- and C-terminus
CRISPR	clustered regularly interspaced short palindromic repeats
DMEM	Dulbecco's modified Eagle's medium
DNA	deoxyribonucleic acid
dNTP	deoxyribonucleotide triphosphate
ε	extinction coefficient
E. coli	*Escherichia coli*
EDTA	ethylenediaminetetraacetic acid
Em	emission
ep	error-prone
eq.	equilibrium
ER	endoplasmic reticulum
Exc	excitation
FACS	fluorescence activated cell sorting
FBS	fetal bovine serum
FP	fluorescent protein
FRET	fluorescence resonance energy transfer
FWHM	full width at half maximum
GFP	green fluorescent protein
gRNA	guide ribonucleic acid
HAL/HAR	homology arm left/right
HygroR	Hygromycin resistance
KanR	Kanamycin resistance
LB	lysogeny broth
MCS	multiple cloning site
MINFLUX	nanoscopy with minimal photon fluxes

NA	numerical aperture
P2A	*porcine teschovirus*-1 2A self-cleaving peptide
PAGE	polyacrylamide gel electrophoresis
PALM	photoactivatable localization microcopy
PBS	phosphate-buffered saline
PCR	polymerase chain reaction
PSF	point spread function
PuroR	Puromycin resistance
QY	quantum yield
RESOLFT	reversible saturable optical fluorescence transitions
RSFP	reversibly switchable fluorescent protein
SDS	sodium dodecyl sulfate
SIM	structured illumination microscopy
STED	stimulated emission depletion
SV40	simian virus 40
T2A	*thosea asigna* virus 2A self-cleaving peptide
TEMED	tetramethylethylenediamine
Tris	tris(hydroxymethyl)aminomethane
wt	wild-type

Acknowledgement

Ich möchte mich bei allen ganz herzlich bedanken, die mich während meiner Doktorarbeit unterstützt haben.

Zunächst möchte ich Prof. Dr. Stefan Jakobs und Prof. Dr. Stefan W. Hell dafür danken, dass sie mir ermöglicht haben, meine Doktorarbeit in ihrer Arbeitsgruppe bzw. in ihrer Abteilung unter hervorragenden Bedingungen anzufertigen. Bei Prof. Dr. Stefan Jakobs möchte ich mich insbesondere für die Betreuung der Arbeit bedanken.

Prof. Dr. Helmut Grubmüller und Prof. Dr. Stefan W. Hell danke ich für die Unterstützung im Betreuungsausschuss und bei Prof. Dr. Helmut Grubmüller bedanke ich mich für die Begutachtung meiner Dissertation.

Mein Dank gilt auch Prof. Dr. Michael Müller, Prof. Dr. Silvio O. Rizzoli und Dr. Dieter Klopfenstein als weitere Mitlgieder meiner Prüfungskommission.

Bei Dr. Alexey I. Chizhik bedanke ich mich für die Messungen der Fluoreszenzlebenszeiten.

Ich möchte mich bei Dr. Nickels Jensen für die tolle Betreuung, für die Unterstützung und für die wertvollen wissenschaftlichen Diskussionen bedanken.

Bei Dr. Sebastian Schnorrenberg bedanke ich mich für die Hilfe am RESOLFT Mikroskop und für aufschlussreiche Gespräche.

Sylvia Löbermann, Tanja Gilat und Rita Schmitz-Salue danke ich für die hervorragende technische Assistenz und die Hilfe bei allen Anliegen.

Bei Dr. Dirk Kamin, Dr. Nickels Jensen und Jaydev Jethwa bedanke ich mich für das Korrekturlesen meiner Arbeit.

Ich bedanke mich bei allen aktuellen Mitgliedern und Ehemaligen der Abteilung NanoBiophotonics für die tolle Arbeitsatmosphäre. Insbesondere möchte ich mich bei meinem Arbeitsehemann Timo Konen dafür bedanken, dass wir vier Jahre lang jedes Leid, aber auch jede Freude und jede Errungenschaft miteinander geteilt haben. Till Stephan danke ich besonders für seine Hilfsbereitschaft und für ein offenes Ohr.

Ich bin sehr dankbar dafür, dass ich in der Abteilung besondere Menschen kennen lernen durfte und Freunde gefunden habe. Für großartige Pausen, liebe Worte und schöne Aktivitäten danke ich Jennifer, Jasmine, Timo, Sebastian, Philipp, Christian, Dirk, Steffi, Till, Nickels, Florian, Felix, Peter, Daniel und allen weiteren, die zur Core Group gehören.

Ein großes Dankeschön möchte ich Dirk aussprechen für die unbeschreibliche Unterstützung in der letzten Zeit und dafür, dass er es geschafft hat, dass ich nicht an meiner Doktorarbeit verzweifle.

Zuletzt möchte ich mich bei meiner Familie für die Liebe und den Rückhalt bedanken. Meinen Eltern danke ich besonders dafür, dass sie mir meinen Weg ermöglicht haben.